KU Leuven
Biomedical Sciences Group
Faculty of Medicine
Department Imaging & Pathology

KU LEUVEN
DOCTORAL SCHOOL
BIOMEDICAL SCIENCES

PET-MR IN ANIMAL MODELS OF ADDICTION

FOCUS ON THE GLUTAMATERGIC SYSTEM

Bart de Laat

Jury:

Promoter:	Prof. dr. Koen Van Laere
Copromoter:	dr. Cindy Casteels
Chair:	Prof. dr. Tania Roskams
Secretary:	Prof. dr. Rudi D'Hooge
Jury members:	dr. Mark Schmidt Prof. dr. Evan Morris Prof. dr. Geert Dom Prof. dr. Jan de Hoon

Dissertation presented in partial fulfilment of the requirements for the degree of
Doctor in Biomedical Sciences

Leuven, December 20th 2017

Acknowledgements

It has been a great pleasure and honour to be part of the academic population these last four years. More than ever, I realize what the phrase ‘standing on the shoulders of giants’ means. Not only does it reflect that one cannot achieve scientific advances without the consistent and considerable help of others, it also implies that the giant will have to bend down and pick you up. Once arrived upon the shoulder, efforts can be made to achieve new heights. Whereas sparse breaks from these efforts provide the opportunity to gaze into the panorama of men’s achievements.

In any doctorate, the fundament is laid by its promotor long before the candidate’s attempts to execute this. I am very grateful for the extensive fundament that was laid by my promoter prof. Van Laere. He provided a high-level environment, ranging from tangible matters, such as infrastructure, to intangible benefits, including an extensive network and reputation that opened many a door. It has been a pleasure to work in your group and to witness how a long-term vision is being realized into a state of the art department of nuclear medicine. Equipment is hardly of any use without the expertise required to operate it. My copromoter, dr. Casteels, provided not only this, but also her extensive experience with the consequent data processing and reporting. Your endless patience to assure the correctness of every detail and to entertain any ambitious proposal are much appreciated.

The internal jury members of this doctorate, prof. de Hoon and prof. D’Hooge, have always demanded that the research met their high standards and consequently improved the quality of this PhD with their input. Also the external jury members have been invaluable in this process, for which I would like to thank dr. Schmidt, prof. Dom, and prof. Morris. Thank you for investing your valuable time, it has improved the thesis, but also my own scientific capabilities. I would also like to thank prof. Morris explicitly for hosting me in his group and offering me the opportunity to pursue my passion even further.

Our group harbours several experts on different aspects of the multi-faceted world of PET imaging. Although my course has never crossed with some, I am very grateful to

those who shared their knowledge and insights. This was particularly true for dr. Leurquin-Sterk, as it was great to have a partner in crime in the translational mGluR5 project. Although on a very different project, dr. Holvoet is thanked for his rigorous condemnation of anything less than excellent science. No question unanswered, no question unasked. Scientists excel in some things, but not in lab management or financial guideline adherence. Happily this was orchestrated by our departmental manager Peter Vermaelen, who seemed to have an answer to every question and access to every account. BSc. Van Santvoort is thanked for being a rescue beacon with her impressive talent to place an injection needle in any tail in only one attempt. I am grateful for the company and assistance from BSc. Buellens, whose heart-warming laughter is now heard by those accompanying her on her new adventures. A thanks and good luck to MSc. Crabbé, who is now the tower of strength of our department in the MoSAIC.

One of the essential pillars of this work has been erected with the help of prof. Koole and his extensive experience in kinetic modelling. In addition, MSc. Devrome, who is impacting the role of artificial intelligence in neuroimaging is thanked for his enthusiasm and expert knowledge in this field. Special thanks go out to dr. Ceccarini, who shared so much of her work with time-variant models to prepare me for the collaboration with prof. Morris at Yale university. Finally, I would like to express my gratitude to prof. Nuyts, who, despite his immense workload, remains calm and cheerful during any project. This is also reflected on the people under his supervision that I have had the pleasure of working with. In a combined effort, dr. Bickell, dr. Turco, and dr. Schramm proved how different backgrounds can seamlessly transform into synergism and friendship.

Every ambition to include additional techniques, modalities or analyses in one's research rely on the benevolence of experts in those respective fields to share their knowledge and infrastructure. Two laboratories have played a major role in that light for this doctorate. Firstly, the laboratory of radiopharmacy where every door was always open. For this, I would like to thank prof. Bormans, who has a unique way of combining a ferocious professional mentality with exceptional personal pleasantness. The way you inspire your laboratory to be positive, motivated, and productive will remain a lifelong example. I am very grateful for the time and discussion I could spend

with the people in this happy bunch, many of whom I am happy to count among my friends. In chronological order, I would like to give a special mention to; BSc. Cornelis for introducing me to microsurgical procedures, autoradiography and so many other techniques; dr. Celen, not only for your crucial work in the preparation of the FPEB radiotracer, but also for introducing me to the radiopharmaceutical lingo; dr. de Groot, for being a cheerful beacon of the familiar Northern no-nonsense in the times of radiotracer production stress; MSc. Sannen, for his expert knowledge of virtually any radiopharmaceutical device and his tireless explanations of HPLC columns; dr. Ory, for so generously including me in my first official collaboration, but also the discussions about houses and whiskey; dr. Declerq, your near magic excel skills have saved me many a times from gamma counter catastrophes, but your generous laughter, both in the lab and on exclusive parties, could cheer me up any time; dr. Cleeren, for getting me into those exclusive parties and our exciting ongoing collaboration; Msc. Siemons, for your never-ending ambitious energy, always combined with impeccable elegance: may we become the ultimate strategy managers; BSc. Haspeslagh, for making it seem as if any problem was surmountable; dr. Billaud, for our collaboration on the exciting application of antibody labelling. Finally a big thanks to dr. Funke, MSc. Attili, MSc. Vermeulen, and MSc. Luyten, I do hope that our paths will cross again in the future.

The second laboratory that has added an immense value to this work is the Biomedical MRI unit. This laboratory is led by prof. Himmelreich, who always has the best interest for the MoSAIC at heart. Thank you for your faith and encouragement and for showing that one can have a huge impact while always being gentle. Another key player, dr. Gsell, has provided so much experience and technical improvements, that many studies came to their full potential through your ‘get things done’ mentality, for which many thanks. A sincere thank you also goes out to all members of this laboratory, many who have also been my direct colleagues: MSc. Weerasekera, if it were not for you, spectroscopy might not have been a part of this work, whereas now it is a key component. I always had much respect for your balance act between the biological mayhem and the exact algorithms that are combined in spectroscopy quantification. MSc. Poelmans, for her tireless efforts to have all introvert scientists engage in social behaviour, including the shared experience of the BMIC board; MSc. Govaerts, for all the hands-on help with navigating the labyrinth of python scripts, virtual machines, and setting up the resting-state pipeline; dr. Liang, thanks for the good times on the football

field and your humour in the lab; MSc. Saini, for our talks on child raising perspectives; BSc. Wouters, your open mind and active tolerance are an example to all of us in the current times; MSc. Ribeiro, always vigilant for any gender inequality issues; and finally dr. Guldris, Dr. Reséndiz Sharpe, MSc. Belderbos, MSc. Van Herp, MSc. Llambrich, and MSc. Dekoster good luck with all your projects, as you are the future of our center.

A welcome exotic influence has always come from the laboratory of theragnostics. Not only the rhythmic Cuban presence of dr. Cona, but also her cigar smuggling were always appreciated. Thanks also to dr. Ting and MSc. Liu, because of you there always was a little light burning in our office, no matter what time in the weekend or at night. Along the years, many individual colleagues have been so instrumental that they should be acknowledged. As mentioned in the introduction, I would like to thank dr. Teuns, as her input to the procedure for surgical implantation of catheters has critically improved the outcome of all self-administration experiments. Setting up the self-administration cages at our facility would not have been possible without the help, experience, and sugar pellets of dr. Beurms and dr. Maes. My gratitude also goes out to dr. Deprez, dr. Luyck, and dr. Van Kuyck for our conversations about travelling, academia, and the IWT preparation sessions. Next to the entire team at the Gasthuisberg Animalium, a special thanks goes out to dr. De Vleeschauwer for her advice on perioperative care. On a more general note, I would like to express my thanks to the University of Leuven, for providing such a great scientific environment, which includes so many workshops and courses all aimed at becoming a broader and better scientist. This includes DOC and LRD for their input on the funding applications, the HR department and LSTAT for all training opportunities, and rector Torfs who made time to be on every science slam to emphasize its importance: ‘Obamas are not bred in attics’.

I could not have reached this point without my parents. Thank you for enabling my curiosity and providing regular doses of adventure in my life. My good friend Dr. Post, I want to thank you for the endless energy and ambition that you radiate so relentlessly. In the scarce moments of frustration and despair, you invariably told me “this is where true character distinguishes itself”. For my wife, my love: our endless love collapses any dimension into an enlightened multiverse of understanding, righteousness, and serenity.

Contents

SUMMARY ..... **I**

SAMENVATTING ..... **V**

CHAPTER 1: INTRODUCTION **1**

1.1 ADDICTION 1
1.2 DRUGS OF ABUSE AND ADDICTION 2
1.3 ADDICTION AND THE REWARD SYSTEM 4
1.4 NEUROBIOLOGY OF ADDICTION 9
1.5 MGLUR5 AND ADDICTION 12
1.6 ANIMAL MODELS OF ADDICTION 15
1.7 NEUROIMAGING OF ADDICTION 19
1.8 OVERVIEW 29

CHAPTER 2: PRECLINICAL EVALUATION AND QUANTIFICATION OF ^{18}F-FPEB AS A RADIOLIGAND FOR PET IMAGING OF THE METABOTROPIC GLUTAMATE RECEPTOR 5 ..... **31**

2.1 ABSTRACT 32
2.2 INTRODUCTION 33
2.3 MATERIALS AND METHODS 34
2.4 RESULTS 39
2.5 DISCUSSION 44

CHAPTER 3: AGE AND SEX RELATED DIFFERENCES IN ^{18}F-FPEB BINDING TO THE METABOTROPIC GLUTAMATE RECEPTOR 5 (MGLUR5) IN THE RAT BRAIN: A POSITRON EMISSION TOMOGRAPHY STUDY **49**

3.1 ABSTRACT 50
3.2 INTRODUCTION 51
3.3 MATERIALS AND METHODS 52
3.4 RESULTS 54
3.5 DISCUSSION 61

CHAPTER 4: GLUTAMATERGIC BIOMARKERS FOR COCAINE ADDICTION: A LONGITUDINAL STUDY IN SELF-ADMINISTERING RATS USING MRS AND MGLUR5 PET **65**

4.1 ABSTRACT 66
4.2 INTRODUCTION 67
4.3 MATERIALS AND METHODS 68
4.4 RESULTS 73
4.5 DISCUSSION 81

CHAPTER 5: EFFECTS OF ALCOHOL EXPOSURE ON THE GLUTAMATERGIC SYSTEM: A COMBINED LONGITUDINAL ^{18}F-FPEB AND ^{1}H-MRS STUDY IN RATS **87**

5.1 ABSTRACT 88
5.2 INTRODUCTION 89
5.3 MATERIALS AND METHODS 90
5.4 RESULTS 94
5.5 DISCUSSION 99

CHAPTER 6: *IN VIVO* SILENCING OF MGLUR5 IN THE RAT BRAIN WITH NAKED SIRNA: A PROOF-OF-PRINCIPLE STUDY USING ^{18}F-FPEB AUTORADIOGRAPHY **105**

6.1 ABSTRACT 106
6.2 INTRODUCTION 107
6.3 MATERIALS AND METHODS 110

6.4 RESULTS 114
6.5 DISCUSSION 119

CHAPTER 7: THE EFFECT OF NICOTINE SELF-ADMINISTRATION ON ^{18}FDG UPTAKE AND RESTING-STATE FUNCTIONAL CONNECTIVITY: A MACHINE LEARNING APPROACH 123

7.1 ABSTRACT 124
7.2 INTRODUCTION 125
7.3 MATERIALS AND METHODS 127
7.4 RESULTS 131
7.5 DISCUSSION 138

CHAPTER 8: ACUTE CHANGES IN RAT BRAIN METABOLISM AFTER INTRAVENOUS ADMINISTRATION OF ALCOHOL, COCAINE, AND NICOTINE: A SIMULTANEOUS PET/MR STUDY WITH DYNAMIC ^{1}H-MRS AND CONTINUOUS INFUSION ^{18}FDG. 141

8.1 ABSTRACT 142
8.2 INTRODUCTION 143
8.3 MATERIALS AND METHODS 145
8.4 RESULTS 147
8.5 DISCUSSION 151

CHAPTER 9: LOGAN PLOTS: A COMPARISON BETWEEN SUMMARY STATISTIC APPROACHES AND ANALYSIS WITH GEE, SECOND-LEVEL, OR MIXED MODELS 157

9.1 ABSTRACT 158
9.2 INTRODUCTION 159
9.3 MATERIALS AND METHODS 164
9.4 RESULTS 169
9.5 DISCUSSION 174

CHAPTER 10: GENERAL DISCUSSION 179

BIBLIOGRAPHY 188

CURRICULUM VITAE 217

PUBLICATION LIST 218

Summary

Addiction is a complex psychiatric disorder with a major impact on healthcare and economy. Treatment of this disorder remains challenging, in particular because of a high rate of relapse even after long periods of abstinence. Classically, addiction was explained by the large dopamine release induced by drugs of abuse. Although this remains a central axis, there is an increasing amount of evidence that other neurotransmitter systems should also be explored for therapeutic options. In this light, interest exists in the glutamatergic system and its controlling function. The control exerted by the glutamatergic system affects not only the dopaminergic system, and its sensitivity to drugs of abuse, but also behavioral aspects such as impulsivity and decision-making. These behavioral aspects have been associated with addiction and could play a pivotal role in an individual's vulnerability to the unnaturally large reward that drugs of abuse can offer. A more extensive introduction to this subject and the techniques used in this thesis can be found in the first chapter (**Chapter 1**).

In this thesis, we aimed to investigate the role of mGluR5 in animal models of addiction with the radiotracer ^{18}F-FPEB. To validate results obtained in later experiments we extensively characterized this radiotracer and its quantification (**Chapter 2**). This provided the confirmation that ^{18}F-FPEB is an mGluR5 specific radiotracer, that can be reliably quantified with the cerebellum as reference region. In addition, we evaluated the physiological variation caused by age and gender differences in Wistar rats using ^{18}F-FPEB PET (**Chapter 3**). Although gender differences were found to be not significant, we observed that the mGluR5 availability increased with age. Specifically, brain regions with high densities of mGluR5 in the adult brain showed the largest increases, whereas this was less in regions with low mGluR5 availabilities.

In our first study of addiction, we applied ^{18}F-FPEB PET and ^{1}H-MRS in a cocaine self-administration model (**Chapter 4**). We followed rats for six weeks to obtain measurements before drug-exposure, during two weeks of cocaine self-administration, two weeks of forced withdrawal, and a final week of regained access to mimic relapse. During each phase, rats were scanned weekly with both ^{18}F-FPEB PET and ^{1}H-MRS. In addition, we performed the rodent Iowa Gambling Taks (rIGT) to evaluate decision-

making at baseline. We observed that the mGluR5 availability was decreased when animals had access to cocaine, in both the first self-administration period and the relapse phase. Although this decrease was observed in several regions, including the prefrontal cortex, the most pronounced change occurred in the bilateral hippocampus. ^{1}H-MRS showed a similar trend for the glutamate concentration in the prefrontal cortex. Moreover, glutamate levels at baseline were found to be associated with the amount of cocaine self-administered later in the experiment. This association was also found for the prefrontal glycine concentration, as well as the rIGT score. In conclusion, we observed that cocaine could perturb parts of the glutamatergic system, namely mGluR5 and prefrontal glutamate concentration, but that these changes normalized during withdrawal. Furthermore, prefrontal glutamate and glycine were identified as potentially predictive biomarkers for cocaine use.

To evaluate whether these effects would also be induced by alcohol, we studied an alcohol self-administration experiment **(Chapter 5)**. Due to the different reward profile, this protocol consisted of seven weeks of 24/48 hours self-administration of a 20% v/v alcohol solution, preceded by a week of baseline and followed by a week of withdrawal. ^{18}F-FPEB PET was performed, before and after self-administration, and again showed a decrease in mGluR5 availability in both the hippocampus and striatum. Moreover, the prefrontal glutamate concentrations also showed a similar trend as described above, i.e. a decrease when animals had access to alcohol, which normalized during the week of withdrawal. In contrast to the cocaine experiment, no predictive value was found for the glutamate concentration in the prefrontal cortex. However, such an association was observed for the mGluR5 availability for the bilateral nucleus accumbens. This association was also found for the total distance a rat travelled in the open field test, which was performed at baseline. In conclusion, despite their distinctly different subjective effects, cocaine and alcohol do have a similar influence on specific parts of the glutamatergic system.

To further establish the causal role of mGluR5 in cocaine and alcohol use, we wanted to evaluate whether self-administration could be reduced by decreasing the availability of mGluR5. Therefore, we evaluated the potential of naked siRNA to induce in vivo gene silencing (**Chapter 6**). siRNA was administered via intracranial injection or intranasal

administration. However, both methods did not reliably reduce mGluR5 availability, as evaluated with ^{18}F-FPEB autoradiography. As the mGluR5 has an indirect influence on the neuronal activity, we investigated whether ^{18}FDG PET and resting-state fMRI would identify the same regions that were identified in Chapter 4 and 5 (**Chapter 7**). In this experiment, rats were subjected to the same self-administration protocol used in Chapter 4, but received nicotine as reward. Pattern-recognition algorithms did not achieve high classification accuracies when distinguishing between scans obtained at baseline and self-administration, or baseline and withdrawal, but did assign most weight to the hippocampus and nucleus accumbens. In addition, pattern recognition did detect a significant correlation between the amount of self-administration and an ^{18}FDG pattern, which identified the frontal cortex and striatum as most important regions.

The decrease in the prefrontal glutamate concentration when exposed to both cocaine and alcohol in Chapter 4 and 5 was observed after multiple days of self-administration. To study whether this decrease would also be present immediately after the exposure to these drugs, we conducted a simultaneous PET-MR study (**Chapter 8**). In this study, we applied dynamic ^{1}H-MRS to detect these acute changes in prefrontal glutamate. In addition, we acquired a continuous ^{18}FDG PET scan to assess the influence of the drugs of abuse on the cerebral glucose metabolism rate simultaneously. The included drugs of abuse in this study were alcohol, cocaine and nicotine, which were all injected intravenously. We observed that only cocaine had a significant effect on the cerebral glucose metabolism, but also on the prefrontal glucose and creatine concentration as measured with ^{1}H-MRS. Alcohol also increased creatine and glucose in the prefontal cortex, but also reduced the glutamate concentration transiently directly after the alcohol injection. Previous studies have shown that these acute effects of drugs of abuse do depend on the dosage that is injected. Therefore, future studies exploring this dose response curve would be of interest.

Longitudinal data can be reduced to a single summary statistic. This is common in biomedical sciences, but frowned upon by statisticians as appropriate statistical models exist for these data. In the final chapter, we evaluated whether dynamic PET data would indeed benefit from analysis with the appropriate models (**Chapter 9**). We observed that summary statistics perform well and do not violate any statistical assumptions. An

interesting alternative is the second-level analysis, which is based on the summary statistics, but uses their uncertainty measure to allow for population inference. Therefore, results obtained with this model can be extrapolated to the entire population, rather than being limited to the available sample. Finally, a small gain in power can be achieved with this method, thus potentially allowing easier detection of differences between groups.

In conclusion, this thesis provides information on the effect of drugs of abuse on several aspects of the rat brain. A more detailed discussion of the obtained results and their limitations can be found in the respective chapters or in the general discussion (**Chapter 10**).

Samenvatting

Verslaving is een complexe psychiatrische aandoening die een zware last legt op de gezondheidszorg en economie. De behandelingsmogelijkheden van deze aandoening schieten te kort, wat zich voornamelijk uit in het grote aandeel van patiënten dat hervalt, zelfs na lange periodes van onthouding. Klassiek werd verslaving verklaard met de grote dopamine vrijstelling die verslavende drugs kunnen veroorzaken. Hoewel dit een centrale spil blijft, is er groeiend bewijs dat andere neurotransmitter systemen ook relevant zouden kunnen zijn voor therapieën. In dit licht bestaat er interesse in het glutamaterge systeem en diens controlerende functie. Deze controlerende functie heeft niet alleen invloed op het dopaminerge systeem en diens gevoeligheid voor verslavende drugs, maar ook op bepaalde gedragsaspecten, zoals impulsiviteit en besluitvorming. Deze gedragsaspecten zijn geassocieerd met verslaving en zouden een belangrijke rol kunnen spelen in de gevoeligheid van een individu voor de onnatuurlijk grote beloning die verslavende drugs kunnen zijn. Een meer uitgebreide introductie tot dit onderwerp en de technieken die gebruikt werden in deze thesis vindt men in het eerste hoofdstuk (**Chapter 1**).

Het doel van deze thesis was om de rol van de metabotrope glutmaat receptor type 5 (mGluR5) in diermodellen van verslaving te onderzoek met de radiotracer ^{18}F-FPEB. Om de resultaten die verkregen zouden worden in latere experimenten te valideren werd begonnen met een uitgebreide karakterisatie van deze radiotracer en diens kwantificatie (**Chapter 2**). De resultaten hiervan toonden aan dat ^{18}F-FPEB een mGluR5 specifieke radiotracer is, die met hoge betrouwbaarheid gekwantificeerd kan worden door het cerebellum als referentie regio te gebruiken. Bijkomend werd ook de fysiologische variatie bestudeerd in Wistar ratten van verschillende leeftijd en beide geslachten (**Chapter 3**). Hieruit bleek dat de beschikbaarheid van mGluR5 toenam met de leeftijd, maar niet verschilde naargelang het geslacht. Het effect van leeftijd werd voornamelijk geobserveerd in hersenregio's met een hoge mGluR5 densiteit, terwijl dit effect minder uitgesproken was in regio's met lagere mGluR5 beschikbaarheid.

In de eerste verslavingsstudie van deze thesis werd ^{18}F-FPEB gecombineerd met ^{1}H-MRS voor de opvolging van een cocaïne zelf-toedieningsmodel (**Chapter 4**). Tijdens dit

experiment werden ratten gedurende zes weken opgevolgd, om zo metingen te bekomen voor, tijdens, en na hun blootstelling aan cocaïne. In de laatste week werd een herval nagebootst, waarbij de dieren opnieuw toegang hadden tot cocaïne. Tijdens iedere fase werden ratten wekelijks gescand met zowel ^{18}F-FPEB PET, als ^{1}H-MRS. Bijkomend werd ook de besluitvormingscapaciteit van iedere rat geëvalueerd, voor de blootstelling aan cocaïne, met een gedragstest genaamd *rodent Iowa Gambling Task* (rIGT). ^{18}F-FPEB PET toonde aan dat de mGluR5 beschikbaarheid verminderd was wanneer dieren toegang hadden tot cocaïne, zowel tijdens de eerste zelf-toediening als tijdens de herval-fase. Deze vermindering werd waargenomen in verschillende hersenregio's, waaronder de prefrontale cortex, maar was meest uitgesproken in de bilaterale hippocampus. Een gelijkaardige trend werd gevonden met ^{1}H-MRS voor de glutamaat concentratie in de prefrontale cortex. Bovendien werd aangetoond dat de glutamaat concentratie op baseline geassocieerd was met de hoeveelheid cocaïne die een rat later in het experiment zou zelf toedienen. Dezelfde associatie werd ook gevonden voor de prefrontale concentratie van glycine, als ook voor de rIGT score. Wij konden daarom concluderen dat cocaïne verschillende delen van het glutamaterg systeem kan beïnvloeden, met name mGluR5 en de prefrontale glutmaat concentratie, maar dat deze veranderingen normaliseren bij onthouding. Daarnaast werden de prefrontale concentratie van glutamaat en glycine geïdentificeerd als potentiele voorspellende biomarkers voor cocaïne gebruik.

Om te bestuderen of de hierboven beschreven effecten ook door alcohol geïnduceerd zouden kunnen worden werd een alcohol zelf-toedieningsexperiment uitgevoerd **(Chapter 5)**. Omdat alcohol een ander soort beloning vormt dan cocaïne werd een ander experimenteel protocol gebruikt. In dit nieuwe protocol kregen dieren, na een week baseline metingen, 24 van de 48 uur toegang tot een alcoholoplossing in een drinkfles gedurende zeven weken. Na deze zeven weken bestond opnieuw een onthoudingsfase van een week. ^{18}F-FPEB PET werd voor en na de zelf-toediening uitgevoerd en toonde opnieuw een daling in mGluR5 beschikbaarheid aan in zowel de hippocampus als het striatum. Bovendien vertoonden ook de prefrontale glutamaat spiegels dezelfde trend als hierboven, dat wil zeggen een afname wanneer dieren toegang hadden tot alcohol, dewelke normaliseerde tijdens de onthoudingsfase. De voorspellende waarde van glutamaat concentraties in de prefrontale cortex, zoals hierboven beschreven voor cocaïne, werd niet gevonden in dit experiment. Een gelijkaardige associatie werd echter

wel gevonden voor de mGluR5 beschikbaarheid in de bilaterale nucleus accumbens. Daarnaast werd ook hier een associatie gevonden met een gedragstest die werd uitgevoerd op baseline, namelijk de *Open Field Test*. Het werd geobserveerd dat de totale afstand die ratten aflegden in tien minuten negatief geassocieerd was met hun voorkeur voor alcohol later in het experiment. Als conclusie kan worden gesteld dat cocaïne en alcohol, ondanks de verschillen in subjectieve ervaring, een gelijkaardige invloed hadden op deze specifieke delen van het glutamaterg systeem.

Om de causale rol van mGluR5 in de predispositie van het gebruik van cocaïne en alcohol verder te bevestigen, werd onderzocht of zelf-toediening beïnvloed zou kunnen worden door een verlaging van mGluR5 beschikbaarheid te induceren. Voor deze reden werd het vermogen van naakt *silencing* RNA (siRNA) om de *in vivo* mGluR5 beschikbaarheid te verlagen geëvalueerd (**Chapter 6**). siRNA werd zowel intracranieel als intranasaal toegediend, maar beide methodes waren niet in staat om een betrouwbare daling in mGluR5 beschikbaarheid, bepaald met ^{18}F-FPEB autoradiografie, te bewerkstelligen. Omwille van de indirecte invloed van mGluR5 op neuronale activiteit werd onderzocht of ^{18}F-FDG PET en resting-state fMRI een rol zouden uitwijzen voor dezelfde regio's als diegene geïdentificeerd in hoofdstuk 4 en 5 (**Chapter 7**). In dit experiment werden ratten geplaats in hetzelfde experimentele protocol als gebruikt in hoofdstuk 4, maar ditmaal met nicotine als beloning. Patroonherkenning algoritmes waren niet in staat om met hoge accuraatheid dieren te classificeren in de juist experimentele fase. Een interessante bevinding desalniettemin was dat de verdeling van patroon-gewichten over de verschillende hersenregio's. Deze waren namelijk meest belangrijk in de hippocampus en nucleus accumbens. Daarnaast vond een patroon regressie een significante correlatie tussen de hoeveelheid zelf-toegediende nicotine en een ^{18}FDG patroon, waarin het meeste gewicht werd toegekend aan de frontale cortex en het striatum.

De daling in de prefrontale glutamaat concentratie tijdens blootstelling aan cocaïne en alcohol werd pas na enkele dagen van zelf-toediening gemeten. Om na te gaan of deze afname ook al direct na de blootstelling aanwezig zou zijn, werd een simultane PET-MR studie ingericht (**Chapter 8**). In deze studie werd dynamische ^{1}H-MRS gebruikt om deze acute veranderingen in prefrontaal glutamaat te detecteren. Daarnaast werd simultaan een continue infusie ^{18}FDG scan uitgevoerd om ook het acute effect van deze verslavende

drugs op het cerebraal glucosemetabolisme in te schatten. De drugs die werden gebruikt in deze studie waren alcohol, cocaïne, en nicotine, welke steeds intraveneus werden geïnjecteerd. Enkel cocaïne was instaat om een significante invloed uit te oefenen op het cerebraal glucosemetabolisme, maar daarnaast ook op de prefrontale glucose en creatinine concentratie zoals gemeten met ^{1}H-MRS. Alcohol deed ook creatinine en glucose toenemen in de prefrontale cortex, maar verminderde ook tijdelijk de glutamaat concentratie direct na de alcohol injectie. Eerder studies hebben aangetoond dat acute effect sterk afhankelijk zijn van de dosis waarin verslavende drugs toegediend worden. Derhalve kijken wij uit naar toekomstige studies die de bovengenoemde effecten evalueren op verschillende punten in de dosis-respons relatie.

Longitudinale data kan vaak samengevat worden in een enkel getal of aggregaat. Dit is gebruikelijk in de biomedische wetenschappen, maar wordt afgekeurd door statistici, omdat modellen voor longitudinale data beter presteren. In het laatste hoofdstuk werd geëvalueerd of dynamische PET-data inderdaad voordeel zou kunnen hebben van analyse met de juiste modellen (**Chapter 9**). Er werd aangetoond dat de bovengenoemde aggregaten goed presteren en geen directe overtreding zijn van statistische assumpties. Een interessant alternatief is de zogenaamde *second-level analysis* methode, welke ook gebaseerd is op deze aggregaten, maar de mate van onzekerheid hierover gebruiken om een bredere statische besluitvorming te rechtvaardigen. Dit wil zeggen dat resultaten van deze methode geëxtrapoleerd mogen worden naar de gehele populatie, in plaats van enkel geldig te zijn binnen de onderzochte selectie van die populatie. Een laatste voordeel is de kleine winst in *power* die bereikt kan worden met deze methode, waardoor verschillen tussen groepen makkelijker gedetecteerd kunnen worden.

Samenvattend draagt deze thesis informatie bij over het effect van verslavende drugs op verschillende aspecten van de hersenen van de rat. De bekomen resultaten en de beperkingen hiervan worden meer uitgebreid besproken in de respectievelijk hoofdstukken en in de algemene discussie (**Chapter 10**).

Chapter 1: Introduction

1.1 Addiction

Addiction is defined by Merriam-Webster as the compulsive need for, and use of, a habit-forming substance, characterized by tolerance and well-defined physiological symptoms upon withdrawal. To its own definition it adds: "*broadly*: persistent compulsive use of a substance known by the user to be harmful" (Merriam-Webster.com 2011). A few interesting aspects in this definition can be highlighted. For example, the requirement that one should use this substance to be addicted, implying that withdrawal would also end one's addictive state. Also, the strict ruling that addiction applies only to substances is debatable in our current understanding of this word (Holden 2010). Another interesting aspect of this definition is the requirement that the "user" is aware of the substance's harmfulness. This definition makes us wonder what state one would be in, when compulsively using this substance unaware of its potential harmful nature, as might have been the case after the introduction of alcohol to native Americans (Beauvais 1998). Additionally, this definition implies that we cannot be addicted to substances that are not harmful to the user. This rapidly becomes an almost philosophical discussion, since the negative effect of most substances are subject to the law "Sola dosis facit venenum" (Latin: the dose makes the poison, meaning: a dangerous poison can be harmless or even beneficial in low doses, whereas substances not considered to be toxic can become so in extreme dosages, e.g. water (Rowntree 1926)). Finally, we might wonder about the "well-defined physiological symptoms" that withdrawal would be able to elicit. This is in direct contradiction with the current lack of objective addiction measures, which complicate the treatment and diagnosis of addicted patients (Garrison and Potenza 2014).

Despite this debatable definition and the often naïve intuition of what addiction means, it is a complex, multi-faceted phenomenon, which is reflected in its professional definition in the DSM V (Buchman, Skinner, and Illes 2010; Barry et al. 2014; American Psychiatric Association 2013). This complexity is partly why addiction is still an important socio-economic issue, which influences the lives of a significant portion of

almost any nation or culture. Moreover, this complexity is the most important reason why modern medicine and its practitioners are not able to aid every individual sufficiently (Koob and Mason 2016).

This manuscript bundles findings from different preclinical experiments, which aimed to contribute to our understanding of this pathology, as advanced understanding might help us with the guidance and treatment of individuals influenced by addiction. After the introduction of the current knowledge of addiction, including available animal models, we introduce the focus of this work, as well as a brief introduction to the techniques that were used. After this general introduction, the details of every experiment, including the obtained results and their interpretation are presented, followed by a general discussion.

1.2 Drugs of abuse and addiction

The American National Institute on Drug Abuse defines drugs of abuse as drugs people use to change the way they feel. This can be either illegal drugs, or drugs exclusively for adults, such as alcohol and cigarettes. In general the motivation to take drugs can be based on three kinds of motivation: to feel good, to feel better or to perform better (National Institute for Drug Abuse 2007). Some drugs can be used for each of these motivations, such as cocaine, whereas other typically are more restricted, such as alcohol. Over thirty groups of drugs are commonly abused. Legal drugs include non-medical use of prescription drugs, such as opioids, but also commercially available products, like paint thinners (National Institute for Drug Abuse 2017). Among the most common drugs are nicotine, alcohol, and cocaine, which have been used in this work and will thus be discussed in more detail.

Nicotine use has decreased over the last years, but is still considered as one on the most important health problems worldwide. This is mainly due to its addictive nature, as about 70% of smokers would like to quit, of which 40% does so for at least one day, but only 3% achieves an abstinence longer than one year (Benowitz 2010b). The primary binding site of nicotine are the nicotinic cholinergic receptors in the VTA, which physiologically bind acetylcholine. Upon binding of nicotine, these receptors open a channel through which calcium can enter the cell. The influx of cations causes other, voltage-dependent,

calcium-channels to open, which leads to an increased neurotransmitter release (Dajas-Bailador and Wonnacott 2004). This release occurs predominantly in the prefrontal cortex, striatum, and mesolimbic area, and consists mostly of dopamine. Other neurotransmitters that are released by nicotine binding are both glutamate, facilitating excitation and thus more dopamine release, and GABA, with the opposite effect. However, chronic exposure desensitizes those receptors that triggered GABA release, thus making an individual more sensitive to reward (Kenny and Markou 2006). An additional mechanism contributing to nicotine's addictive nature is the inhibition of the monoamine oxidase A and B, which normally catalyse the metabolism of several neurotransmitters, including dopamine (Hollander et al. 2008).

Alcohol has a complex neuropharmacological profile to such an extent that it was long thought to be a non-specific agent (Vengeliene et al. 2008). However, recently primary binding sites have been recognized as the primary targets. These include the NMDA receptor, which is inhibited by alcohol exposure. This inhibition was shown to be related to the neural and cognitive impairment of alcohol intoxication (Peoples et al. 1997). Other identified targets are the $GABA_A$ and glycine receptors, as well as serotoninergic and nicotinic ACh receptors (Mihic 1999; Narahashi et al. 1999; Lovinger 1999). All these receptors are made up of different sub-units, and can consist of different combinations hereof. Which combination of sub-units is used can have an influence on the affinity and effect of alcohol, making its neurobiology, and potential treatment development, exponentially complex. In addition to these receptors, alcohol also exerts an influence on two types of ion-channels, a Ca^{2+} and a K^+ channel, able to influence neurons in both an excitatory and inhibitory way. In general however, the most important effect of alcohol is attributed to the inhibition of the NMDA receptor and activation of the inhibitory GABAergic system (Vengeliene et al. 2008). It is not surprising therefore, that alcohol exerts a depressing influence on the brain and behaviour in general. This aligns with the general motivation of chronic alcohol abusers, which is typically to drown anxiety, stress and pain. In effect, despite the initial use for euphoria, alcohol increasingly becomes a negative reinforcing drug, i.e. it is indirectly rewarding by relieving negative aspects in a patients subjective state (Koob 2013). This is in contrast with stimulants, like cocaine, which are generally taken as a positive reinforcer, due to their capability to induce an instant pleasurable state. This also has profound implications on the

implementation and interpretation of animal models. Where positive reinforcers can mimic the human situation, as they are taken for the similar reasons, the interpretation of self-administration of negative reinforcers is more complex. In effect, animals are unlikely to experience the above mentioned stressors to a level that requires pharmacological alleviation. Furthermore, it is likely that rodents, who have a high environmental alertness in anticipation to potential confrontation with predators, avoid intoxicated states with decreased mobility and cognitive ability.

The effect of cocaine on global health is significantly smaller than that of alcohol or nicotine. However, a hallmark of cocaine addiction is the high rate of relapse after detoxification (O'Brien 1997). Cocaine is an alkaloid, which binds to the transporters of several neurotransmitters, such as serotonin and dopamine (Ritz, Cone, and Kuhar 1990). This prevents their reuptake in to the neurons, which continue to fire at their regular rate, thus creating a sharp increase in synaptic neurotransmitter concentrations. In addition to its influence on the dopaminergic system, cocaine has also been reported to have an extensive indirect influence on almost every part of the glutamatergic system (Schmidt and Pierce 2010). The most important influence is on the limbic, glutamatergic neurotransmission, including the nucleus accumbens, which produces persistent changes in neuronal functioning and the consequent effects of cocaine on behaviour (Gass and Olive 2008). An excellent review of the current knowledge of these changes in detail can be found in (Schmidt and Pierce 2010).

1.3 Addiction and the reward system

Simple organisms can rely on non-selective feeding (Moore 2008). For example, mussels pump water through a biological filter, which extracts nutrients needed for their growth and maintenance. However, for most organisms this way of feeding does not supply sufficient energy and nutrients. This is particularly the case in environments with a high spatial heterogeneity of these nutrients. For example, a bumblebee might only have to visit a dozen flowers to collect a sufficient amount of nectar, but if it would randomly fly through our world, the chances of landing on twelve flowers in a day would be astronomically small (Moller 1995). Therefore, individuals, be it bumblebees or humans,

that were able to make the distinction between nutrient-rich and nutrient-poor sources performed better in the evolution towards the fittest (Barron, Sovik, and Cornish 2010). In effect, a vast majority of the members of the animal kingdom have evolved to a form where this distinction was possible, such as moths and bumblebees (Cunningham 2004). However, making the distinction alone would not result in an evolutionary advantage, instead individuals more motivated to pursue these identified sources of nutrition would have the upper hand. This is where the reward system finds it origin: a neuronal circuit using motivation through pleasure to order an organism's behaviour (Aunger and Curtis 2013). In other words, animals born with the right triggers of the reward system would be motivated to show behaviour that increased their fitness. Although the focus might have been primarily toward food, other behaviours could be motivated with the same system. Indeed, a male fish or bird constructing an elaborate nest does so, because this triggers a pleasurable feeling (Hall, Healy, and Meddle 2015). Most activations of the reward system that we experience are recorded by our memory (Adcock et al. 2006). This record is used later to motivate our behaviour towards a similar outcome. For example, the first red apple that our ancestor found will have been eaten with suspicion. However, the ingested nutrients would have activated his reward system, and a memory would be established about the link between a red apple and this pleasurable feeling. Setting up the system in this way allowed for a flexible imprinting of the reward system. Rather than evolutionary programming all favourable foods into the genetic code, organisms could adapt to new situations, such as new territories or seasons. Furthermore, since the reward system responds proportional to the value of stimuli, organisms could use their memories to decide which opportunity to pursue. In most natural environments, this combination of learning and reward lead to a major increase in fitness, as it provided a balance between self-preservation and procreation. These natural environments however, also consisted of competitive participants (Kunstler et al. 2016). For example, a berry carrying plant would be able to grow faster than other plants in certain parts of a forest, but be outgrown itself in the majority of all places. This competition limited the supply of berries, as it did for almost any source of nutrients, be it flowers, plants or prey. Moreover, this competitive environment entailed considerable uncertainty about the availability of nutrient sources in the future. In effect, food could be found by competitors, be taken or get spoiled. Therefore, greatest fitness could be achieved by consuming any available

nutrient without delay (van den Bos and de Ridder 2006). The reward system evolved therefore in such a way that consuming more resulted in an increased reward experience.

This remains the status quo in most animals, for example obesity only occurs in domesticated dogs and can be fully explained by the amount of food made available by its owners (Bland et al. 2009). Our ancestors however, underwent further brain development, which allowed for a more rational assessment of these acute supply situations (Coolidge and Wynn 2001). Although rationally the answer could still be to consume everything at once, it opened the door towards long-term reward consideration. Long-term vision, or reward delay, was the most important step towards our modern society, as it significantly influenced our behaviour (Coolidge and Wynn 2009). In effect, inhibiting our direct consumption drive led to early forms of agriculture, reserves and trading. An individual could choose not to opt for the certain direct reward, but go for a calculated long-term reward. The outcome of this calculation depended on several factors, but two primarily. Firstly, the consequences of either action, consume or store, and their probability. Secondly, the magnitude of the direct reward is negatively associated with the delay discount. Delay discounting implies that the value of a reward declines with increasing delay (Johnson and Bickel 2002). In other words, receiving 100 dollars now might feel the same as receiving 125 dollars next month, but is likely to be a more pleasurable feeling than the knowledge of receiving the same 100 dollars next month. A similar phenomenon exists for the negative consequences, e.g. the minutes of life lost per cigarette lose a substantial part of their impact on the decision-making process, as they are only long-term negative effects (Weinstein, Marcus, and Moser 2005).

When an individual is confronted with natural nutrients sources only, such as agricultural products and meat, the measure of reward delay can reach an objective optimum for the average of the population (Kelley and Berridge 2002). This is likely the result of centuries of evolution in an environment with relatively stable reward intensities. Still, as with any biological parameter, variation will exist between individuals in their reward-consequence calculation. Extremes in this variation can indeed provide an increased fitness compared to peers in certain situations. For example, an individual who shifts substantially more of his resources into reserves might survive a harsh winter, but he may also be the first to perish when forced into a physically intensive migration. In our modern

society however, we are able to create or obtain reward intensities that surpass the natural rewards for which our reward system has been optimized, e.g. high-sugar and high-fat products, such as coke and fries (Schulte et al. 2015). As discussed above, reward discounting increases with reward value. This means that a larger part of the population will tend to make choices with, objectively, suboptimal outcomes. In effect, problems like the obesity pandemic find their roots for a large part through this mechanism (Stice et al. 2013).

An interesting and very complex aspect of this decision-making behaviour, are the contributing factors used for these semi-rational choices. A good example is cigarette smoking. Originally, smoking was not considered harmful to one's health, and except for its cost, few downsides could be found to this rewarding habit. This led to massive use of nicotine in the beginning of the last century (Peto et al. 1996). Besides the unknown harmful effects, this widespread use and/or addiction was potentially possible because of the relatively low rewarding effect of nicotine. That is, although pleasurable, the majority of users will not engage in criminal activities to obtain nicotine. Due to this weaker rewarding character, the use of nicotine was also possible to halt through non-coercive measures. The information about harmful effects brought many smokers to, at least try to, quit. In combination with education (particularly effective before the onset of a smoking habit), financial and logistic discouragement, most western societies have been able to reduce the number of nicotine users more than fifteen percent (Ng et al. 2014). This success story is in stark contrast with the failure of the prohibition in the United States, in which alcohol was banned to halt the widespread alcoholism, family violence and corruption (Figure 1) (Tyrell 1997). A probable reason for this failure, is that alcohol is a more addictive drug than nicotine, particularly with a more intense withdrawal (Carlson et al. 2012). The main reason however, may have been the individual's unwillingness to stop alcohol consumption.



Figure 1. The drunkards progress by Nathaniel Currier, 1846. Step 1: A glass with a friend, Step 2: a glass to keep the cold out, Step 3: A glass too much, Step 4: Drunk and riotous, Step 5: The summit attained. Jolly companions. A confirmed drunkard, Step 5: Poverty and disease, Step 6: Forsaken by friends, Step 7: Desperation and crime, Step 8: Death by suicide.

Interestingly, the desire to stop is now one of the criteria used to diagnose addiction, as is the continuance despite negative consequences (American Psychiatric Association 2013). These two criteria outline a familiar, but tragic state, in which the addicted patient realises the negative consequences, which are reflected in his desire to quit, but is not able to forsake his habit. From a scientific point of view, this is an interesting development as it suggests that primal systems can overrule rational reasoning (Sanfey et al. 2006). This represents the current view of addiction, as a brain disease or psychiatric disorder and has therefore be named the "medical model" (Volkow and Li 2004). According to this model, addiction should be considered as a compulsion beyond the addict's control (Wilbanks, 1989). This is a large contradiction with the older models of addiction that have been proposed: the moral model considered addiction to be a choice. It was thought that an individual could choose to stop his addiction at any point, but

choose not to. A third model, the "learning model", finds it place somewhere between these two, as it poses that every person has an individual choice space, which is delimited by previous experiences. Therefore, it can be harder for one individual than for the other, but both ultimately make their own choice (Acker 1993). Although most addiction medicine professionals currently agree to a large extent with the medical model, interesting literature points out that a strict reading of this model has far-reaching consequences (Hall, Carter, and Forlini 2015). In effect, an addicted individual, who commits a crime related to his addiction, should not be held responsible for his actions in a criminal court according to the definition of this model. For example, it could be argued that robbing for money or driving under the influence are symptoms rather than choices and should not receive the same punishment as a not-addicted individual would receive (Wexler 1981).

1.4 Neurobiology of addiction

The motivation of an organism to pursue rewarding actions has been associated with the dopaminergic system (Arias-Carrion et al. 2010). Despite dopaminergic neurons comprising less than one percent of the total number of neurons in the brain (Arias-Carrion and Poppel 2007), they have been studied in great detail. The dopaminergic neurons in this system are heterogeneously distributed throughout the brain and have been classified into three major pathways, although this distinction is functionally not entirely clear (Figure 2). The mesolimbic pathway consists of neurons in the ventral tegmental area (VTA) that project towards nucleus accumbens, and also innervates the amygdala and hippocampus. Whereas the mesocortical pathway also starts in the VTA, but extends to the prefrontal, cingulate and perirhinal cortex. Due to their overlap and common role in emotion-related behavior, they are often collectively referred to as the mesocorticolimbic system (Phillips, Vacca, and Ahn 2008; Wise 2005). The shortest dopaminergic projection pathway, the nigrostriatal system, connects the substantia nigra pars compacta with the caudate-putamen nucleus, and plays an important role in voluntary movement (Smith and Villalba 2008). The caudate-putamen is one of the brain regions that differ in nomenclature between rats and humans. As the distinction between these regions is not clear in rats, often times it has been addressed as striatum, which is

also the nomenclature we will use in this manuscript. Another region where the neuroanatomy of humans and rats is not directly translatable is the prefrontal cortex. Although it has been established that rats do have a prefrontal cortex, the division into sub-regions and their functional implications is not without discussion (Ongur and Price 2000).

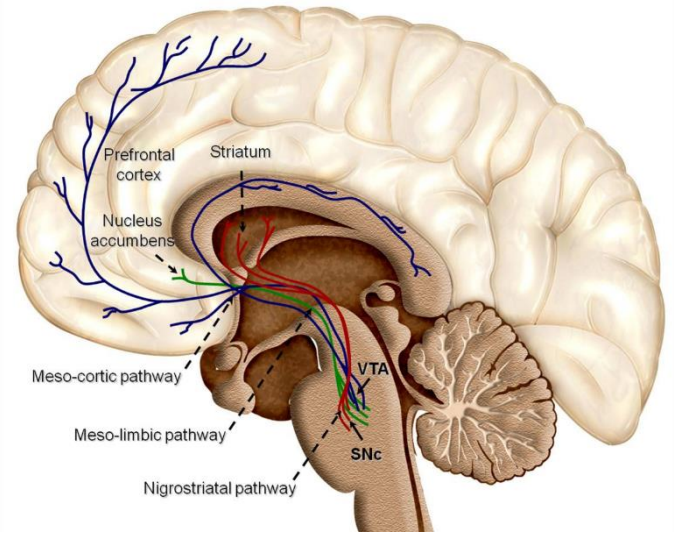


Figure 2. Overview of reward structures in the human brain (Arias-Carrion et al. 2010).

Imbalances in the dopaminergic system have been associated with a multitude of disorders not related with reward. Two examples of such disorders are movement disorders and schizophrenia (Tremblay et al. 2015). Dopamine itself is biosynthesized from tyrosine, via L-Dopa, by neuronal aromatic amino acid decarboxylase (Elsworth and Roth 1997). After its synthesis, dopamine is stored in specialized storage vesicles with 10 – 1000 times higher concentrations than in the cytosol. Whenever an action potential induces a calcium influx in the terminal region of a neuron, the vesicles fuse with the cell membrane. An integral part of the dopaminergic signalling pathway are the dopamine transporters, which invariably exist in dopaminergic nerve terminals. These transporters actively pump dopamine back into the pre-synaptic nerve terminal, thus modifying the extent and duration of the dopamine release. An interesting extra element of this system are the autoreceptors (Roth 2006). By definition, these receptors are influenced by the neurotransmitter released by the neuron on which the receptor is located. These dopaminergic autoreceptors are particularly interesting as they provide

input to the negative-feedback loop, which decreases the firing-rate of dopaminergic neurons, but also decreases the release and synthesis of dopamine.

This aligns with the reduced dopamine levels that have been observed in rats chronically exposed to cocaine (Rossetti, Hmaidan, and Gessa 1992). Substantially lowered dopamine levels can cause depression or a state called anhedonia (Dailly et al. 2004; Wise 2008). Anhedonia is used to describe a state in which an individual has become relatively insensitive to rewards and has been robustly linked to patients withdrawing from a drug addiction (Wise 2008; Wang et al. 2004). Since drugs of abuse can elicit dopamine release that is much greater than induced by natural reward, the negative-feedback loop goes in overdrive (National Institute for Drug Abuse 2007). This means that natural rewards will not be able to induce a dopamine level experienced by the patient as pleasurable. In effect, patients in full withdrawal often describe their anhedonic state as "living in a gray world". In their eyes, there is no behaviour possible that will results in a noticeable reward, except for re-engaging in drug use. Although somewhat oversimplified, this is now considered a major motivation for relapse (Janiri et al. 2005). A positive side however, is that this negative feedback system of dopaminergic autoreceptors will decrease their inhibitory effect in the absence of these massive dopamine release elicited by drug-use. Therefore, prolonged abstinence can typically restore the sensitivity of the dopaminergic system to a normal level (Figure 3) (National Institute for Drug Abuse 2007).

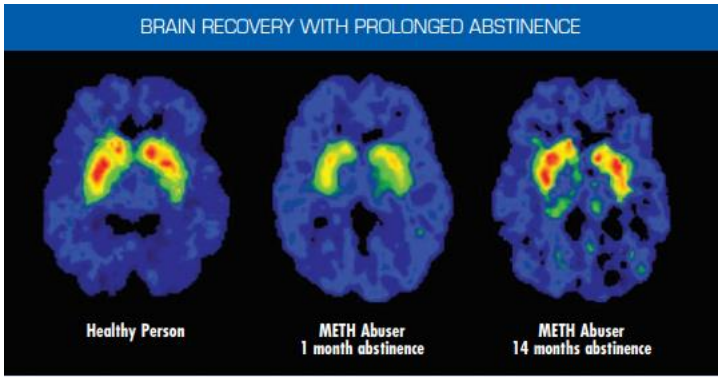


Figure 3. Density of dopamine transporter in the striatum during short and prolonged methamphetamine withdrawal. Note that the number of dopamine transporters becomes higher with longer abstinence, towards the level of a healthy individual (National Institute for Drug Abuse 2007).

Kumar et al. 2013; Parsons and Hurd 2015). For example, serotonergic neurotransmission changes after acute drug exposure and in addicted patients (Muller and Homberg 2015). Potentially the most investigated neurotransmitter system besides the dopaminergic system in this context is the glutamatergic system (Tzschentke and Schmidt 2003). This is mainly based on both clinical and preclinical evidence that chronic exposure to drugs of abuse imbalances the glutamatergic system (Kalivas 2009). A consequent hypothesis was that the glutamatergic system is involved in processing the effect of drugs of abuse on the dopaminergic system. In other words, individuals that experience a similar rewarding effect and equally large dopamine releases do not necessarily respond to these drugs in the same way in the long term. The interplay of these neurotransmitters system can be understood when looking at a specific limbic circuit. Specific limbic structures, such as the hippocampus, amygdala, and prefrontal cortex send glutamatergic projections to the nucleus accumbens (Meredith et al. 2008). The nucleus accumbens, in turn, sends inhibitory GABAergic neurons to the ventral pallidum and VTA (Groenewegen et al. 2006). Both these regions are the start of new GABAergic connections running towards the thalamus (Groenewegen 2003). The circuit is completed by the glutamatergic input to the prefrontal cortex originating from the thalamus (Heimer 2003). This demonstrates the complex, multi-system fine-tuning of the dopaminergic reward system.

1.5 mGluR5 and addiction

The glutamatergic system is extensive and comprises several receptor types. These receptors can be classified into ionotropic and metabotropic receptors. Ionotropic receptors are defined as ion-channel coupled receptors, whereas metabotropic receptors are coupled to 1,4,5-triphosphate turnover, which is mediated by G protein (Tsai, Gastfriend, and Coyle 1995). The most abundant glutamatergic ionotropic receptor is the N-methyl-D-aspartate (NMDA) receptor, which is the main excitatory receptor in the mammalian brain present in virtually every brain region (Zeiler 2015). An interesting aspect of the NMDA receptors is that a co-factor is required to induce the activation. In physiological conditions, it is glycine that acts as the co-agonist, however, as described below, alcohol can compete for this binding location (Buller et al. 1996). The metabotropic class of receptors also contains three groups of receptors: group I receptors

include the metabotropic glutamate receptor (mGluR) 1 and 5, group II receptors contain mGluR2/3, whereas group III consists of mGluR 4, 6, 7, and 8. Although the relevance to addiction of multiple receptors has been studied, most research has been done on mGluR2/3 and mGluR5 (Figure 4) (Moussawi and Kalivas 2010).

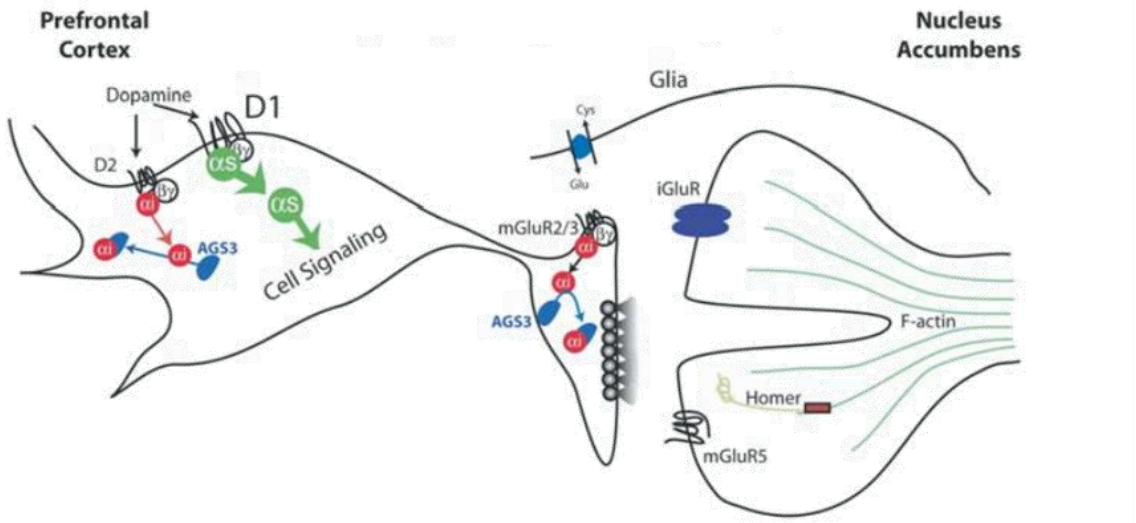


Figure 4. Schematic overview of the interplay between the dopaminergic and glutamatergic system between the prefrontal cortex and nucleus accumbens (Kalivas, Volkow, and Seamans 2005).

The metabotropic glutamate receptor 5 is a G-coupled protein receptor, which is expressed predominantly on the post-synaptic neurons. Upon activation by glutamate, a conformation change occurs that activates G_q protein signalling, thus activating phospholipase C (PLC). This enzyme can, through hydrolysis of phosphatidylinositol-4,5-biphosphate (PIP_2) induce the release of 1,2-diacylglycerol (DAG) and inositol triphosphate (IP_3). The former activates protein kinase C (PKC), which plays an important role in a range of signalling cascades. IP_3 on the other hand induces endoplasmic calcium release, generating complex Ca^{2+} concentration-dependent signals, such oscillations and wave propagations (Figure 5) (Piers et al. 2012). A specific example of the effect of mGluR5 activation is the inhibition of the dopamine transporter, which could be prevented by addition of selective PKC inhibitors (Page et al. 2001).

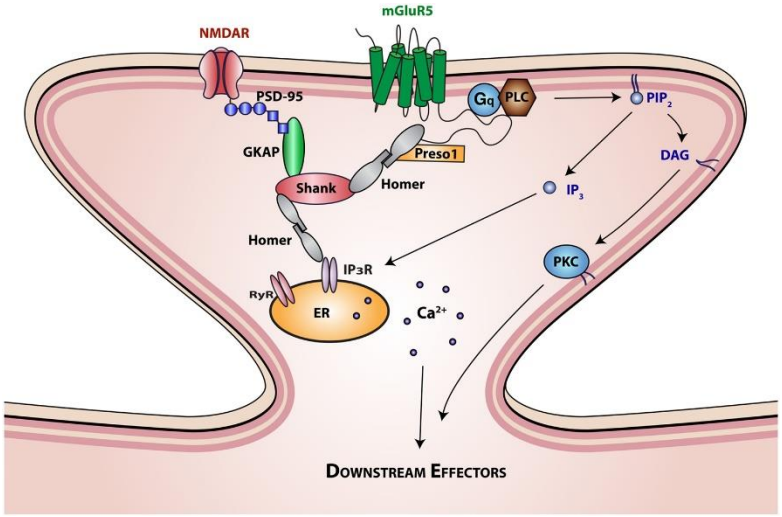


Figure 5. Intra-cellular pathway of mGluR5 induced effects (Piers et al. 2012).

The metabotropic class of glutamate receptors were discovered almost thirty years ago and linked to addiction not long after (Ishida et al. 1990). A particularly interesting finding came in 2001, when it was shown that mGluR5 knock-out mice did not show increased locomotor activity after a cocaine injection, despite having a similar dopamine release in the nucleus accumbens (Figure 6) (Chiamulera et al. 2001). This relation was confirmed with numerous pharmacological studies, particularly involving negative allosteric modulators, such as MPEP or MTEP (Backstrom et al. 2004; Hodge et al. 2006; McGeehan and Olive 2003; Paterson et al. 2003; Brown et al. 2012). These compounds were observed to influence self-administration behaviour and drug-memory formation in different stages and for different drugs (Nickols et al. 2016). However, both clinical and preclinical studies suggested that mGluR5 NAM blockade can induce adverse effects, including cognitive and memory impairments, and psychotomimetic effects (Abou Farha, Bruggeman, and Balje-Volkers 2014; Campbell et al. 2004). This prompted two research lines: a pharmacological search for partial mGluR5 blockers, with potentially lower levels of side-effects, and studies into the physiology of mGluR5 and its pathophysiological role in specific disorders (Nickols et al. 2016; Elmenhorst et al. 2016). An important role in the latter is reserved for neuroimaging, which is able to non-invasively characterize the differential expression of receptors in the presence of a suitable imaging probe and will be discussed below.

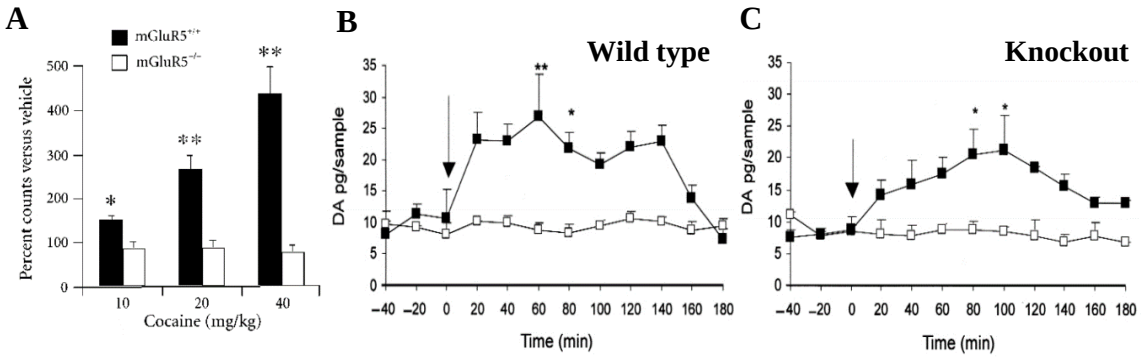


Figure 6. **A**) Locomotor activity after cocaine injection in both wild-type and mGluR5 knock-out mice, and the dopamine release in the nucleus accumbens for the respective groups (**B** and **C**) (Chiamulera et al. 2001).

1.6 Animal models of addiction

Animal models have several advantages that make them a central tool in biomedical research. These advantages include possibility of performing *ex vivo* techniques, such as histology, but also allow pharmacological or neurosurgical interventions, that have not yet been approved for human application. Furthermore, genetic modifications can be created either at birth or during the animal's life. The most important downside of animal experiments are questions of their translational validity. Although, this translational value can vary immensely between different models and different diseases, e.g. neoplastic models, in which cultured cancer cells are injected to simulate spontaneous tumours are notoriously oversimplifications of the real world situation (Gould, Junttila, and de Sauvage 2015). This oversimplification is thought to be, among many other factors, one of the reasons that new treatment targets identified in animal models have led to disappointing results in clinical trials. This poor performance of preclinical findings is particularly true for psychiatric diseases, in which medication developed in preclinical models have clinical efficacy in only less than ten percent of cases (Kaiser and Feng 2015). Intuitively, this can be understood as many psychiatric diseases manifest themselves in subjective ways, which are verbally communicated by the patient. For example, hallucinations or the sense of impending doom are clinically diagnostic tools that cannot be evaluated in animal models (Mayr and Schmid 2010). Therefore, surrogate markers have been proposed to evaluate aspects of an animal's behaviour, thought to

reflect these more subjective symptoms. However, it can be difficult to assess whether these surrogate markers are oversimplifications of the clinical situation, e.g. does the time a mouse hangs from a bar fully reflect the state of mind of the depressed patient (Hellwig et al. 2016)?

Animal models in addiction have a substantial benefit over many other psychiatric diseases, as they rely on a very similar reward system as present in humans. However, actual addiction is again difficult to objectively achieve or diagnose. Several criteria have been proposed that show indications of substantial use, compulsive drug-taking, and continuance despite negative consequences (Deroche-Gamonet, Belin, and Piazza 2004). The latter for example, is assessed by animal's having to withstand an electrical shock when earning a drug reward. This method does divide the entire population in two groups: those willing to endure the electrical shock, and those not motivated enough by the drug to do so. The distribution over these two groups will shift with increasing shock-intensity, thus reflecting motivation to obtain the drug. Whether this constitutes drug addiction in the same sense as in the addicted patient who faces health risks or commits crimes to support his habit remains debatable. Equally debatable however, is the notion that addiction is a categorical diagnosis, rather than a continuous multi-dimensional spectrum (Helzer, Van den Brink, and Guth 2006). Indeed, an individual might not make the required number of DSM-VI criteria to be diagnosed as an addict, but still show behaviour that places him closer toward the diagnosis than a non-drinking individual. Considering addiction as a dimensional disorder, brings us to one of the main advantages of animal models in addiction: the possibility to record variation in baseline values of specific biomarkers. In practice, addicted patients are typically only enrolled in scientific studies at the summit of their addiction. In other words, specific relevant baseline measurements are not present for the addicted patient seeking help to end his habit. Measurements taken at this moment can be compared to an abstinent state, and thus provide information about the neurobiological changes elicit by this change. However, it is unknown whether all biomarkers normalize after drug-use is stopped, particularly since individual baselines do show variation. Therefore, with these data it is not possible to identify those biomarkers that indicate a larger vulnerability, or motivation for, drugs-of-abuse. Identification of these biomarkers would of be great interest however, as they might shed new light on the complex pathophysiology of addiction.

Animal models of addiction can be classified into two large groups: forced and voluntary exposure. In the first group, the researcher forces animals to be in contact with the drug under investigation. For example, through intraperitoneal injections or providing drug solutions as the only liquid source (Ding et al. 2016). Although it is likely that some animals will experience a rewarding sensation by these exposures, and even enter an addictive state, a certain proportion of the population will not. To link observed changes to addiction is therefore, a difficult and ambiguous task, as only exposure to the drug can be verified. The other group of animal models allow animals to choose the moment and quantity of their intake. For example, drug rewards can be earned by pushing a lever or multiple drinking bottles are presented containing both solution with and without alcohol (Gardner 2000). Within this class of voluntary exposure models, an important distinction can be made by the way the drug is administered to the animal. The three most-used methods are either oral consumption, vaporization or intra-venous administration. Oral consumption has the benefit of being closest to natural exposure. However, two main disadvantages can play, to a certain extent, a role. Firstly, most drugs are not palatable to rats, e.g. alcohol solutions are typically disliked by both rats and people. Therefore, extensive schedules have been used to make alcohol solutions more palatable by adding a sweetener, such as sucrose, or by only intermittently providing the alcohol solution (Simms et al. 2008). The former complicates however, the interpretation of the solution intake, as sucrose itself can also provide both caloric value and salience. The second potential downside of oral consumption is the lack of control over the actual consumption. On the one hand, this can be the case for liquids that are dispensed or presented in bottles, as they can evaporate, leak or wet other parts of the animal. On the other hand, there is a latency between when an oral reward is earned and when it is actually consumed. For example, a pile of sugar pellets can sometimes be found in receptacles of animals that responded well during their task, but did not consume (all of) their rewards. Several systems to counteract this have been applied, such as the infrared beams, which are breached when an animal accesses the receptacle. However, these systems can still err in several situations, which are not discussed here.

Vaporization typically provides a robust uptake, although respiratory frequency can have an influence, but is an unnatural way of uptake which can be experienced as stressful by

the animal (Rogers, Wiener, and Bloom 1979). Intravenous models also come with a downside, i.e. the need for the surgical implementation of a permanent IV catheter. Their obvious benefit though, is that the experimenter has full control of the administered drug quantity, and has exact information about its timing.

The surgical implantation of the IV catheter is a relatively complex microsurgery, particularly due to the permanent placement, which opens up the possibility of many long-term complications, such as infection or obstruction. Particularly, the latter has been an important issue, as up to twenty per cent of animals were lost during some experiments. Counter-measures to prevent obstruction, mostly caused by blood-clots, included daily flushing and filling the catheter with 'locking solutions' (Schober et al. 2013). These solutions consist of a viscous polyvinylpyrrolidone-heparin mixture, which remains inside the catheter and prevent blood from entering and clotting inside the catheter. However, aspiration of this stopping solution could be problematic, whereas its injection has been shown to have biological effect, despite its alleged inertia, such a nephritis (Fonseca et al. 2010). Another complication, albeit short-term in the majority of cases, was the result of placement of the catheter in the v. jugularis up into the right atrium. Misplacement, movement during the surgery, or animal movement could therefore irritate the atrial wall and cause arrhythmias or fibrillation with acute death as a result.

In this work, we used a new generation of IV catheters that was developed by a collaboration of Janssen pharmaceutica and Instech. We particularly acknowledge Greet Teuns, Scientific Director Toxicology at Janssen pharmaceutical research & development, who has shared not only this information, but also provided a hands-on demonstration of the implantation technique. In an extensive experiment by Janssen pharmaceuticals, several catheters were compared for their ease of implementation and particularly the long-term patency. The latter increased from ~75% to 100% with this newly developed catheter. This new design had three major improvement points. Firstly, a high quality anti-coagulant silicon tubing system for insertion into the vein. Additionally, this tubing had a decreased diameter, which prohibited aspiration of blood, but also prevented blood clot formation without a stopping solution. Secondly, a longer tube was used that ran from the dorsal access point between the shoulder blades to the

femoral vein, rather than the jugular vein. This tube was inserted into the femoral vein, but fed up to a pre-determined distance, that placed the tip of the catheter in the v. cava caudalis at the height of the kidneys. As the v. cava. caudalis at this point is the largest vein in the body, a slower blood velocity is encountered, thus reducing the risk for blood clot formation. Furthermore, the long insertion prevented the catheter from coming out of the vein when the animal moved, something which happened regularly with the atrial placement due to its short insertion length of 3 cm. A final improvement was the addition of a surgical mesh around the base of the catheter. This allowed for stable subcutaneous incorporation, and due to its softness at body-temperature was experienced as less painful and irritating by the animals. A downside of this catheter model was the 1 cm inguinal incision required for its placement. Earlier models required a surgical incision in the throat region, which cannot be visually inspected by the animal. This is not the case for the inguinal region, which therefore requires suture placement with a decent technique.

1.7 Neuroimaging of addiction

Some of the most valuable information in addiction science has come from neuroimaging studies. This is particularly true for data obtained from patients, as neuroimaging can provide a unique window of non-invasive functional biomarkers, thus allowing longitudinal studies of the same subject. Two modalities have provided most information in this field, and in clinical neuroimaging in general, namely magnetic resonance imaging (MRI) and positron emission tomography (PET). Where PET has the flexibility, and limitation, of being able to study whatever radiotracer is available, MRI has been developed beyond the initial imaging techniques into a vast array of applications. These sequences provide the opportunity to use the same machine for different applications, such as structural images, perfusion measurements, blood vessel visualization and metabolite concentration determination. Below a short introduction is given for both modalities and the specific applications that were used for the experiments in this thesis.

1.7.1 Principles of PET imaging

Positron Emission Tomography (PET) is an imaging modality, which can be used to visualize radioactive isotopes called β-ray emitters. These unstable isotopes, often

containing one proton more than the stable natural species can decay by emitting a positron, the anti-particle of an electron. An example is the decay of ^{18}F:

$$^{18}_{9}F \rightarrow {}^{18}_{8}O + e^{+} + \nu_e$$

where the decay results in oxygen, a positron (e^+) and a neutrino (ν_e). However, fluorine-18 is not the only β-emitter that is used for PET imaging, others include ^{11}C, ^{15}O, ^{68}Ga and ^{124}I. These different isotopes each have their own characteristics, such as decay rate and branching ratios. Suitable radiotracers for PET imaging would need a short half-time, i.e. the time in which half of the isotopes decay, and high branching ratio, i.e. high probability of decaying through the beta-decay process rather than other forms of decay. The positron, upon emission, travels a short distance before annihilating with an electron of the surrounding matter. The length of this distance travelled depends on the kinetic energy of the positron, and on the abundance of electrons in the surrounding matter. After this annihilation, a short-lived positronium comes into existence, that rapidly annihilates into two or more photons (Figure 7).

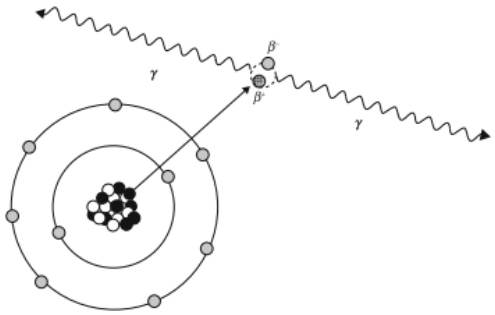


Figure 7. Schematic diagram of an ^{18}F radiotracer positron emission and annihilation (Livieratos 2012).

These photons, with an energy of 511 keV, are almost exactly antiparallel, and can thus be detected simultaneously by the detector ring surrounding the radioactive source, i.e. the PET scanner, as a 'coincidence' (Figure 8). Based on these characteristics, a simultaneously detected pair of photons can be used to construct a line of response between the two detecting crystals. However, without additional information, it is not possible to identify where along this line the annihilation took place. Therefore, uniform probability is given to each possible point along the line of response. If this is done for a

sufficient number of coincidences it becomes possible to reconstruct the distribution of radioactivity within the field of view of the scanner (Kearfott and Votaw 1995). Modern PET systems however, are equipped with time-of-flight techniques, that can, to a certain extent, localize the coincidence based on the small time difference between the detection of the two photons of a pair (Conti 2009).

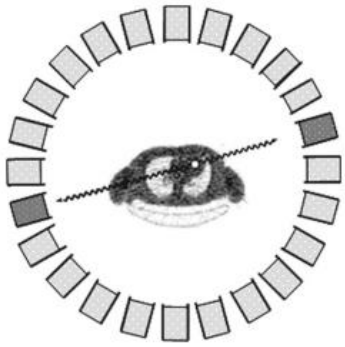


Figure 8. Annihilation photons detected by opposing detectors in coincidence (Livieratos 2012).

The distribution of the radioactivity *in vivo* is determined by the radiotracer that is used. Radiotracers typically consist of two parts; a molecule with a certain biological behaviour, and a radioactive isotope. The first part is designed with consideration of the target that is to be visualized. Examples are glucose metabolism, brain receptors or cell-reporters specifically implemented for this purpose. The second part, the radioactive isotope, is determined by several factors, including the chemical properties of the molecule of interest, and the purpose of the radiotracer, e.g. commercially sold products benefit from longer half-times allowing storage and transportation (Kearfott and Votaw 1995).

1.7.1.1 Principles of Kinetic Modelling

When PET data are recorded statically over the entire scan time inference can only be made about the spatial distribution of the radiotracer, which answers questions like 'where is glucose metabolism happening?' for the glucose derivative ^{18}F-deoxy-glucose (^{18}FDG) or 'what is the distribution of this receptor in the brain?'. However, when dynamic data are provided more quantitative measures can be obtained, such as the concentration of receptors being expressed in the brain. This information cannot be

readily assessed visually since the resolution of a PET image does not allow the distinction between the different locations a radiotracer might be located in. For example, we can imagine that the radiotracer bound to a receptor is surrounded by other radiotracer molecules not specifically bound to the target receptor, but rather floating through the extracellular spaces, and circulating in the blood. These different states, also called compartments, can however, be separated by mathematical approximations. These compartmental models describe the flow between different compartments classically starting from the first compartment; arterial blood (Figure 9). Indeed, radioactive tracer distribution to other compartments strongly depends on the concentration, which is made available to the tissue over time, which practically means the arterial concentrations of radiotracer. From here, the radiotracer can experience an influx to the tissue compartment, or sub-compartments within this tissue compartment, for example the specific and non-specific tracer compartment, and the metabolite compartment (Morris et al. 2004).

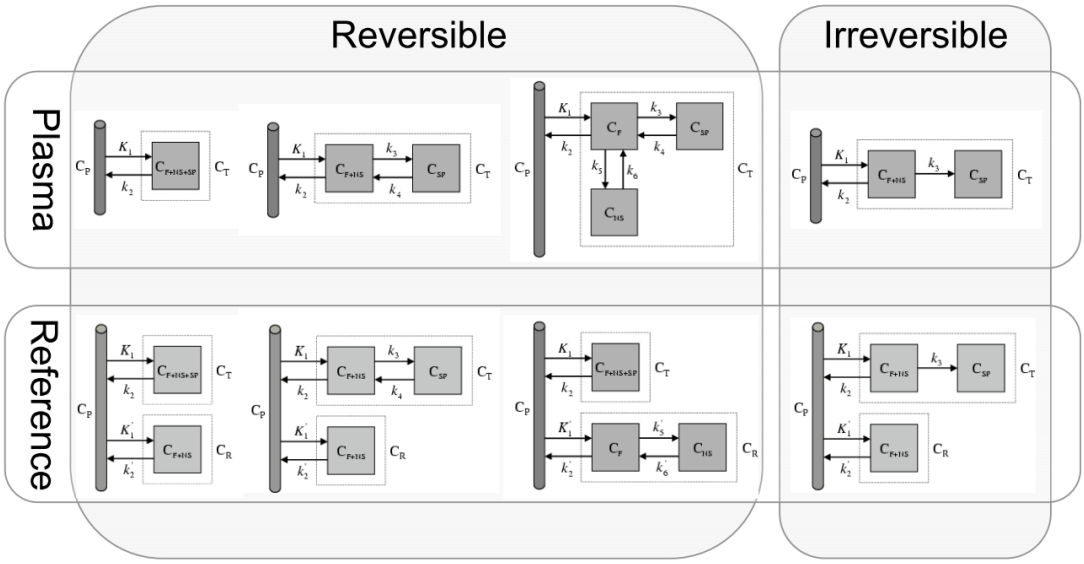


Figure 9. A range of compartment models used for the quantification of PET radiotracers. These include models for tracers that exhibit reversible and non-reversible behaviour and use either plasma or reference input functions (Gunn et al. 2002). C_P, C_T,C_R = concentration of radiotracer in plasma, tissue, or reference respectively. C_F, C_{SP},C_{NS} = free radiotracer, and specifically and non-specifically bound radiotracer respectively. K1, k2, k3, and k4 = rate constant describing the movement from tracer from one compartment to the other.

Depending on the quality of the data and the biological behaviour of the radiotracer more or less complex compartmental models can be fitted by setting the differential equations in the model to constants reflective of the kinetic properties of that specific radiotracer. Then by comparing the output of such a model with the experimentally obtained PET data, these kinetic parameters can be assessed. An assumption on the obtained data parameters however, is that they are time-invariant, at least over the time of the study. This means that a PET scan provides a snapshot of the relation between the biological system and the tracer at that specific time. It can be expected therefore, that scans between similar subjects, or even on the same subject, can result in slightly different estimations, as biological systems typically display a complex and dynamic behaviour, which is influenced by a vast number of factors.

Measuring the arterial radiotracer concentration is a cumbersome process as it requires an arterial catheter to repeatedly obtain blood samples. For human subjects, this process can be experienced as painful, whereas in the preclinical research setting the placement of an arterial catheter is a terminal procedure, thus prohibiting longitudinal study setups. Additionally, practical issues, like time-lags between blood sample collection and image acquisition can complicate quantification. Therefore, alternatives have been extensively investigated, with several potential surrogates for invasive blood sampling. For example, if large volumes of blood are placed within the field of view of the camera, the signal originating from these regions, e.g. the left ventricle or aorta, can be used as a surrogate to calculate the arterial input function (Mourik et al. 2009). The most popular approach however is to use a reference tissue model for quantification. The reference region is defined according to the radiotracer and research question; for example, for brain receptor studies a region is chosen that is virtually devoid of the target receptors (Figure 10).

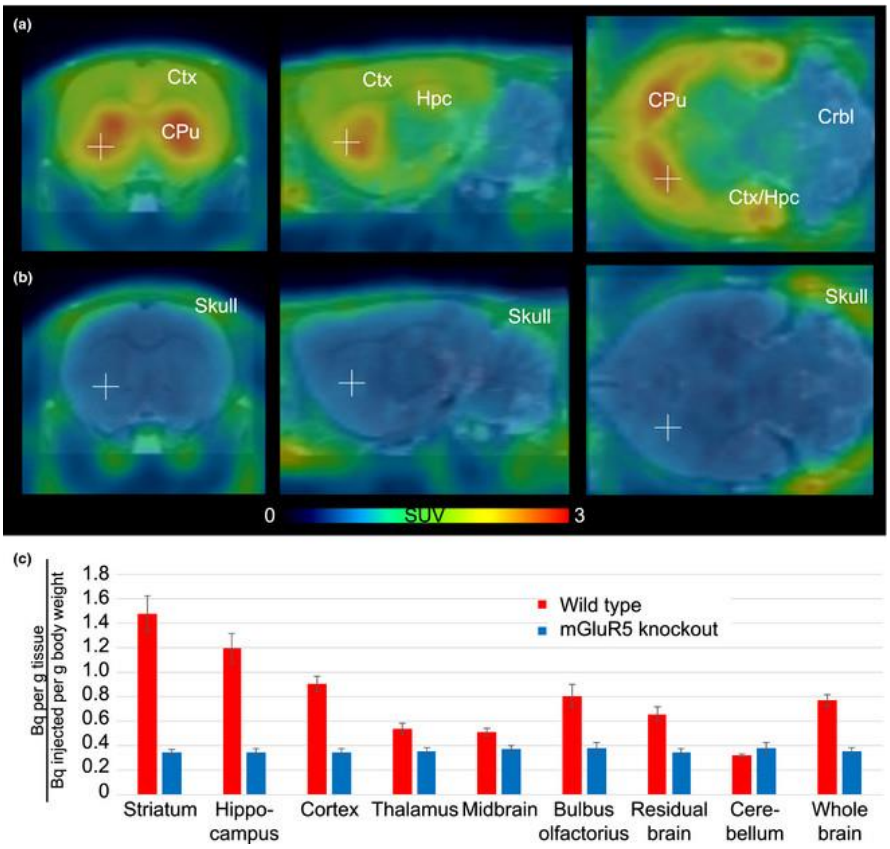


Figure 10. Example of a preclinical PET scan visualizing mGluR5 availability with [^{18}F]PSS232 in both wild type and mGluR5 knockout rat brains. Notice the absence of binding in the cerebellum (Crbl), i.e. no difference between both strains of rats, which can indeed be used as a reference region for this radiotracer (see also chapter 2). Ctx = Cortex, CPu = caudate putamen, Hpc = hippocampus (Muller Herde et al. 2015).

Based on the compartmental models described above we can expect that the signal originating from this region contains two major contributors of the radioactive signal, namely the blood and non-specific binding, but not a third: the specifically bound radiotracer (Figure 11). However, several assumptions are made using such a reference tissue quantification method. Firstly, the ratio of the kinetic parameters K1 and k2, describing the respective influx and efflux between blood and non-specific compartment respectively, is assumed equal for all regions. A second assumption is the absence of the radiotracer target in the reference tissue, if not, variation in this target concentration between states or individuals would bias the obtained quantification results for regions of interest. Additional modifications to the model can be made to account for small

amounts of specific binding in the reference region, but are not discussed here (Watabe 2017).

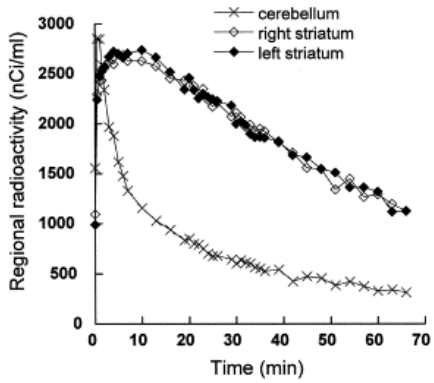


Figure 11. Example of a time-activity curve for ^{11}C-raclopride in the left and right striatum and the reference region, the cerebellum, in cats (Ginovart et al. 2002).

The development of suitable PET radioligands for imaging of the mGluR5 receptor started more than ten years ago (Hamill et al. 2003). The first radiotracer used in vivo, ^{18}F-FPEB, had good characteristics, but its radiosynthesis was problematic (Hamill et al. 2005). Consequent tracers faced *in vivo* defluorination, which was the case for [^{18}F]FPECMO (Lucatelli et al. 2009), [^{18}F]-FE-DABP688 (Honer et al. 2007) and ^{18}F-PSS223 (Sephton et al. 2012). However, [^{18}F]-FDEGPECO, an ABP688 analogue, did not suffer from defluorination, but had low signal-to-noise and radioactivity ratios (Wanger-Baumann et al. 2011). The first tracer suitable for both preclinical and clinical use, ^{11}C-ABP688, was developed by Ametamey *et al*. in 2006 (Ametamey et al. 2006). Using ^{11}C-ABP688 *in vivo,* increased mGluR5 binding was reported in patients with high obsession scores and after sleep deprivation (Akkus et al. 2014; Hefti et al. 2013). On the contrary, decreased binding was seen after both nicotine and cocaine addiction (Akkus et al. 2013; Martinez et al. 2014; Hulka et al. 2014). Despite its favorable characteristics, the major limitation of ^{11}C-ABP688 remains the short half-life of its radioisotope. This limits its use to centers with onsite cyclotrons preventing both more extensive study setups and satellite use in facilities without the infrastructure to produce radioactive compounds. Acknowledging this situation, Wong *et al.* optimized the cumbersome and low-productive radiosynthesis of ^{18}F-FPEB by simplifying the process and increasing the radioactive yield. They additionally performed an *in vivo* distribution study in humans, that confirmed the previously described pharmacokinetics (Wong et al. 2013). At this

time, three radiotracers have been fully optimized in humans, namely ^{11}C-ABP688, ^{18}F-SP203, and ^{18}F-FPEB (Li et al. 2012). The latter will be validated for preclinical use and applied for mGluR5 availability measurements in experiments described in this work.

1.7.2 Principles of MR imaging

Magnetic resonance imaging is performed using a magnetic field in which certain atomic nuclei can absorb and re-emit energy at a specific frequency, known as the resonance frequency. The resonance frequency depends on the gyro magnetic ratio (γ) of the atoms and on magnetic field strength (B_0). The most commonly used atom for MRI is the hydrogen atom, because of its high gyro magnetic ratio (γ = 42,57 MHz/T) and its abundance in biological tissue. Hydrogen atoms or protons are suitable for MR imaging as they have a non-zero spin of $\boldsymbol{I}$ = ½. This non-zero spin allows every proton to create a small magnetic field. The net magnetization field does not increase with the number of protons, as the direction of this field is randomly distributed. Due to this random distribution a multitude of protons will neutralize each other's magnetic fields, thus balancing out the net magnetism. However, inside the magnetic field of the MR scanner, hydrogens position themselves parallel or anti-parallel to this field. Since the parallel orientation is a lower energy state, this orientation is more common among all protons in the field. Besides this change in orientation, protons will start to circle around their central axis, a phenomenon called precessing. This precessing occurs at the Larmor frequency $\omega_0 = \gamma * B_0$. When a radiofrequency pulse is delivered to the protons in the magnetic field, they will absorb the energy of this pulse. However, this energy transfer can only happen for protons precessing at the exact same frequency. Through absorbance of this energy the spin axis of each proton is flipped to a certain extent, for example ninety degrees. From this excited state, protons will slowly come back to their natural state by emission of their excess energy. This process is called relaxation, which consists of two independent parts. Firstly, the net magnetic field will move back towards the original orientation, i.e. upwards or along the z-axis in a 3D system. Therefore the amplitude of the magnetic field in this direction will steadily grow back to its original strength. The speed with which this process, called T1 relaxation, advances is specific per tissue type and is thus essential for the contrast of MRI. The second part of the relaxation can be measured as the amplitude of the net magnetic field in the horizontal or X-Y plane. Immediately after the radiofrequency pulse all protons will spin

harmonically in this plane. We can therefore imagine that, if we would spin the X-Y axes with equal speed, that we could measure the net strength of the field in this direction. However, since the radiofrequency pulse is only short-lived, the spin of the protons in this plane will progressively slow down. The speed with which this happens depends on the environment of the proton, and since this is not equal for all protons, particularly in vivo, the net magnetization in this direction will diminish as the magnetic field direction of the individual protons becomes progressively more randomly distributed. This process, called T2 relaxation is therefore also a tissue specific time-constant.

This contrast however, is not useful without being able to locate its original position. For this reason, an MR scanner is equipped with three gradient coils, one for every spatial dimension. For example, the influence of the Z-gradient on the magnetic field will create a slice where protons spin with center frequency, i.e. the frequency that will be detected by the scanner. Therefore, when the radiofrequency pulse is delivered, only protons in this slice will be affected and consequently imaged. Similarly, the radiofrequency pulse also has a certain frequency and phase, this can be used for localization as protons will have the same characteristics in a specific voxel due to the influence of the X- and Y-gradient (Oldendorf and Oldendorf 1988).

1.7.2.1 resting-state functional-MRI

A special application of MR imaging has been developed to image regional blood oxygenation changes over time. Imaging this provides functional information and has hence been named functional MRI (fMRI). Since cellular energy metabolism requires oxygen and glucose, neuronal activity can influence this blood oxygenation level. Specifically, sudden increases in metabolic activity increase the cerebral metabolic rate of oxygen, thus creating a relative oxygen depletion in its direct vicinity. This is a physiological trigger for localized vasodilation to increase the regional blood flow and restore the oxygen level. Typically, the increased flow of oxygen results even in a transient overshoot. Oxygen in the blood is transported by hemoglobin, which can exist in its oxygenated or deoxygenated form. Interestingly, the magnetic properties of hemoglobin are determined by its oxygenation, and can therefore be used as a surrogate marker for oxygen concentration and thus neural activity (Glover 2011). In effect, oxygenated hemoglobin is diamagnetic, whereas its deoxygenated form is paramagnetic.

The latter creates local gradients in the magnetic field in function of the hemoglobin concentration (Thulborn et al. 1982). In this way, it is possible to receive a blood-oxygen level dependent (BOLD) signal.

Clinical fMRI scans require the subject to perform a task intermittently during the sequence. In this way, the brain activation can be compared between the active and inactive state, or between control and experimental condition. An interesting finding however was that during the inactive state, fluctuations in the BOLD signal were also observed (Biswal et al. 1995). These fluctuations can be considered activity of the brain in a resting state. Potentially, the most important discovery about these fluctuations during resting state was that different brain regions showed similar patterns (Scholvinck et al. 2010; Biswal et al. 1995). After extensive investigation, it has been shown that this can be considered as neural communication between regions, as activity in one would prompt activity in the other. These apparent communication lines have been hypothesized to reflect functional connectivity, i.e. high correlations between patterns of both regions could be interpreted as intense neural linking. However, the value of resting-state fMRI has not been without controversy. These fluctuations typically have a low signal-to-noise ratio and can be disturbed by a number of factors. For example, physiological variations in heart rate or blood pressure can influence their pattern. Moreover, the activity in a target region might depend on the input of several other regions, thus resulting in low correlation with each individual region (van den Heuvel and Hulshoff Pol 2010).

1.7.2.2 Magnetic Resonance Spectroscopy

A technique that is rapidly gaining interest in both research and clinical practice is proton magnetic resonance spectroscopy (^{1}H-MRS). Especially for brain imaging, this method can provide information that was previously inaccessible. Furthermore, this is possible on most MRI systems, without the need of additional software (Blüml 2013). Where MR imaging uses the interaction of water protons and tissue, spectroscopy is based on hydrogen atoms built into other chemical structures. In effect, rather than one water peak, multiple peaks are mapped at different radiofrequencies. These frequencies depend on the chemical environment of the protons and specific peaks can therefore be associated with certain molecules. Since these molecules are present in much lower concentrations than water, MRS has a lower spatial resolution, up to a thousand times, than MRI. This

typically results in voxels, the region of interest where the measurements take place, of 1 – 10 mm^3. With this size, molecules with concentrations exceeding 0.5 µmol/g can be detected. Most neurotransmitters can therefore not be detected with this method, with exceptions of glutamate, GABA and aspartate.

If an electron is close to its proton, it can shield it, thus reducing the magnetic field strength to which it is subjected. This results in a slightly shifted resonance frequency of the proton. The position of the electron depends on the chemical structure of the molecule and the consequent shift in resonance frequency has therefore been named "chemical shift". This chemical shift can even differ between protons of the same molecule, depending on their respective position. An additional influence on the detected peak signature of a molecule is called J-coupling. J-coupling describes the indirect interaction between different protons within the same molecule. This modulation of signal intensity is related to several acquisition parameters, such as echo time.

An interesting modification of the classical one-voxel MRS is chemical shift imaging (CSI). CSI is typically performed in a 2D plane, although 3D CSI scans have been reported, which is subdivided into a raster of smaller voxels. The potential benefit of CSI is two-fold: firstly, a larger area of the brain is typically imaged, providing information about chemical profiles in different brain regions. Secondly, a larger classical MRS voxel might measure in several brain regions at the same time. Since only an averaged spectrum within this voxel is obtained, subtle spatial differences may be lost. Therefore, the smaller voxels typically obtained with CSI can be considered an advantage. Another interesting modification of ^{1}H-MRS is its dynamic application. For this, short spectroscopy scans are repeatedly performed to be able to study the change in chemical profiles in physiological systems not in steady-state (Brechtel et al. 2001).

1.8 Overview

This introduction aimed to provide the reader with a background on addiction and the techniques used in this thesis. The next two chapters describe the characterization of ^{18}F-FPEB on one hand and of the physiological variance of mGluR5 in rats on the other hand. Subsequently, two chapters describe the observed changes in the glutamatergic system in animals that self-administer alcohol and cocaine. Chapter 6 describes an experiment

where silencing RNA is used to alter mGluR5 expression, whereas the application of machine learning to metabolic data obtained from rats self-administering nicotine is described in chapter 7. Chapter 8 is a report of those effects observed after acute injection of drugs of abuse on both the cerebral metabolic rate of glucose, as well as the simultaneous changes in brain analytes. The final experimental chapter is an assessment of different analysis methods that can be used for statistical inference on PET data. In the last chapter, the translational value of the observed results, as well as their limitations are discussed.

Chapter 2: Preclinical evaluation and quantification of ^{18}F-FPEB as a radioligand for PET imaging of the metabotropic glutamate receptor 5

Bart de Laat · Gil Leurquin-Sterk · Sofie Celen · Guy Bormans · Michel Koole · Koen Van Laere · Cindy Casteels.

Published: Journal of Nuclear Medicine (2015), 56 (12), pp. 1954 – 1959.

2.1 Abstract

Introduction: The metabotropic glutamate receptor 5 (mGluR5) is a high interest target for PET imaging as it plays a role in several pathologies, including addiction, schizophrenia and fragile X syndrome. We studied the pharmacokinetics of ^{18}F-FPEB, a selective PET radioligand for mGluR5, and used it to quantify mGluR5 in rat brain.

Materials & Methods: Quantification was performed using both arterial sampling in combination with compartment models as well as simplified reference methods. SRTM, MRTM0, and Logan Non-Invasive were tested as reference models with BP_{ND} as outcome parameter. Additionally, test-retest scans were performed in six animals.

Results: ^{18}F-FPEB uptake in rat brain was consistent with its known distribution. No radiometabolites were present in the brain and binding was specific as shown in blocking experiments, which also confirmed the cerebellum as a viable reference region. A two tissue compartment model was used to determine BP_{ND} for the striatum (11.7±1.5), nucleus accumbens (10.6±2.0), hippocampus (9.0±1.2), cortex (7.2±1.0) and thalamus (4.0±0.9). Reference methods were able to estimate these values with small bias (<2%). Test-retest analysis showed high repeatability between scans below 6 %, also for shorter scan durations of 30 and 60 min.

Conclusion: Due to its favorable reversible kinetics, high specificity and absence of brain radiometabolites ^{18}F-FPEB proves a highly useful tracer for *in vivo* visualization of the mGluR5 in rat brain. Moreover, reference tissue models allow non-invasive, rapid scanning with good test-retest.

2.2 Introduction

The metabotropic glutamate receptor type 5 (mGluR5) is a post-synaptic G-protein coupled glutamate receptor predominantly located extra-synaptically (Shigemoto et al. 1993). mGluR5 is thought to regulate and react on the extra-synaptic glutamate, arriving from synaptic spill-over and the glial cysteine-glutamate antiporter (Baker et al. 2002). Contrary to the rapid fluctuations of glutamate levels inside the synapse, extra-synaptic levels have slower temporal dynamics allowing for longer-lasting changes in activity states of both glial and neuronal cells (Coutinho and Knopfel 2002; Vermeiren et al. 2005).

The mGluR5 has been implicated in several psychiatric and genetic disorders, such as schizophrenia (Ohnuma et al. 1998), fragile X syndrome (Fatemi et al. 2013), and addiction (Chiamulera et al. 2001). In the latter, it has been shown that mGluR5 plays a crucial role in the capability of cocaine to induce self-administration or increase locomotor activity. Additionally, mGluR5 contributes to the self-administration of metamphetamine, alcohol and opiates (Chesworth et al. 2013; Parkitna et al. 2013; Veeneman et al. 2011). In humans, this receptor has been related to the susceptibility to alcohol addiction (Schumann et al. 2008).

Non-invasive imaging could be a valuable tool allowing a better understanding of the role of mGluR5 in these pathological situations. Indeed, effective PET radioligands may act as biomarker and can guide dosing of therapeutic agents. Therefore, much work has been done on creating PET imaging ligands for this receptor (Li et al. 2012). The first tracer suitable for both preclinical and clinical use, ^{11}C-ABP688, was developed by Ametamey *et al*. in 2006 (Ametamey et al. 2006). Using ^{11}C-ABP688 *in vivo*, increased mGluR5 binding was reported in patients with high obsession scores and after sleep deprivation (Akkus et al. 2014; Hefti et al. 2013). On the contrary, decreased binding was seen in both nicotine and cocaine addiction (Akkus et al. 2013; Hulka et al. 2014; Martinez et al. 2014). Despite its favorable characteristics, the major limitation of ^{11}C-ABP688 remains the short half-life of its radioisotope. This limits its use to centers with onsite cyclotrons preventing both more extensive study setups and satellite use in facilities without the infrastructure to produce radioactive compounds.

Acknowledging this situation, Wong *et al.* optimized the cumbersome and low-productive radiosynthesis of ^{18}F-FPEB by simplifying the process and increasing the radioactive yield. They additionally performed an *in vivo* distribution study in humans, which confirmed the previously described pharmacokinetics (Wong et al. 2013). This pharmacokinetic profile is shown to allow quantification of mGluR5 levels in the brain in humans without exceeding prescribed maximum radiation doses (Kessler et al. 2014). Despite these promising results in humans, no published studies have confirmed the applicability of this ligand in preclinical models.

We report here on the preclinical characterization and quantification of ^{18}F-FPEB in rat brain. As the primary objective, we assessed the pharmacological specificity of brain uptake and binding characteristics of ^{18}F-FPEB. As second objective, we quantified the imaging data by compartmental modelling and high frequency serial arterial measurements of both parent radiotracer and radiometabolites. Outcome measures were the V_T, i.e. the ratio between concentrations in tissue over plasma, and the non-displaceable binding potential (BP_{ND}), representing the ratio between the distribution volumes of specific and non-displaceable binding. Finally, simplified modelling method estimates were evaluated in order to overcome the need for arterial sampling in this species.

2.3 Materials and methods

2.3.1 ^{18}F-FPEB characteristics and preparation

^{18}F-FPEB was synthesized starting from the nitro-precursor using microwave irradiation. A detailed description of the radiosynthesis will be published elsewhere.

2.3.2 Animals

Experiments were conducted in 30 male Wistar rats (Janvier laboratories, Le Genest St. Isle, France) weighing on average 281 ± 18 g at the time of the experiments. All animals were housed two or 3 to a cage in an average room temperature of 22 °C and a 12-h light-dark cycle with free access to food and water. The research protocol was approved by

the local Animal Ethics Committees of the University of Leuven (P156/2013), and was carried out in accordance with European Ethics Committee guidelines (decree 86/609/EEC).

2.3.3 Small-animal PET imaging

Imaging experiments were performed on an LSO (lutetium oxy-orthoscilicate) detector-based small-animal tomograph (FOCUS-220; Siemens Medical Solutions USA, Knoxville, TN), which has a transaxial resolution of 1.35 mm in full-width at half-maximum. Data were acquired in a 128×128×95 matrix with a pixel width of 0.475 mm and a slice thickness of 0.796 mm. The coincidence window width was set at 6 ns. During PET imaging, rats were kept under gas anaesthesia (2.5 % isoflurane in oxygen at a flow rate of 1.5 l/min), and their body temperature was maintained between 36.5 and 37 °C with a heating pad. On average 37.6 ± 5.6 MBq (specific activity range: 35 – 150 GBq/µmol, mass dose range: 1.03 – 5.64 µg) was injected into the tail vein using an infusion needle set. Individual dynamic 180-min scans were started simultaneously with the injection of ^{18}F-FPEB to assess the kinetics of ^{18}F-FPEB using compartmental modeling (n=10) and for pretreatment evaluation (n=3).

For the pretreatment experiment, MTEP-hydrochloride (3-[(2-methyl-1,3-thiazol-4-yl)ethynyl]pyridine hydrochloride; Sigma-Aldrich USA, St. Louis, MO), an mGluR5 NAM, was dissolved to a concentration of 20 mg/ml in distilled water. MTEP was administered intra-peritoneally 15 minutes before and, 45 and 95 minutes after ^{18}F-FPEB injection. The dose of 20 mg/ml and the time of treatments were based on previous reports to ensure complete blocking of mGluR5 receptors (Anderson et al. 2003; Simeon et al. 2007).

List-mode acquisition data were Fourier-rebinned in 33 frames (4×15, 4×60, 5×180, 8×300, and 12×600s). Sinograms were reconstructed using an iterative maximum a posteriori probability algorithm with ordered subsets (MAP; 18 iterations, 9 subsets, fixed resolution: 1.5 mm) (Cheng, Shoghi, and Laforest 2012). All scans were corrected by means of a ^{57}Co-attenuation scan.

2.3.4 Measurement of ^{18}F-FPEB in plasma

To measure the concentration of ^{18}F-FPEB in rat plasma, an arterial cannula was placed in the femoral artery. After slow bolus injection of ^{18}F-FPEB, arterial blood was continuously collected for 1 min (15 samples, approximately one sample every 4 s), followed by 100 µl samples at 90, 120 and 150 s and 200 µl samples at 3, 5, 10, 25, 40, 60, 120 and 180 min. All blood samples were immediately stored on ice to minimize possible tracer metabolism. The plasma time–activity curves were corrected for the fraction of unchanged radioligand using reversed-phase HPLC separation (LaChrom Elite HPLC system, Hitachi; Chromolith C18, 3×100 mm, Merck). Plasma samples were isolated from whole blood by centrifugation at 3,000 rpm for 5 min and spiked with authentic FPEB reference (25 µl) prior to HPLC analysis. The HPLC separation was achieved with gradient mixtures of 0.05 M sodium acetate (pH 5.5) (A) and CH_3CN (B) (1 % B, flow rate 0.5 ml/min, from 0 to 4.1 min; 1 % B, flow rate 1.0 ml/min, from 4.1 to 9 min; 90 % B, flow rate 1.0 mL/min, from 9.0 to 12.0 min; 90 % B, flow rate 0.5 mL/min, from 12.0 to 12.1 min; and 1 % B, flow rate 0.5 mL/min, from 12.1 to 15.0 min). The HPLC eluate was collected after passing through an inline ultraviolet detector (296 nm). Collection was performed per minute, except for the period between 8 and 12 min where samples were collected every 15 seconds. This period of higher temporal resolution allowed better delineation of the parent tracer and one of the radiometabolites. Radioactivity in all fractions was measured using an automated γ–counter equipped with a 7.62-cm NaI(TI) well crystal coupled to a multichannel analyser (2480 Wizard; Wallac). Results were corrected for background radiation, physical decay and counter dead time.

2.3.5 Measurement of ^{18}F-FPEB radiometabolites in the brain

For each time point, two rats were infused with approximately 37 MBq of ^{18}F-FPEB under isoflurane anaesthesia as described above. At 10, 30, 60, 120 and 180 min after injection, rats were euthanized using a 180 mg/kg overdose of sodium pentobarbital (Nembutal, Ceva Sante Animale, Brussels, Belgium) and perfused transcardially with saline. The brain was carefully removed from the skull, after which the cerebrum and cerebellum were separated. After homogenization, in 3 and 2 ml CH_3CN respectively, the supernatant was collected and filtered with a Centrifee ultrafiltration membrane. One

ml of this filtrate was diluted with 1 ml water after which 0.5 ml of this solution was spiked with authentic FPEB reference and injected onto the HPLC consisting of an analytical XBridge column (C_{18}, 5 μM, 3 mm×100 mm; Waters) eluted with a mixture of 0.05 M sodium acetate (pH 5.5) and CH_3CN (50/50 v/v) at a flow rate of 0.8 ml/min. HPLC eluates were collected every minute after passing through a UV detector (296 nm). Radioactivity in the fractions was measured using the automated γ–counter.

2.3.6 In vitro rat brain and blood stability studies

Fresh rat blood, plasma and homogenized perfused brain were incubated with about 18 MBq tracer at 37 °C. After 60 min of incubation, samples were cooled on ice. Blood and brain homogenate samples were processed and analyzed by RP-HPLC as described above.

2.3.7 Small-animal PET analysis

PET images were normalized to a custom-made rat brain template in Paxinos stereotactic space, allowing the use of a predefined volume of interest map. The procedure for spatial normalization and its validation have been described previously by our group (Casteels et al. 2006a). Time–activity curves were generated for the bilateral caudate-putamen, nucleus accumbens, hippocampus, cortex and cerebellum of each individual scan using PMOD software (version 3.6; PMOD Technologies, Zurich, Switzerland). The macrostructures that were used were based on the spatial resolution of the FOCUS-220 system (Tai et al. 2005). The radioactivity concentration in each brain region was normalized to the injected dose and body weight, and expressed as standardized uptake value (SUV).

2.3.8 Compartmental modelling of ^{18}F-FPEB in the rat brain

All ^{18}F-FPEB input curves were obtained after correction for ^{18}F decay and radiometabolite correction, which was based on a hill-function fitting of the radiometabolites. One- and two-tissue compartment models were considered to describe ^{18}F-FPEB kinetics in the rat brain using the metabolite-corrected plasma input function. Blood fraction volume was fixed at 5%. Fittings were obtained for different scan durations and evaluated both by visual assessment and model selection criterion (MSC) values. The MSC is a modified form of the Akaike Information Criterion (AIC), which

is widely used to select the best-fitting model when those under consideration do not contain the same number of parameters (Akaike 1974). The MSC modification allows to obtain an information criterion which is also independent from the number of data points (MicroMath 1995). The model with the largest MSC value is considered the most appropriate one (Berry and Likar 2007; Wagner 1993). V_T and BP_{ND} were used as outcome parameters. BP_{ND} was calculated as $V_T/V_{Ref} - 1$, where V_{Ref} is the distribution volume of the reference region.

To determine the time-stability of the tracer and the minimum scanning time necessary to obtain reliable estimates for BP_{ND}, we analyzed PET data from each rat after removing variable durations of the terminal portion of the scans. We analyzed data of all animals for the periods between 0 – 30, 60, 90, 120 and 180 min. Estimates of BP_{ND} were compared with the reference value obtained with the best fitting dataset. The solution was considered acceptable if the result was within 10 % of that from the analysis of the reference value.

2.3.9 Simplification of ^{18}F-FPEB quantification

As arterial blood sampling in rats is technically demanding and a terminal procedure, it hampers serial small-animal PET studies in this species. Therefore, we also explored the possibility of simplifying ^{18}F-FPEB quantification in rat studies. For this purpose SRTM (Lammertsma and Hume 1996), Logan Non-Invasive (Logan et al. 1996) and $MRTM_O$ (Ichise et al. 2003) were tested as reference models with BP_{ND} as the outcome parameter. Reference models were compared to the best-fitting compartmental model.

2.3.10 Test-Retest variability

Six animals were scanned twice for 120 min with one week interval to evaluate the (short-term) inter-scan variation between different scans of the same animal. Intraclass correlation coefficient (ICC) was used to assess within-subject variability relative to the between-subject variability. Additionally, percent difference was also calculated as the difference between test and retest values on the same subject divided by their average, i.e. $(Y_1 – Y_2) / ((Y_1 + Y_2)/2)$.

2.3.11 Statistical analysis

The reported values are mean ± SD. Conventional statistics were carried out using GraphPad Prism v5.0 (San Diego, CA). This includes reported biases, which are obtained with the Bland-Altman method. Intraclass correlations (ICC) were calculated with SPSS 22 for absolute agreement in a two-way mixed model on individual measurements. Significance was defined at the 95 % probability level. Goodness-of-fit by nonlinear least-squares analysis was evaluated using a modified version of Akaike information criterion, i.e. the model selection criterion (MSC) (MicroMath 1995).

2.4 Results

2.4.1 Plasma kinetics

The percentage of intact ^{18}F-FPEB in arterial plasma over time is shown in Figure 1A (dots). At 3 min after injection, 68±7 % of the total radioactivity in arterial plasma corresponded to intact ^{18}F-FPEB. This fraction declined to 44±9 % at 10 min, 26±6 % at 40 min, 19±5 % at 60 min, 16±5 % at 120 min and 11±3 % at 180 min after tracer injection. In rat plasma two radiometabolites were observed, which eluted earlier (at 3 and 9 min) than ^{18}F-FPEB (R_t = 10 min) on the HPLC and are therefore more hydrophilic (polar) than the parent radioligand (Figure 1B). No radiometabolites with higher lipophilicity than ^{18}F-FPEB were detected.

2.4.2 In vitro and ex vivo radiometabolite analysis in rats

^{18}F-FPEB was shown to be metabolically stable in rat whole blood, rat plasma and rat brain homogenates in vitro as the fraction of radiometabolites observed after 60 min incubation at 37 °C was less than 2%. To assess whether ^{18}F-FPEB radiometabolites are also present in the in vivo brain, 2 rats were sacrificed at 10, 30, 60, 120, and 180 min after ^{18}F-FPEB injection. Polar radiometabolites were present in the cerebrum after 60 min, but never accounted for more than 5% of the total radioactivity in the samples (Figure 1A). Total radioactivity in the cerebellum never exceeded 1.5% of the cerebrum.

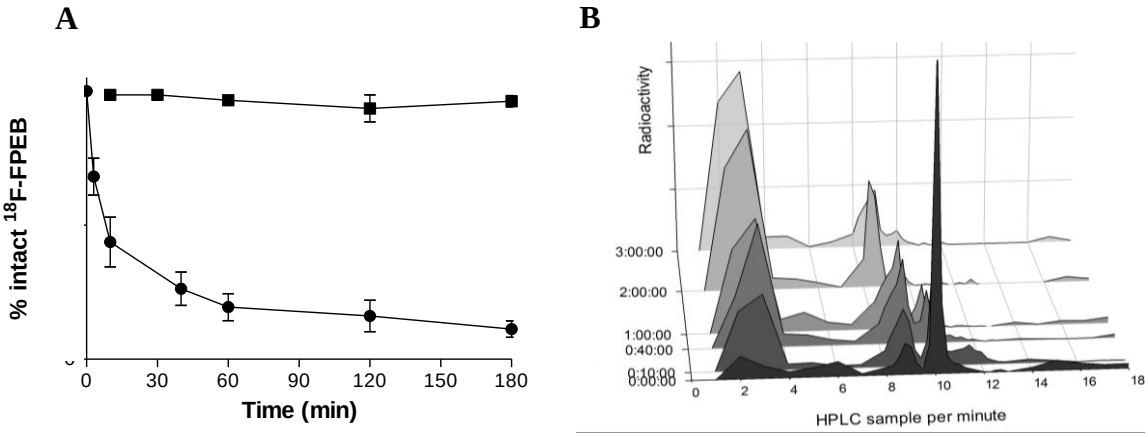


Figure 1. **A**) Intact percentage of ^{18}F-FPEB over time in cerebrum homogenate (squares) and plasma (dots). **B**) Reconstructed chromatograms showing the intact tracer eluting at 10 min. Two polar radiometabolites eluting at 3 and 9 min were observed.

2.4.3 Brain kinetics

After injection of ^{18}F-FPEB, all rats showed radioactivity in the brain in a pattern consistent with the distribution of mGluR5, i.e. highest concentrations in the caudate/putamen, nucleus accumbens, hippocampus and low concentrations in both cerebellum and brainstem (Romano et al., 1995) (Figure 2A). ^{18}F-FPEB uptake in receptor-rich regions increased to a peak around 25 min, after which a slow and approximately linear decline was observed towards 25% of the maximal amplitude at 3 hours (Figure 2B).

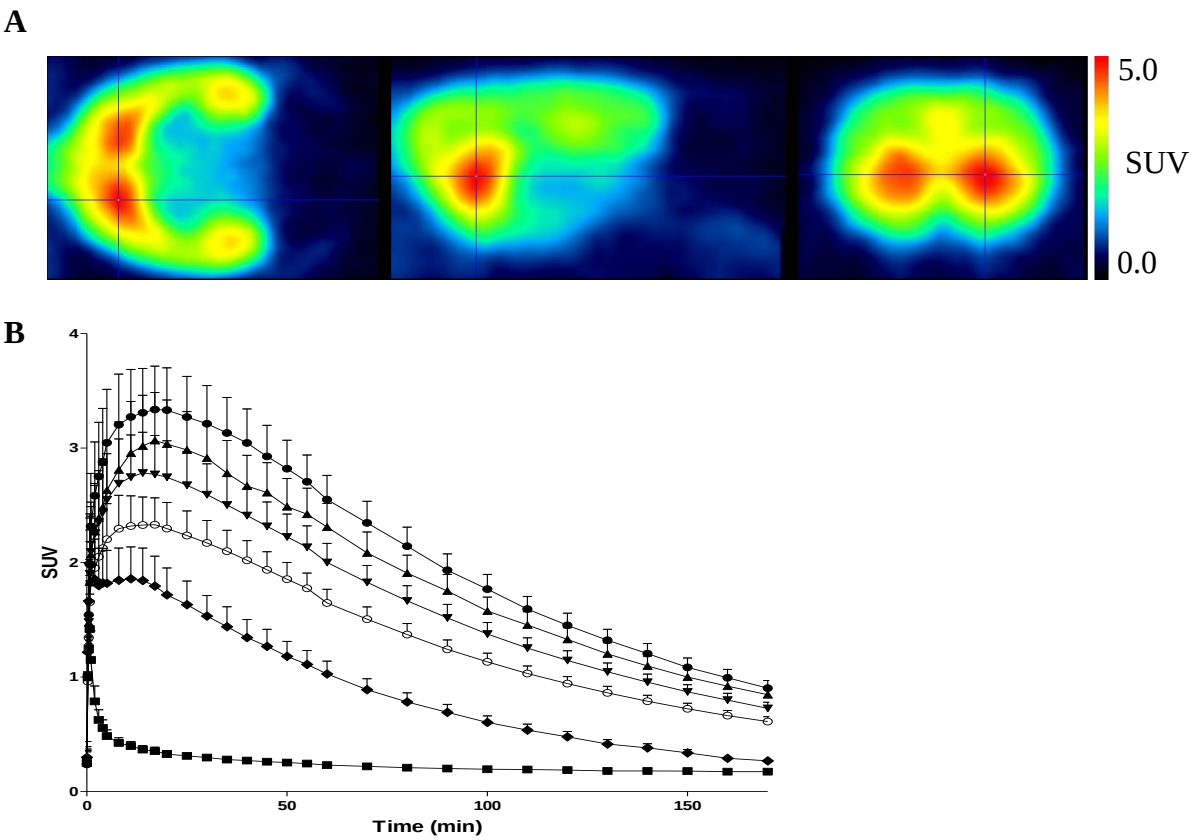


Figure 2. **A**) A representative small animal PET image of rat brain after ^{18}F-FPEB injection averaged from 10 to 60 min. **B**) Averaged time activity curves after venous injection of ^{18}F-FPEB for (from high to low) striatum (dots), nucleus accumbens (upward triangles), hippocampus (downward triangles), cortex (circles), thalamus (aces) and cerebellum (squares). Error bars represent one standard deviation.

2.4.4 Specificity and binding characteristics of ^{18}F-FPEB in rats

^{18}F-FPEB was selective for the mGluR5 receptor in rats as assessed by pharmacological pretreatment with the highly selective mGluR5 NAM, MTEP (Cosford et al. 2003). Full blockage was obtained by injecting 20 mg/kg of MTEP every 50 min, starting 15 min before the injection of ^{18}F-FPEB. The ratio of the area under the curve (AUC) between receptor-rich and reference region TACs (e.g striatum/cerebellum) decreased from 110 to 1.10 (Figure 3). Based on these results, the cerebellum is used as the reference region for the following kinetic modelling analyses.

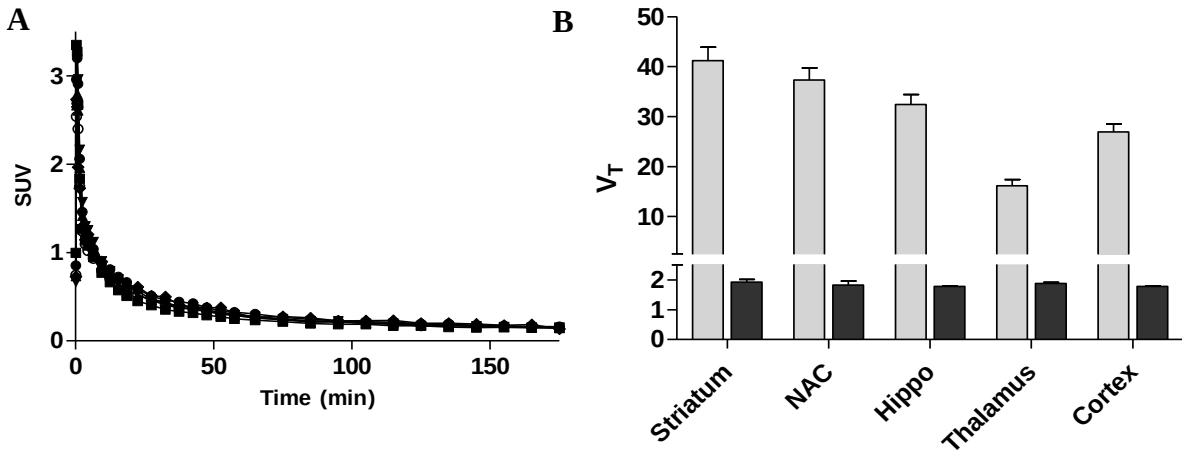


Figure 3. **A**) Time-activity curves expressed in SUV after pretreatment with MTEP for the same regions as shown in Figure 2. **B**) Results of blocking with 20 mg/kg MTEP in comparison with baseline V_T as obtained with the 2TC model. .

2.4.5 Compartmental modelling of ^{18}F-FPEB in the rat brain

Two-tissue compartmental modelling showed to be superior to the one-tissue compartmental model with both better visual fit and higher MSC values. Both criteria were optimal for the scan duration of 120 min. The V_T values obtained with the 2TC model were high for both striatum (41.2 ± 7.7) and the nucleus accumbens (37.3 ± 6.9), intermediate for both hippocampus (32.4 ± 5.6) and cortex (26.9 ± 4.6) with lower values for the thalamus (16.2 ± 3.5).

2.4.6 Simplification of ^{18}F-FPEB quantification

Binding potentials obtained with the 2TC model are closely approximated by the evaluated reference models (Table 1). Of the latter, a clear reduction in variance can be observed for values obtained with SRTM and $MRTM_O$.

	2TC	SRTM	$MRTM_O$	Logan NI
Striatum	11.36 (1.66)	11.33 (0.99)	11.30 (1.02)	11.12 (1.23)
Nc. Accumbens	10.29 (2.05)	9.99 (1.33)	9.95 (1.36)	9.81 (1.51)
Hippocampus	8.76 (1.32)	8.81 (0.78)	8.79 (0.80)	8.64 (0.98)
Cortex	7.10 (1.0)	7.21 (0.60)	7.20 (0.62)	7.06 (0.77)
Thalamus	3.88 (0.91)	4.28 (0.55)	4.22 (0.55)	4.0 (0.65)

Table 1. Binding potentials (mean, (SD)) obtained with both a plasma corrected 2TC model and 3 simplified reference models for 120 min data.

For SRTM and $MRTM_O$ this bias remained stable for the shorter time-frames of 90 (-2.0 and -2.2% respectively), 60 (-5.85 and -5.3%) and 30 min (-2.9 and 0.3%) scan durations. Logan NI however, showed an increasing underestimation ranging from -2.6% at 90 minutes to -20.8% at 30 minutes. All 3 methods showed a relatively large overestimation for 180 min scan duration as compared to 120 min (SRTM 7.2%, $MRTM_O$ 9.6% and Logan NI 17.2%) (Figure 4).

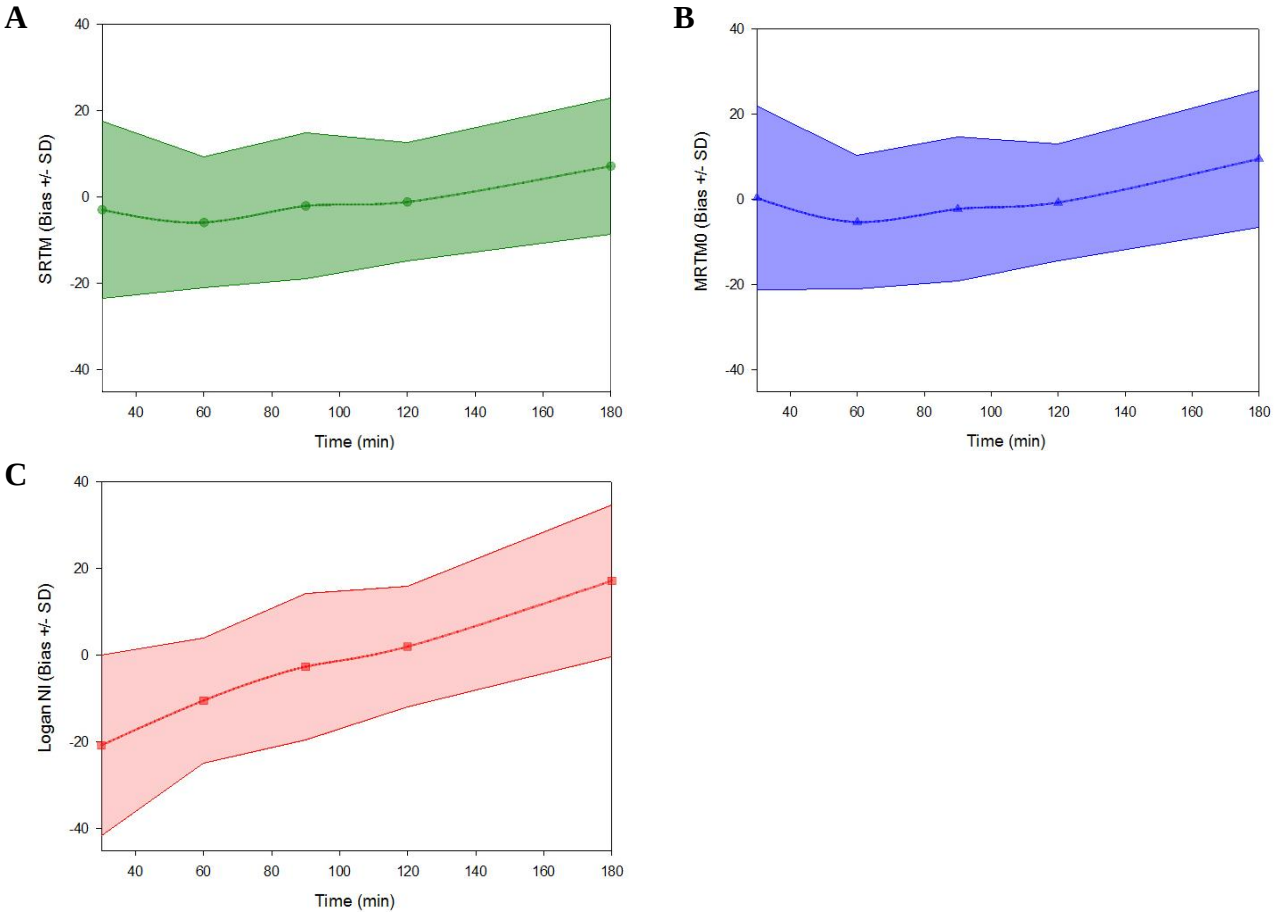


Figure 4. Bias, as compared to the 2TC model, with confidence band (± SD) for SRTM (A), $MRTM_O$ (B) and Logan NI (C) for scan durations of 30, 60, 90, 120 and 180 min.

2.4.7 Test-Retest variability

High repeatability was found for every reference method in all time-frames (Table 2). However, highest repeatability was found for scan-durations of 30 min for SRTM (ICC = 0.92) and $MRTM_O$ (ICC = 0.93) and 60 min for Logan NI (0.88). This was also reflected in the average test-retest values of all regions studied with minimal differences

at 60 min for $MRTM_O$ (-2.3 ± 14.9%) and Logan NI (-1.0 ± 15.3%), and at 30 min for SRTM (-2.7 ± 12.6%).

	SRTM		$MRTM_O$		Logan NI	
Time	ICC	PD	ICC	PD	ICC	PD
120	0.80	-6.7 (18.6)	0.78	-7.6 (19.4)	0.70	-11.8 (23.4)
90	0.85	-3.9 (16.2)	0.84	-3.5 (17.1)	0.81	-3.6 (18.7)
60	0.88	-3.4 (14.4)	0.88	-2.4 (14.9)	0.88	-1.0 (15.3)
30	0.92	-2.7 (12.6)	0.93	-3.0 (11.4)	0.86	-6.0 (15.9)

Table 2. ICC and percent difference (mean ± SD) values for all regions of test-retest scans using SRTM, $MRTM_O$ and Logan NI for different scan durations.

Individual regions showed no more than 10% bias for any scan duration except when evaluated with Logan NI in the 120 min scan duration (<13.9%). Additionally, biases of individual regions also decreased in the 60 time frame to below 5% (Table 3).

	SRTM	$MRTM_O$	Logan NI
Striatum	-2.7 (10.5)	-1.8 (10.8)	-0.1 (9.5)
Nucl. Accumbens	-4.5 (19.5)	-3.2 (27.7)	-1.2 (29.7)
Hippocampus	-5.0 (7.5)	-4.1 (7.7)	-2.8 (7.8)
Thalamus	0.2 (13.7)	1.2 (14.8)	1.7 (15.0)
Cortex	-4.8 (9.8)	-3.8 (10.2)	-2.2 (9.3)

Table 3. Percent difference (mean ± SD) values per region for SRTM, $MRTM_O$ and Logan NI for the 60 min scan duration data.

2.5 Discussion

The evaluation of ^{18}F-FPEB in rats demonstrated uptake in the brain consistent with the known distribution of mGluR5 (Romano et al. 1995; Wyckhuys et al. 2013). Binding was almost 100% specific. Two polar radiometabolites were present in plasma, but these

did not enter the brain. BP_{ND} values obtained with 2TC modelling in combination with arterial sampling corresponded excellently with values obtained by evaluated simplified reference methods, i.e. SRTM, $MRTM_O$ and Logan NI. Test-retest scans proved high consistency and low inter-scan variation with ^{18}F-FPEB.

Plasma radiometabolite analysis showed a rapid conversion of parent to polar radiometabolites contributing to 46% and 89% of the radioactivity at 10 and 180 min, respectively. This pattern is similar to the one reported in humans by Wong et al., but slower than in monkeys (Hamill et al. 2005; Wong et al. 2013). The detection of only one polar radiometabolite by Hamill et al. however, could suggest that the radiometabolite eluding directly before the parent fraction (Figure 1B) might have been missed.

The in vitro evaluation of ^{18}F-FPEB in rats showed no radiometabolite formation in either plasma, blood or brain homogenates. This is also in agreement with data from Hamill et al. showing metabolism of ^{18}F-FPEB in vitro only after addition of liver microsomes (Hamill et al. 2005). Our study is the first to show that there is no significant ex vivo radiometabolite presence in the cerebrum up to 180 min after injection for the ^{18}F-FPEB radiotracer. Although the cerebellum showed minor radiometabolite presence (<6.5%), the total absolute activity in the cerebellum was very low (only 1.5% when compared to the cerebrum). This observation could be explained by incomplete wash-out of radioactivity in the circulatory system, which can be seen with saline perfusion (Graham et al. 1990). Quantification of the mGluR5 receptor using ^{18}F-FPEB is thus feasible when relying on the radiometabolite-corrected ligand input function only.

The in vivo evaluation of ^{18}F-FPEB in rats demonstrated uptake in the brain in a pattern consistent with the known mGluR5 receptor distribution pattern of both ex vivo (Romano et al. 1995) and in vivo (Wyckhuys et al. 2013) data. Tracer binding was shown to be reversible with favorable kinetics allowing accurate quantification with short scan durations of minimally 60 minutes. Moreover, low inter-subject variability (Table 2) allows sensitive comparison between individuals and groups. Finally, calculating the receptor occupancy with the Michaelis-Menten equation (Innis et al. 2007), using the free fraction of ^{18}F-FPEB determined in humans (Sullivan et al. 2013), confirmed that

occupancies in all studies remained below 1.3% and thus well below the pharmacological threshold and in the range of microdosing.

Scans performed after the administration of MTEP showed a decrease in signal from receptor-rich regions to the same level of the reference region, i.e. the cerebellum, thus confirming the high specificity of ^{18}F-FPEB (Cosford et al. 2003; Elmenhorst et al. 2010)(Figure 3). A similar trend was reported for another mGluR5 tracer, ABP-688, in rats. However, for this tracer no full blockage was achieved (Elmenhorst et al. 2010). This can either be explained by the use of MPEP, which has a lower affinity than MTEP, or by a lower specificity of this tracer compared to ^{18}F-FPEB (Anderson et al. 2003).

Modelling showed that a 1TCM was unable to fit the data, but a 2TCM provided good fits in all regions. When different scan durations were considered, best results were obtained with scan data of 120 min according to both visual assessment and MSC values. The 2TC model has also been reported appropriate for ABP-688 in rats by Elmenhorst *et al*. who also show that the cerebellum can be used as a reference region for mGluR5 PET imaging (Elmenhorst et al. 2010). However, their approximation with RTMs of the values obtained with the 2TC model is only evaluated by correlation analysis and not using Bland-Altman plots and is therefore hard to interpret (Bland and Altman 1986). Although the ordering of regions according to BP_{ND} values (e.g. striatum highest, cerebellum lowest) is the same as for ABP-688, absolute BP_{ND} values are not. Indeed, BP_{ND} values found, both with 2TCM and RTMs, for ^{18}F-FPEB are on average 4 to 5 times higher. This could theoretically be explained by a difference in receptor density between the two scanned populations, but is more likely a result of the higher affinity of ^{18}F-FPEB for mGluR5 (K_D = 0.05 nmol/L versus K_D = 1.7 nmol/L) (Ametamey et al. 2006; Patel et al. 2007).

To avoid cumbersome arterial sampling in future animal model scans, the results of the 2TCM for 120 min were compared to SRTM, $MRTM_O$ and Logan NI. Minimal bias was obtained with SRTM and $MRTM_O$ for 120 min data frames (-1.1 +/- 13.7% and -0.7 +/- 13.7 respectively). Furthermore, this bias remained stable and below 6% for 30, 60 and 90 min with both methods (Figure 4). High ICCs were obtained for these time-frames with test-retest scans using SRTM (0.92, 0.88 and 0.85 respectively) and $MRTM_O$ (0.93,

0.88 and 0.84 respectively) (Table 2). This consistency between scans was also confirmed by the small bias on all regions combined (<3.0%) and individual regions (<5%) (Table 3). These results are similar to the ones obtained for ABP-688 in rats (Elmenhorst et al. 2012) and baboons (DeLorenzo et al. 2011).

Mild defluorination is observed in the later time-frames by the appearance of bone structures on the PET images. Defluorination is a common problem for fluorine-18 labeled tracers and can be so rapid that it impedes their practical use (Lucatelli et al. 2009). For ^{18}F-FPEB, the influence of bone uptake was neglectable in receptor-positive regions, but is noticeable in the reference region directly adjacent to bone. Therefore, the reference region used in this study was delineated within the cerebellum, including both grey and white matter, but evading spill in from bone structures. Additionally, this influence might be more pronounced in late time-frames, when radioactivity concentrations in the brain have decreased. This could explain the less optimal fit of the 2TCM for the 180 min data as compared to the 120 min scans. Interestingly, after MTEP administration no bone uptake of radioactivity was present on PET images. HPLC analysis of plasma after MTEP administration also showed absence of the most polar metabolite. Therefore, this most polar radiometabolite, is the probable cause for the uptake of radioactivity in bone.

In conclusion, we have shown that ^{18}F-FPEB is a suitable radioligand for the in vivo visualization and quantification of mGluR5 in rats. Because of the highly specific signal and low inter-subject variability it provides a sensitive tool for preclinical research on mGluR5 related topics. The presence of a valid reference region allows reliable and accurate simplified quantification using SRTM and $MRTM_O$. Moreover, test-retest ICC scores of > 0.88% for 30 and 60 min scans allow for high-throughput and longitudinal experimental designs. Our data suggest that optimal results with ^{18}F-FPEB can be obtained with SRTM and $MRTM_O$ for scan s of 60 min.

Chapter 3: Age and sex related differences in ^{18}F-FPEB binding to the metabotropic glutamate receptor 5 (mGluR5) in the rat brain: a positron emission tomography study

Bart de Laat · Gil Leurquin-Sterk · Guy Bormans · Cindy Casteels · Koen Van Laere

In preparation for submission

3.1 Abstract

Introduction: The metabotropic glutamate receptor type 5 (mGluR5) has been implicated in several disorders and is consequently studied in both clinical and preclinical experiments. However, the interpretation of the preclinical experiments is hampered by the lack of information on the effect of sex and age on mGluR5 availability.

Materials & Methods: Six male and female Wistar rats were scanned on the age of 21, 42, 84, and 168 days with the mGluR5 specific PET tracer ^{18}F-FPEB. Kinetic modelling analysis was performed for every age, and the resulting binding potential was compared between different sex and age groups. Additionally, a voxel-wise analysis was performed to highlight the brain regions in which the most significant effects were located. Finally, a correlation map was created to evaluate brain differentiation over time.

Results: mGluR5 availability, as measured with ^{18}F-FPEB, is shown to progressively increase in the rat brain between the age of 21 and 168 days. The pattern of this increase differed significantly between different regions, whereas sex did not have a significant influence. Voxel-wise analysis located clusters of age dependent increases in the bilateral hippocampus, striatum and the prefrontal cortex. Network analysis showed the emergence of functional networks with age, consisting of cortical and limbic regions, suggesting a central role for the prefrontal cortex.

Conclusion: Preclinical experiments evaluating mGluR5 availability should take the influence of age into account.

3.2 Introduction

The metabotropic glutamate receptor 5 (mGluR5) is a post-synaptic G-protein coupled glutamate receptor located outside the synapse (Hermans and Challiss 2001). Due to this location the mGluR5 is exposed to slower changes in glutamate concentration when compared to the rapid fluctuations inside the synapse. These slower dynamics allow for longer lasting changes in the activity states of both glial and neuronal cells. This lasting effect could be why this receptor has been implicated in several pathologies, such as fragile X syndrome, addiction and Parkinson's disease (Lohith et al. 2013; Tison et al. 2016; Chiamulera et al. 2001).

In vivo imaging of mGluR5 by positron emission tomography (PET) has been applied in the investigation of several pathologies, including psychiatric diseases, such as depression, obsessive compulsive disorder, and addiction (Leurquin-Sterk et al. 2016; Akkus et al. 2014). PET scans targeting mGluR5 have also been applied to animal models of several of these diseases in order to further elucidate their respective etiologies. However, no *in vivo* information is available about the changes in mGluR5 availability between young and adult, or male and female rats. Our group recently reported a moderate negative correlation between age and mGluR5 availability as measured with ^{18}F-FPEB in healthy volunteers, in contrast with previous studies that did not find a difference (Leurquin-Sterk et al. 2015; DuBois et al. 2016). Both studies, did not find a difference between male and female subjects, which is in contradiction with earlier findings (Akkus et al. 2013).This information is not available for preclinical imaging, which hampers comparison between studies using rats of different age, as well as the interpretation of longitudinal protocols.

This study investigated age and sex related differences in mGluR5 availability for specific brain regions in Wistar rats. Rats of both sexes were scanned at the ages of 21, 42, 84, and 184 days. After this assessment of mGluR5 availability, data were explored by cluster and correlation analysis to describe the post-natal differentiation of mGluR5 networks in the rat brain.

3.3 Materials and Methods

3.3.1 Animals

This experiment was performed on four groups of Wistar rats with different ages, namely 21, 42, 84, and 196 days (Janvier laboratories, Le Genest St. Isle, France). Each group contained 6 males and 6 females weighing 73 ± 6 / 73 ± 6 at 21 days, 217 ± 6 / 164 ± 15 at 42 days, 433 ± 18 / 241 ± 9 at 84 days, and 464 ± 69 / 228 ± 72 respectively. All animals were individually housed at an average temperature of 22 °C with free access to food and water. The research protocol was approved by the local Animal Ethics Committees of the University of Leuven (P156/2013), and was carried out in accordance with European Ethics Committee guidelines (decree 86/609/EEC).

3.3.2 Small-animal PET imaging

PET scans were performed on an LSO (lutetium oxy-orthoscilicate) detector-based small-animal tomograph (FOCUS-220; Siemens Medical Solutions USA, Knoxville, USA), which has a transaxial resolution of 1.35 mm in full-width at half-maximum. Data were acquired in a 128×128×95 matrix with a pixel width of 0.95 mm and a slice thickness of 0.796 mm. The coincidence window width was set at 6 ns. During PET imaging, rats were kept under gas anaesthesia (2.0 % isoflurane in oxygen at a flow rate of 1.5 l/min), and their body temperature was maintained between 36.5 and 37 °C with a heating pad. Animals were scanned at approximately the same time of day to avoid diurnal changes in mGluR5 availability (Elmenhorst et al. 2016).

On average 18.5 ± 3.6 MBq (specific activity range: 80 – 301 GBq/µmol, mass dose range: 1.03 – 5.64 µg) was injected into the tail vein using an infusion needle set. Dynamic 120-min scans started simultaneously for three animals upon the injection of ^{18}F-FPEB. List-mode acquisition data were Fourier-rebinned in 33 frames (4×15, 4×60, 5×180, and 8×300). Sinograms were reconstructed using an iterative maximum a posteriori probability algorithm with ordered subsets (MAP; 18 iterations, 9 subsets, fixed resolution: 1.5 mm). All scans were attenuation corrected with a ^{57}Co-point source scan.

PET images were normalized to a custom-made rat brain template in Paxinos stereotactic space, allowing the use of a predefined volume-of-interest (VOI) map and of statistical parametric mapping (Casteels et al. 2006b). Non-displaceable binding (BP_{ND}) was calculated with the previously validated simplified reference tissue model for ^{18}F-FPEB in rodents using PMOD 3.6 (PMOD Technologies, Zurich, Switzerland)(de Laat et al. 2015). For evaluation of changes in ^{18}F-FPEB binding between different time-points, with a maximal use of information without *a priori* knowledge, PET data were analyzed voxel-wise with a full factorial design using age and gender as factors using SPM12 (Statistical Parametric Mapping, Wellcome Department of Cognitive Neurology, London, UK) (Paxinos, Watson, and Emson 1980).

3.3.3 Statistics & data exploration

All statistical analyses were performed using SAS JMP pro 12.1 (SAS institute Inc., Cary, U.S.A.). The influence of age and gender on binding potential in separate regions, i.e. bilateral striatum, nucleus accumbens, thalamus, hypothalamus, prefrontal cortex, lateral and medial temporal cortex, sensorimotor cortex, lateral and medial globus pallidus, substantia nigra, and hippocampus, was evaluated using a regression model. In this model, binding potential was used as outcome, with age a continuous covariate, and gender and region both nominal covariates. Since observations of different regions originating from one animal are more correlated than observations from different animals. This was taken into account by including a random effect for animal (Aarts et al. 2014). PET data were analyzed using SPM as described above using a cluster extent threshold of 150 voxels. Significance was defined at the 95% confidence level. The reported values are mean ± standard deviation.

To provide further insight into the data two exploratory analyses were performed. Firstly, a random forest model was generated with the same three covariates as in the regression model described above. The optimal model was defined as the model with the lowest AIC. The corresponding random forest plot gives insight in the structure of the data beyond the overall significance obtained with regression. Additionally, we constructed a correlation plot for each age group. This represents the correlation between the ^{18}F-FPEB binding potential of different regions. These correlation plots provide an intuitive visualization of the changing spatial correlation structure at different developmental stages.

3.4 Results

With age, the weight of animals increased for both males and females to 73±6 / 69±6 at 21 days, 217±6 / 164±15 at 42 days, 433±18 / 241±9 at 84 days, 464±69 / 228±72 at 168 days respectively. All animals showed radioactivity uptake consistent with the known distribution of mGluR5 (Figure 1).

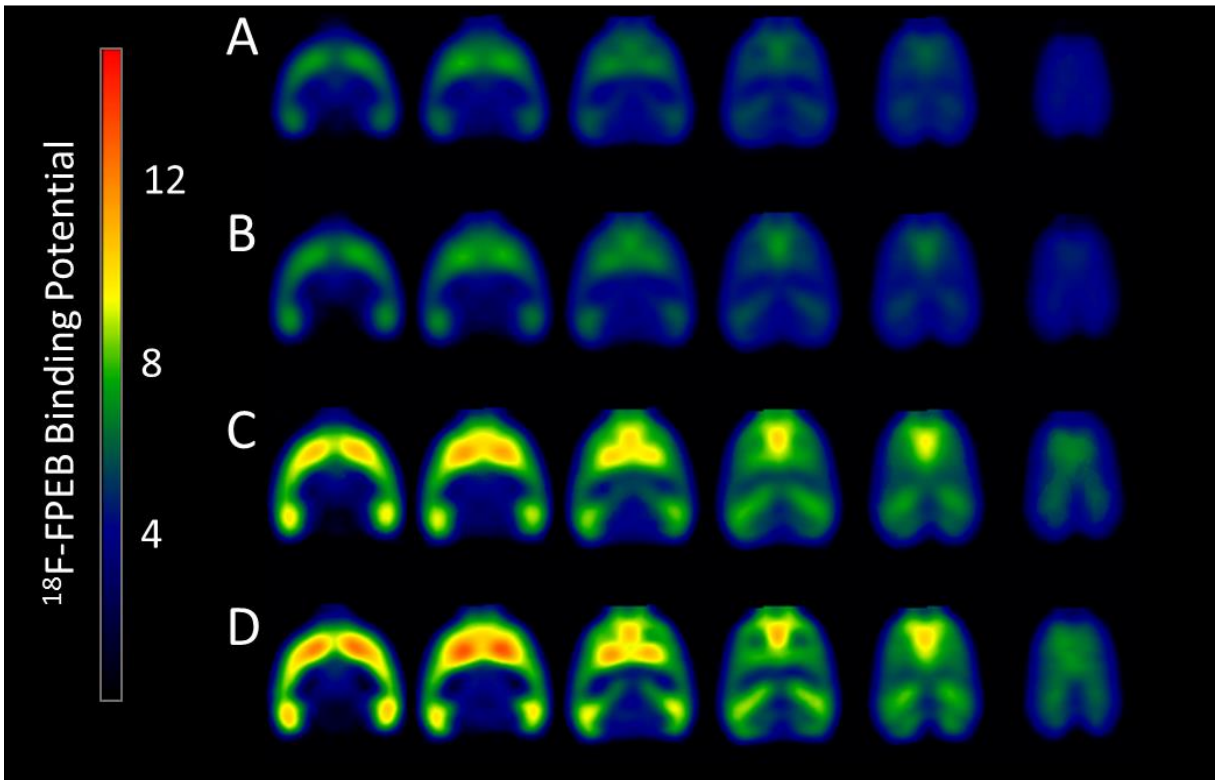


Figure 1. Average distribution of ^{18}F-FPEB binding at 21 (A), 42 (B), 84 (C), and 168 (D) days of age.

Regression was performed using all evaluated regions of interest, i.e. bilateral striatum, nucleus accumbens, thalamus, hypothalamus, prefrontal cortex, lateral and medial temporal cortex, sensorimotor cortex, lateral and medial globus pallidus, substantia nigra, and hippocampus. These were used as covariates, together with age and gender, to explain the observed variance in the average ^{18}F-FPEB binding potential. Based on this model we found that age ($p = 0.0004$) and region ($p < 0.0001$) were significantly associated with ^{18}F-FPEB binding potential. Additionally, the interaction effect between age and region was found to be significant ($p < 0.0001$), proving that the effect of age significantly differed between different regions (Figure 2).

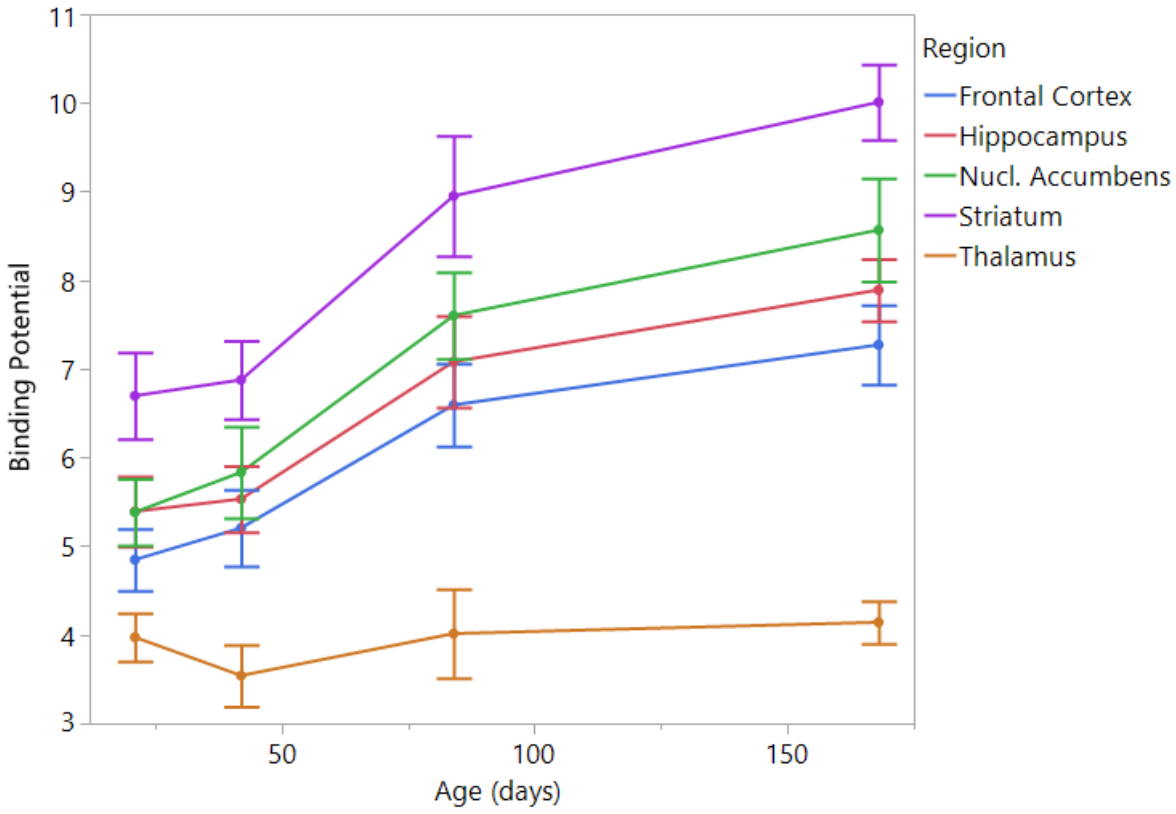


Figure 2. Evolution of average ^{18}F-FPEB binding potential with age, in function of 5 brain regions.

To quantify the pharmaco-kinetic behavior of ^{18}F-FPEB, we performed kinetic modelling of the acquired time-activity curves for the bilateral hippocampus, nucleus accumbens, striatum, and thalamus, and the entire cerebral cortex with the simplified reference tissue method using the cerebellum as reference region. Next to the estimated measure for receptor density, BP_{ND}, the obtained mean k_2, and k_2', the transfer of tracer from the region of interest and reference region respectively, and their standard deviation can be found in Table 1. Whereas BP_{ND} increased with age, no other parameters changed significantly over the time-points or between both genders.

Voxel-wise analysis was performed with SPM12 to find clusters of voxels that changed significantly between the different age groups. Five clusters were found to overcome the set minimum size threshold of 150 voxels (Figure 3). These clusters were located in the bilateral hippocampus, striatum and prefrontal cortex. Detailed results of the analysis can be found in Table 2.

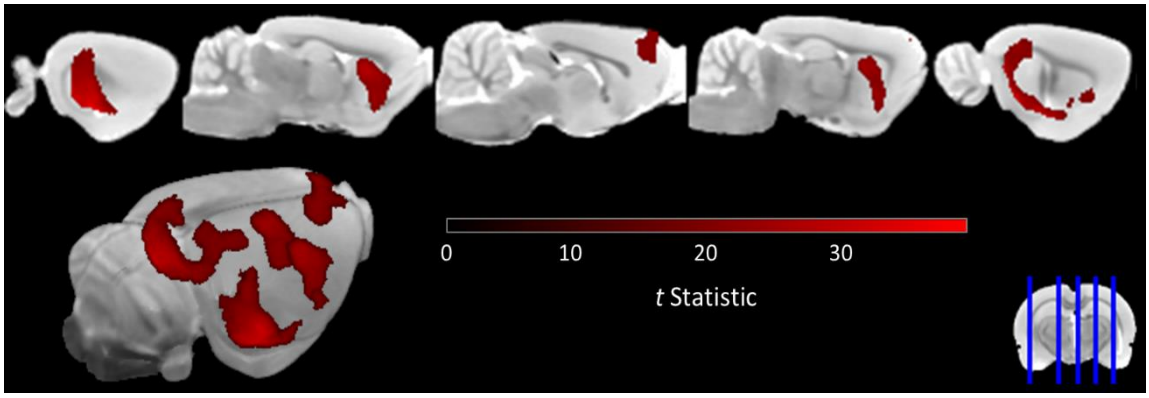


Figure 3. Clusters of voxels with significantly changed mGluR5 availability between 21, 42, 84 and 168 days of age.

Since receptor availability for mGluR5 is distinctly heterogeneous, we wanted to further explore the structure of the data. Therefore, we created a random forest model using the same covariates as used in the regression model above. The output of this can be visualized as a random forest plot, which shows the covariate that can explain most variance in the outcome, here ^{18}F-FPEB binding potential, at that level. The plot generated for our data (Figure 4) shows at the first level a distinction between regions with high and low binding potential, independent from the age group. However, further steps showed the most important differences to lie between the first and last two age groups. Both have similar region clustering, although the nucleus accumbens behaves more similarly with the striatum at 84 and 168 days, hinting towards a higher degree of differentiation. Finally, it can be noted that although gender is included as a covariate in the model, it does not appear in the forest plot. This shows that gender has a smaller influence than both the region and age on binding potential, thus confirming our regression analysis.

Correlation heat maps representing the correlation between the mGluR5 availability between the different evaluated regions show a similar pattern (Figure 5). In effect, at the youngest age of 21 days, a high, relatively homogenous correlation is observed between all regions, except the cerebellum. The cerebellum is almost devoid of mGluR5 receptors in rats (de Laat et al. 2015), which is reflected here by the observed low correlation at each time-point. The homogenous correlation observed at 21 days is progressively shaped into three main clusters for the older age groups. The smallest consists only of

the hypothalamus and thalamus, whereas the second cluster contains the substantia nigra, and the medial and lateral globus pallidus. The largest cluster contains most high-expressing regions, including the cortical regions, striatum, nucleus accumbens, and the striatum. However, within this cluster two separate clusters appear at 168 days. Firstly, the hippocampus, striatum and sensorimotor cortex, whereas the second cluster contains the nucleus accumbens, and medial and lateral temporal cortex. Interestingly, these two clusters are joined by the prefrontal cortex, which correlates with both subclusters.

			Prefrontal cortex			Hippocampus			Nucl. accumbens			Striatum			Thalamus		
Age	Gender		BPnd	k2'	k2a	BPnd	k2'	k2a	BPnd	k2'	k2a	BPnd	k2'	k2a	BPnd	k2'	k2a
21	F	Mean	3,63	0,91	0,18	4,52	0,93	0,18	3,64	0,64	0,15	5,64	1,26	0,19	3,48	0,80	0,25
		Std Dev	0,59	0,20	0,03	1,06	0,28	0,05	0,92	0,22	0,05	1,29	0,42	0,05	0,78	0,24	0,06
	M	Mean	2,95	0,95	0,28	4,23	0,86	0,24	3,28	0,67	0,20	5,17	1,19	0,28	3,58	0,83	0,36
		Std Dev	0,89	0,27	0,16	1,31	0,26	0,15	0,74	0,21	0,12	1,66	0,49	0,20	0,87	0,31	0,24
42	F	Mean	4,59	0,70	0,10	5,42	0,69	0,10	4,83	0,56	0,08	6,66	1,13	0,10	3,48	0,59	0,13
		Std Dev	0,98	0,16	0,03	0,68	0,19	0,03	0,57	0,16	0,03	1,55	0,52	0,04	0,83	0,20	0,05
	M	Mean	4,01	0,98	0,17	4,64	1,03	0,17	4,50	0,92	0,16	5,53	1,30	0,17	2,94	1,33	0,34
		Std Dev	1,21	0,38	0,10	1,19	0,49	0,11	1,37	0,44	0,12	1,35	0,21	0,08	0,78	1,62	0,39
84	F	Mean	5,55	0,55	0,08	6,49	0,50	0,07	5,18	0,47	0,09	8,47	0,63	0,07	3,95	0,39	0,11
		Std Dev	1,87	0,13	0,01	1,58	0,15	0,02	1,26	0,17	0,05	2,47	0,22	0,01	1,18	0,13	0,04
	M	Mean	5,10	0,74	0,09	6,15	0,74	0,09	6,06	0,67	0,08	7,80	1,05	0,09	3,44	0,53	0,12
		Std Dev	1,45	0,05	0,04	1,30	0,06	0,04	1,67	0,07	0,03	2,37	0,16	0,05	1,06	0,08	0,06
168	F	Mean	5,72	0,70	0,08	7,29	0,72	0,07	6,63	0,56	0,06	9,53	0,97	0,07	4,03	0,49	0,10
		Std Dev	0,97	0,13	0,03	1,16	0,17	0,03	2,28	0,16	0,02	1,43	0,32	0,03	0,74	0,11	0,03
	M	Mean	5,98	0,56	0,09	7,16	0,57	0,08	6,58	0,50	0,08	9,34	0,86	0,08	3,51	0,49	0,14
		Std Dev	1,14	0,16	0,03	1,21	0,25	0,02	1,17	0,19	0,03	1,86	0,66	0,02	0,70	0,07	0,05

Table 1. Descriptives of kinetic parameters obtained by applying SRTM to ^{18}F-FPEB PET scans of rats in different age and gender groups for the evaluated regions. Nucl. accumbens = nucleus accumbens, Std Dev = standard deviation. k_2 = transfer of tracer from the region of interest to the plasma compartment, k_2' = transfer of tracer from reference region to the plasma compartment.

Table 2 Voxel-wise clusters of significant difference between age-groups

	Threshold	Cluster level		Voxel level		Coordinates			Anatomic structure
	P	P_{FWE}	K_E	T	P_{FWE}	X	Y	Z	
Age	0.0001 (FWE)	<0.0001	2511	39.4	<0.0001	-6.0	-6.6	5.9	Hippocampus L
		<0.0001	2397	35.4	<0.0001	6.2	-5.2	6.1	Hippocampus R
		<0.0001	1859	29.3	<0.0001	1.7	0.5	4.1	Striatum R
		<0.0001	1096	27.5	<0.0001	-2.1	0.0	4.0	Striatum L
		<0.0001	846	23.0	<0.0001	-1.7	3.9	1.3	Prefrontal cortex (Cg, PrL)

Abbreviations: FWE = family-wise error corrected, K_E = cluster extent, L / R = left, right. Anatomic structures: Cg = cingulate cortex, PrL = prelimbic cortex.

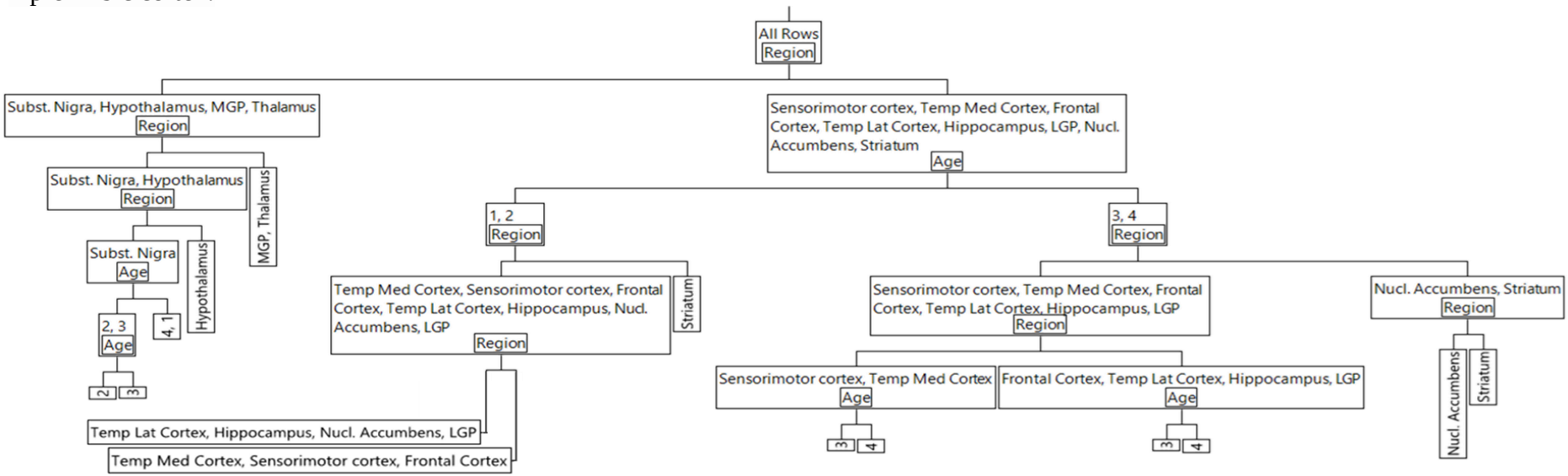


Figure 4. A random forest plot showing which covariates can explain most variance in binding potential. Temp. Lat. / Med. Cortex = temporal lateral / medial cortex, Med. / Lat. Glob. Pal. = Medial / Lateral Global Pallidus, Subst. Nigra = Substantia nigra.

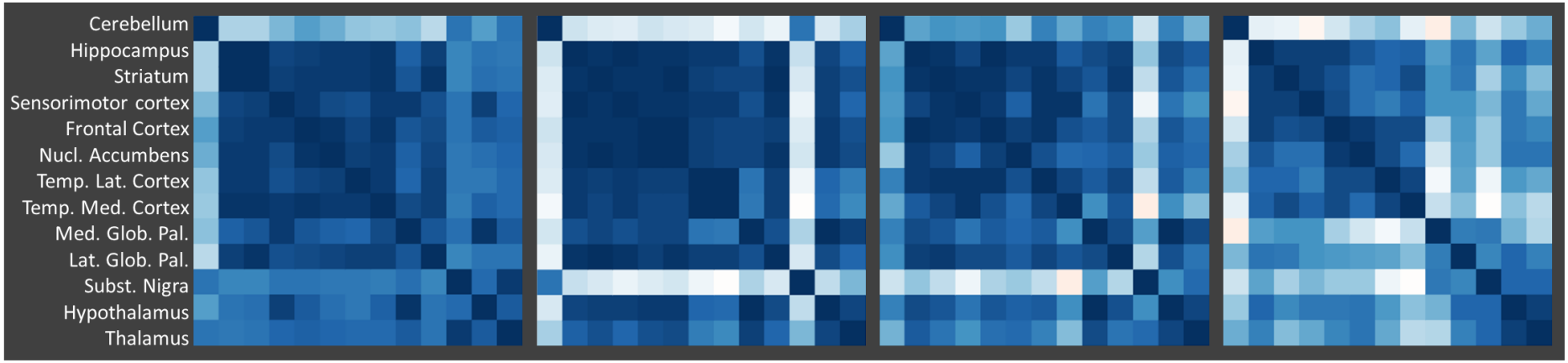


Figure 5. Correlation heat maps show emerging cluster formation in mGluR5 expression. Nucl. Accumbens = nucleus accumbens, Temp. Lat. / Med. Cortex = temporal lateral / medial cortex, Med. / Lat. Glob. Pal. = Medial / Lateral Global Pallidus, Subst. Nigra = Substantia nigra.

3.5 Discussion

We report mGluR5 availability, as measured with ^{18}F-FPEB, to progressively increase in the rat brain between the age of 21 and 168 days. The pattern of this increase differed significantly between different regions, in contrast gender did not have a significant influence. Additionally, we show that age does not influence kinetic parameters estimated by the simplified reference region, with the exception of BP_{ND}. Data clustering showed that after an initial division in high and low mGluR5 availability regions, only subtle differences in clustering between age groups remained. However, network analysis showed the emergence of functional networks that changed with age, consisting of cortical and limbic regions, with a potential pivotal role for the prefrontal cortex.

Protein expression in mammals is known to be influenced by physiological factors such as age and gender in several organ systems, such as striated muscles and the brain (Bischoff-Ferrari et al. 2004; Quadros and Wagner 2008). In the brain for example, different types of receptors have been shown to follow specific and distinctly different expression levels in function of age and brain region, even within the same family of receptors (Letiembre et al. 2007). For example, D2 receptors have been shown to decrease linearly in humans between 20 and 70 years of age (Wong et al. 1984; Antonini and Leenders 1993). On the other hand, preclinical evidence has shown glutamate transporters to increase with age (Ullensvang et al. 1997). A third major pattern seems to be an inverted parabola, observed for example with estrogen and glutamate receptors in rats between 3 and 24 months or 4 and 60 days of age respectively (Pellegrini-Giampietro, Bennet, and Zukin 1991; Wilson et al. 2002). The expression of mGluR5 has been described in the rat for specific brain regions at different ages. For example, the first detectable mGluR5 levels have been reported in Cajal-Retzius cells and pioneer neurons of the marginal zone around the 18th day of the embryonal development (López-Bendito et al. 2002). During the consequent development an important change in distribution has been described, with now expression on interneurons and pyramidal cells throughout the cortex 21 days after birth (López-Bendito et al. 2002). Macroscopically, a relatively uniform expression has been observed by histological staining at P10, although the adult pattern is already emerging (Romano, Van den Pol, and O'Malley 1996). Most information about this period of development, i.e. late embryological and

early post-natal, is derived from either protein expression techniques, such as Western blotting, or usi ng mRNA expression evaluation with PCR (Romano, Van den Pol, and O'Malley 1996). The results of both techniques can be in disagreement, as an abundance of mRNA does not necessarily translate into higher protein expression, due to rate-limiting translational steps. In contrast, the opposite can also be true, when, for example, proteins are less prone to degeneration and equal or higher expression levels can be found in combination with less mRNA concentrations. In the literature of mGluR5, the effect of age is described to be different for protein expression than for mRNA transcription. Also, their relation is not constant in the present literature, with reports of a stronger decrease in protein expression, than mRNA transcription with age in rats between P7 and adult rats. Older rats were reported to have an increasing mGluR5 expression at 3, 12, and 25 months, but decreased mRNA expression in different brain regions (Simonyi et al. 2005). Specifically, an increase in mGluR5 protein expression in the caudate putamen, frontal cortex, but not cerebellum, thalamus or hippocampus was described (Simonyi et al. 2005).

This increase of protein expression with age is contradictory with evidence from investigations at younger ages, which compared P7 with adulthood, or P9 with adulthood for cerebellum and thalamus, and spinal cord (Berthele et al. 1999; Casabona et al. 1997). However, this increase is in agreement with our results, comparing mGluR5 availability at P21, P42, P84, and P168. This discrepancy could be explained by a steep decrease between P9 and P21 in mGluR5 protein expression, which might be reversed into increasing expression at P21. However, such a pattern seems improbable, particularly considering the dynamics of other glutamatergic system parts, which gradually increase up to adulthood (Ullensvang et al. 1997). Therefore, it seems more likely that we have measured functionally available mGluR5, rather than all mGluR5, including endocytosed receptors in vesicles, as is done for example by Western blots (Fourgeaud et al. 2003).

Receptor distribution patterns have been hypothesized to reflect the organizational structure of the brain (Zilles et al. 2002). In effect, these distribution patterns can be tightly correlated with architectonics and functions of specific brain regions, which do not necessarily follow structurally delineated areas (Amunts and Zilles 2015). Although different from the classical temporal network analysis, functional receptor networks have

been shown inherently connected to the temporal activation behavior described by resting-state network analysis (Brier et al. 2016; De Vico Fallani et al. 2014). Moreover, the expression pattern or "fingerprint" of specific receptors has been associated with pathologies, such as schizophrenia (Valles et al. 2014; Zilles et al. 2015). Here we show that the mGluR5 fingerprint in the rat brain changes into specific high correlation clusters. It would be interesting to also assess this functional network strength in pathological situations, e.g. in addiction.

Although ^{18}F-FPEB has been validated as a sensitive and specific method to quantify mGluR5 availability *in vivo*, two potential influences should be kept in mind when interpreting the results reported here. Firstly, due to growth of the brain, structures can be expected to be more compactly positioned at the earlier time-points. As all scans were performed using the same PET scanner, smaller brains will have suffered more from the limited resolution of the PET scanner. In effect, a voxel is more likely to contain a mixture of high and low binding regions in a smaller brain. This phenomenon, called partial volume effect, could therefore have led to an underestimation of the early differentiation when scanning compact younger brains. Secondly, PET results can be ambiguous to a certain extent due to competition between the endogenous ligand and the radiotracer. Here we did not perform glutamate measurements at the different time-points, and thus cannot exclude this potential bias. However, since ^{18}F-FPEB does not bind at the primary glutamate binding place, but rather at a negative modulator binding site, this effect is unlikely to have played a significant role.

In conclusion, we show that the distribution of mGluR5 in the rat brain shows significant post-natal development and differentiation. Specifically, mGluR5 availability is observed to increase with age in highly expressing regions in the rat brain. This increase seems to plateau at the later time-points. We are the first to publish these *in vivo* mGluR5 availability in rats of different ages and are convinced that an animal's age should be taken into account in longitudinal preclinical studies. Additionally, the presented literature evidence supports such a practice not only for mGluR5, but for all receptor density studies. An interesting next step would be to correlate these neuroimaging data with behavioral tests, to assess whether these would demonstrate the same patterns. This could be in combination with a more clinically oriented step, to see whether the

prevalence of mGluR5 related pathologies follows a similar age-dependent pattern and confirm this with a clinical PET study to assess mGluR5 in different age groups.

Chapter 4: Glutamatergic biomarkers for cocaine addiction: A longitudinal study using MRS and mGluR5 PET in self-administering rats

Bart de Laat · Akila Weerasekera · Gil Leurquin-Sterk · Guy Bormans · Uwe Himmelreich · Cindy Casteels · Koen Van Laere

Manuscript under review

4.1 Abstract

Background: Cocaine addiction is a disorder for which no diagnostic biomarkers exist and without effective pharmacotherapy. Research is hampered by the lack of longitudinal data starting before exposure to drugs. The glutamatergic system has been implicated in several components of cocaine and other forms of addiction. Here we present findings in a rat model of cocaine self-administration that was followed longitudinally using the mGluR5 receptor tracer ^{18}F-FPEB PET, ^{1}H-MRS and behavioral tests.

Materials & Methods: Forty-two Wistar rats were scanned with ^{18}F-FPEB PET and ^{1}H-MRS before and after sucrose or IV cocaine self-administration, during withdrawal and relapse. All animals performed a rodent Iowa Gambling Task (rIGT) at baseline to evaluate decision making. Baseline values were used in a mixed model to assess associations with later cocaine use and follow-up measurements were compared to the values before drug exposure.

Results: An increase in pre-exposure rIGT scores were significantly related to both cocaine and sucrose use during the drug-exposure phase. However, only access to cocaine showed a decrease in ^{18}F-FPEB binding compared to pre-exposure binding ($\geq$12$\pm$7%, $p \leq 0.002$). This decrease was most pronounced in the bilateral hippocampus. In this region, mGluR5 availability correlated with the amount of cocaine used during relapse ($p < 0.001$). Compared to the sucrose group, a larger decrease was observed in the hippocampal-prefrontal cortex pathway ($\geq$13%, $p < 0.0001$). Pre-exposure glutamate and glycine concentrations in the prefrontal cortex were significantly associated with cocaine use during the drug-exposure phase ($p < 0.001$). Moreover, prefrontal glutamate exhibited a distinct, reversible decrease (>22%, $p \leq 0.011$) when animals had access to cocaine, but not sucrose.

Conclusion: Baseline values of prefrontal glutamate and glycine are associated with future cocaine use. Furthermore, baseline rIGT scores are associated with the intake of both sucrose and cocaine. Finally, we found that both glutamate concentration and mGluR5 availability decrease during exposure to cocaine.

4.2 Introduction

Substance use disorders are estimated to occur in 10% of the 246 million people using illegal drugs worldwide (UN office on drugs and crime 2015). Beside the heavy burden this places on health systems, a high number of drug users lose their lives prematurely, particularly due to overdoses in polydrug use (Gossop et al. 2002). To date, despite intensive research, therapeutic options for drug use disorders remain limited. This holds especially true for cocaine addiction, largely due to its dynamic and complex neurobiology of addiction to this particular drug (Soyka and Mutschler 2016). For example, prolonged use of cocaine will make it increasingly difficult to achieve the same magnitude of dopamine release as with initial exposures. This is due to several neurological control mechanisms of dopamine release that start playing a more pronounced role. These control mechanisms also influence behavior and their reduced presence can result in the traits that have become associated with cocaine abuse, such as poor decision-making, impulsivity and compulsivity (Kalivas and Volkow 2005; Grant and Chamberlain 2014). Cocaine users are known to perform worse on the Iowa gambling task, a widely used measure of decision-making (Verdejo-Garcia et al. 2007). An important part of these control mechanisms is the glutamatergic system with the prefrontal cortex as its predominant enforcer (Koob and Volkow 2016). In this light, extrasynaptic metabotropic glutamate receptors have gained considerable interst (mGluR) (Anwyl 2009). These receptors, in particular mGluR type 2 and type 5 have a modulatory role which is hypothesized to be disturbed in several psychiatric disorders, including addiction but also autism and obsessive-compulsive disorder (Matosin and Siegel 2016; Conn and Jones 2009). In cocaine addiction, mGluR5 knockout mice have been used to prove mGluR5's role in conditioned locomotor activity and in the signaling cascade involved in the propensity to self-administration (Bird et al. 2010; Chiamulera et al. 2001).

Several drugs have been designed to modulate the glutamatergic system aiming at an anti-addictive effect (Schmidt and Pierce 2010). However, most of them were plagued by toxicity and side-effects or lacked convincing results in clinical trials (Tomek et al. 2013). It has been hypothesized that the latter might be due to our lack of understanding of the dynamics of the addiction process and the absence of suitable biomarkers, as no objective markers to guide pharmaco-psychological treatment currently exist (Garrison and Potenza 2014). Addicted patients normally present themselves after a long history of

their addiction, which is often of a multi-drug nature (Jones, Mogali, and Comer 2012). Therefore, it remains unclear whether observed neurobiological adaptations in long-term addicts are innate characteristics, predisposing the individual for addiction, or rather consequences of the prolonged drug use. Because of these issues, demand has risen to elucidate in more detail the role of the different aspects of the glutamatergic system during different phases of addiction, such as drug-exposure, withdrawal and relapse (Cosgrove 2016).

In this context, we conducted a longitudinal experiment in a cocaine self-administration rat model. This protocol commenced before the exposure to cocaine and followed each animal through its initial drug-exposure, withdrawal and relapse. In every phase, animals were characterized using ^{18}F-FPEB positron emission tomography (PET) for mGluR5 imaging as well as non-invasive proton magnetic resonance spectroscopy (MRS) for glutamate and glutamine. Additionally, at baseline a behavioral test for decision making, namely the rodent Iowa Gambling Task (rIGT) was performed. This information was used to study whether there are baseline markers associated with future drug use. Secondly, assessed where and how these potential markers changed during the different phases of the addictive process.

4.3 Materials and Methods

4.3.1 Animals

Cocaine exposure experiments were performed in duplicate, with in total 36 animals originating from two identical and independent experimental blocks (time difference 14 weeks) (Figure 1). In both blocks, we used 18 adult (110 – 115 days) male Wistar rats (Janvier laboratories, Le Genest St. Isle, France) weighing on average 500 ± 40 g. Additionally, a control group of matched age, gender and weight was installed to control for cocaine independent effects. Since these animals were only exposed to sucrose, a natural reward, no influence of experimental phases were anticipated. Therefore, a smaller number of animals, i.e. 6, was included in this group. All animals were housed individually at an average temperature of 22 °C and under an inversed 12-h light-dark cycle with free access to water. During the experiments animals were kept on a diet of 20 ± 1 g food (Ssniff, Soest, Germany) per day to maintain a stable body weight. At least 7 days before the start of self-administration sessions, rats had a catheter in the femoral

vein inserted. These polyurethane 22G catheters (Instech Laboratories, Plymouth Meeting, USA) were inserted through the femoral vein in cranial direction for 7 cm. A vascular access button was mounted between the shoulder blades using a Dacron® mesh. The research protocol was approved by the Animal Ethics Committees of the University of Leuven (P156/2013), and was carried out in accordance with European Ethics Committee guidelines (decree 86/609/EEC).

4.3.2 Self-administration

Nine experimental test chambers (Med Associates, Fairfax, USA) equipped with a custom-made solid floor, and equipped with two levers were used for self-administration (SA) experiments. One light stimulus above the active lever and acoustic stimulus (2900 Hz) mounted on the opposite wall were activated for the duration of the injection when the active lever was pressed. All test chambers were housed in sound attenuating chambers to mitigate external sounds and light sources. The rats were trained to use the levers with sucrose pellets (45 mg, TestDiet, St. Louis, USA) as reward in ten trainings sessions, until 100 responses within one hour were achieved. After baseline measurements with all tests, rats were given access to cocaine for 3 h per day for 14 consecutive days (Lucantonio et al. 2015). During this time range, they could self-administer cocaine hydrochloride (0.3 mg/kg/infusion) by pressing the active lever one time (FR1 schedule). Cocaine dissolved in NaCl 0.9% was administered IV via a pump infusing 0.05 ml / infusion over 2 seconds. Each administration resulted in a 15 s time-out to prevent lethal doses. After these 14 days, rats were withdrawn from cocaine for 14 days, during which they were not placed in the self-administration boxes. This forced withdrawal period was followed by regained access for 7 days, mimicking a relapse (Figure 1). Catheter patency was tested using 4 mg/kg propofol (Propovet, Abott, Berkshire, United Kingdom) before the first SA sessions and whenever animals showed a decrease in lever presses over 20% within 3 days. Control animals followed the same experimental phases, but continued to receive sucrose pellets as reward and were only scanned at baseline, the second week of self-administration and withdrawal, and in the relapse phase, i.e. week 1, 3, 5, and 6.

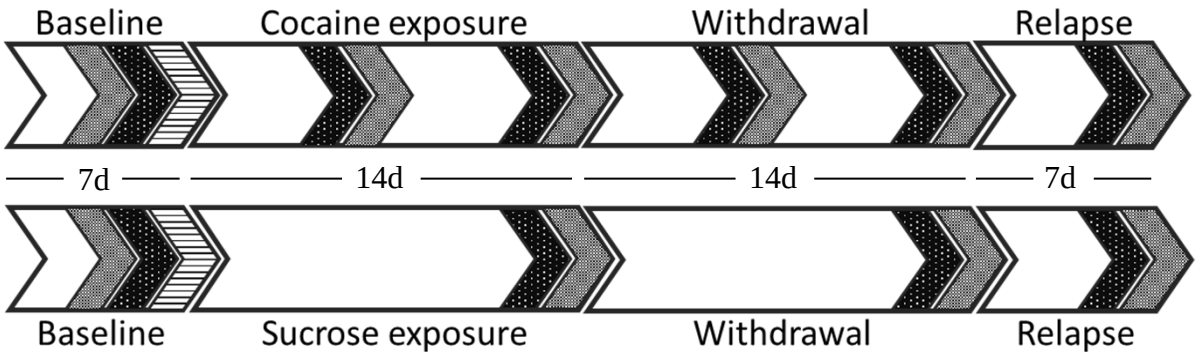


Figure 1. Schematic overview of the experimental design. ▤ = rodent Iowa Gamling Test, ▩ = ^{18}F-FPEB PET, ▩ = ^{1}H-MRS.

4.3.3 Rodent Iowa Gambling Task

Decision making was assessed before exposure to cocaine with the rodent Iowa Gambling Task (rIGT). Behavioral testing took place in a standard five-hole operant chamber with pellet dispenser in a sound-attenuating cabinet (Med Associates, Fairfax, USA). Nose-poke responses were detected with an infrared beam in the five response holes and the pellet receptacle, which were all equipped with tray lights. Before the actual rIGT, two training steps had to be completed with more than 30 responses in 30 minutes. In the first step, animals were trained to make a nose-poke into any response hole, all of which were illuminated. A response turned off the tray lights of the response holes and the food magazine became illuminated, until its infrared beam was breached and this cycle restarted. In the second training step, a random response hole was illuminated, with the exception of the middle nose-poke hole, and a reward was returned only when the animal made a nose-poke in the illuminated hole. In this step, every hole had its own reward-punishment profile (chance of success, reward size (number of pellets), time-out duration (s)) as described by Zeeb *et al*. (Zeeb, Robbins, and Winstanley 2009). More specifically, the maximal reward could be obtained by solely choosing the (P=0.8,2,10) response hole, whereas a more risky choice of the (P=0.4,4,40) option resulted in the least rewards. Smaller losses were experienced with the other two, (P=0.9,1,5) and (P=0.5,3,30) response holes. Finally, in the rIGT task, 4 response holes, with the same reward-punishment profile as before, were illuminated and animals were free to respond during 30 minutes. The outcome, decision making score (DM), was calculated according to the following formula.

$$DM = \frac{\#\ pellets\ rewarded}{\#\ nose\text{-}pokes} - C$$

With C = 2, i.e. the score of optimal decision making.

4.3.4 Small-animal PET imaging

PET scans were performed at approximately the same time during the dark phase on an LSO (lutetium oxy-orthoscilicate) detector-based small-animal tomograph (FOCUS-220; Siemens Medical Solutions USA, Knoxville, USA), which has a transaxial resolution of 1.35 mm in full-width at half-maximum. During PET imaging, rats were kept under gas anaesthesia (2.0% isoflurane, 1.5 l/min O_2), and their body temperature was maintained between 36.5 and 37 °C with a heating pad. Animals were scanned at baseline (n = 33), both drug-exposure weeks (n = 24, n = 25 respectively), both withdrawal weeks (n = 15, n = 21 respectively), and during relapse (n = 22), as a function of the available amount of radiotracer produced and its specific activity. On average 18.5 ± 3.6 MBq (specific activity range: 80 – 301 GBq/µmol, mass dose range: 1.03 – 5.64 µg) was injected into the tail vein using an infusion needle set. Dynamic 60-min scans started simultaneously for three animals with the injection of ^{18}F-FPEB.

List-mode acquisition data were Fourier-rebinned in 33 frames (4×15, 4×60, 5×180, and 8×300). Sinograms were reconstructed using an iterative maximum a posteriori probability algorithm with ordered subsets (MAP; 18 iterations, 9 subsets, fixed resolution: 1.5 mm). All scans were corrected by means of a ^{57}Co-attenuation scan.

PET images were spatially normalized to a custom-made rat brain template in Paxinos stereotactic space (Casteels et al. 2006b). Non-displaceable binding (BP_{ND}) parametric images were calculated with the previously validated simplified reference tissue model (SRTM) for ^{18}F-FPEB in rodents, using the cerebellum as reference region (de Laat et al. 2015). To assess the value of baseline measurements, we performed a VOI-based analysis using PMOD 3.6 (PMOD Technologies, Zurich, Switzerland). For evaluation of changes in ^{18}F-FPEB binding between different phases with a maximal use of information without *a priori* knowledge, PET data were analyzed voxel-wise using SPM12 (Statistical Parametric Mapping, Wellcome Department of Cognitive Neurology, London, UK) (Paxinos, Watson, and Emson 1980). For the SPM analysis, data were analyzed with a

flexible factorial design using subjects and experimental phase as factors (Table 1 & 2). In addition, a voxel-based correlation analysis between the median self-administration per phase and ^{18}F-FPEB BP_{ND} was performed through a multiple regression with median lever presses, and prefrontal glutamate MRS concentration as covariate vector.

4.3.5 Magnetic Resonance Spectroscopy

MRS was performed in a subset of 18 randomly selected animals of the cocaine group, which were scanned each week, as well as all six animals in the sucrose group. All MR images and spectra were acquired with a 9.4T Biospec small animal MR scanner (Bruker Biospin, Ettlingen, Germany) equipped with a horizontal bore magnet and an actively shielded gradient set of 600mT/m (117 mm inner diameter) using a 7 cm linearly polarized resonator for transmission and an actively decoupled dedicated rat surface coil for receiving (Rapid biomedical, Rimpar, Germany). For the selection of MRS voxels, 2D T2-weighted MR images were acquired (RARE sequence, TE = 12.3 ms, TR = 3500 ms, In-plane resolution = 0.14 mm, 12 slices, slice thickness = 0.5 mm). Spectroscopy voxels were manually placed over two *a priori* selected regions: the left nucleus accumbens (2.5x2.5x2.5 mm) medioventrally to the caudate putamen, and the pre-frontal cortex (2x3x2.5 mm) caudally from the rhinal fissure and craniodorsally of the corpus callosum (Supplemental Figure S1). Localized Fast Map shimming was performed before the PRESS sequence (320 averages, TE/TR; 20ms/1.8s). Analyses were performed with jMRUI v5.2. Evaluated metabolites were total creatine (Cr + PCr), γ-aminobutyrate (GABA), glucose, glutamate, glutamine, glycine, lactate, N-acetylaspartate, and taurine. Quantification was performed with the QUEST algorithm using a measured metabolite basis set (Ratiney et al. 2004).

4.3.6 Statistical analysis

All statistical analyses were performed using SAS JMP pro 12.1 (SAS institute Inc., Cary, U.S.A.). By design, the reported data of animals exposed to cocaine were pooled from two independent experiments to minimize the number of false positive results. Moreover, effects are only retained when significant for both blocks or significant for one and consistent in the other, i.e. the estimate of a significant effect in one block contained the estimate of the other block within its 95% confidence intervals. Therefore,

no additional multiple test comparison is applied to avoid false negatives. This approach is not adopted for the reported SPM results due to the nature of its output.

The ability of baseline measurements to explain variability in drug-use during the drug-exposure phase was assessed with linear mixed models including a random effect per animal and animal*day. To visualize these results, we divided the animals in 3 groups based on the baseline value of the variable of interest such that each group contained approximately one third of the total number of animals. The self-administration results were then plotted for these three groups. Differences between the different phases of the experiment are non-parametrically evaluated with a Kruskall-Wallis test, which, if significant, was followed by a Wilcoxon pair comparison. PET data were analyzed using SPM as described above. Significance was defined at the 95% confidence level. The reported values are mean ± standard error of the mean (SEM).

4.4 Results

4.4.1 Self-administration

All catheters remained patent during the experiment. Animals readily self-administered cocaine (median; IQR) during the first (34; 17 - 53) and second (60; 19 - 100) drug-exposure week. Moreover, cocaine intake increased significantly ($z = 9.53$, $p < 0.0001$) during the relapse week (89; 57 – 116) with on average 25 ± 2 lever presses per 3 hours compared to the first drug-exposure period. Sucrose intake by the control group showed a different profile with significantly higher intake during the first (134; 103 – 180, $z = 5.55$, $p < 0.0001$) self-administration week, but no difference between the second self-administration (89; 74 – 123) and relapse week (88; 69 – 104). Median inactive lever presses remained low throughout both the first (1; 0 -4) and second (0.5; 0 – 4) drug-exposure week, as well as during the relapse phase (1; 0 – 4).

4.4.2 Rodent Iowa Gambling Task

Animals performed the rIGT actively with a mean of 164 ± 10 responses in 30 min with a mean DM score of 0.09 ± 0.31. This provided them with 50 ± 3 rewards consisting in total of 98 ± 6 pellets. Mixed model analysis of baseline DM score showed a significant

association with the increase in lever presses during the cocaine exposure phase ($F_{3,78}$ = 9.19, p = 0.001) (Figure 2). Indeed, an increase in DM score with one standard error (0.31) increased the predicted number of lever presses by 36 ± 8. Interestingly, a positive association was also found in the sucrose group ($F_{2,6}$ = 15.71, p = 0.005), with a 66 ± 26 increase in predicted lever presses for the same increase in DM.

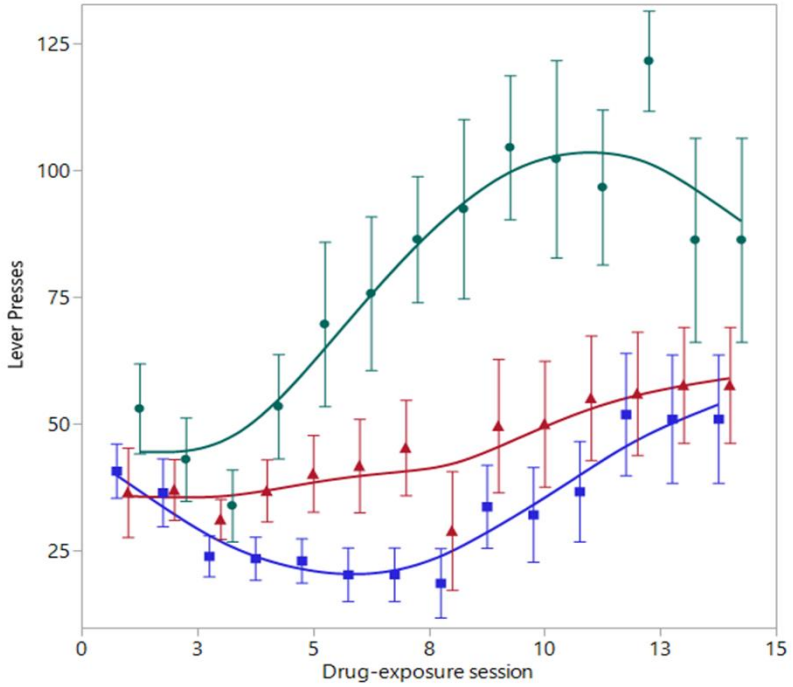


Figure 2. Number of lever presses during the self-administration phase. Cocaine use can be partially explained by pre-exposure scores of decision making in the Iowa gambling task. To visualize this, animals were grouped according to low (■, 0 – 0.15), average (▲, 0.15 – 0.35), and high (●, 0.35 – 0.60) levels of decision making score, with each category containing one third of the observations.

4.4.3 Small-animal PET imaging

All animals showed regional brain-uptake of ^{18}F-FPEB in accordance with the known distribution of mGluR5 (de Laat et al. 2015). Baseline VOI-based BP_{ND} values were used as covariates in a mixed model to assess if there was an association with substance use during the drug-exposure phase, but no significant results were found for either the cocaine or the sucrose group.

We compared the evolution of BP_{ND} in animals self-administering cocaine to that of animals with access to sucrose. Cocaine induced a more pronounced decrease than sucrose, when baseline was compared to the drug-exposure phase in the bilateral nucleus accumbens, agranular insular cortex, and orbital cortex. Additionally, the bilateral CA1 and subiculum regions of the hippocampi showed a significantly larger decrease (Table 1A). During withdrawal, these differences returned to the same differences observed at baseline. However, during the relapse phase, the same regions as during the self-administration were significantly different between both groups (Figure 3). During all phases a significantly lower BP_{ND} was found for the sucrose group in the bilateral striatum, however, this difference was already present at baseline and was therefore not further evaluated in the light of this comparison.

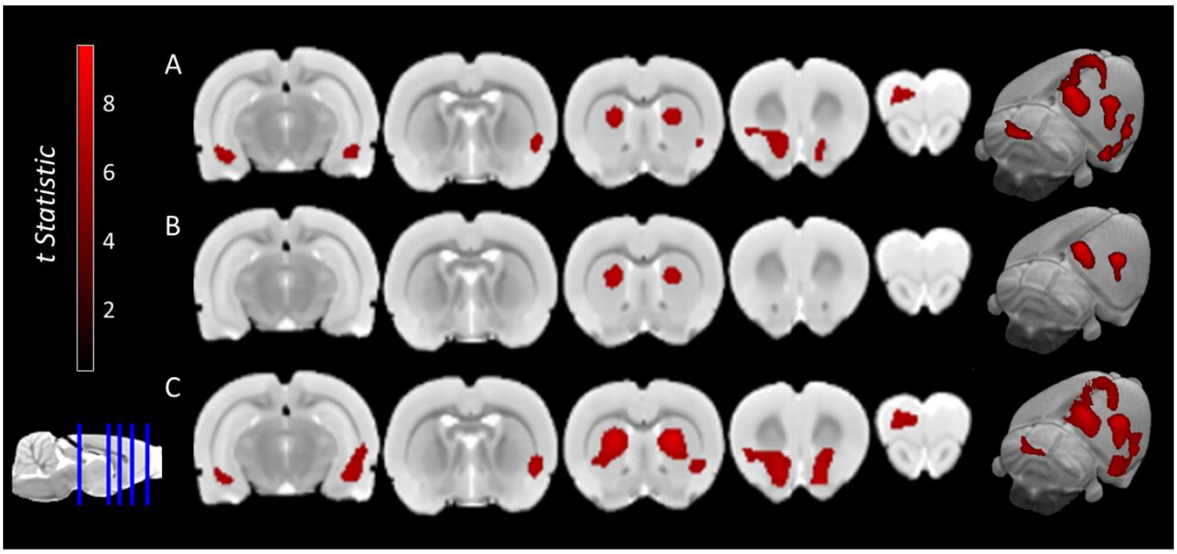


Figure 3. Significant SPM clusters ($p < 0.00001$ FWE) locate the significant differences between animals self-administering sucrose or cocaine during **A**) Drug-exposure, **B**) Withdrawal, and **C**) Relapse.

Voxel-based analysis of the cocaine group demonstrated decreased ^{18}F-FPEB BP_{ND} in the hippocampus bilaterally during the second drug-exposure week, and the relapse phase as compared to baseline (Table 1B). A smaller cluster of decrease was observed during the first and second withdrawal week (Figure 4). During the first week of drug-exposure FPEB BP_{ND} only decreased in the right hippocampus. Other regions that showed a decrease in mGluR5 BP_{ND} in comparison to baseline were the prefrontal cortex during

the second drug-exposure week and relapse. Lastly, a decrease of 14 ± 5% was observed in the bilateral cingulate cortex during the second week of withdrawal.

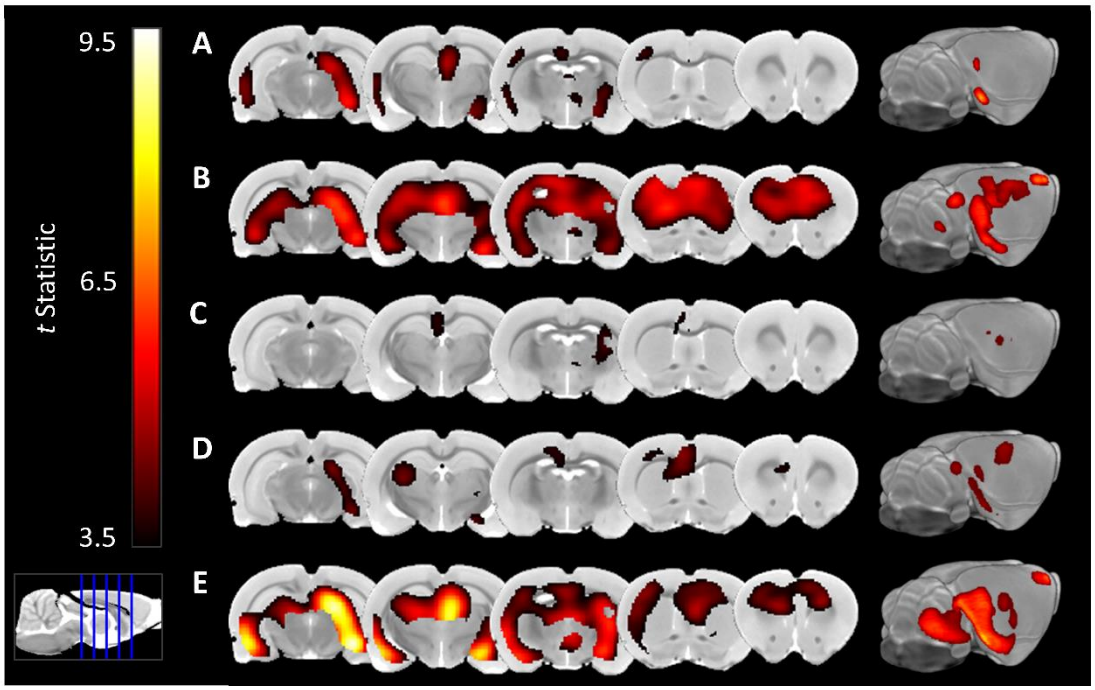


Figure 4. Significant SPM clusters ($p < 0.0005$ Uncorrected) locate the decrease in mGluR5 BP_{ND} of the cocaine group during **A**) Drug-exposure week 1, **B**) Drug-exposure week 2, **C**) Withdrawal week 1, **D**) Withdrawal week 2, and **E**) Relapse. Most extensive clusters of decrease are observed during the weeks of drug exposure in the bilateral hippocampus. A normalization can be observed during both withdrawal weeks (C and D).

Table 1 SPM results for clusters of ^{18}F-FPEB binding

A SPM results for clusters of difference in mGluR5 availability between the cocaine and sucrose group

	Threshold	Cluster level					Voxel level	Coordinates			Anatomical structure
	P	P_{Corr}	K_E	ΔS	ΔC (%)	T	P_{Corr}	X	Y	Z	
Baseline > DE 2	0.00001 (FWE)	<0.0001	1631	3	-14	7.90	<0.0001	2.1	-0.9	5.2	CPU L, NAC L, AI L, OC L
		<0.0001	780	-0	-15	7.82	<0.0001	-2.3	-0.8	5.0	CPU R, NAC R
		<0.0001	397	-3	-16	6.85	<0.0001	-5.5	-1.0	6.5	AI L, OC L
		<0.0001	439	-2	-15	6.69	<0.0001	-5.2	-6.8	6.7	Hippocampus R (CA1, S)
		<0.0001	234	0	-13	6.34	<0.0001	-5.2	-5.8	7.2	Hippocampus L (CA1, S)
Baseline > W2	0.00001 (FWE)	<0.0001	502	0	-15	7.67	<0.0001	-2.3	-0.8	5.0	CPU L, NAC L
		<0.0001	701	5	-14	7.65	<0.0001	2.1	-0.5	4.7	CPU R, NAC R
Baseline > Relapse	0.00001 (FWE)	<0.0001	2478	-0	-24	9.67	<0.0001	-2.3	-0.8	5.0	CPU L, NAC L, AI L, OCL
		<0.0001	2892	0	-13	9.34	<0.0001	2.1	-0.7	5.1	CPU R, NAC R, AI R, OCR
		<0.0001	387	-5	-15	6.89	<0.0001	5.2	-6.8	6.7	Hippocampus R (CA1, S)
		<0.0001	387	-7	-13	6.69	<0.0001	-6.0	-6.0	6.0	Hippocampus L(CA1,S,DG)

B Longitudinal analysis of effect cocaine self-administration on mGluR5 availabilty

	Threshold	Cluster level				Voxel level	Coordinates			Anatomical structure
	P	P_{Corr}	K_E	Decrease (%)	T	P_{Corr}	X	Y	Z	
Baseline > DE 1	0.005 (FWE)	<0.0001	1470	37±6	5.95	0.01	3.2	-6.2	6.6	Hippocampus R (DG)
Baseline > DE 2	0.005 (FWE)	0.0003	533	20±8	6.90	<0.0001	-0.4	-5.4	2.4	Prefrontal cortex (FAC,PLC)
		<0.0001	20986	25±8	6.68	<0.0001	2.2	-4.8	5.6	Hippocampus BL, CPU (DG)
Baseline > Relapse	0.005 (FWE)	<0.0001	14223	19±7	9.50	<0.0001	3.8	-6.4	6.8	Hippocampus R (DG)
		0.0003	539	12±7	9.04	<0.0001	-0.2	-5.8	2.4	Prefrontal cortex (PLC)
		<0.0001	4108	14±8	8.35	<0.0001	-6.0	-5.2	7.2	Hippocampus L (CA1)
Baseline > W1	0.0005 (Unc)	0.003	2330	19±6	4.18	0.02	0.6	-1.2	4.4	Hippocampus BL (FoHC)
Baseline > W2	0.0005 (Unc)	0.002	2866	14±5	4.62	0.004	-0.4	-0.4	2.0	Cingulate cortex (A2)
		0.03	807	4±4	4.57	0.005	-3.2	-4.4	4.0	Hippocampus L (CA3)
		0.04	2229	12±5	4.55	0.005	3.8	-6.4	7.0	Hippocampus R (DG)

Table 1. Abbreviations: DE 1 / 2 = drug-exposure week 1 / 2, W1 /2 = withdrawal week 1 / 2, FWE = family wise error corrected, Unc = uncorrected, K_E = cluster extent, ΔS = difference in BP_{ND} for the sucrose group, when compared to baseline images, ΔC = difference in BP_{ND} for the cocaine group, when compared to baseline images. Anatomical structures: DG = dentate gyrus, FAC = frontal association cortex, PLC = prelimbic cortex, S = subiculum, CA1 = region CA1 of the hippocampus, FoHC = fimbriae of hippocampus, A2 = region A2 of the cingulate cortex. CPU = striatum, NAC = nucleus accumbens, AI = agranular insular cortex, OC = orbital cortex.

Voxel-based correlation analysis showed a positive correlation ($z = 3.55$, $p < 0.001$) between the median lever presses value per cocaine, but not sucrose, administration phase and the paired absolute ^{18}F-FPEB BP_{ND} in the left ($K_E = 281$, x = -3.2, y = 8.0, z = 2.8, $p_{Cluster\ Level} = <0.0001$) and right ($K_E = 234$, x = 3.2, y = 8.2, z = 3.2, $p_{Cluster\ Level} = <0.0001$) subiculum of the hippocampus. Classification of animals based on ^{18}F-FPEB BP_{ND} in this cluster showed that this effect was most important during the relapse phase (Figure 5).

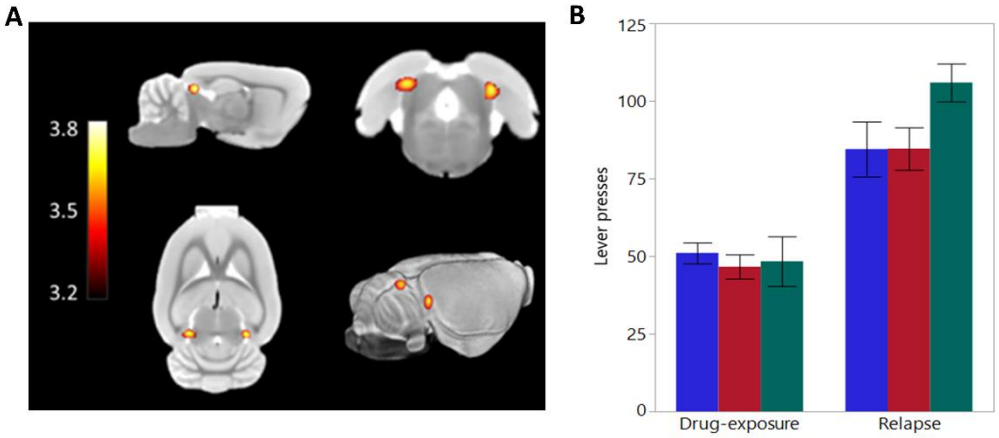


Figure 5. **A**) Clusters of mGluR5 binding that positively correlated with the quantity of cocaine use in the bilateral subiculum. **B**) The positive correlation with lever presses is only distinguishable during the relapse phase. Observations are categorized by low (1.1 – 2.5), average (2.5 – 3.2) or high (3.3 – 4.4) ^{18}F-FPEB binding potential, with each group containing approximately one third of all observations. Error bars represent SEM.

4.4.4 Magnetic Resonance Spectroscopy

All measured metabolites were in line with previously reported ranges for healthy rats (Pfeuffer et al. 1999). For example, average prefrontal concentrations of glutamate at 6.2 ± 0.08 mmol/L and glycine at 0.5 ± 0.006 mmol/L at baseline were measured. Interestingly, mixed models showed a significant association for prefrontal glutamate ($F_{2,36} = 8.98$, $p < 0.001$) and glycine ($F_{2,36} = 17.41$, $p < 0.001$) with cocaine use during the drug-exposure phase (Figure 6). Indeed, an animal with 1 mmol/L higher prefrontal glutamate concentrations was related to, on average, 14.9 ± 4.1 more lever presses per session. On the other hand, an increase of 1 mmol/L in prefrontal glycine was related to an overall increase of 13.6 ± 2.6 lever presses. The only metabolite for which a significant effect of cocaine exposure was found on the measured prefrontal concentration was glutamate. In particular, a decrease was observed when animals had access to cocaine in the first week of drug-exposure (1.46 ± 0.53 mmol/L, $z = 2.74$, $p = 0.006$), and during the relapse phase (1.37 ± 0.54 mmol/L, $z = 2.54$, $p = 0.011$) compared to baseline. Additionally, a significant difference was also observed between the first and second withdrawal week and the same phases, i.e. the first drug-exposure week (0.93 ± 0.56, $z = 2.15$, $p < 0.031$ and 1.01 ± 0.65, $z = 2.46$, $p < 0.013$) and relapse (0.85 ± 0.56, $z = 1.96$, $p = 0.049$ and 0.93 ± 0.66, $z = 2.32$, $p = 0.020$) (Figure 6). No significant differences were found between the different phases in any metabolites, nor were there any significant associations with baseline measurements for the nucleus accumbens region and the sucrose group.

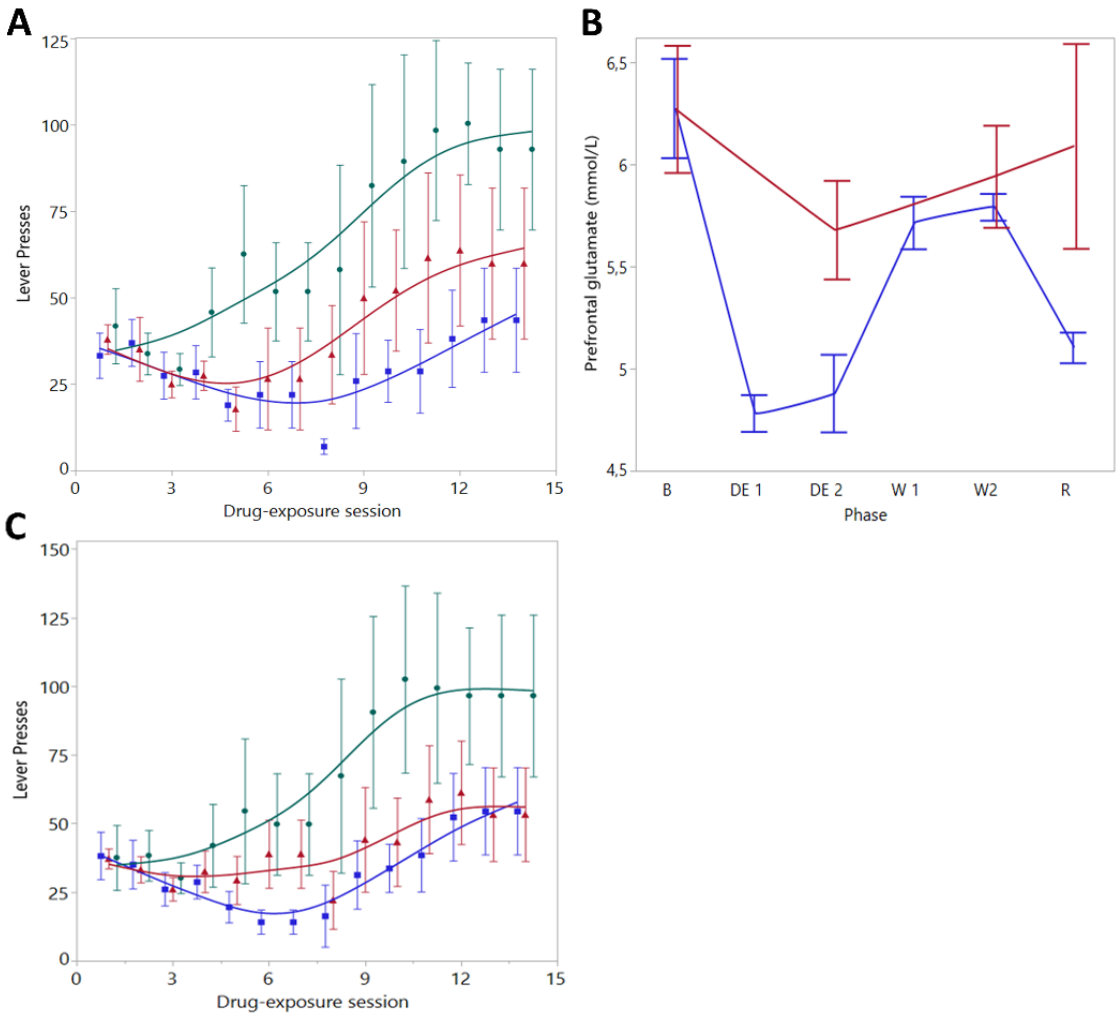


Figure 6. **A**) Number of lever presses during the self-administration phase. Cocaine use can be partially explained by the level of prefrontal glycine concentration (mmol/L). For visualization purposes, animals were categorized in low (■, 0.20 – 0.45), average (▲, 0.45 – 0.55) and high (●, 0.55 – 1.00) concentrations, with one third of observations in each category. **B**) Prefrontal glutamate levels as measured with *in vivo* MRS show a strong, but reversible, effect of exposure to cocaine (blue), but not sucrose (red). **C**) Cocaine use during the drug-exposure phase as explained by prefrontal glutamate concentration. **A**nimals are categorized in low (■, 4.3 – 5.5), average (▲, 5.5 – 6.8) and high (●, 7.2 – 13.5) concentrations, with one third of observations in each category. Error bars represent SEM.

A possible relation among the reported significant baseline measurements was investigated using a non-parametric correlation analysis. No significant correlation was found between the rIGT and either prefrontal glutamate or glycine concentrations.

However, between the latter two, a significant correlation of $\rho = 0.77$ ($p < 0.0001$) was found.

Finally, since prefrontal concentrations of glutamate showed significant changes between the different phases, we also investigated a relationship between glutamate and the mGluR5 BP_{ND} in the prefrontal cortex, as measured with ^{18}F-FPEB PET. However, no significant association was found with the voxel-by-voxel analysis.

4.5 Discussion

In a longitudinal rat model of cocaine self-administration, we showed that baseline measurements of the rIGT, prefrontal glycine and glutamate can be associated with future cocaine use as expressed by the number of lever presses. Furthermore, by mimicking withdrawal and relapse after the initial drug-exposure, we observed that this induced a distinct cocaine dependent pattern in prefrontal glutamate. A similar pattern was found in mGluR5 availability, explicitly for the hippocampus. Moreover, hippocampal mGluR5 availability decreases were associated with the level of cocaine intake during the drug-exposure and relapse phases. Compared to sucrose self-administration decreases were found in the bilateral hippocampus, nucleus accumbens, insular and orbital cortex during the phases with drug-exposure.

Patients with substance abuse disorders typically show an impaired ability of decision making (Bechara 2005). More specifically, they have on average more difficulty evaluating negative consequences of a choice (Paulus 2007). A long-standing question in addiction research is whether this character trait is pre-existing or a result of the neurobiological changes induced by the drug use or the resulting addiction (Grant and Chamberlain 2014). Research in patients has been unable to answer this question definitively, as most studies are performed only after the transition into addiction. Recently, the rodent Iowa Gambling task has been proposed and validated to evaluate decision making in rats (Zeeb, Robbins, and Winstanley 2009). Using this test, we were able to show that animals with lower rIGT scores had higher future intake of either sugar or cocaine. This might indicate an inverse relation between decision making and reward salience that transcends reward type (Dichter, Damiano, and Allen 2012). The described

relation considers both the predictor variables and the future drug-use as continuous variables, rather than the discrete classification of "addicted". We opted for this approach, not only since addiction can be considered as a dimensional diagnosis, but also since diagnosing addiction in animals can be problematic (Helzer, Van den Brink, and Guth 2006; Deroche-Gamonet, Belin, and Piazza 2004).

We compared the change in mGluR5 availability after exposure to cocaine, to that after sucrose self-administration. When animals had access to their respective reward, a significant decrease was observed in the bilateral nucleus accumbens, insular and orbital cortex, and the CA1/Subiculum region of the hippocampus. This cluster of regions is known as the hippocampo-prefrontal cortex pathway in the rat (Thierry et al. 2000). This pathway originates in the CA1/Subiculum fields and projects to the orbital cortex, while both sites have projections towards the nucleus accumbens. Its central role in motivational processes is confirmed by preclinical genetic studies, as well as clinical imaging studies of cocaine dependent patients (Winstanley et al. 2007; Milella et al. 2014). The robust difference in mGluR5 availability in these region between both groups is interesting and relevant to the ongoing debate whether food rewards should be considered on the same scale as drugs of abuse, or rather as a separate group of motivators (DiLeone, Taylor, and Picciotto 2012). Although sucrose can be an equally strong, or stronger, incentive than cocaine, it does not directly interfere with the dopaminergic system (Cantin et al. 2010). This could lead to the hypothesis that the observed neurobiological changes are due to unnaturally high synaptic dopamine levels elicited by cocaine, rather than the inherently pleasurable effects of both sucrose and cocaine.

This is the first addiction study, in which mGluR5 availability is assessed longitudinally. We report a decrease in mGluR5 availability after exposure to cocaine, particularly in the hippocampus, although other regions, such as the prefrontal cortex, are also implicated. This is in accordance with literature reports in humans showing decreased mGluR5 binding in cocaine dependent individuals (Milella et al. 2014). Withdrawal from cocaine induced normalization of mGluR5 availability, although localized smaller decreases remained. This normalization is similar to the one observed in the prefrontal glutamate concentration and could hint towards a general downregulation of the glutamatergic system during drug-exposure. Interesting is the observed cortical increase in mGluR5

availability during access to sucrose, without involvement of the hippocampus. A differential effect on synaptic activity between heroin and sucrose has already been described, and could explain this observation (Schmidt et al. 2005).

The cocaine induced decreases were most explicit in the hippocampus, which can be considered as a corroboration of the hypothesis that addiction is in part a pathologically strong learning process (Berridge, Robinson, and Aldridge 2009). According to this hypothesis, individuals start off with sporadic drug use, but these seemingly harmless exposures are key in the formation of memories that will later drive the compulsive behavior typical for addiction. Indeed, lesions in the hippocampus, and more specifically the subiculum, reduce cocaine use in rats (Caine et al. 2001). Interestingly, the bilateral cluster within the hippocampus we found to be associated with the amount of cocaine use is located in the subiculum. Specifically, higher mGluR5 densities in this region are related to higher drug intake during relapse. This could suggest that mGluR5 availability in the subiculum is involved in the formation of drug-associated memories, which later induce craving. This is in line with the existing hypothesis that addictive behavior arising from the center of the nucleus accumbens is heavily influenced by glutamatergic input from the subiculum (Everitt et al. 1999).

The glutamatergic system acts as an essential conductor of the response to drugs on both a molecular and behavioral level (Brown, Kupchik, and Kalivas 2013). In the prefrontal cortex, one of the main effectors of the mesolimbic reward system, lower glutamate levels have been measured with ^{1}H-MRS in human chronic cocaine users (Yang et al. 2009). Additionally, lower extra-cellular basal glutamate levels have also been reported in rats after methamphetamine self-administration (Parsegian and See 2014). Here we confirm this decrease in cocaine exposed animals as measured with ^{1}H-MRS and show that normalization occurs during withdrawal. This complements the data of Hermann *et al*., who show that drug-exposure leads to an increase in prefrontal glutamate lasting up to 60 hours after exposure, which then progressively decreases lower than the baseline (Hermann et al. 2012). Additionally, in humans a similar normalization is observed during alcohol-abstinence (Umhau et al. 2010). Indeed, Meshul *et al.* report a significant decrease after 2 days of withdrawal, which is no longer present after 14 days (Meshul et al. 1998). However, cross-sectional results alone can be misleading, e.g. based on O'Neill *et al*. the decrease in glutamate could be considered a direct effect of withdrawal, whereas

we show here that it is rather a remnant of the earlier exposure to cocaine (O'Neill et al. 2015). This emphasizes the need for longitudinal experiments in addiction research, allowing us to study the temporal dynamic of biological processes.

Glycine is an obligatory co-agonist of glutamate at the NMDA receptor (Turecek and Trussel 2001) and plays an important role in the dopamine-elevating properties of drugs (Chau, Soderpalm, and Ericson 2011). Indeed, several rat studies have shown that antagonists of glycine can reduce the addictive properties of cocaine (Zhou et al. 2012). However, we are the first to report that glycine levels before drug-exposure can have an explanatory value for cocaine use in rats. Furthermore, we report that exposure to and withdrawal from cocaine nor sucrose influenced these concentrations. Although glycine has not yet been implicated in addicted patients, a clinical trial with the glycine transporter-1 inhibitor Org 25935 was performed in patients with alcohol dependence (de Bejczy et al. 2014). The trial was stopped midway when evidence of efficacy was lacking. However, no complete dose-response study was performed, making it difficult to evaluate the true value of this trial. Other pathologies, in which dysregulation of the glutamatergic system is also believed to be fundamental, namely schizophrenia, glycine has been found to be correlated with the severity of symptoms (Hons et al. 2010). Therefore, we believe glycine could be an interesting target deserving future studies into the pathophysiology and therapy of cocaine addiction.

In conclusion, we report the temporal dynamics of several important mediators of cocaine self-administration in rats, before and after drug-exposure. Specifically, prefrontal glycine and glutamate are found to be very interesting biomarkers of vulnerability for cocaine use. Furthermore, we show that mGluR5 availability and prefrontal glutamate concentrations are influenced by exposure to cocaine in a different way than by sucrose. Finally, decision making is observed to be associated with future drug use. Considering the high degree of similarity in pathophysiology, preclinical data as presented here may be considered of translational value (Koob 2014). Although these findings are an advancement in our understanding of the pathophysiology of addiction, a more complete picture could result from the following steps. Firstly, similar setups should be imposed on animals with access to other drugs, such as e.g. nicotine and alcohol. Secondly, the important decrease in mGluR5 in the hippocampus warrants localized ^{1}H-MRS

observations in this region. Thirdly, the findings of this paper should be confirmed in more experimental setups, for example with localized gene-knock down or glycine synthesis inhibitors before drug-exposure. Despite this required future work, our study already provides a reference for longitudinal studies and can guide the interpretation of both clinical and preclinical cross-sectional studies.

Supplemental Figure

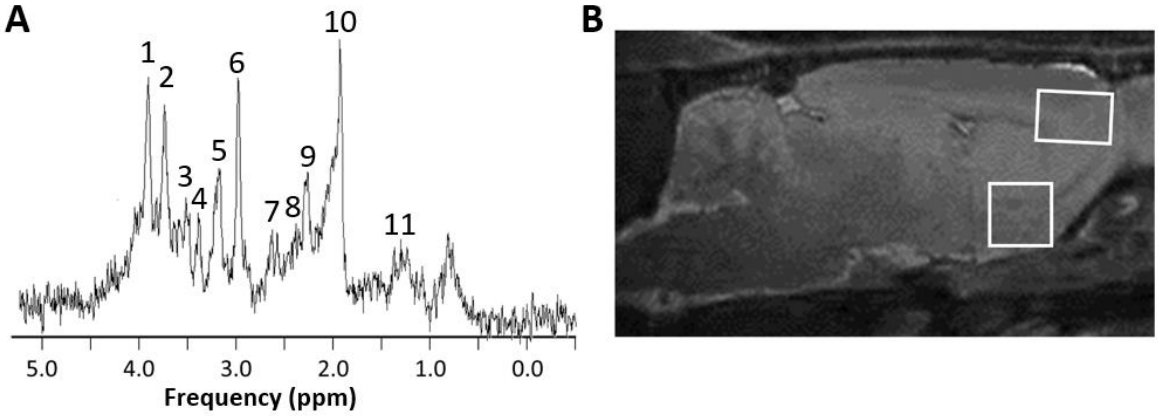


Figure S1. A) Example of a spectrum obtained from the prefrontal nucleus voxel. 1 = Creatine; 2 = Ascorbate, glutamine, glutamate, glutathione; 3 = myo-inositol; 4 = Taurine; 5 = Taurine, glycerophosphocholine, phosphocholine; 6 = Creatine, 7 = Aspartate, N-acetylaspartate; 8 = N-acetylaspartate, glutamine; 9 = glutamate; 10 = N-acetylaspartate; 11 = Alanine, lactate. **B)** Illustration of voxel position for spectroscopy on a sagittal image.

Chapter 5: Effects of alcohol exposure on the glutamatergic system: A combined longitudinal ^{18}F-FPEB and ^{1}H-MRS study in rats

Bart de Laat · Akila Weerasekera · Gil Leurquin-Sterk · Willy Gsell · Guy Bormans · Uwe Himmelreich · Cindy Casteels · Koen Van Laere

Manuscript under review

5.1 Abstract

Introduction: Alcohol use disorders (AUDs) are an important health and socio-economic issue. Although limited pharmacological and behavioral treatments exist, these are not very effective and a large number of individuals with AUDs remain. This is in part due to its elusive neurobiological dynamics. Recent studies have implicated an important role for the glutamatergic system in impulse control. As rodent models allow instatement of alcohol abuse and follow-up to a withdrawal phase, we conducted a longitudinal study on specific glutamatergic and behavioral aspects of alcohol exposure in rats, using a two-bottle choice paradigm.

Materials & Methods: In this paradigm, rats had 24h alternating access to either water alone or water and a solution consisting of 20% v/v alcohol, or 10 mM saccharin for control animals. Rats were followed through a baseline, exposure and withdrawal phase with ^{1}H-magnetic resonance spectroscopy to measure prefrontal glutamate and glycine concentrations. Additionally, ^{18}F-FPEB PET was used to assess metabotropic glutamate receptor 5 (mGluR5) availability before and after exposure to alcohol or saccharin. Finally, anxiety levels of rats were assessed with an open field test at baseline.

Results: We found that the total distance travelled in the open field test and mGluR5 availability in the nucleus accumbens were associated with future alcohol preference ($p = 0.02$). Furthermore, prefrontal glutamate decreased significantly during alcohol exposure ($> -1.25 \pm 0.55$ mmol/L, $p = 0.038$) and normalized during withdrawal. Finally, voxel-based analysis of the ^{18}F-FPEB PET showed that exposure to alcohol resulted in decreased mGluR5 availability in the hippocampus (>14±3%, $p_{Cluster} = 0.047$) and amygdala (>16±2%, $p_{Cluster} = 0.004$), whereas saccharin exposure induced decreases in the prefrontal cortex (11±1%, $p_{Cluster} = 0.035$) and hippocampus (15±2%, $p_{Cluster} = 0.003$). A direct comparison of both groups showed differences in mGluR5 availability in the striatum bilaterally (-2±4% vs +2±2%, $p_{Cluster} = <0.0001$) and hippocampus (-16±4% vs -5±4%, $p_{Cluster} = <0.0001$).

Conclusion: this study corroborates the anxiolytic effect of alcohol, and provides evidence for mGluR5 downregulation in the amygdala as potential underlying mechanism. Saccharin and alcohol self-administration differentially influence the prefrontal glutamate concentrations, but both induce an mGluR5 decrease, potentially to modulate the dopamine release that can be elicited.

5.2 Introduction

The worldwide alcohol consumption is estimated to be on average 6.2 liters of pure alcohol, used in this article as a synonym for ethanol, per person. This results in alcohol being responsible for 5.1% of the global burden of disease and injury (World Health Organization 2014). Consumption is initially motivated by the induced euphoria, but chronic alcohol abuse is often attributed to its negative reinforcing capacities (Koob 2013), which also explains some of the associations that exist between alcohol abuse and mental illnesses, such as anxiety disorders (Lai et al. 2015). The positive reinforcement of alcohol consumption, is thought to be mainly the result of both a direct excitability effect on dopaminergic neurons, and an inhibitory effect on the GABAergic transmission to dopaminergic neurons (Trantham-Davidson and Chandler 2015; Xiao and Ye 2008). Next to this dopaminergic pathway, the glutamatergic system is also influenced by alcohol. This influence can be attributed to an inhibition of the NDMA receptor, not only through the maintenance of the protein kinase C (PKC) mediated phosphorylation hereof, but also by alcohol being a competitive inhibitor of glycine, a co-agonist of the NMDA receptor (Chen and Roche 2007; Woodward 1990). Recently, it has been shown that the acute reduction in prefrontal functioning by alcohol, commonly seen in patients with alcohol use disorders, is glycine receptor dependent (Badanich et al. 2013).

The effects of alcohol on the glutamatergic system are however, not restricted to the NMDA receptor. Our group recently showed that patients addicted to alcohol have decreased metabotropic glutamate receptor type 5 (mGluR5) availability using ^{18}F-FPEB PET (Leurquin-Sterk et al., submitted). Interestingly, Schwendt *et al.* showed that PKCε is also a downstream signaling target of mGluR5, whose translocation can induce the internalization of the mGluR5 (Schwendt and Olive 2016). Additionally, using mice with selective mGluR5 knock-down in dopaminergic neurons, it was shown that mGluR5 is involved in alcohol relapse (Parkitna et al. 2013). Moreover, the mGluR5 antagonist 6-methyl-2-(phenylethynyl)pyridine (MPEP) was shown to be able to reduce ethanol consumption in mice, through a PKCε dependent mechanism (Olive et al. 2005).

There has been a call for longitudinal experiments in addiction research, not only on a behavioral level, but also on the dynamic molecular changes occurring during exposure to alcohol (Cosgrove 2016). Neuroimaging provides a unique opportunity to non-invasively study the intact brain, thus allowing a systems biology approach integrating interactions and interplay of many levels of biological information (Tabakoff and

Hoffman 2013). In this light, animal studies are especially suitable, since they can, unlike clinical studies, provide a pre-exposure baseline measurement. These baseline measurements allow a more quantitative interpretation of changes observed after drug exposure and can thus make a distinction between pre-existing traits and drug induced changes. Moreover, patient studies are typically plagued by the prevalent comorbid nicotine exposure, which complicates the deciphering of the neurobiology of alcohol addiction (Chou et al. 2016). Therefore, animal models are valuable as translational models for the molecular basis of the effect of alcohol exposure (Spanagel 2003).

In this context, we conducted a longitudinal experiment in which rats could choose between water and a 20% v/v alcohol solution, or 10 mM saccharin for the control group, for 24 hours. This was alternated with 24 hours during which only water was accessible (Simms et al. 2008). The protocol commenced before the exposure to alcohol or saccharin and followed animals through a seven week exposure, as well as a one week forced withdrawal phase. In every phase, animals were characterized using non-invasive proton magnetic resonance spectroscopy (^{1}H-MRS). Additionally, a subset of animals was scanned with ^{18}F-FPEB PET for mGluR5 imaging before and after exposure to alcohol or saccharin. Finally, anxiety was assessed at baseline using the open field test. The gathered data were used to study whether baseline markers could be identified that are associated with future drug use. Secondly, we hypothesize that alcohol will be able to induce changes between the different experimental phases, which will only be the case to a lesser extent for sucrose.

5.3 Materials and Methods

5.3.1 Animals

Experiments were conducted on 24 adult male Wistar rats (Janvier laboratories, Le Genest St. Isle, France) weighing on average 343 ± 18 g at the time of the experiments. All animals were individually housed in an average room temperature of 22 °C under an inversed 12-h light-dark cycle. During the experiments animals were kept on a diet of 20 ± 1 g food (Ssniff, Soest, Germany) per day to maintain a stable body weight. The research protocol was approved by the local Animal Ethics Committees of the University

of Leuven (P156/2013), and was carried out in accordance with European Ethics Committee guidelines (decree 86/609/EEC).

5.3.2 Self-administration

After baseline measurements, animals were subject to an alternating 24 hour access two-bottle paradigm, which was previously shown to reliably induce alcohol intake in Wistar rats (Simms et al. 2008). During the exposure phase, access was granted to either a water bottle alone or to both a water and a solution bottle, changing between both every 24 hours (Simms et al. 2008). This solution consisted of a 20% v/v dilution of 99% v/v percent stock alcohol (VWR, Leicestershire, U.K.) for 18 experimental animals, or a 10 mM saccharin solution (Sigma-Aldrich, St. Louis, USA) for 6 control animals. Both groups also underwent an 8-day withdrawal phase, during which only a bottle of water was made available, to assess the reversibility of alcohol induced changes (Figure 1). Alcohol or sucrose preference, calculated as the ratio between the solution and water consumption, was used as outcome. As manipulation and placement of bottles led to a spill of approximately 1 g, consumption was defined as the weight difference before and after placement minus one. For the two bottle days, the side of the substance solution was alternated to avoid side-preference bias.

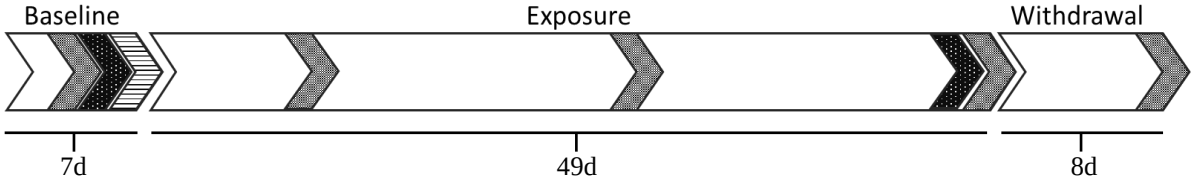


Figure 1. Schematic overview of the experimental design. = Open Field Test, = ^{18}F-FPEB PET, = ^{1}H-MRS.

5.3.3 Open Field Test

The open field consisted of a standard arena with an 80 cm diameter with surrounded by a 40 cm rim. Rats were recorded with a Logitech C920 1080p HD camera (Logitech, Romanel-sur-Morges, Switzerland), which allowed custom-built videotracking software to determine the rat's position in one second intervals (30 frames). Extracted parameters were the total distance travelled during one session and the average distance from the center of the field during this period, which have been used as surrogate markers for anxiety (Prut and Belzung 2003).

5.3.4 Magnetic Resonance Spectroscopy

Magnetic resonance spectroscopy (MRS) was performed at baseline, exposure week 5, and after withdrawal. Additionally, alcohol exposed animals were also scanned at exposure week 2 and 7. All scans were acquired with a 9.4T Biospec small animal MR scanner (Bruker Biospin, Ettlingen, Germany) equipped with a horizontal bore magnet and an actively shielded gradient set of 600mT/m (11.7 cm inner diameter) using a 7 cm linearly polarized resonator for transmission and an actively decoupled dedicated rat surface array coil for receiving (Rapid Biomedical, Rimpar, Germany). During MR imaging, rats were kept under gas anaesthesia (2.0 % isoflurane in oxygen at a flow rate of 1.5 l/min), and their body temperature was maintained between 36.5 and 37.0 °C with a circulating warm water bed. Spectroscopy voxels were manually placed on the pre-frontal cortex (2 x 3 x 2.5 mm) caudally from the rhinal fissure and craniodorsally of the corpus callosum. Localized Fast Map shimming was performed before the PRESS sequence (320 averages, TE/TR; 20ms/1.8s). A representative obtained spectrum and the spectrum location can be found in Figure S1. Analyses were performed with jMRUI v5.2 to assess glutamate and glycine concentrations (Stefan et al. 2009). Quantification was performed with the QUEST algorithm using a measured metabolite basis set (Ratiney et al. 2004).

5.3.5 Small-animal PET imaging

A subset of animals were scanned before and after exposure to alcohol or saccharin, on a LSO (lutetium oxy-orthoscilicate) detector-based small-animal tomograph (FOCUS-220; Siemens Medical Solutions USA, Knoxville, TN), which has a transaxial resolution of 1.35 mm in full-width at half-maximum. Data were acquired in a 128×128×95 matrix with a pixel width of 0.95 mm and a slice thickness of 0.796 mm. The coincidence window width was set at 6 ns. During PET imaging, rats were kept under gas anesthesia (2.0 % isoflurane in oxygen at a flow rate of 1.5 l/min), and their body temperature was maintained between 36.5 and 37 °C with a heating pad. Animals were scanned at baseline (n = 15) and after drug-exposure (n = 21) depending on the available amount of radiotracer and its specific activity. On average 14.9 ± 0.4 MBq (specific activity range: 88 – 100 GBq/µmol, mass dose range: 2.27 – 3.93 µg) was injected into the tail vein using an infusion needle set. Dynamic 60-min scans started simultaneously with the injection of ^{18}F-FPEB per three animals.

List-mode acquisition data were Fourier-rebinned in 33 frames (4×15, 4×60, 5×180, and 8×300). Sinograms were reconstructed using an iterative maximum a posteriori probability algorithm with ordered subsets (MAP; 18 iterations, 9 subsets, fixed resolution: 1.5 mm). All scans were corrected by means of a ^{57}Co-attenuation scan. PET images were normalized to a custom-made rat brain template in Paxinos stereotactic space, allowing the use of a predefined volume-of-interest (VOI) map and of statistical parametric mapping (Casteels et al. 2006b). Non-displaceable binding (BP_{ND}) was calculated with the previously validated simplified reference tissue model (SRTM) for ^{18}F-FPEB in rats using the cerebellum as reference region (de Laat et al. 2015). To evaluate the value of baseline measurements, we performed a VOI-based analysis on the nucleus accumbens, hippocampus, prefrontal cortex and striatum using PMOD 3.6 (PMOD Technologies, Zurich, Switzerland). For evaluation of changes between baseline and post-exposure ^{18}F-FPEB binding with a maximal use of information without *a priori* knowledge, PET data were analyzed voxel-wise with SPM12 (Statistical Parametric Mapping, Wellcome Department of Cognitive Neurology, London, UK) using a flexible factorial design with the maximally stringent threshold, which was in this case p_{Uncor} = 0.002. This design was also used to directly compare the effect of alcohol versus saccharin, but here with a more stringent threshold of p_{Uncor} = 0.00002. In addition, a voxel-based correlation analysis of baseline ^{18}F-FPEB BP_{ND} and total distance travelled was performed through a multiple regression with total distance travelled as covariate vector.

5.3.6 Statistical analysis

All statistical analyses were performed using SAS JMP pro 12.1 (SAS institute Inc., Cary, U.S.A.). The ability of baseline measurements to explain variability in drug-use during the exposure phase was assessed with linear mixed models using an autoregressive covariance matrix to take into account the longitudinal nature of the data. To visualize the significant results of this analysis, the group of animals was divided into high and low groups based on the variable of interest. Respective curves were then plotted for these two virtual subgroups.

Differences in prefrontal glutamate and glycine concentrations between different phases of the experiment were evaluated with a Kruskal-Wallis test, whereas comparisons with baseline were assessed using a Wilcoxon signed-rank test. The Mann-Whitney U test was

used to interrogate the difference in total fluid consumption with and without access to alcohol. The reported values are mean ± standard error and significance was defined at the 95 % confidence level.

5.4 Results

5.4.1 Self-administration

Animals consumed on average 4.8 ± 0.2 g/kg alcohol per 24 hour session with an average alcohol preference of 32 ± 1%. The latter increased over time ($p < 0.001$) with significantly higher preference during the sixth (36 ± 7%, $p < 0.0001$) and seventh (19 ± 7%, $p = 0.035$) exposure week compared to the first. The saccharin group consumed on average 0.01 g/kg/24h saccharin, and showed no significant differences between the different phases. On days that animals had access to both alcohol and water they consumed on average 27.1 ± 0.4 g water, on days where only a water bottle was present this increased to 32.6 ± 0.5 g. The total fluid consumption however, was higher during days when animals also had access to alcohol (35.3 ± 0.4 g, $p < 0.0001$). This effect was also present in the sucrose group ($p < 0.0001$), which consumed 53.7 ± 1.5 g when both sucrose and water were available and 30.1 ± 0.9 g when only water was present. Finally, bottles were compared for consistently providing more liquid, as this might have been indicative of leakage, but no abnormalities were identified.

5.4.2 Open Field Test

One open field test was performed at baseline to provide surrogate markers of animal's individual anxiety levels. Videos of animals inside the open field test were analyzed with automated software. This provided two outcome measures, which did not differ significantly between both groups: total distance travelled (mean = 272 ± 13 cm) and distance from center (mean = 36 ± 3 cm). Interestingly, animals who travelled a larger distance had on average lower alcohol preference during the exposure phase (Figure 2A). It was estimated that one meter of extra distance travelled was associated with an average lower alcohol preference of 10.5 ± 4.5% ($p = 0.02$). No significant relationships were found for the distance-from-center outcome, nor for the saccharin group.

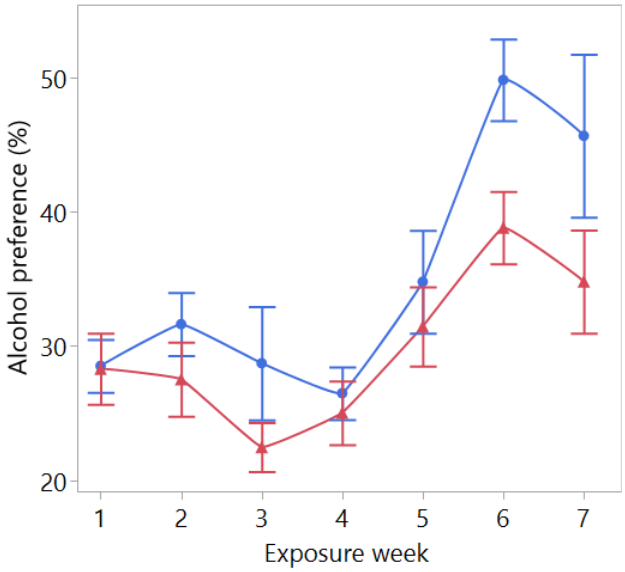


Figure 2. Alcohol preference as a function of exposure week. Animals were categorized into two subgroups based on their OFT locomotor activity, with each group containing half of all observations. Animals with lower activity (●, 224 ± 9 cm) had higher alcohol preference than those who travelled a larger distance (▲, 320 ± 9 cm).

5.4.3 Small-animal PET imaging

All animals showed regional brain-uptake of ^{18}F-FPEB in accordance with the known distribution of mGluR5 (de Laat et al. 2015). The predictive value of pre-exposure ^{18}F-FPEB PET scans was evaluated using a VOI-based analysis, for *a priori* selected regions (bilaterally defined), i.e. the nucleus accumbens, hippocampus, prefrontal cortex and striatum. A significant relationship was found between the baseline ^{18}F-FPEB BP_{ND} in the nucleus accumbens bilaterally and future alcohol preference ($p = 0.0053$). Specifically, an increase of one in BP_{ND} was associated with an average 11.6 ± 4.1% higher alcohol preference (Figure 3).

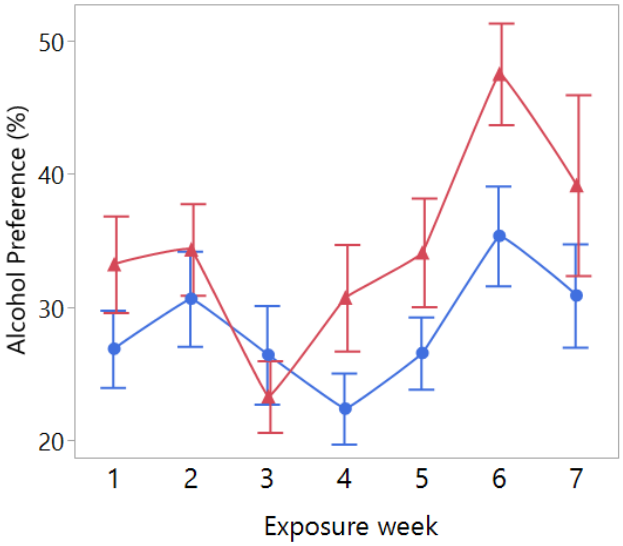


Figure 3. Alcohol preference as a function of exposure week. Animals are categorized into two sub-groups based on the ^{18}F-FPEB binding potential in the nucleus accumbens, with each group containing half of all observations. Animals with higher mGluR5 availability (▲, 7.2 ± 0.4) had significantly higher alcohol preference than those who demonstrated lower mGluR5 availability (●, 6.1 ± 0.2).

For the parametric voxel-wise analysis, we applied a flexible factorial design to evaluate the influence of alcohol and saccharin on baseline mGluR5 availability. Additionally, this design was used to locate where these influences were significantly different between both substances. Detailed results of the analysis can be found in Table 1, but are summarized here. Exposure to alcohol significantly reduced mGluR5 availability in a cluster located in the bilateral hippocampus (>14 ± 3%) and amygdala (>16 ± 2%). Saccharin exposure also induced reduced availability in the bilateral hippocampus (15 ± 2%) and in the prefrontal cortex (11 ± 1%). A comparison of both groups showed that alcohol induced significantly larger decreases in mGluR5 availability in the bilateral hippocampus (-16 ± 4% vs -5 ± 4%) and the striatum (-2 ± 4% vs +2 ± 2%). Finally, a correlation between ^{18}F-FPEB at baseline and the total distance travelled in the OFT was performed, but no significant relationship was found.

Table 1 Voxel-based clusters of significant difference

Baseline vs Exposure

	Threshold	Cluster level				Voxel level	Coordinates			Anatomical structure
	P	P_{Uncor}	K_E	Difference	T	P_{Uncor}	X	Y	Z	
Alcohol	0.002 (Uncor)	0.039	1569	-16±2%	6.6	<0.001	3.2	-6.0	7.3	HippoC R (DG)
		0.001	215	-20±3%	6.5	<0.001	3.7	-4.1	9.2	Amygdala R
		0.004	191	-16±2%	6.4	<0.001	-4.2	-4.1	7.8	AmygdalaL HippoC L
		0.047	191	-14±3%	5.5	<0.001	-4.0	-7.2	6.3	HippoC R (PrS)
	Threshold	Cluster level				Voxel level	Coordinates			Anatomical structure
	P	P_{Uncor}	K_E	Difference	T	P_{Uncor}	X	Y	Z	
Saccharin	0.002 (Uncor)	<0.001	522	-15±2%	7.2	<0.001	4.8	-7.4	5.6	HippoC R (S)
		0.003	342	-16±2%	6.3	<0.001	-4.4	-7.3	3.5	HippoC L (S)
		0.035	145	-11±1%	5.7	<0.001	1.8	-4.6	3.3	PFC R (FrA)
		0.002	350	-15±1%	5.4	<0.001	0.3	-2.6	2.6	PFC & Cing Ctx BL

Alcohol vs Saccharin

	Threshold	Cluster level					Voxel level	Coordinates			Anatomical structure
	P	P_{Uncor}	K_E	ΔS (%)	ΔA	T	P_{Uncor}	X	Y	Z	
Alcohol < Saccharin	0.00002 (Uncor)	<0.0001	1569	-2±2	-5±3	10.6	<0.0001	3.9	-1.0	7.1	Striatum, HippoC R
		<0.0001	215	-5±4	-16±4	8.3	<0.0001	-4.0	-5.5	5.6	HippoC L
		<0.0001	191	2±2	-2±4	8.0	<0.0001	-3.9	-1.6	5.5	Striatum L

Abbreviations: Uncor = uncorrected, K_E = cluster extent, ΔS / ΔA = % difference in BP_{ND} for the sucrose or alcohol group resepectively, when compared to baseline images. BL / L / R = bilateral, left, right. Anatomical structures: HippoC = hippocampus, DG = dentate gyrus, AHiAL = amygdalohippocampal area, CA2 = hippocampal CA2 region, PrS = pre-subiculum, S = subiculum, PFC = prefrontal cortex, FrA = frontal association cortex, PrL = prelimbic cortex, Cing. ctx = cingulate cortex.

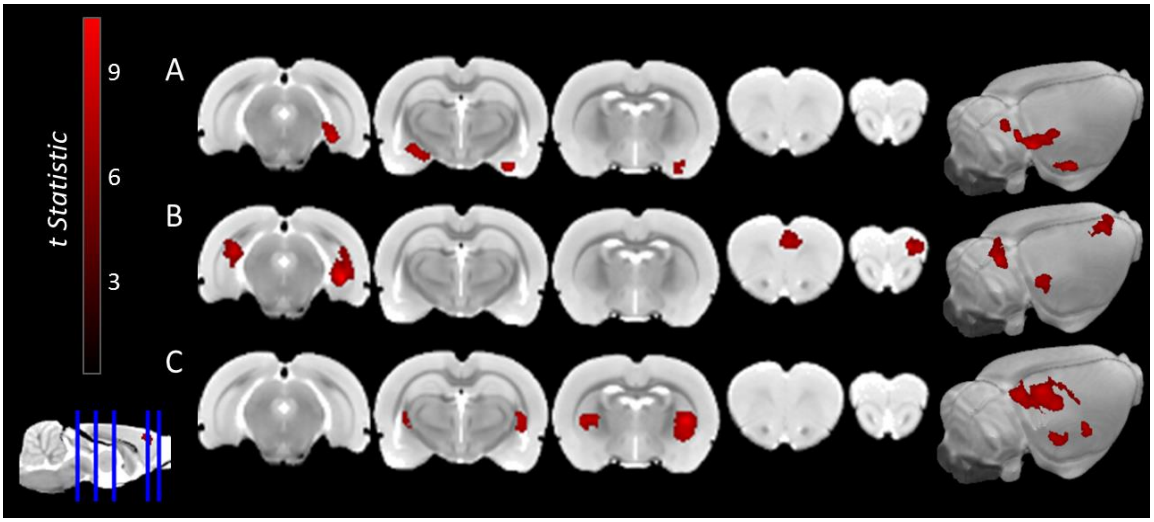


Figure 4. Voxel-based analysis showed significant decreases in mGluR5 availability compared to baseline after **A**) alcohol exposure, **B**) saccharin exposure. **C**) Direct comparison of the effect of alcohol versus saccharin significant decreases were observed in the bilateral hippocampus and striatum.

5.4.4 Magnetic Resonance Spectroscopy

All measured metabolites were found to be in previously reported ranges for healthy rats (Pfeuffer et al. 1999). For example, average prefrontal concentrations of glutamate at 11.1 ± 0.3 mmol/L and glycine at 0.42 ± 0.04 mmol/L at baseline were measured. No significant associations were found between baseline measurements and future alcohol preference for neither glutamate nor glycine. However, glutamate was influenced by exposure phase in the alcohol group ($p = 0.026$) with significant decreases at the first (-1.38 ± 0.49 mmol/L, $p = 0.016$), second (-1.35 ± 0.46 mmol/L, $p = 0.007$) and last (-1.25 ± 0.55 mmol/L, $p = 0.038$) time point. During withdrawal a normalization was observed and no significant difference with baseline remained (Figure 5). The temporal pattern for glycine showed no overall phase effect ($p = 0.11$). Finally, both metabolites did not show significant changes over time for the saccharin group.

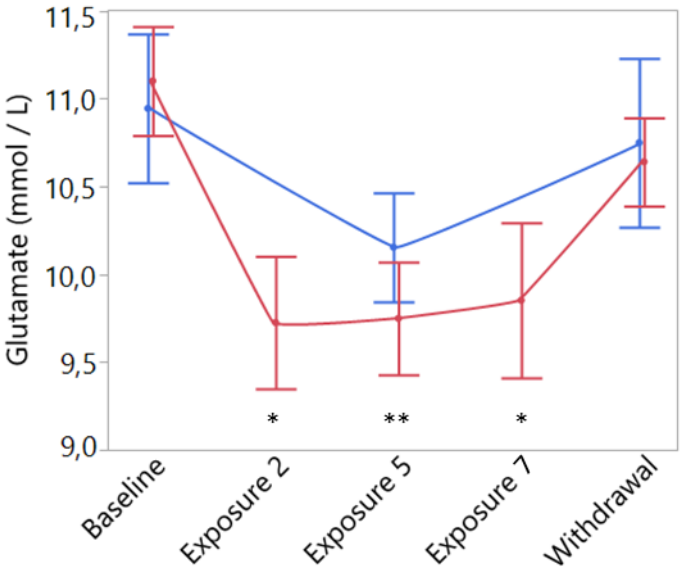


Figure 5. Prefrontal concentrations of glutamate, as measured with ^{1}H-MRS, showed a significant decrease compared to baseline for all three alcohol exposure time-points, which was no longer present after withdrawal from alcohol (red). Exposure to saccharin (blue) induced a similar pattern, but this did not reach significance. * = $p < 0.05$, ** = $p < 0.01$.

5.5 Discussion

In a longitudinal rat model of alcohol consumption, we showed that animals with higher activity in the open field test showed significantly lower preference for alcohol, but not saccharin. Exposure to alcohol decreased glutamate in the prefrontal cortex, whereas a normalization occurred during withdrawal. ^{18}F-FPEB PET scans revealed that pre-exposure mGluR5 availability in the nucleus accumbens is associated with future alcohol preference, although alcohol exposure did not change mGluR5 availability. Finally, alcohol exposure induced a decrease in the bilateral hippocampus and amygdala mGluR5 expression compared with baseline, and in the hippocampus and striatum compared with saccharin. Saccharin exposure itself induced decreases located in the hippocampus and prefrontal cortex.

This study used saccharin as the control condition, as has been done before in addiction studies (Logrip et al. 2014). However, specific aspects of the relationship between

saccharin and alcohol should be kept in mind when interpreting the results presented here. Firstly, alcohol has a naturally aversive taste, which is only overcome by its rewarding properties. In contrast, saccharin has a sweet taste and is thus immediately preferred over plain water. Secondly, saccharin has no caloric value, whereas alcohol does provide a relatively high amount of energy per gram. In effect, the lack of satiation after saccharin consumption might have increased its consumption compared to alcohol. Finally, it has been shown that a rats propensity to consume saccharin is also reflected in its alcohol consumption (Gosnell and Krahn 1992). Therefore, differences reported here, e.g. the relation with open field behavior, highlight an interesting incongruity between both types of reward.

Anxiety disorders are associated with alcohol abuse disorders (Grant et al. 2015). Indeed, patients with high anxiety levels can use the anxiolytic properties of alcohol to cope with their subjective situation (Anker et al. 2016; Kushner, Abrams, and Borchardt 2000). A molecular corroboration is the preclinical evidence that the central amygdala is pivotal in both disorders, and that aberrant epigenetics could predispose to both alcoholism and anxiety (Gilpin, Herman, and Roberto 2015; Moonat et al. 2013). Anxiety in rats can be assessed with the open field test as it will negatively influence their locomotor activity (Prut and Belzung 2003). Here we show that rats with lower locomotor activity, possibly due to a more anxious state, have a higher alcohol preference. Similar findings have been reported by Pelloux *et al.*, who showed that more anxious rats in a light/dark box test had higher alcohol intake, particularly when a lower alcohol concentration was offered (Pelloux, Costentin, and Duterte-Boucher 2015). Since mGluR5 has also been implicated in anxiety, we also evaluated this anxiety profile with the measured mGluR5 availability at baseline, but did not find a significant association (Ballard et al. 2005).

The role of the NMDA receptor in the effect of alcohol has been proven with both experimental and observational studies (den Hartog et al. 2013; Nona, Li, and Nobrega 2014). Specifically, alcohol is known to differentially upregulate the expression and activity level of the NMDA receptor (Chen, Michaelis, and Michaelis 1997; Hu, Follesa, and Ticku 1996). This is interesting as we showed a prefrontal decrease of its agonist glutamate after exposure to alcohol. Glutamate has been studied extensively in alcohol addiction research, but longitudinal studies remain scarce. This study provided evidence

for a hyperglutamatergic state during early abstinence, which normalized within 14 days (Hermann et al. 2012; Bauer et al. 2013). Additionally, Hermann *et al*. also showed a short-lasting increase in medial prefrontal cortex glutamate at 12 hours after acute forced alcohol administration in rats (Hermann et al. 2012). We believe our data complement these existing results, as we show a decrease during alcohol exposure, which normalized after one week of withdrawal. Interestingly, acamprosate, an FDA approved therapy against relapse, prevents the glutamatergic rise after alcohol withdrawal (Dahchour et al. 1998). Our data suggest however, in corroboration with those of Hermann *et al*., that acamprosate could lose its function in prolonged withdrawal, when the short peak in glutamate concentrations in early withdrawal has already normalized. This provides therefore a possible mechanism for the findings of a randomized clinical trial with acamprosate (Paille et al. 1995). In this clinical trial, a significant effect of acamprosate was only found at the first time-point after abstinence, but lost at the second time-point. This pattern has been confirmed in a recent meta-analysis on when acamprosate has proven most useful (Maisel et al. 2013). As proposed by Nam *et al*., serum glutamate could be used as a biomarker for the efficacy of acamprosate in order to personalize anti-dependence therapy (Nam et al. 2015).

The nucleus accumbens plays a central role in alcohol addiction, for example, deep-brain stimulation there can enhance alcohol liking in rats and is therefore explored as a treatment option for patients (Hadar et al. 2016; Muller et al. 2013). Although the exact molecular mechanism is not fully elucidated, research has shown a role for both PKCε and mGluR5 expression in the nucleus accumbens in the consumption of excessive amounts of alcohol (Cozzoli et al. 2012; Cozzoli et al. 2016). Moreover, it has been shown that first exposure to alcohol can induce translation of the Homer protein, which binds to the mGluR5, possibly promoting subsequent alcohol intake (Beckley et al. 2016; Marton, Hussain Shuler, and Worley 2015). Therefore, our finding that mGluR5 binding in the nucleus accumbens bilaterally is associated, with future alcohol preference can be considered an *in vivo* support of these earlier *in vitro* findings.

Exposure to both saccharin and alcohol decreased mGluR5 availability in the hippocampal subiculum, although this decrease was more pronounced after alcohol exposure. The ventral subiculum projects towards the nucleus accumbens, and these

projections have been shown to be essential to alcohol-dependence related behavior in rats (Marchant et al. 2016). Moreover, mGluR5 in this region, as well as in the ventral striatum and amygdala, have been shown to play a role in both novelty-seeking and alcohol drinking (Parkitna et al. 2013). Interestingly, we also observed that alcohol, but not saccharin, exposure decreased mGluR5 availability in the bilateral amygdala. The amygdala has been proposed before as an integrative hub for anxiety and alcohol use disorder (Gilpin, Herman, and Roberto 2015), which aligns with our results. In effect, animals with more anxious behavior self-administered higher levels of alcohol, which in itself could lower mGluR5 availability on D2R expressing neurons in the amygdala. This is interesting in the light that mGluR5 can inhibit dopamine transporter capacity and therefore indirectly reduce the level of synaptic dopamine, and thus lower neuronal activity in this region creating a possible anxiolytic effect (Bueno, Zangrossi, and Viana 2005; Page et al. 2001).

Both saccharin and alcohol can elicit dopamine release in the striatum, which can be blunted by reducing mGluR5 activity (Golembiowska 2003). It could be hypothesized that the decrease observed in both groups, albeit stronger in the alcohol group, is related to this phenomenon. The observations here are in line with our previous human result that alcohol dependent patients show reduced mGluR5 availability in this region (Leurquin-Sterk et al., submitted 2017). An interesting difference is that saccharin induced an mGluR5 availability decrease in the prefrontal cortex, which was not found after alcohol exposure. Literature on the influence of either substance on prefrontal mGluR5 is sparse, and no direct comparison has been published before. A similar difference has been found before by Hamilton *et al*., who showed that an mGluR5 related intra-cellular protein, c-fos, was shown to be influenced in the prefrontal cortex of rats exposed to saccharin, but not alcohol. However, also considering the limited number of animals used in this substudy, further research is required to confirm these results. An interesting general contradiction is found with the data presented by Nandi *et al*. (Nandi et al. 2016), who showed an increase in mGluR5 availability in cortex, hippocampus and striatum after 14 day exposure to alcohol as measured using ^{18}F-FPEB PET. Differences in study setup impair direct comparison with our results however, e.g. the use of forced alcohol administration, lower dose (2.5 mg/kg/24u), shorter exposure duration (14d), and smaller group size (n = 4).

In conclusion, we report the temporal dynamics of several important mediators of alcohol preference in rats, before, during, and after alcohol exposure. Specifically, we show that animals with higher anxiety levels before alcohol exposure have a tendency towards higher alcohol preference. A similar association was also found with mGluR5 availability in the bilateral nucleus accumbens before drug exposure. Furthermore, we show that prefrontal glutamate levels are observed to be lower after alcohol exposure, but normalize during withdrawal. Finally, it is shown that alcohol and saccharin differentially decrease limbic mGluR5 availability. Considering the similarity of findings between clinical and preclinical research, as well as the use of a translational model of alcohol abuse, we feel that these results advance our understanding of preclinical and clinical alcohol dependence. Particularly, the new information on the dynamic of prefrontal glutamate could be of interest to practitioners prescribing acamprosate, although a more detailed corroboration is required before translation into clinical practice.

Supplemental figure:

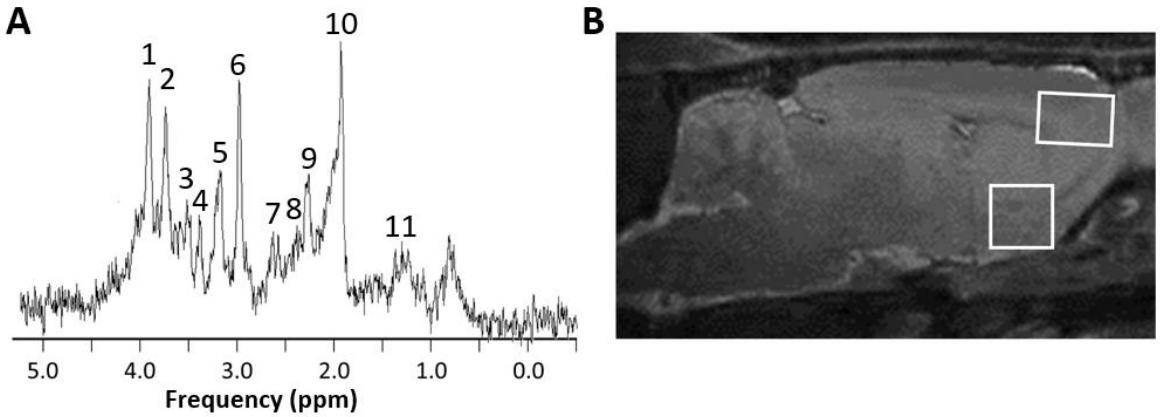


Figure S1. A) Example of a spectrum obtained from the prefrontal nucleus voxel. 1 = Creatine; 2 = Ascorbate, glutamine, glutamate, glutathione; 3 = myo-inositol; 4 = Taurine; 5 = Taurine, glycerophosphocholine, phosphocholine; 6 = Creatine, 7 = Aspartate, N-acetylaspartate; 8 = N-acetylaspartate, glutamine; 9 = glutamate; 10 = N-acetylaspartate; 11 = Alanine, lactate. **B)** Illustration of voxel position for spectroscopy on a sagittal image.

Chapter 6: *In vivo* silencing of mGluR5 in the rat brain with naked siRNA: A proof-of-principle study using ^{18}F-FPEB autoradiography

Bart de Laat · Celine Aelbrecht · Guy Bormans · Cindy Casteels · Koen Van Laere

Manuscript in preparation

6.1 Abstract

Introduction: There is observational evidence from neuroimaging studies that mGluR5 plays a role in clinical addiction. In addition, we have observed in animal models of addiction that drugs of abuse significantly influence mGluR5 availability. Therefore, it would be interesting to study the influence of reduced mGluR5 availability on self-administration behaviour in rats. Here, the ability of modified naked small RNA fragments to induce *in vivo* mGluR5 silencing is studied.

Materials & Methods: Twenty-eight rats received a single stereotactic injection with mGluR5 Accell siRNA in the left lateral ventricle. A second group of six rats received a high-dose of mGluR5 Accell siRNA intranasally. Control groups for anaesthetics and control substance were used to exclude their influence on mGluR5 availability. *Ex vivo* mGluR5 expression was evaluated with autoradiography using the specific radiotracer ^{18}F-FPEB.

Results: Two days after intracranial siRNA injection, a reduction in ^{18}F-FPEB signal was observed. However, a similar trend was observed in the control group. In a second experiment, a full factorial design was used to investigate the cause of this decrease. Anaesthetics nor injected substances were able to significantly lower mGluR5 availability.

Conclusion: Despite the reduction of ^{18}F-FPEB signal 2 days after siRNA injection, no conclusive evidence was found that this reduction was specifically due to the injected siRNA. Therefore, *in vivo* gene silencing was not reliably obtained after a single intracranial or intranasal administration of siRNA.

6.2 Introduction

Only a minority of individuals exposed to addictive substances develop dependence, which is thought to be dependent on a pre-existing combination of environmental and genetic factors (Hiroi and Agatsuma 2005). This genetic contribution is complex as multiple genes contribute, which include genes related to dopamine and serotonin, but also personality traits, such as impulsivity, risk taking, stress responsivity (Hiroi and Agatsuma 2005). Family and twin studies have shown that the genetic factors account for 30-60% of the variance in risk for development of addiction (Goldman, Oroszi, and Ducci 2005; Kreek et al. 2005).

One of the key glutamate receptors involved in addiction is the metabotropic glutamate receptor subtype 5 (mGluR5) (Olsen et al. 2010). This receptor, predominantly located postsynaptically, is widespread in the brain with high expression in the cortex, striatum, hippocampus and low to absent expression is seen in the cerebellum of humans and rats, respectively (Shigemoto et al. 1993; Ametamey et al. 2007; de Laat et al. 2015). The mGluR5 uses Gq/G11 to activate phospholipase C (PLC), which will release diacylglycerol and inositol triphosphate (Kew and Kemp 2005). These molecules mobilize intracellular calcium, which causes an increase of the neuronal excitability and enables an array of downstream pathways. Next to this pathway, the receptor is also strongly associated with postsynaptic proteins that regulate signalling and localization, namely Homer, Preso-1 and Shank. These scaffolding proteins have a role in signalling mechanisms, but are also important in cross-linking complexes, and the regulation of synergistic effects between mGluR5 and the N-methyl-D-aspartate (NMDA) receptor (Piers et al. 2012).

It has been shown that pharmacological manipulation of mGluR5, for example with negative allosteric modulators or antagonists can cause a reduction in cue- and cocaine-reinstated drug seeking in animal models (Wang et al. 2013). Furthermore, studies of mGluR5 knockout mice showed that without this receptor the locomotor stimulant effects of cocaine remain absent (Chiamulera et al. 2001). Additionally, a downregulation of mGluR5 in the nucleus accumbens, has been associated with cocaine use escalation. This observed reduction of mGluR5 expression could therefore represent an adaptation that further enhances cocaine-seeking behaviour (Hao, Martin-Fardon, and Weiss 2010). This

decrease has also been observed in clinical imaging studies. For example, a ^{11}C-ABP688 PET study by Akkus *et al*. showed a decrease in mGluR5 availability in smokers and ex-smokers in comparison with non-smokers (Akkus et al. 2013). Another study demonstrated that mGluR5 availability in cocaine addicted individuals was reduced compared to healthy volunteers in multiple brain regions, including the striatum, putamen, anterior cingulate, prefrontal and temporal cortex, thalamus, and occipital cortex (Martinez et al. 2014). Furthermore, we showed in the previous experiments that both alcohol and cocaine self-administration induce a decrease in mGluR5 availability. The results of these studies implicate a probable role for mGluR5 in addiction, but it is not clear whether its role is causal. Therefore, it would be of great interest to change the mGluR5 expression experimentally and study addiction-associated behavioural consequences.

RNA interference is a post-transcriptional process to obtain gene silencing, i.e. reduced expression of translated genes, through degradation of cytoplasmic mRNA (Figure 1). It is a natural mechanism for protection against viruses or transposons, which is triggered by the presence of long dsRNA in the cytoplasm (Tijsterman, Ketting, and Plasterk 2002). The long dsRNA causes activation of the Dicer protein complex, an endoribonuclease that splices long dsRNA to dsRNA duplexes of an appropriate length (21-23 nt) for loading onto an Argonaute (Ago) protein (Whitehead, Langer, and Anderson 2009). The Ago protein is a part of the RNA induced silencing complex (RISC) that performs cellular surveillance for long dsRNA. During the loading of the siRNA onto the Ago protein, the passenger strand of the siRNA is eliminated and the antisense guide strand is incorporated. Hereafter, the RISC complex is able to bind and cleave complementary mRNA. If enough target mRNA is degraded, a depletion of the target protein is obtained through its natural turnover. Depending on the half-life of the target protein, noticeable gene knockdown is typically achieved 1 or 2 days after administration of siRNA, but will be limited in time (Brazas et al. 2005).

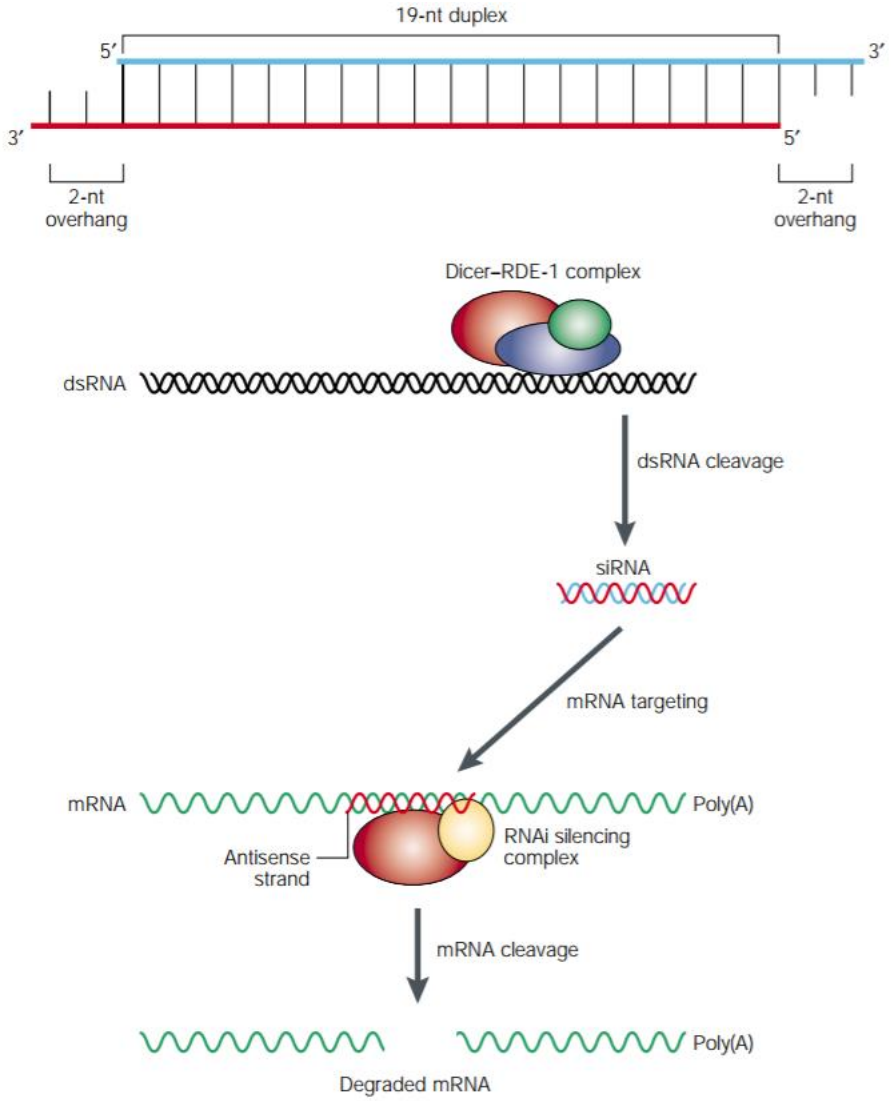


Figure 1. RNA interference pathway. RISC activity lead to post-transcriptional gene silencing through degradation of mRNA (McManus and Sharp 2002).

To deliver the siRNA efficiently to the target cells, several delivery mechanisms have been investigated. Viral vectors, electroporation or transfection with liposomes or nanoparticles, can be used to facilitate administration of exogenous siRNA into the cytoplasm of the living target cells (Shum and Rossi 2016). However, the siRNA can also be delivered without a vehicle, namely as naked siRNA. This is however, only possible if the size and charge of the siRNA are chemically modified to allow easy crossing of cellular membranes. Moreover, unmodified siRNA is easily degraded by endogenous enzymes and can cause a non-specific immune reaction by activation of Toll-like receptors (Whitehead, Langer, and Anderson 2009). *In vivo* administration of siRNA is typically done via an injection directly into the target tissue. However, as this is

complicated and invasive for the brain, intranasal applications have successfully been applied for the delivery of siRNA into the brain or the lungs (Kim et al. 2012; Zafra et al. 1996). If successful, this administration method could facilitate therefore, repeated administrations in longitudinal animal models and translation into clinical therapy.
In this study, we present the findings of a cross-sectional proof-of-principle study to assess the feasibility of silencing mGluR5 expression with naked siRNA. Animals were sacrificed one to seven days after siRNA administration to estimate when maximal silencing was achieved. Two routes were compared, namely intracranial and intranasal administration. To quantify mGluR5 expression we optimized and applied ^{18}F-FPEB (3-[^{18}F]fluoro-5-(2-pyridinylethynyl)benzonitrile) autoradiography.

6.3 Materials and Methods

6.3.1 Animals

All experiments were performed with approval of the Animal Ethics Committee of the University of Leuven. Fifty-two adult male Wistar rats weighing 306 ± 12 (R. Janvier, Le Genest-St-Isle, France) were housed per three in a cage in a temperature- and humidity-controlled room with a 12 h light/dark cycle. Food and tap water were available ad libitum. Animals were habituated for at least one week before surgery and randomly assigned to one of the experimental or control groups.

6.3.2 siRNA

mGluR5 Accell siRNA consisted of a mixture of 4 siRNA sequences complementary to specific sequence regions of mGluR5 mRNA of rats: 5'-CUAGCCACCUUAUUCGUUA-3', 5'-CUUUCAUUCUCAUCCUGUAU-3', 5'-GUUUGAUGAUUAUUAUCUG-3', 5'-GGAUUAUUGAUUUUGAGUU-3'. After briefly centrifuging, the 5 nmol siRNA pellet was resuspended in RNAse free 1x siRNA buffer (Dharmacon, Lafayette, CO, USA) to a final concentration of 100 µM. For the cerebral injection the Accell siRNA stock solution was diluted with Accell delivery medium (Dharmacon, Lafayette, CO, USA) to three final concentrations of 7.5 µM, 15 µM and 30 µM. For the intranasal delivery concentrations of 37.5 µM and 75 µM were used. Control rats received a 2 µL injection of Accell delivery medium (Dharmacon, Lafayette, USA) in the same conditions. After

the experiment, administered siRNA concentrations were verified with a NanoDrop spectrophotometer (ThermoFisher Scientific, Waltham, USA).

6.3.3 siRNA administration

Animals were anesthetised with a mixture of 50 mg/kg ketamine (100 mg/ml, Nimatek, Eurovet, Bladel, the Netherlands) and 0.3 mg/kg medetomidine (1 mg/ml, Domitor, Orion Pharma, Espoo, Finland) injected intraperitoneally (IP). During the whole procedure, a heating pad was used to avoid hypothermia. When a sufficient level of anaesthesia had been achieved, ophthalmic ointment (Vidisic, Bausch lomb, Schiphol-Rijk, the Netherlands) was applied to both eyes, the crown of the rat was shaved and the incision area was scrubbed with a surgical handbrush (4% chlorhexidrine, Vygon, Ecouen, France). Subsequently the animal was mounted onto the stereotactic apparatus. An anterior/posterior incision of 1 cm was made at the midline of the skull and the periosteum was removed. Using the described coordinates (−1.1 mm posterior to bregma, 1.5 mm lateral to midline, and −3.6 mm ventral to the skull surface), a 2 mm hole was made with a drill (Paxinos et al. 1985). Next, a 5 µL Hamilton syringe (Hamilton Company, Nevada, USA) was lowered gradually to the right depth. Subsequently, rats received a 2µL injection at a rate of 0.5 µL/min using a microinfusion pump (Quintessential Stereotaxic Injector, Stoelting, USA) (Nakajima et al. 2012). After the infusion was complete, the syringe was left in place for 10 min and then slowly withdrawn to avoid backflow of the injected fluid.

Rats received IP amoxicillin/clavulanic acid 93 mg/kg (140 mg/ml amoxicillin trihydrate, 35 mg/ml potassium clavulanate, Noroclav, Fendigo, Brussels, Belgium), 0.05 mg/kg buprenorphine (0.3 mg/ml, Vetergesic, Ecuphar, Oostkamp, Belgium) and 5 mg/kg Carprofen (50 mg/ml, Rimadyl, Zoetis, Louvain la Neuve, Belgium) as part of the peri-operative care. Upon completion of the surgery animals were injected with 0.5 mg/kg Atipamezole (5 mg/ml, Antisedan, Orion Pharma, Espoo, Finland) to reverse the effects of the medetomidine.

6.3.4 Autoradiography

Animals were decapitated and their brains were removed and snapfrozen by immersion in 2-methyl butane (Isopentane, Sigma Aldrich, St. Louis, MO, USA) at -35 °C for 30 seconds. The frozen brains were kept at -30 °C and afterwards 20 µm slices, covering the

entire brain, were cut on a -20°C cryostat (Cryotome™ FSE Cryostat, Thermo Scientific, MA, USA) and thaw-mounted onto microscope slides (StarFrost, Waldemar Knittel, Braunschweig, Germany). Per animal, 10 successive slices were made in the axial plane, starting approximately 4 mm below bregma and stored at -30 °C until use (Paxinos et al. 1985).

Brain slices were thawed and dried prior to a 10 min preincubation with Tris buffer (Tris-HCl 50 mM, pH 7.4) at room temperature. After the preincubation, slices were dried again before 10, 30, or 60 min incubation with 400 µL of Tris-BSA buffer (Tris-HCl 50 mM, pH 7.4, 0.3 % BSA) containing 80 µCi/ml ^{18}F-FPEB to determine the optimal exposure protocol. Brain slices were washed 2 times in cold Tris-BSA buffer for 10 min and subsequently a short dip in ice cold water was performed. Following the washing steps, all brains slices were dried and exposed to phosphor imaging plates for 2, 5 or 10 min before scanning on a Cyclone Plus Storage Phosphor System (PerkinElmer, Waltham, USA). Analysis of the obtained digital autoradiograms was performed using Optiquant software (Packard Instruments Company, Meriden, USA). The optimal protocol would be identified by visually comparing the obtained autoradiograms with the reported mGluR5 distribution. In addition, it was ascertained that sufficient radiotracer was taken up, but without oversaturating the imaging system.

Region-of-interest (ROI) analyses of the resulting autoradiograms were performed to quantify and examine the spatial distribution of ^{18}F-FPEB. ROIs were manually delineated and mean ligand uptake minus background was calculated. In all analyses, the cerebellum served as a reference region, based on previous studies (de Laat et al. 2015; Patel et al. 2007). Two analyses were performed: one where the entire cerebrum was used as ROI, and a second analysis in which 6 ROIs, were delineated to investigate region specific decreases in mGluR5 availability: the PFC, the striatum and the hippocampus in both hemispheres (Sengmany and Gregory 2015).

Experiment 1

To examine the effect of the administered siRNA concentration on the mGluR5 expression, three different siRNA concentrations were injected: 0.1 µg/µL (n = 14), 0.2 µg/µL (n= 8), 0.4 µg/µL (n=6) (Figure 10). To assess the time course of the siRNA effect a flexible factorial design was used. For this, animals were sacrificed and brains were collected at day 1 (n=6), 2 (n=4), 3 (n=3), 4 (n=2), 5 (n=2), 6 (n=4) and day 7

(n=5) after the injection. Animals in the control group (n = 5), which received a delivery medium injection, were also sacrificed at different time-points (day 2, 3, 5, and 7) to detect possible time-dependent changes.

Experiment 2

To confirm results of the above-described experiment, we used the same protocol, but excluded potentially confounding factors. To investigate an effect of the ketamine/medetomidine anaesthesia, we compared this protocol (n = 3) with animals anaesthetised with 60 mg/kg pentobarbital (60 mg/ml, Nembutal, Ceva Santé Animale, Brussels, Belgium) injected intraperitoneally (n = 4). The effect of the delivery medium was assessed by injecting animals with either the delivery medium (n = 3) or physiological saline (n = 3), both under ketamine/medetomidine anesthesia. Additionally, a group of animals did not undergo stereotactic surgery, but was only anaesthetised with a ketamine/medetomidine mixture (n=3) in order to study possible non-specific surgery related phenomena, such as neuroinflammation. Since animals in the first experiment received atipamezole to reverse the medetomidine effects, two animals received only an injection of Atipamezole. Untreated healthy animals (n=3) were included as a final control group. As described above, autoradiographic images based three brain slices per animal were used to calculate the mean cerebrum/cerebellum ratio. It has been reported that Accell siRNA can be delivered to the brain via intranasal administration. Therefore, a single dose of 0.5 µg/µL (n=3) or 1 µg/µL (n=3) mGluR5-targeting siRNA, or delivery medium only for the control group (n=3), was given through both nostrils of the rat. For this procedure, rats were anesthetized with 2.5 % isoflurane (Isovet 100 mg/ml, Piramal Healthcare, London UK) in 100% oxygen at a flow rate of 2 L/min. Heating pads were used to avoid hypothermia. After 10 min of anaesthesia, rats were placed in a supine position with their nose upwards against the side of the induction box. A nose drop of 10 µL siRNA solution or delivery medium was administered by pipette in the left and right nostril. Between the two drops, a 2 min interval was respected to prevent simultaneous obstruction of the nostrils. Additionally, the animal remained in this position for two additional minutes after the last administration. Animals were sacrificed 48 hours after administration.

6.3.5 Statistical analysis

All statistical analyses were performed with JMP Pro 12.1.0 software (SAS, Cary, USA). Normality assumption was justified using the Shapiro-Wilk test. Obtained data for the ^{18}F-FPEB signal were analysed using One Way ANOVA. Tukey's HSD tests were used for further post hoc comparisons. P-values < 0.05 were considered statistically significant.

6.4 Results

6.4.1 ^{18}F-FPEB autoradiography optimization

Firstly, the autoradiography protocol was optimized and best results (highest contracts and specific signal?), were obtained after 30 min incubation with ^{18}F-FPEB, in combination with 5 min phosphor screen exposure (Figure 3).

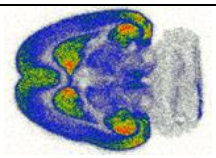
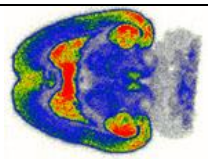
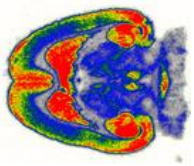
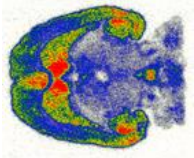
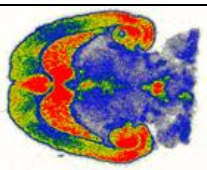
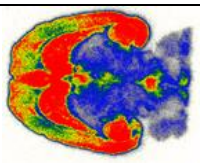
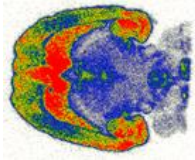
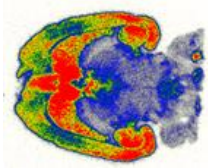
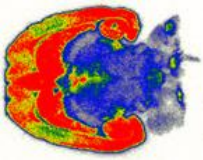
	Phosphor screen 2 min	Phosphor screen 5 min	Phosphor screen 10 min
10 min			
30 min			
60 min			

Figure 3. Distribution of ^{18}F-FPEB in rat brain sections. An incubation time of 30 min with the ^{18}F-FPEB and 5 min exposure to the phosphor screens are optimal conditions to perform *in vitro* receptor autoradiography with the ^{18}F-FPEB radiotracer.

6.4.2 Experiment 1

mGluR5 Accell siRNA was stereotactically injected into the rat lateral ventricle in order to induce *in vivo* mGluR5 knockdown in the rat brain. Three concentrations of siRNA solution were injected to establish whether there was a concentration effect on the mGluR5 expression level. Animals were sacrificed 1-7 days after surgery to evaluate the onset and duration of potential down-regulation. For each animal, autoradiography was performed on three brain slices. The obtained cerebrum/cerebellum ratio for each slice was used to calculate the mean cerebrum/cerebellum ratio of these three slices, representative for one animal.

The results revealed a significant effect of time on the ^{18}F-FPEB signal (one way ANOVA, $p = 0.0067$). Tukey's HSD test was used for post-hoc comparisons and showed a significant lower ^{18}F-FPEB signal at day 2 after injection in comparison with day 1, 3, 4, 6 and 7 ($p < 0.028$) (Figure 4). In contrast, different siRNA concentrations did not significantly change the temporal patterns of the ^{18}F-FPEB signal ratio between cerebrum/cerebellum (one-way ANOVA, $p = 0.70$).

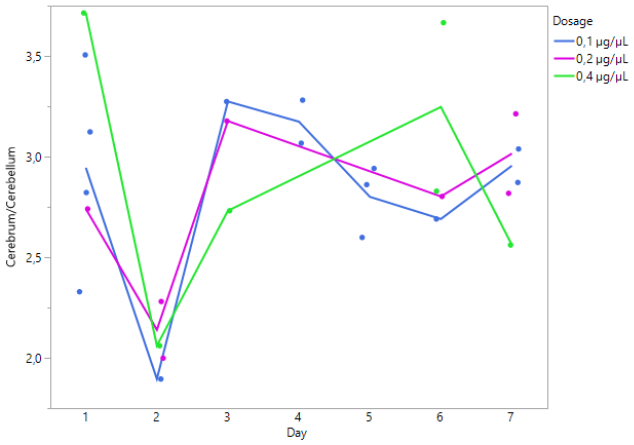


Figure 4. Ratio of ^{18}F-FPEB signal between the whole cerebrum and the cerebellum over time following a single injection of mGluR5-targeting Accell siRNA. There is no significant concentration effect on mGluR5 availability. Significant decreases in ^{18}F-FPEB signal were observed at day 2 ($p = 0.0067$) with an average reduction of 34.5 % compared to day 1. No significant changes in ^{18}F-FPEB signal at later time points were observed.

To evaluate whether this effect was region specific or differed between the right and left hemisphere, a ROI analysis was performed. The results from this analysis confirmed the

significant effect of time in ^{18}F-FPEB signal (one way ANOVA, $p < 0.0001$). Specifically, post-hoc comparisons revealed that there was a significantly reduced ^{18}F-FPEB signal at day 2 in comparison with all other days ($p < 0.0001$). However, there was no significant difference in change of ^{18}F-FPEB signal between delineated regions per day ($p = 0.93$) (Figure 5A). Finally, no significant difference was found between the left and the right hemisphere ($p = 0.49$). Comparing the results from the control group with the experimental group, no significant differences were observed ($p = 0.16$). However, at day 2 a decrease of ^{18}F-FPEB signal was also observed for the control animal ($n = 1$) (Figure 5B).

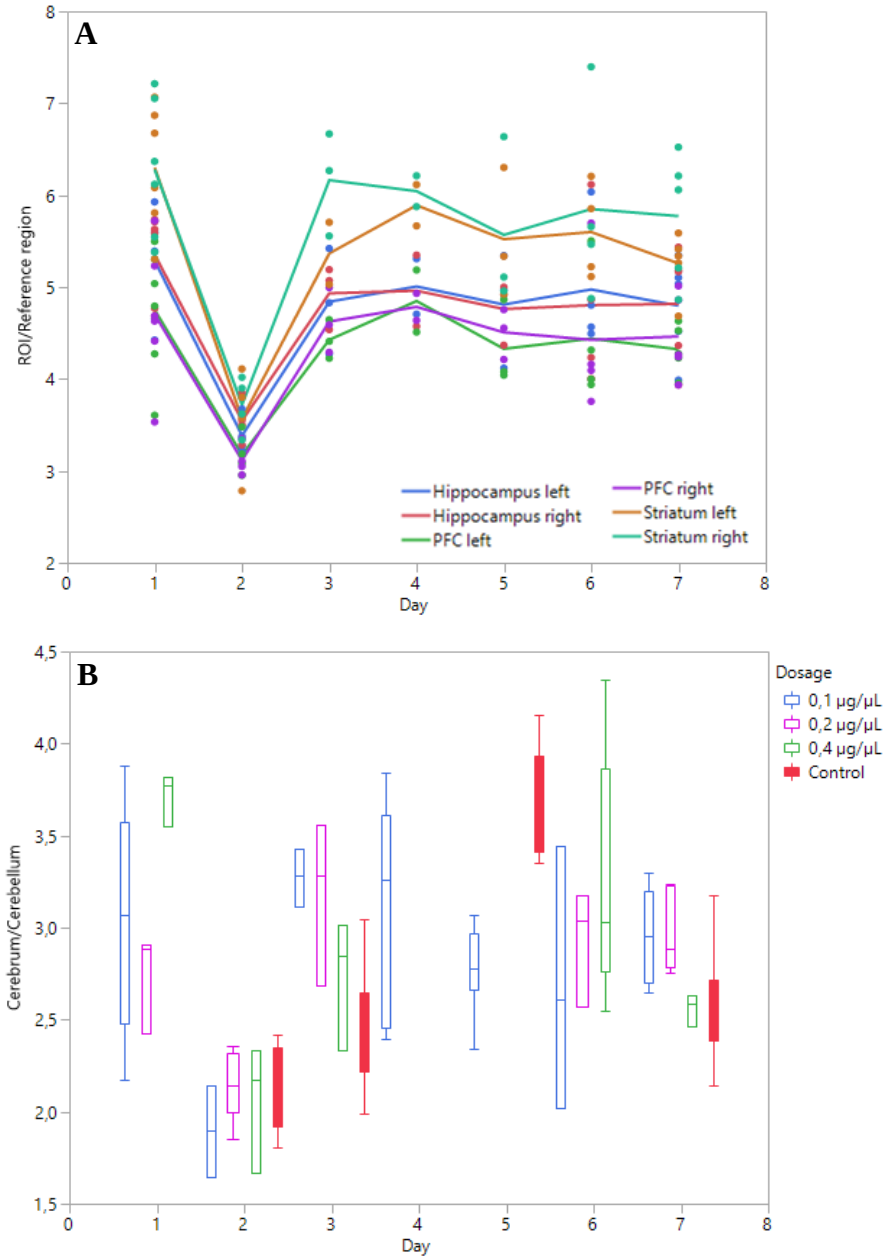


Figure 5. **A)** ^{18}F-FPEB signal in the striatum, hippocampus and PFC after a single injection of mGluR5 siRNA. No significant difference in ^{18}F-FPEB signal was observed between the left and the right hemisphere per region ($p = 0.49$). In addition, there were no significant difference seen in change of ^{18}F-FPEB signal between delineated regions per day ($p=0.93$). **B**) ^{18}F-FPEB signal in the cerebrum of siRNA treated and control animals. Control animals received an injection of delivery medium and were sacrificed at day 2, 3, 5 and 7 after injection. The control animal that was sacrificed at day 2 had a similar decrease in ^{18}F-FPEB signal as the treated animals. No significant differences between control animals and mGluR5 siRNA injected animals were obtained ($p = 0.16$).

6.4.3 Experiment 2

In the previous experiment, a decrease in mGluR5 expression was observed on day 2 in both the control group and the siRNA group. To verify whether the observed was an induced by the siRNA injection, we repeated the experiment for this time-point. Additionally, we evaluated the influence of the used anaesthesia and control substance, i.e. the delivery medium used in both groups. Considering the previous results, all animals in this experiment were sacrificed at day 2 after administration and siRNA animals received the highest dose evaluated in the previous experiment, i.e. 0.4 µg/µL siRNA injection.

No significant differences between all evaluated conditions were found (one way ANOVA, p = 0.88). In addition, intranasal administration revealed no significant decrease in ^{18}F-FPEB signal between the controls and different concentrations (one way ANOVA, p=0.88) (Figure 7).

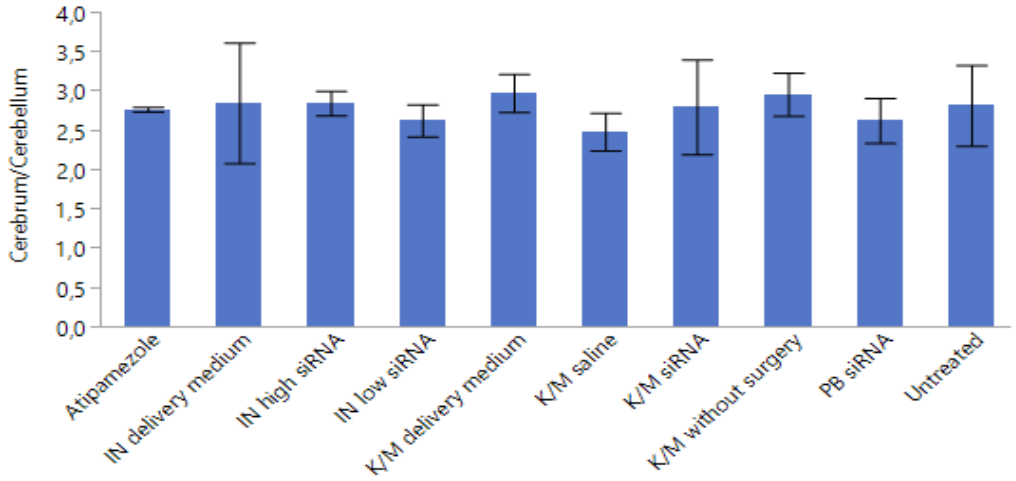


Figure 7. ^{18}F-FPEB signal in the rat brain for the different conditions evaluated in experiment 2. Rats received an intranasal administration of 0.5 µg/µL siRNA (IN low siRNA), 1 µg/µL siRNA (IN high siRNA) or delivery medium (IN delivery medium). Using the cerebral injection procedure rats, anaesthetized with ketamine/medetomidine, received 0.4 µg/µL siRNA (K/M siRNA) or, delivery medium (K/M delivery medium) or saline (K/M saline) as control. Rats anaesthetized with pentobarbital received an injection with 0.4 µg/µL siRNA (PB siRNA). Additional control conditions were healthy untreated rats (Untreated) or rats IP injected with ketamine/ medetomidine (K/M without surgery) or with Atipamezole (Atipamezole). Comparisons between all conditions revealed no significant differences (p=0.88).

6.5 Discussion

In this study, we aimed to induce mGluR5 knockdown, as measured with ^{18}F-FPEB autoradiography, through mGluR5 Accell siRNA injections in the left lateral ventricle. We were not able to prove that *in vivo* gene silencing of mGluR5 can be achieved with this method in the rat brain. Although a significant reduction of ^{18}F-FPEB signal was observed two days after the siRNA injection, we were not able to confirm these results in a follow–up experiment. Finally, we report a 30 min incubation and 5 min exposure time autoradiography protocol, which is observed to be optimal in combination with the 400 µL of 80 µCi/ml ^{18}F-FPEB dose that was used (Voytas and Ke 2001).

There are several genetic techniques to alter the expression of a receptor. The most drastic techniques result in knockout models which lack proteins encoded by this gene to a certain extent. Knockout models have been used to study the contribution of mGluR5 in addiction. For example, Chiamulera et al. demonstrated that mGluR5 null mutant mice have an absence of cocaine self-administration and no increased locomotor activity (30). Although knockout models can provide useful information, their results are ambiguous. In effect, it has been shown that animals lacking a gene will find alternative pathways to alleviate the effects of the absent gene (Rossi et al. 2015). This can cause fundamental changes in the physiology of animals, thus invalidating them as a model for organisms with this gene present (Osokine et al. 2008). A possible alternative is to reduce the expression of a protein *in vivo*. Previously, antisense oligonucleotides (ASO) have been used to achieve *in vivo* gene silencing of mGluR5 expression (Mao and Wang 2003; Dorri et al. 1997). However this method is not used regularly, because ASO are very bioactive molecules and off-target effects are frequent (Lebedeva and Stein 2001). An alternative method to reduce protein expression involves the use of loci called ‘Clustered Regularly Interspaced Short Palindromic Repeats' (CRISPR). CRISPR interference is a technique to acquire specific gene silencing at the transcriptional level on a genome-wide scale. This method is more predictable and specific than ASO due to its specific design. This makes CRISPR interference a promising technique to achieve gene silencing but optimization is necessary for *in vivo* use (Larson et al. 2013). RNA interference is an attractive technique to reduce the expression of proteins *in vivo*, as it is a simple and rapid method. In addition, efficient siRNA delivery *in vivo* is possible, although also RNA

interference can cause off target effects and toxicity (Kim and Rossi 2008; Shim and Kwon 2010).

Injection of siRNA into a lateral ventricle has been reported to achieve widespread and specific gene knockdown in the rat brain (Nakajima et al. 2012; Huang et al. 2015). Accell siRNA is particularly suited for this application, because of its proven performance and efficacy in neuronal cell types and its ability to enter cells without the need for a transfection reagent (Nakajima et al. 2012; Mitchnick et al. 2015). We observed that mGluR5 availability at 1 to 7 days after stereotactic administration of siRNA decreased 2 days after intracranial siRNA administration. However, this reduction was very limited in time with a recovery of normal mGluR5 expression levels 3 days after injection and a similar effect was observed in the control group. A confirmation experiment was unable to reproduce any siRNA specific results. RNA interference is known to be influenced by several factors, which can impede its efficacy. Firstly, the magnitude of siRNA induced silencing can decrease when the target mRNA is abundantly present (Arvey et al. 2010). Secondly, a high turnover rate of the mRNA can also limit the efficiency of the siRNA (Larsson, Sander, and Marks 2010). Thirdly, if the target protein has a long half-life, the mRNA levels can be restored before a significant protein reduction has occurred, whereas the exogenous siRNA will have been depleted (Bartlett and Davis 2006). For mGluR5, the turnover rate of mRNA and the receptor protein have not been reported.

It has been reported that siRNA has a short-lasting effect, which impedes its use in longitudinal animal models, often used in self-administration paradigms. Therefore, we wanted to explore administration techniques that were minimally invasive and could easily be applied repeatedly. The intranasal route, which meets these criteria, has been used before to deliver siRNA to the brain. Kim et al. demonstrated that siRNA molecules were able to penetrate neural cells after intranasal delivery (Kim et al. 2012). The target gene was significantly reduced in multiple brain regions such as the PFC and the striatum, which indicates a global knockdown rather than restriction to brain regions associated with the olfactory nerve pathway. Disadvantages of intranasal administration of siRNA do however also exist. For example, olfactory epithelium in the nose is subject to active mucociliary clearance and enzymatic activity, which can cause rapid removal and

degradation of RNA. In addition, there is a large inter-individual variability in the delivery efficiency to the CNS, which on average is rather low (Lochhead and Thorne 2012). We report here that intranasal application of siRNA is indeed feasible and practical, but did not result in detectable mGluR5 knockdown.

In conclusion, the first experiment in this study showed that a reduction in ^{18}F-FPEB signal could be achieved 2 days after a single ICV injection with mGluR5 targeting Accell siRNA. There was no concentration effect present and the duration of the effect was limited in time. However, a second experiment was unable to reproduce the observed decrease. Consequently, there is no evidence that ventricular injection of siRNA leads to a robust and significant reduction in mGluR5 expression. In addition, intranasal administration of siRNA was also not able to knockdown the mGluR5 expression. Future studies are necessary to verify whether *in vivo* gene silencing can be obtained using naked siRNA.

Chapter 7: The effect of nicotine self-administration on ^{18}FDG uptake and resting-state functional connectivity: A machine learning approach

Bart de Laat · Silke Vanden Wyngaert · Willy Gsell · Uwe Himmelreich · Cindy Casteels · Koen Van Laere

Manuscript in preparation

7.1 Abstract

Introduction: Nicotine addiction is a major health concern with a high relapse rate despite the development of novel therapeutic strategies. Metabolic brain signatures hold promise for the elucidation of the underlying mechanisms of both the addictive properties of nicotine and the associated relapse.

Materials & Methods: 18 Wistar rats had access to IV nicotine self-administration for two weeks, followed by a two week forced withdrawal and final week of relapse. During this time, rats underwent weekly ^{18}FDG PET and resting-state fMRI scans. Dimension reduction was performed on the latter by eigenvector centrality mapping (ECM). We applied pattern classification and pattern regression to these functional neuroimaging data to determine whether patterns could be associated with drug-use.

Results: We here show for the first time that pattern classification can be used on ^{18}FDG and ECM images to differentiate between time-points where animals could self-administer nicotine or not, with up to 70% balanced accuracy. When comparing baseline with self-administration or withdrawal phases, a visually distinct distribution of weights over all voxels is observed, i.e. positive weights in the nucleus accumbens bilaterally, and negative weights in the hippocampus, colliculus and cortical regions. Finally, pattern regression identified an ^{18}FDG uptake pattern significantly correlated with a rat's nicotine intake.

Conclusion: Weight distributions suggests that the nucleus accumbens and the hippocampus play important roles in this disorder, although the roles of these regions is suggested to be opposing. Finally, these results show that ^{18}FDG PET scans could potentially have value as objective biomarker for nicotine use, but further optimization is required.

7.2 Introduction

Tobacco smoking is the leading cause of preventable disease and death in developed countries, with an annual death toll of 7 million (World Health Organization 2015). A lifetime of smoking is estimated to advance an individual's death by 10 years compared to non-smokers (Doll et al. 2004). These health problems are the consequence of toxic and carcinogenic substances inhaled with the smoke (Program 2015). This knowledge, and the increasing financial burden, prompts a desire to quit in 68% of the smoking population. Effectively, 55% of all smoker quit for at least one day, but only 7% of the smokers are able to quit successfully (Babb et al. 2017). An individual's susceptibility to smoking addiction depends on several factors: pharmacological, social, conditional, environmental, and genetic influences (Benowitz 2010a). The positive rewarding effects of nicotine include heightened concentration and task performance (Heishman and Singleton 2010), but additional negative reinforcement is due to the induced reduction of stress and anxiety (Hughes and Hatsukami 1986). The rewarding effects of nicotine are primarily mediated through the release of dopamine, although other non-nicotinic molecules, such as monoamine oxidase (MAO) inhibitors, contribute to addictive nature of cigarette smoking (Corrigall et al. 1992; Lewis, Miller, and Lea 2007). Binding of nicotine to neuronal nicotinic acetylcholine receptors (nAChRs), opens ligand dependent ion channels open and allow sodium and calcium to enter the intracellular compartment. These cations trigger other ion channels to open thus further decreasing the neuron's membrane potential and facilitating neurotransmitter release (Dajas-Bailador and Wonnacott 2004).

From a neurobiological perspective, dopaminergic neurons in the ventral tegmental area (VTA) are the primary targets of nicotine (Adinoff 2004). These neurons are able to release dopamine in the nucleus accumbens, which is experienced as pleasurable and required for spontaneous use (Benowitz 2010a; Corrigall, Coen, and Adamson 1994). A key difference between natural cholinergic transmission and its nicotinic variant are their temporal dynamics. Where acetylcholine typically occurs in millisecond bursts of high concentration, before it is hydrolyzed by acetylcholinesterase, nicotine is present in lower concentrations, but for a much longer time (Dani and De Biasi 2001). Therefore, nicotine can initiate a long dopamine release, but will desensitize the acetylcholinergic receptors hereafter (Mansvelder and McGehee 2002). This desensitization will slow the turn-over

of receptors on the cell membrane, eventually resulting in an excess of acetylcholinergic receptors. However, this excess becomes only clear when all receptors reappear on the cell membrane, which is the case in the absence of nicotine. This can lead to a neuronal overstimulation hypothesized to contribute to the restlessness experienced during withdrawal (Mansvelder and McGehee 2002).

Over the past few decades, PET studies have been used to show that nicotine increases the availability of nAChRs, as measured with 2-[^{18}F]fluoro-A-85380, but that these receptors also mediate nicotine self-administration in monkeys (Mukhin et al. 2008; Le Foll et al. 2009). Additionally, studies using [^{11}C]befloxatone showed that smokers have lower availability of cerebral monoamine oxidases, whereas [^{11}C]raclopride has been used to assess whether brain dopamine concentrations were influenced by exposure to nicotine (Leroy et al. 2009; Montgomery et al. 2007). Another group of studies has used ^{18}FDG to study the influence of nicotine on the cerebral glucose metabolism (CMR_{glc}). These showed that acute nicotine exposure causes a global reduction in CMR_{glc} (Stapleton et al. 2003). Moreover, Rose *et al*. reported that changes in smoking behavior can reversibly change regional CMR_{glc}, particularly in the striatal reward and corticolimbic regulatory pathways (Rose et al. 2007). Interestingly, resting-state fMRI data also show a change in functional connectivity in executive control networks and regions implicated in reward processing; this changes is moreover negatively correlated with withdrawal symptoms (Cole et al. 2010).

Classical neuroimaging analysis aimed to identify biomarkers by applying univariate analyses to obtain regionally specifics about abnormalities in brain function (Singh 2012; Singh et al. 2013). Recently, additional analysis techniques have been introduced at the junction of machine learning and neuroimaging, such as pattern recognition which can be used to classify datasets into discrete groups or to associate patterns with their continuous outcomes (Kloppel et al. 2012; Lemm et al. 2011). The latter has been applied to associate symptoms of behavioral and emotional dysregulation with fMRI data obtained from a reward paradigm (Portugal et al. 2016). In this study, fMRI is converted from 4 dimensional to 3 dimensional beta images, through the use of a generalized linear model regressing the time-series in function of the recorded stimuli periods. To apply these algorithms to resting-state fMRI, without losing its spatial organization or spatial resolution, we used eigenvector centrality mapping to spatially characterize the

functional connectivity by attributing network properties to voxels (Wink et al. 2012). Eigenvector centrality is the influence of a node in a network and is calculated by the strength of the connections with its neighbors taking into account the centrality of these neighbors. Therefore, eigenvector centrality takes into account the entire pattern of the network, has no region selection bias and is interpretable in the same space as the acquired brain scans (Lohmann et al. 2010).

In this study, we investigated the effect of nicotine self-administration on ^{18}FDG PET and resting-state fMRI data with pattern classification and regression analysis. Data were collected from a longitudinal nicotine self-administration protocol, where rats were scanned weekly during different phases of addiction. These different experimental phases included baseline, two weeks of self-administration, two weeks of forced withdrawal and a final week in which access to nicotine was regained. These experimental phases aim to reflect the different situations typically endured by the addicted patient. Classification analysis was performed to evaluate accuracy of the binary classification algorithm on differentiating scans acquired at baseline and after nicotine self-administration. In addition, we evaluated differences between baseline and withdrawal, and all time-points with versus without exposure to nicotine. Pattern regression analysis was performed to predict total self-administration based on baseline scans, as well as weekly average self-administration during every nicotine-exposure phase, i.e. self-administration and relapse. All analyses were performed for both ^{18}FDG and resting-state fMRI. In addition, classification was also performed when information from both modalities was used, a feature not yet available in the used software for pattern regression analysis.

7.3 Materials and Methods

7.3.1 Animals

Eighteen adult male Wistar rats (Charles River laboratories, Wilmington, USA) weighing 343 ± 19 g, were housed individually in a temperature controlled room and kept on a 12h reverse light-dark cycle (lights off at 7 am) with free access to water. During the experiments animals were kept on a diet of 20 ± 1 g food (Ssniff, Soest, Germany) per day to ascertain nicotine self-administration and prevent an excessive increase in body weight. At least 7 days before the start of the self-administration sessions, a catheter was

implanted in the femoral vein. These polyurethane 22G catheters (Instech Laboratories, Plymouth Meeting, USA) were inserted through the femoral vein in cranial direction for 7 cm. A vascular access button was mounted between the two shoulder-blades using a Dacron® mesh. The research protocol was approved by the local Animal Ethics Committees of the University of Leuven (P156/2013), and was carried out in accordance with European Ethics Committee guidelines (decree 86/609/EEC).

7.3.2 Self-administration

Nine experimental test chambers (Med Associates, Fairfax, USA) with custom-made solid floor, and equipped with two levers were used for SA experiments. One light stimulus above the active lever and acoustic stimulus (2900 Hz) mounted on the opposite wall were activated for the duration of the injection when the active lever was pressed. All test chambers were located in sound attenuating boxes to mitigate external sounds and light sources. Ten training sessions**,** during which sucrose pellets (45 mg, TestDiet, St. Louis, USA) functioned as reward, were installed to train rats until 200 responses within one hour were achieved. After baseline measurements with all tests, rats were given access to nicotine for 2 h per day for 14 consecutive days. During this time range, they could self-administer nicotine bitartrate dihydrate (0.03 mg/kg/infusion, Sigma-Aldrich, St. Louis, USA) by pressing the active lever one time (FR1 schedule). Nicotine dissolved in NaCl 0.9% was administered IV via a pump infusing 0.05 ml / infusion over 2.34 s. Each administration resulted in a 15 s time-out to prevent lethal doses. After these 14 days, rats were withdrawn from nicotine for 14 days, during which they were not placed in the self-administration boxes. This forced withdrawal period was followed by 7 days of regained access, mimicking a relapse (Figure 1). Catheter patency was tested using 4 mg/kg propofol (Propovet, Abott, Berkshire, United Kingdom) before first SA sessions and whenever animals showed a decrease in lever presses over 20% within 3 days.



Figure 1. Experimental design. = rodent Iowa Gamling Test, = ^{18}FDG PET, = ^{1}H-MRS.

Rats were fasted overnight before being scanned on a LSO (lutetium oxy-orthoscilicate) detector-based small-animal tomograph (FOCUS-220; Siemens Medical Solutions USA, Knoxville, USA), which has a transaxial resolution of 1.35 mm in full-width at half-maximum. During PET imaging, rats were kept under gas anaesthesia (2.0% isoflurane, 1.5 l/min O_2), and their body temperature was maintained between 36.5 and 37 °C with a heating pad. On average, 26.2 ± 1.5 MBq of ^{18}F-FDG was injected via a lateral tail vein, which was diluted with 0.9% NaCl (B. Braun, Melsungen, Germany) to a total injected volume of 0.5 mL. Animals were scanned per three and all scans were attenuation corrected using a Co^{57}-point source. Static emission scans were initiated one hour post-injection and lasted 30 min. List-mode acquisition data were reconstructed using filtered back projection and converted to standard uptake value (SUV) images, i.e. SUV = tissue activity x animal weight / injected dose. Using PMOD software (3.0, PMOD Technologies), a custom-made template of the rat brain was registered onto the SUV images (Casteels et al. 2013).

7.3.3 Resting-state fMRI

All MR images were acquired with a 9.4T Biospec small animal MR scanner (Bruker Biospin, Ettlingen, Germany) equipped with a horizontal bore magnet and an actively shielded gradient set of 600mT/m (117 mm inner diameter). A 7 cm linearly polarized resonator was used for transmission and an actively decoupled dedicated rat surface coil for receiving (Rapid Biomedical, Rimpar, Germany). Resting-state fMRI was acquired using single shot gradient echo EPI (Echo Planar Imaging) with TR = 2000 ms and TE = 16.7 ms. Twenty-one slices with 1 mm-thickness were recorded over 150 repetitions, during a 5 min acquisition time. Finally, a high resolution anatomical image was acquired using a Turbo RARE (Rapid Acquisition with Refocused Echoes) sequence (TR = 2500 ms, TE = 33 ms, 21 slices, 4 min acquisition time) for later volumetric and co-registration analysis. Animals were anesthetized using 2% isoflurane mixture for induction and maintenance, but this was reduced to a 1.5% concentration 5 min before and during the EPI acquisition to minimize its effect on the animal's physiology (Nair and Duong 2004). Body temperature was maintained at 37°C with a heated waterbed. Respiration and heart rate were monitored continuously.

Pre-processing was performed using FSL tools for fMRI brain imaging data (Woolrich et al. 2009). EPI data were slope corrected, before motion correction using MCFLIRT (Jenkinson et al. 2002). A band pass filter (0.01 – 0.1 Hz) was applied to the temporal data, resulting in the final temporal data used for further analysis. For registration of the EPI images to the stereotactic MRI brain atlas, we first registered anatomical RARE scans to the atlas. These aligned anatomical scans were then used to register the low-resolution EPI scan of the corresponding individual using FLIRT with 12 degrees of freedom, i.e. affine registration (Jenkinson and Smith 2001). Eigenvector centrality mapping (ECM) images were created from these registered EPI images using the fastECM Matlab package (Wink et al. 2012).

7.3.4 Pattern classification and regression

These analyses were performed with the PRoNTo 2.0 software package (Schrouff, Rosa, et al. 2013). For both types of analyses, ^{18}FDG SUV or ECM images were first masked with the available voxels present for all animals, i.e. voxels on the edges of the brain not present in all animals were discarded for analysis.

To evaluate the external validity we used a leave-one-out (LOO) cross-validation. LOO validation consists of repetitive training the model on all but one subjects, after which a classification or score is assigned to the subject that was left out, which is repeated for all other subjects to be left out. The performance of the classification model was evaluated by the number of correctly classified individuals in total accuracy (TA) and balanced accuracy (BA), i.e. the accuracy if both classes contained an equal number of observations. In addition, we report the sensitivity and specificity for each comparison. For the pattern regression analysis, the Relevance Vector Regression (RVR) was used, as it has previously been applied to neuroimaging based predictions (Portugal et al. 2016). The agreement between the assigned and observed outcome for the regression analysis is reported here by two metrics; Pearson's correlation coefficient and the normalized mean squared error (MSE). For both methods, a p-value was calculated for these performance measures by 1000 permutations. This entails that the same pattern analysis and cross-validation as above are performed, but where the observed score or classifications are permuted between subjects. The number of permutations resulting in

a better performance is divided by 1000 and used a p-value. Results were considered significant if the $p < 0.05$.

7.4 Results

7.4.1 Self-administration

The number of active lever presses quantifies self-administration (SA) behaviour and is illustrated per day in Figure 2. Self-administration starts out high during SA1 (27.7 ± 2.7), but the daily nicotine self-administration declines rapidly over the course of this phase, resulting in a more stable but significantly lower mean during the second week of self-administration (11.8 ± 1.1, $p < 0.0001$) and the relapse phase (9.0 ± 0.9, $p < 0.0001$).

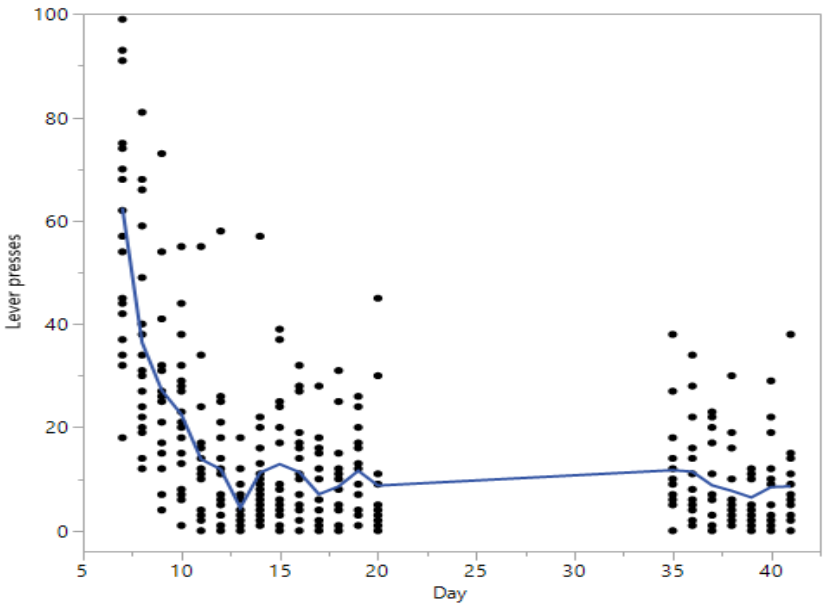


Figure 2. Self-administration over the course of the different experimental phases. Each dot represents the number of lever presses of an individual animal on that day, the line the population average. Note that during the withdrawal phase, i.e. day 19 – 33, no lever press data was be obtained.

7.4.2 Pattern classification

Classification of ECM and ^{18}FDG PET images was performed for three comparisons: firstly, we investigated which patterns could explain the differences between baseline

images and those acquired during both weeks of nicotine-exposure. Secondly, we investigated the reversibility of the nicotine-induced changes by comparing baseline and withdrawal week scans. Finally, all nicotine exposure phases were compared with all weeks where animals did not have access to nicotine, i.e. baseline, and the first and second week of withdrawal.

Detailed results of the first analysis can be found in Table 1. In general, ^{18}FDG scans provided higher classification accuracy than ECM images. This was particularly the case for the correct classification of baseline scans, which was only 5% for ECM. Combining both modalities with one kernel slightly improved the models accuracy compared to ^{18}FDG alone and resulted in a significant BA and specificity.

	TA	**BA**	**Specificity**	**Sensitivity**
^{18}FDG	72.7	58.2 (0.1)	30.8 (0.1)	85.7 (0.65)
ECM	66.7	48.4 (0.7)	5.2 (0.4)	91.5 (0.92)
Both modalities	76.4	57.9 (0.03)	23.1 (0.03)	92.9 (0.38)

Table 1. Classification accuracy of images obtained at baseline and during nicotine self-administration phases, i.e. two weeks of self-administration and one week of relapse. TA = total accuracy, BA = balanced accuracy. P-values are shown in brackets.

Weight maps, also called prediction patterns, for these analyses are shown in Figure 3. ECM showed a visually homogenous pattern, whereas ^{18}FDG images were weighted in a heterogeneous manner. Specifically, a bilateral cluster of high positive weights was observed in the nucleus accumbens, whereas large negative values can be observed in the hippocampus, colliculus, and cortical regions. The difference in sign does not signify a difference in relative importance, but rather that higher intensities in these voxels would either increase or decrease the estimated score respectively. For example, the model will assign a score and classify that scan to the nearest group, i.e. a score of 1.84 will be classified as a nicotine-exposure scan (group 2), rather than a baseline scan (group 1). Negative weights indicate therefore that, when a higher intensity is measured in this voxel or region, the final score will be lower and thus be more likely classified as a baseline scan. Specifically, a higher ^{18}FDG uptake in the hippocampus was associated here with baseline images.

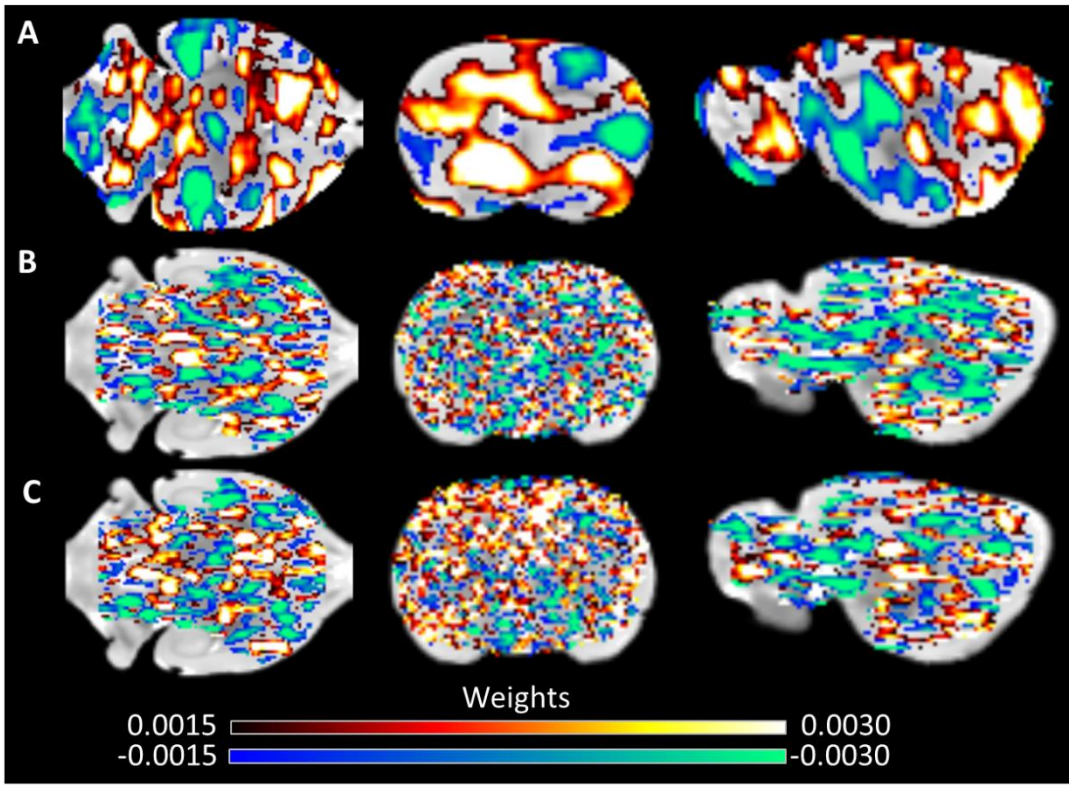


Figure 3. Weight patterns estimated by an algorithm using ^{18}FDG (**A**), ECM (**B**), or both (**C**) to classify subjects in either the baseline phase or nicotine exposure phase.

Interpretation of these feature weight maps should be done with care: the obtained results can only be achieved by using each voxel in the image. Therefore, it is recommended to not perform formal statistical analyses on regional differences, due to their inherent correlation as model parameters. However, it has recently been proposed to summarize regional weights based on an anatomical template (Schrouff, Cremers, et al. 2013). For this we calculated the mean absolute voxel weight for five regions implicated in addiction, namely the frontal cortex, hippocampus, nucleus accumbens, striatum, and thalamus. Additionally, for a clearer comparison between methods, all weights were normalized towards the average weight of all regions in the template, which cover the whole brain.

The heterogenous weight distribution in ^{18}FDG images is confirmed here, with the nucleus accumbens and hippocampus being on average more important for the classification (Figure 4). This distribution of weights was not observed for the ECM images, nor for the bimodal combination.

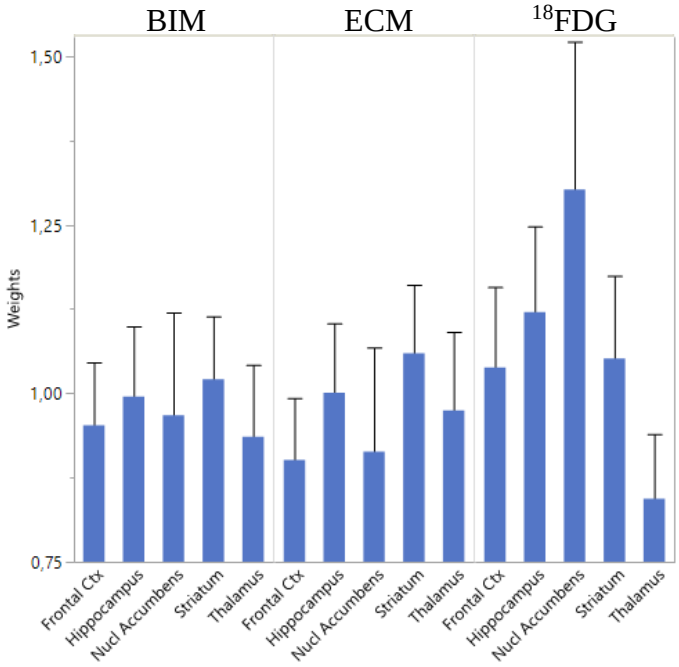


Figure 4. Average weights per anatomical region estimated by an algorithm using ^{18}FDG, ECM, or both to classify subjects in either the baseline phase or nicotine exposure phase. Error bars represent SEM. BIM = bimodal, Frontal Ctx = frontal cortex, Nucl Accumbens = nucleus accumbens.

The second analysis showed that higher classification accuracy could be achieved between scans obtained during baseline and the withdrawal phase. The model using ECM showed higher accuracy in this comparison than ^{18}FDG images. Conversely, the combination of both modalities using one kernel decreased the accuracy below the unimodal levels (Table 2),

	TA	**BA**	**Specificity**	**Sensitivity**
^{18}FDG	73.2	63.9 (0.02)	38.5 (0.07)	89.3 (0.07)
ECM	76.6	75.3 (0.01)	68.4 (0.02)	82.1 (0.39)
Both modalities	68.3	57.2 (0.07)	26.9 (0.13)	87.5 (0.26)

Table 2. Classification accuracy of images obtained at baseline and during the withdrawal phase. TA = total accuracy, BA = balanced accuracy. P-values are shown in brackets.

Pattern localization showed similar results as the analysis described above. In effect, the heterogeneous uptake in ^{18}FDG images is not observed in the ECM or bimodal weight images (Figure 5).

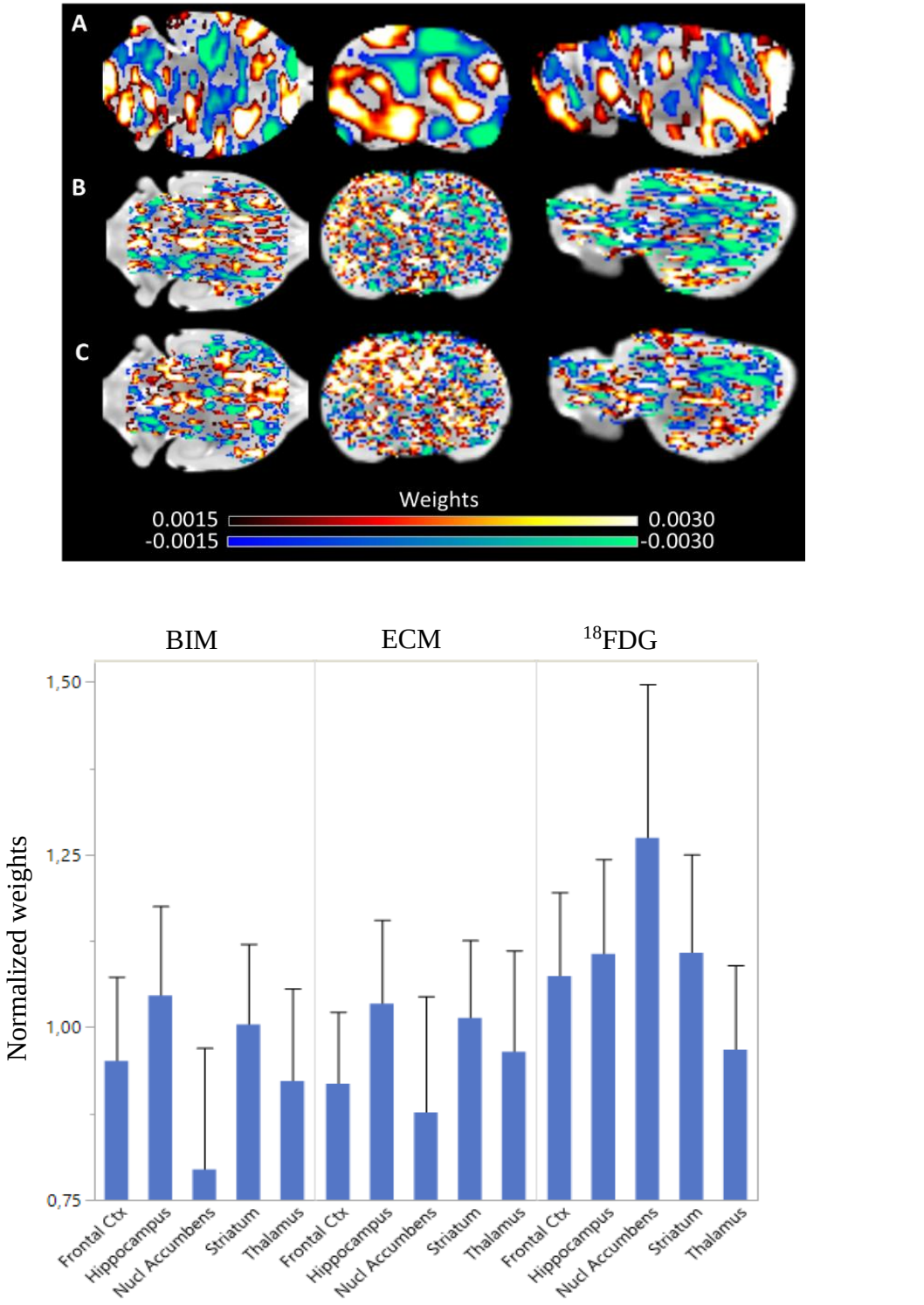


Figure 5. **Left**) Weight patterns, in atlas (**A**) space, estimated by an algorithm using ^{18}FDG (**B**), ECM (**C**), or both (**D**) to classify subjects in either the baseline phase or withdrawal phase. **Right**) Average weights per anatomical region estimated by an algorithm using ^{18}FDG, ECM, or both to classify subjects in either the baseline phase or withdrawal phase. Error bars represent SEM.

7.4.3 Pattern regression analysis

We also performed a regression analysis, in which models were used to predict the outcome variable associated with a scan. Firstly, baseline scans were compared with the total amount of nicotine that a rat self-administered during this experiment. This could potentially shed light on patterns or brain structures associated with an individual's propensity to use nicotine. The second analysis compared scans recorded at each self-administration week, with the average number of lever presses during that week. With this analysis we aimed to assess the pharmacologically induced changes in regional glucose metabolism and functional connectivity, as this could potentially be used as an objective biomarker for nicotine use.

Baseline scans were not able to accurately predict the total amount of nicotine an animal would self-administer (Table 4). A negative correlation in this situation indicates that the model is not able to learn from the data, i.e. high scores were predicted to be low scores and vice versa. The second analysis, associating the weekly number of lever presses with a scan acquired during that week, showed a significant correlation when using ^{18}FDG data.

	Baseline ~ total nicotine amount		**SA phases ~ weekly average lever presses**	
	Correlation	**Norm MSE**	**Correlation**	**Norm MSE**
^{18}FDG	-0.56 (0.86)	10.94 (0.72)	0.49 (0.01)	2.55 (0.01)
ECM	-0.54 (0.71)	10.68 (0.90)	0.05 (0.19)	3.35 (0.15)

Table 4. Pattern regression analysis results showing Pearson's correlation and the normalized mean squared error (Norm MSE), with the respective p-values in brackets. Left two columns show the results from the baseline scans predicting the total amount of self-administered nicotine, the right two columns show the results for scans acquired during self-administration and their association with the weekly average of self-administration, measured as lever presses.

No distinguishable pattern or weight distribution was found for either modality in the baseline analysis. For the second analysis, heterogenous ^{18}FDG images weights were observed, although identification of important anatomical regions was less clear: a cluster of positive weighting was observed in the right striatum, whereas low weighting was observed, as above, in the colliculus. Regional average weighting showed a higher value for the nucleus accumbens based on ECM images, whereas ^{18}FDG uptake associated with nicotine self-administration increased the weights in the frontal cortex and striatum.

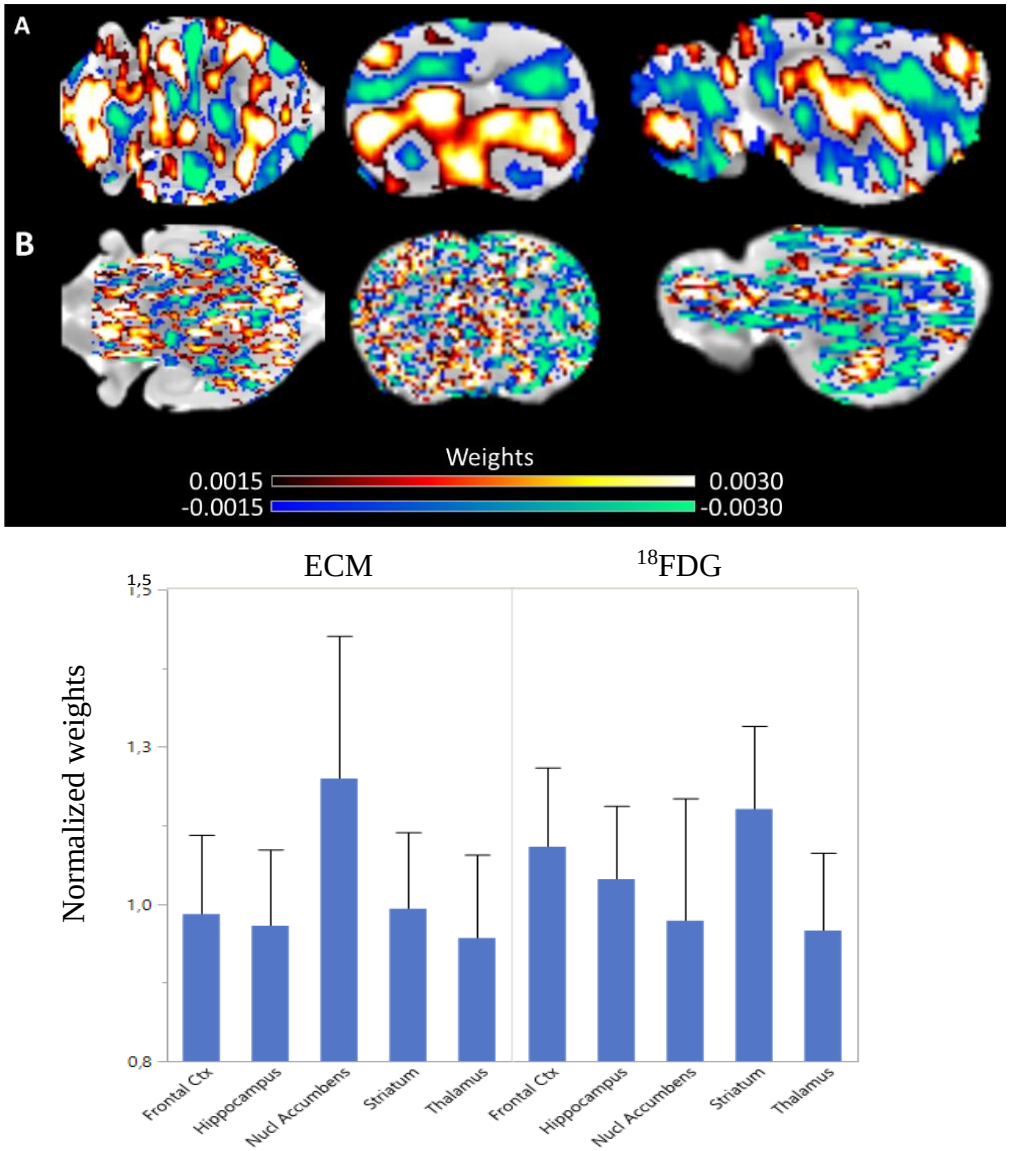


Figure 7. **Left**) Weight patterns, in atlas (**A**) space, estimated by an algorithm using ^{18}FDG (**B**) or ECM (**C**) for pattern regression analysis predicting the weekly average of lever-presses. **Right**) Average weights per anatomical region estimated by an algorithm using ECM (left) or ^{18}FDG (right) to predict the weekly average number of lever presses using scans acquired during self-administration weeks. Error bars represent SEM.

7.5 Discussion

In this work, we followed rats longitudinally before and during two weeks of nicotine self-administration. In addition, we staged a two week forced withdrawal and a final week of regained access. During this time, rats underwent weekly ^{18}FDG PET and resting-state fMRI scans. We applied pattern classification and regression to these functional neuroimaging data to determine whether patterns could be associated with drug-use. We show here that both modalities, separately or combined can identify, patterns associated with nicotine self-administration. Specifically, we have shown for the first time that pattern classification can be used on ^{18}FDG and ECM images to differentiate between time-points where animals could self-administer nicotine or not. In effect, we report that a binary Gaussian classification machine can reach a balanced accuracy up to 70%, when both modalities were combined, which is comparable to accuracies reported before for other psychiatric disorders (Mourao-Miranda et al. 2012). When comparing baseline with self-administration or withdrawal phases, a visually distinct distribution of weights over all voxels is observed, i.e. positive weights in the nucleus accumbens bilaterally, and negative weights in the hippocampus, colliculus and cortical regions.

Both the nucleus accumbens and hippocampus have been reported before to have significantly different functional connectivity when comparing nicotine-dependent smokers to non-smokers (Janes et al. 2012). Furthermore, high doses of nicotine have been reported to increase the $rCMR_{Glu}$ in the nucleus accumbens, but decrease this in the hippocampus, in rats (London et al. 1988). Our results show that, independently of the global reduction, the positively weighted nucleus accumbens became relatively more metabolically active and functionally connected. This is in line with numerous preclinical studies that have shown that nicotine promotes dopamine release, thus triggering energy dependent dopamine transporters of these dopaminergic neurons (Schilstrom et al. 1998). In contrast, the hippocampus showed a negative relation, which could corroborate the hypothesis that nicotine, like other substances of abuse, is able to reduce exploration, activity, and conditioning. This imbalance in the hippocampus – nucleus accumbens system, is thought to contribute to the evolution of hedonically motivated sporadic drug-

use and the habitual and compulsive behavior components that are typical for addiction (Everitt and Robbins 2005).

Pattern regression analysis, using a relevance vector regression algorithm, was able to identify patterns in ^{18}FDG, but not ECM, images that were partially predictive of the amount of nicotine an animal had self-administered in that week. In effect, the strength of this association is similar to that found in previous neuroimaging studies (Portugal et al. 2016). In this context, predictive means that the optimized regression model is able to return a score based on the corresponding imaging data. Although no visual pattern could be recognized, the weight per region summary showed that the striatum and frontal cortex were the two most influential regions when predicting a score for a new dataset. This is in line with the finding, that both these regions play a pivotal role in nicotine addiction. Not only is nicotine able to elicit a dopamine release here, but it can also inhibit the dopamine transporters in both regions (Cao, Surowy, and Puttfarcken 2005; Middleton, Cass, and Dwoskin 2004). A functional link has been proposed in the literature on schizophrenia, were it was observed that reduced prefrontal activity induced exaggerated striatal dopaminergic function (Middleton, Cass, and Dwoskin 2004).

The application of machine learning in biomedical research has exponentially increased in the last decade. On the one hand, this is due to the increasingly sophisticated and accessible algorithms that are available. For the analyses employed here, we used a Matlab package, PRoNTo, which is was designed specifically for neuroimaging and provides advantages, which assure the validity of the obtained results. However, scans cannot be entered with one or more covariates and, for the regression analysis, it is not possible to enter multiple data sources simultaneously into the model. This undermines a major advantage of machine learning algorithms compared to most classical analyses, which assess only one modality at the time in a univariate way. Despite its massive potential, it is generally recommended that results obtained with machine learning should be interpreted with care. In effect, in part due to their black-box character, machine learning techniques can identify irrelevant patterns with a confounding effect (Foster, Koprowski, and Skufca 2014; Begley and Ioannidis 2015). The use of longitudinal data, such as ours, in support vector machines is currently a subject of debate. Correlated observations could influence the external validity of the model, although a recent

comparison found that models ignoring this data clustering typically underperform. Exciting efforts are ongoing to develop kernels for longitudinal data, such as the hierarchical fisher kernel, but are not readily available yet.

The reported results are part of an ongoing study for which further analyses are underway. In effect, data has been collected for both a control group and for a group of animals that self-administered cocaine. The control group will be used to verify that the obtained results indeed result from the self-administered drugs, but not from different behavioral state or progressing adaptation to the environment and executers of the experiment. With the cocaine group we aim to investigate the differences in resting-state fMRI and ^{18}FDG uptake patterns induces by this drug compared to the nicotine induced changes. Finally, we will complement this machine learning analysis with the conventional voxel-based SPM analysis to further elucidate contrast specific significance clusters.

The present study was a proof of concept study to evaluate the potential of pattern regression in preclinical functional neuroimaging applications. Our results suggest that it is possible to identify patterns associated with nicotine use in a rat self-administration model. Concretely, we applied pattern classification and regression to ^{18}FDG PET and resting-state fMRI based eigenvector centrality mapping images. Using a binary classification machine, we were able to achieve 70% balanced classification accuracy, when comparing time-points with and without nicotine exposure. Although encouraging, the value of the pattern, which provided this moderate accuracy, is likely greater for the pathophysiological interpretation than for actual classification purposes. In addition, the weight distribution suggests that the nucleus accumbens and the hippocampus play important roles for this classification, although the roles of these regions is suggested to be opposing. Finally, we showed that ^{18}FDG brain scans could be correlated with the amount of nicotine self-administration at that time-point. This analysis emphasized the potential importance of the bilateral striatum and prefrontal cortex in nicotine use. Although further optimization is required, these results show that ^{18}FDG PET scans could potentially have value as objective biomarker for nicotine use.

Chapter 8: Acute changes in rat brain metabolism after intravenous administration of alcohol, cocaine, and nicotine: A simultaneous PET/MR study with dynamic ^{1}H-MRS and continuous infusion ^{18}FDG.

Bart de Laat · Akila Weerasekera · Gwen Schroyen · Willy Gsell · Cindy Casteels · Koen Van Laere · Uwe Himmelreich

Manuscript in preparation

8.1 Abstract

Introduction: Positron emission tomography (PET) studies have shown a global reduction in the regional cerebral metabolic rate of glucose ($rCMR_{Glu}$) after IV administration of addictive substances such as alcohol, cocaine, and nicotine. It has been hypothesized that this decrease could be mediated by a common mechanism in which glutamate release results in a decrease in $rCMR_{Glu}$. In this study, we combined continuous ^{18}F-deoxy-glucose (^{18}FDG) PET and dynamic proton magnetic resonance spectroscopy (^{1}H-MRS) to investigate the validity of this hypothesis.

Materials & Methods: Twenty-one Wistar rats received a simultaneous PET/MR scan of 50 min. After 25 min an intravenous injection was administered containing either saline or a drug of abuse, i.e. alcohol, cocaine, or nicotine. Using Patlak plot, $rCMR_{Glu}$ was calculated for the first and second 25 min of the ^{18}FDG scan. Dynamic ^{1}H-MRS in the prefrontal cortex was performed simulanteously.

Results: Stable $rCMR_{Glu}$ was observed in the control, alcohol and nicotine groups. Cocaine administration reduced the global CMR_{Glu} significantly (-11.3 ± 3.5 µmol/min/g, $p = 0.0017$). As for MRS, alcohol administration had a significant influence on the prefrontal concentration of ethanol (4.33 ± 0.30 mmol/L, $p < 0.0001$), glucose (1.35 ± 0.54 mmol/L, $p = 0.022$), choline (0.77 ± 0.36 mmol/L, $p = 0.042$), and glutamate (-1.0 ± 0.29 mmol/L, $p = 0.0026$). Cocaine increased glucose (1.26 ± 0.66 mmol/L, $p = 0.073$) and creatine (1.29 ± 0.44 mmol/L, $p = 0.0081$) levels, whereas nicotine did not significantly influence any metabolites.

Conclusion: Simultaneous FDG PET/MRS of the rat brain does not point to a common mechanism through which $rCMR_{Glu}$ can be reduced by drugs of abuse. In this experiment, only cocaine was able to reduce the global $rCMR_{Glu}$. Furthermore, our data show that alcohol can induce a transient decrease in glutamate concentration simultaneous with the peak in ethanol concentration. Since the effects of drugs of abuse on $rCMR_{Glu}$ are known to be dose-dependent, future studies exploring the molecular changes at different point in this dose-response relation are of interest.

8.2 Introduction

Addiction is considered to be the most costly of all psychiatric disorders in Europe, with the highest loss of disability adjusted life years and highest cost-of-illness (Effertz and Mann 2013). Non-invasive brain imaging techniques, such as positron emission tomography (PET) and magnetic resonance imaging (MRI) have paved the way towards better undestanding of the underlying pathophysiology of addiction. For example, several studies have reported the effect of drugs of abuse on global neuronal functioning after intravenous administration, as can be studied by glucose metabolism. Stapleton *et al*. reported a decreased regional glucose metabolism by approximately 10% after 1.5 mg IV nicotine (Stapleton et al. 2003), which was in line with a previous report studying nicotine nasal spray (Domino et al. 2000). Cocaine has been shown to induce a similar global reduction of 14% in regional cerebral metabolic rate of glucose ($rCMR_{Glu}$) in volunteers after intravenous administration (London et al. 1990). In addition, alcohol administration dose-dependently reduces $rCMR_{Glu}$ between 5 to 25% in human volunteers. Low doses of alcohol reduced the $rCMR_{Glu}$ only in cortical regions, whereas a higher dosage also affected subcortical regions (Volkow et al. 2006). This consistent decrease of the $rCMR_{Glu}$ after exposure to the major drugs of abuse have not been observed in preclinical experiments however. $rCMR_{Glu}$ showed dose-dependent increases in the several brain regions in rats, including the subiculum and colliculus, after 0.1 to 1.0 mg/kg intravenous nicotine administration (London et al. 1988). Although contradictory with the human study mentioned above, the relative change in $rCMR_{Glu}$ remains consistent: a reduction in $rCMR_{Glu}$ was observed in most human brain regions, however, not in those identified by an increase in $rCMR_{Glu}$ in rats. Similarly, a high dose of 10 mg/kg cocaine injection was shown to differentially affect the $rCMR_{Glu}$ with increases in some regions of the rat brain, but decreases in others. A similar, but dose-dependent increase was observed after low doses (0.25 g/kg) of alcohol administration, whereas a higher dose (1.0 g/kg) resulted in regional decreases in $rCMR_{Glu}$ (Williams-Hemby and Porrino 1994).

Different mechanisms have been proposed to explain the reduction in $rCMR_{Glu}$ in humans after intravenous administration of drugs of abuse. For alcohol, it has been suggested that the observed reduction in ^{18}FDG uptake might reflect the use of acetate as an alternative energy source, particularly for astrocytes (Cruz et al. 2005; Waniewski and Martin 1998).

Acetate crosses the blood-brain barrier via the monocarboxylate transporter and has a high Km for acetate transport by astrocytes. This might explain the contradiction that exists between these reports of decreased $rCMR_{Glu}$ and the observed increase in activity in frontal, temporal, and occipital brain structures using fMRI and regional CBF assays (Stein et al. 1998; Zubieta et al. 2001). As multiple drugs of abuse seem to reduce $rCMR_{Glu}$ in humans, it has also been hypothesized that this could be caused by a common mechanism. A proposed common mechanism is that drugs of abuse would induce an acute reduction in cerebral glutamate concentration. The molecular fundament of this hypothesis is that, next to its depolarizing effect on neurons, glutamate has been shown to induce glycolysis in astrocytes. The increased glycolysis is established by the Na^+/K^+-ATPase, as the cytoplasmic Na^+ rises through its co-transport with glutamate (Pellerin and Magistretti 1994).

In humans, the typical 30 min uptake period of a ^{18}FDG PET scan is long relative to the subjective effect of nicotine (Stapleton et al. 2003). This issue has been addressed in recent efforts that focused on protocols suitable for acute challenge studies. A proof-of-principle setup for "functional ^{18}FDG PET" has been reported, in which higher temporal resolution could be obtained (Villien et al. 2014). A continuous ^{18}FDG infusion is able to quantify the changes in glucose metabolism during blocks where subjects were finger-tapping, compared to resting control blocks (Hahn et al. 2016). Watabe *et al*. used this protocol to detect changes in the cerebral rate of glucose uptake in the rat brain when their whisker pad was stimulated (Watabe et al. 2016).

In parallel, similar protocols have been established for ^{1}H-MRS to non-invasively measure specific metabolites. Dynamic ^{1}H-MRS protocols have been established to acquire data with high temporal resolution, e.g. 1 min, and have been applied to study changes in muscle energy metabolism, but also to study exercise induced lactate increases in the brain (Brechtel et al. 2001; Prompers et al. 2006; Maddock et al. 2011). In addition, dynamic ^{1}H-MRS has been used to study metabolic changes in the brain after behavioral tasks or psychiatric disorders (Kuhn et al. 2016; Maddock et al. 2009). Since glutamate is one of the metabolites that can be detected with this technique, ^{1}H-MRS could be instrumental to elucidate the validity of the proposed glutamate hypothesis.

We hypothesize that an important glutamate release, induced by drugs of abuse, will results in a temporary depletion of glutamate with the concurrent decrease in glucose metabolism, as measured in previous PET studies. Therefore, we conducted a study in which continuous ^{18}FDG PET and dynamic ^{1}H-MRS are simultaneously acquired using small animal PET/MR, on rats before and after they received a dose of intravenous alcohol, cocaine, or nicotine.

8.3 Materials and Methods

8.3.1 Animals

Twenty-one male Wistar rats (R. Janvier, Le Genest-St-Isle, France) weighing 310 ± 10 g were included. Animals were housed three per cage with *ad libitum* food and water in a temperature- and humidity controlled room with a reversed 12h cycle for at least one habituation week before the experiment. The research protocol was approved by the local Animal Ethics Committee of the University of Leuven (P156/2013), and was carried out in accordance with European Ethics Committee guidelines (decree 86/609/EEC).

8.3.2 Pharmaceuticals and study design

To investigate the molecular basis of the previously reported influence on $rCMR_{Glu}$, we administered a drug of abuse 25 min after the start of both scans into the contralateral tail vein using an infusion needle set. Dosages of alcohol and nicotine were selected from previous studies in which a significant effect on $rCMR_{Glu}$ was observed (Williams-Hemby and Porrino 1994; London et al. 1988). For cocaine, an average of 2.5 mg/kg was taken of literature reported dosages, which ranged from 1 – 10 mg/kg (Zocchi, Conti, and Orzi 2001; Higuera-Matas et al. 2011). The injected solutions therefore, contained either ethanol (400 mg/kg, n = 6, Technisolv 99% v/v), cocaine (2.5 mg/kg, n = 5, UZ Leuven, hospital pharmacy ID 12904), or nicotine (0.3 mg/kg, n = 5, Sigma-Aldrich)(Gao et al. 2012; Anderson and Diller 2010; Picetti et al. 2010). All drugs were dissolved into an injection volume of 0.5 ml 0.9% NaCl (Braun, Hessen, Germany). For the control group (n = 5), no drugs were dissolved, but the same quantity of 0.9% NaCl was injected.

8.3.3 PET-MR

For simultaneous high-field MRS and a ^{18}FDG PET imaging, a 7T Biospec small animal MR system (70/30 USR, Bruker Biospin, Ettlingen, Germany) equipped with a 3-ring Silicon-based photomultiplier detector (SiPM) based PET insert (Bruker Biospin, Ettlingen, Germany) was used. The latter provides a resolution of 0.7 mm at Full Field Accuracy (FFA) with 12% sensitivity. Animals were anesthetized with 1.5% isoflurane in 1.5 L/min O_2, during which their body temperature was maintained with a heating waterbed. Respiration, ECG, and temperature was continuously monitored.

8.3.4 Continuous infusion ^{18}FDG PET

Small-animal PET imaging was performed while continuously infusing 31.6 ± 4.0 MBq ^{18}FDG into the tail vein with a Harvard Apparatus PHD 2000 pump (Harvard Apparatus, Holliston, USA) at an infusion rate of 0.015 mL/min. The radiotracer was diluted to 0.8 ml with a heparin-saline mixture (1:100; 25000 I.E./5ml; Leo, Ballerup, Denmark; Braun, Hessen, Germany). The 50 min PET scan, was started upon the start of injection and simultaneously with the MRS sequence described below. List-mode acquisition data were reconstructed to 50 consecutive frames of 1 min using the mesh-based three-dimensional maximum likelihood expectation-maximization (MLEM) algorithm (12 iterations, 23 x 23 pixels; fixed resolution, 0.5 mm). PET images were registered and spatially normalized to an in-house atlas in Paxinos stereotactic space (Casteels et al. 2013). This atlas included the bilateral striatum, nucleus accumbens, thalamus, and hippocampus. Additionally, the neocortex was divided in the frontal, sensorimotor, and medial and lateral temporal cortex. For these regions time-activity curves were created of each animal using PMOD software (PMOD, version 3.6, PMOD Technologies, Zürich, Switzerland). Patlak plots were generated for quantification of the mean cerebral metabolic rate of glucose (CMR_{Glc}) in R for each region and animal using time-activity curves of the whiskers area of the rat muzzle as reference region (R Core Team 2016; Backes et al. 2011). Slopes obtained from the Patlak plot were corrected for measured glycemia and the lumped constant was set to 0.625 (Watabe et al. 2016).

8.3.5 ^{1}H-MRS

Magnetic resonance was performed using a polarized resonator for transmission (30 cm horizontal bore) together with a rat head coil for receiving (Rapid Biomedical, Rimpar, Germany) and a quadrature volume coil with an internal diameter of 86 mm. A ^{1}H-MRS voxel of 2.5 mm^3 was manually placed in the prefrontal cortex, identified on 2D axial and sagittal T_2-weighted RARE anatomical scans (TR = 2500 ms, TE = 33 ms, 9 slices of 1 mm thickness). A point resolved spectroscopy (PRESS) pulse sequence (TR = 2000 ms, TE = 20 ms, 30 averages, 50 repetitions) was used to obtain 50 separate spectra, each taking one minute and three seconds to acquire. Water was suppressed using a presaturation pulse. Processing was performed with the jMRUI software package version 6.0 beta (Stefan et al. 2009). Quantification was performed with QUEST, an algorithm which fits a time domain model function to the *in vivo* data (Graveron-Demilly 2014). Linewidth H-peak was constrained below 17.5 Hz and broadening was constrained between 0 and 8 Hz, data was excluded if these ranges were exceeded. Individual metabolite amplitudes were estimated relative to the individual water amplitude.

8.3.6 Statistics

All statistical analyses were performed using SAS JMP pro 12.1 (SAS institute Inc., Cary, U.S.A.). The difference between measurements before and after the challenge injection were assessed using a linear mixed model, which included a random effect per animal. The reported values are mean ± standard error and significance was defined at the 95 % confidence level.

8.4 Results

8.4.1 PET

Animals showed a time-activity curve in the brain and blood consistent with previous reports (Figure 1) (Hahn et al. 2016). Linear spline regression was performed on the obtained Patlak plot for each animal, and the resulting slope was used to estimate the $rCMR_{Glu}$ (Figure 1). The average baseline $rCMR_{Glu}$ were 27 ± 9 µmol/min/g in the prefrontal cortex, 31 ± 10 µmol/min/g in the hippocampus, 30 ± 11 µmol/min/g in the nucleus accumbens, and 34 ± 12 µmol/min/g in the striatum, which are similar to previously reported $rCMR_{Glu}$ of anesthetized rats (Watabe et al. 2016).

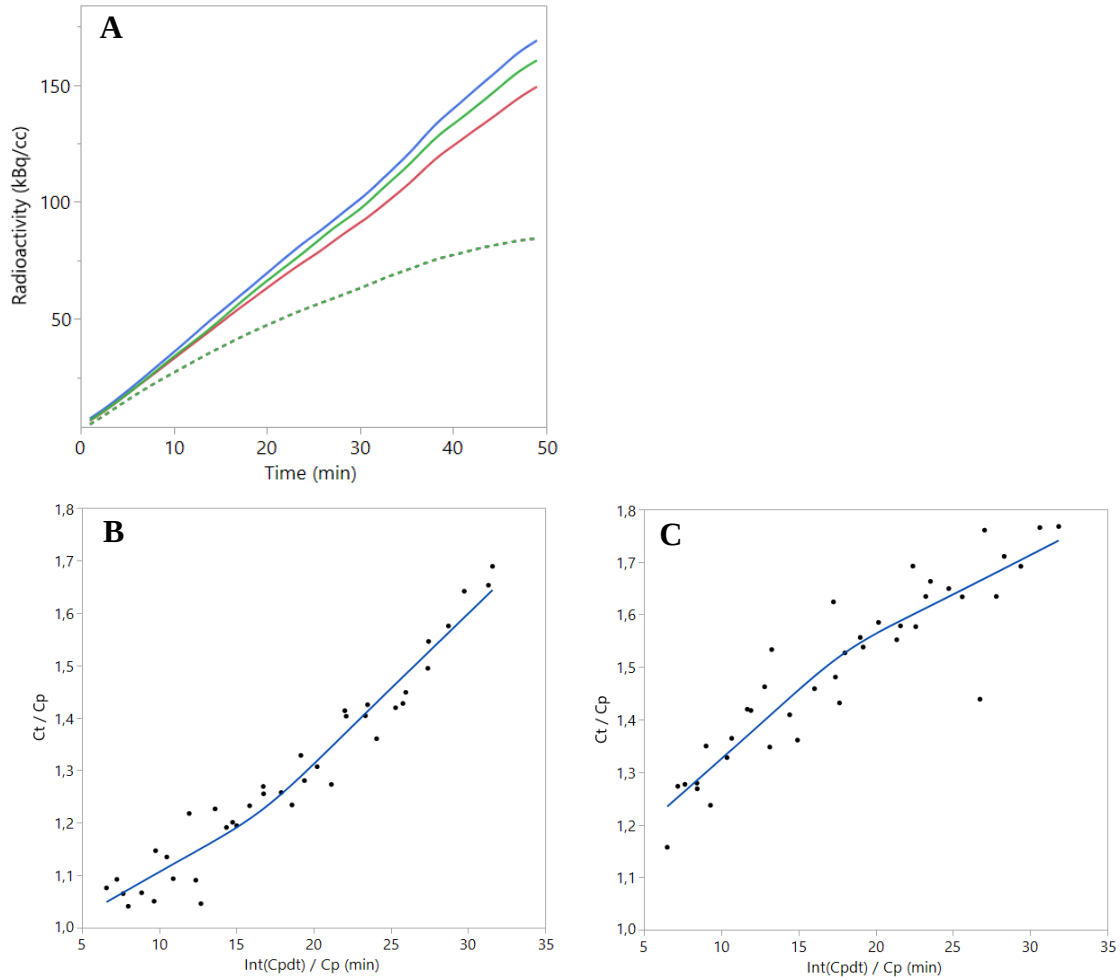


Figure 1. **A**) Average radioactivity concentrations for the plasma input function (dotted) or the right striatum (red), prefrontal cortex (green), and hippocampus (blue). Representative Patlak plots (points) of the right striatum for an animal that received either a saline (**B**) or cocaine (2.5 mg/kg) injection (**C**). A linear fit of the data (line), with a spline at the time of injection, visualizes the difference in pre- and post-injection $rCMR_{glu}$.

No significant over all differences in baseline $rCMR_{Glu}$ between groups were found. An increased $rCMR_{Glu}$ post-injection was observed for the control group, but significance was not reached (7.1 ± 4.1 µmol/min/g, p = 0.089). However, a significant decrease in average $rCMR_{Glu}$ was observed after cocaine injection cocaine (-11.3 ± 3.5 µmol/min/g, p = 0.0017). Change after injection did not differ significantly between the different regions (Figure 3). No other drugs were able to elicit a significant difference in $rCMR_{Glu}$.

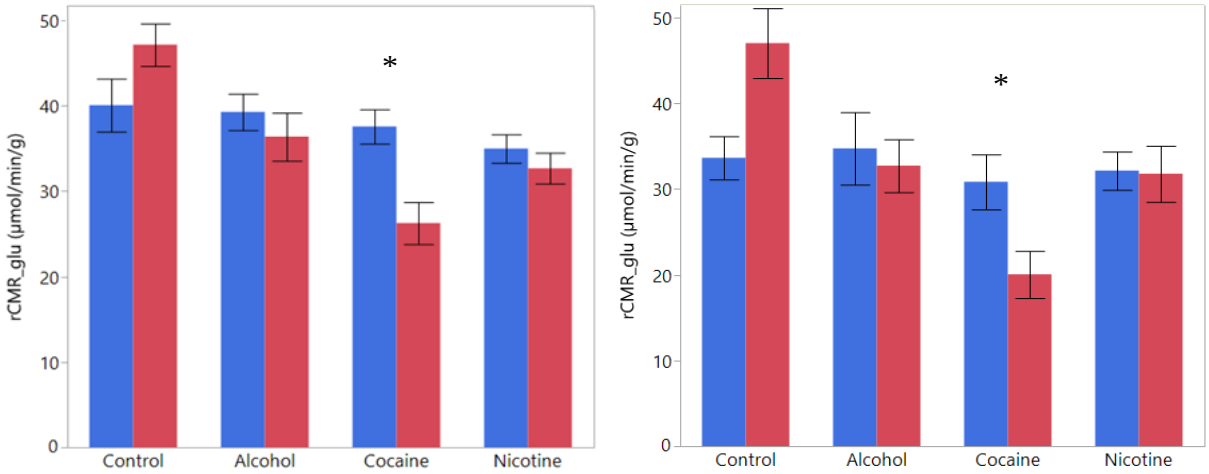


Figure 3. $rCMR_{glu}$ in the first (blue bars) and second (red bars) half of the scan in the bilateral thalamus (left) and prefrontal cortex (right). An increase in $rCMR_{glu}$ was observed in the control group, whereas cocaine induced a generalized decrease. Error bars represent the standard error of the mean. ** = $p < 0.01$

8.4.2 ^{1}H-MRS

All measured metabolites were found to be in previously reported ranges for healthy rats (Pfeuffer et al. 1999). For example, average prefrontal concentrations of glutamate at 8.8 ± 0.2 mmol/L, glucose at 6.6 ± 0.2 mmol/L, and creatine at 7.8 ± 0.1 were measured at baseline. An example of the acquired dynamic spectra can be found in Figure 4.

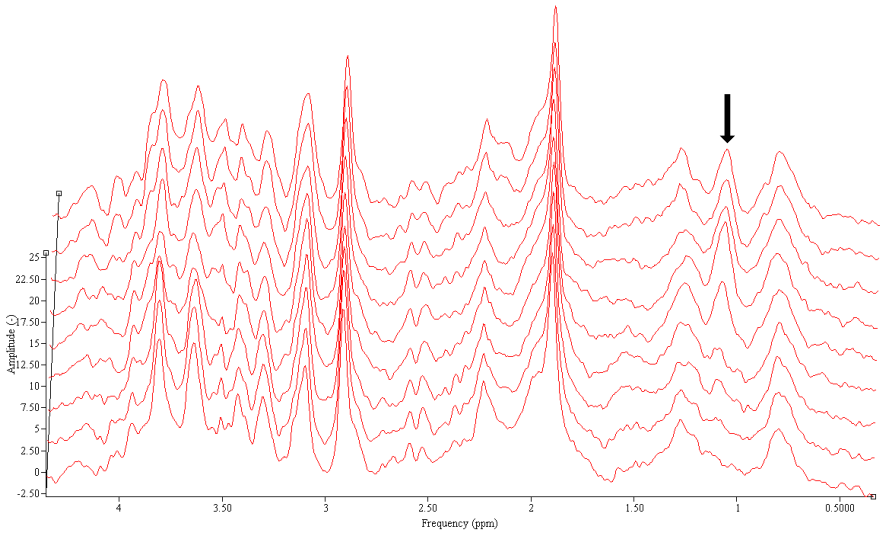


Figure 4. Example of spectra acquired during the dynamic MRS scan of an animal receiving an ethanol injection at 25 min. The black arrow indicates the peak associated with ethanol, which can be seen to rise after 25 min. In this figure, one spectrum represents the average of five one-minute spectra.

Changes between the average of the first and second 25 ^{1}H-MRS measurements showed that alcohol increased the glucose concentration (1.35 ± 0.54 mmol/L, p = 0.022), as well as the creatine (0.77 ± 0.36 mmol/L, p = 0.042), and ethanol concentration (4.33 ± 0.30 mmol/L, p < 0.0001). However, the challenge with alcohol reduced the prefrontal glutamate concentration (-1.0 ± 0.29 mmol/L, p = 0.0026). Cocaine also increased glucose (1.26 ± 0.66 mmol/L, p = 0.073), and creatine (1.29 ± 0.44 mmol/L, p = 0.0081). An interesting result is that nicotine was the only drug that decreased the glucose concentration during the experiment, albeit non-significantly (0.27 ± 0.60 mmol/L, p = 0.65).

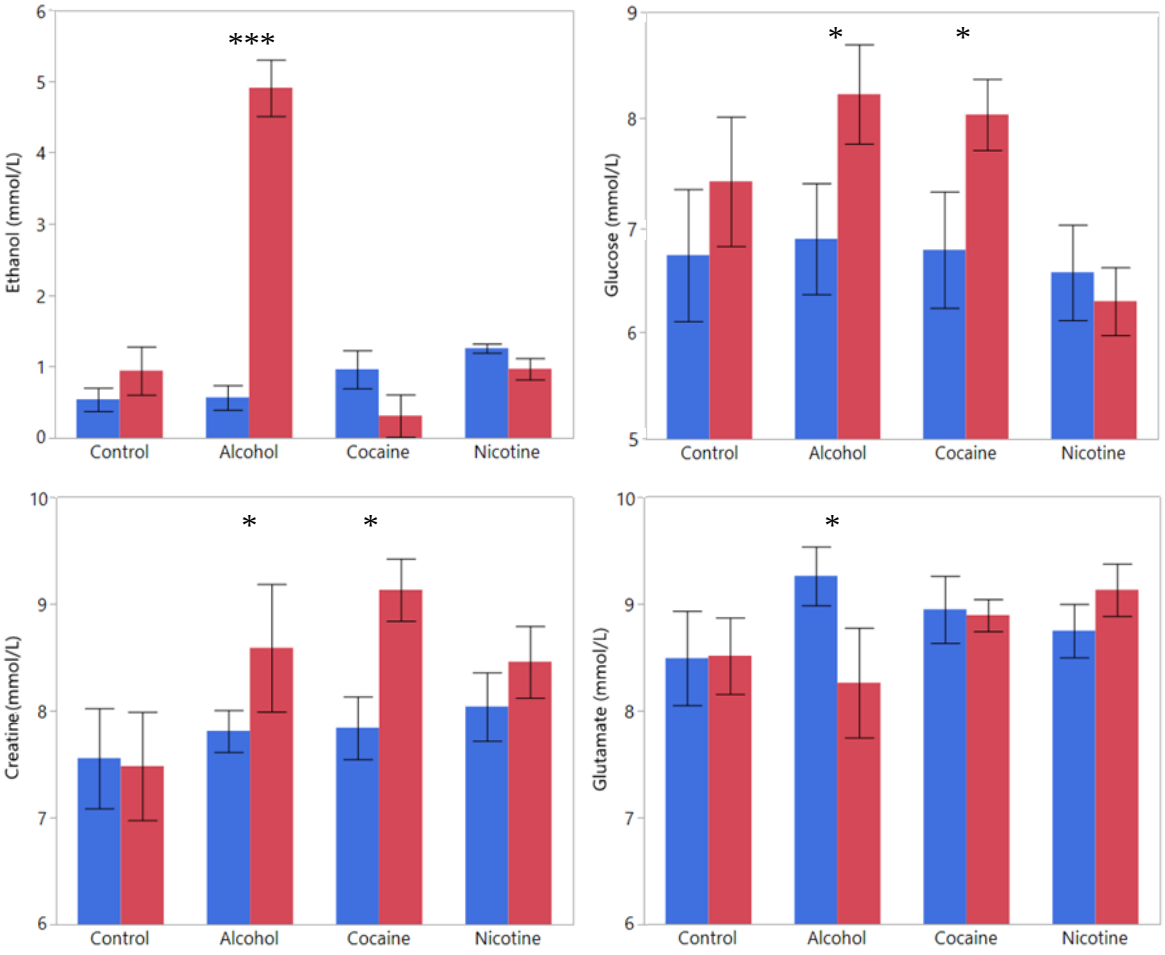


Figure 5. Prefrontal metabolite concentrations before (blue bars) and after (red bars) the challenge injection for each group as measured with ^{1}H-MRS. Error bars represent the standard error of the mean.

To fully exploit the one-minute temporal resolution of the dynamic MRS data, we visually inspected how every metabolite behaved after the respective drug injections. No distinct patterns were found for any drug, except for the alcohol administration. These showed a marked ethanol concentration increase, for which individual variance in peak concentration and clearance could be observed (Figure 6A). In addition, a change in the prefrontal glutamate concentration was found. This seems to visually correspond with the ethanol increase, as the concentration of this metabolite appears to transiently decrease during the peak concentrations of ethanol (Figure 6B).

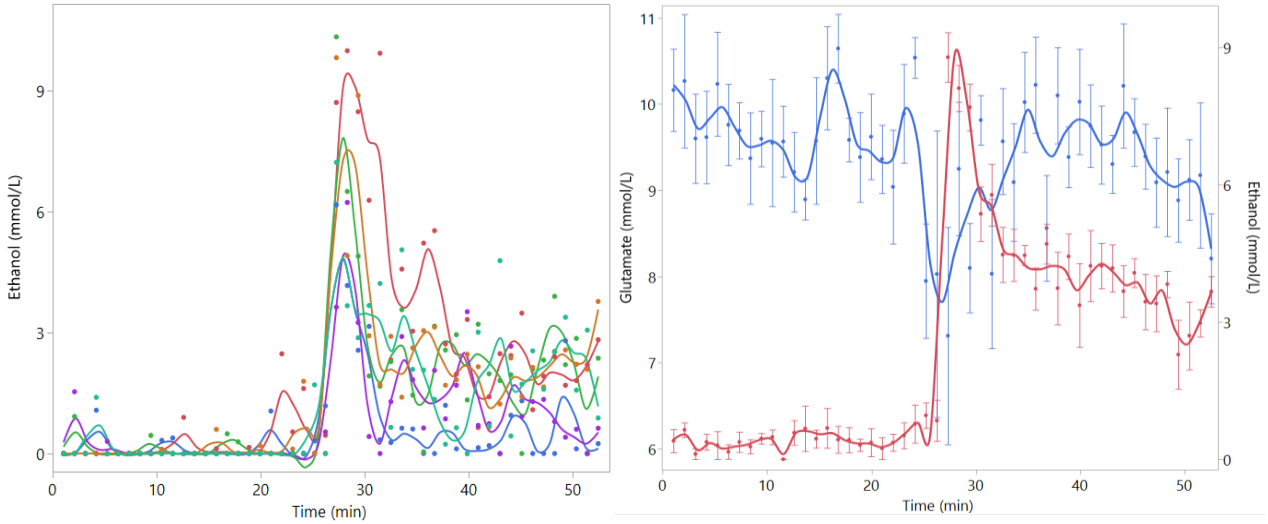


Figure 6. **A)** Concentration of ethanol as measured with ^{1}H-MRS after IV ethanol injection at 25 min. Every repetition is quantified separately resulting in one minute bins of 32 averages. **B)** Average concentration of glutamate (blue, left Y-axis) and ethanol (red, right Y-axis). Points show the average value over all animals with its standard error, a cubic spline smoothing curve is fitted through these points. Note that the increase in standard errors during the respective increase or decrease is due to inter-subject variability of the onset, which is larger for glutamate.

8.5 Discussion

In this experiment, we evaluated the influence of intravenous alcohol, cocaine, and nicotine on the $rCMR_{Glu}$ of rats as evaluated with continuous ^{18}FDG. Dynamic MRS was simultaneously acquired in the prefrontal cortex in an attempt to elucidate the molecular

pathways that would underlie the previously reported changes in $rCMR_{Glu}$. Of the three evaluated drugs, only cocaine was able to significantly reduce the $rCMR_{Glu}$ compared to the pre-challenge rate. However, the control group showed an increase in $rCMR_{Glu}$, which was not present in the nicotine and alcohol group. ^{1}H-MRS showed that cocaine injections increased glucose and creatine concentrations in the prefrontal cortex. In addition, alcohol was found to have a significant effect on the prefrontal concentration of glucose, creatine, ethanol, and glutamate. Furthermore, a dynamic pattern was identified that corroborates the potential association between ethanol and glutamate as mechanism for observed reduction in $rCMR_{Glu}$.

The use of anesthetic agents is common practice in preclinical neuroimaging. However, most anesthetic agents are notorious for their extensive influence on different organ systems, including the brain. Isoflurane in particular has been shown to increase the $rCMR_{Glu}$, and ^{18}FDG uptake upon which this is based, in rodents, when compared to other anesthetic agents such as sevoflurane (Flores et al. 2008). This is in line with our observation that the $rCMR_{Glu}$ is higher, albeit non-significantly, for the control group in the second 25 min of the 50 min ^{18}FDG PET scan. This increase is not observed after alcohol, nor nicotine administration. As we discussed above, the reduction in $rCMR_{Glu}$ in rodents after injection of drug of abuse is strongly dose-dependent. Therefore, it would be interesting to investigate whether a significant reduction could be induced with higher dosages of these drugs. Cocaine however, was able, at the evaluated dosage of 2.5 mg/kg, to reduce the $rCMR_{Glu}$ significantly in all evaluated regions. This is in line with previous reports, but highlights the importance of dose-effect studies to allow further interpretations.

Our PET protocol used a constant infusion of ^{18}FDG, which is a logical explanation for the observed increase in prefrontal glucose concentration by ^{1}H-MRS, as ^{18}FDG will provide the same resonance signature as glucose itself. However, further studies are required to assess whether the low quantity of injected ^{18}FDG, relative to the naturally present glucose concentration, can indeed entirely explain this effect. Interestingly, animals that received an intravenous nicotine injection showed a small decrease in glucose levels. A probable explanation for this, as well as the stable $rCMR_{Glu}$ in this group, is the previously described increased uptake of ^{18}FDG in peripheral adipose tissue

after acute nicotine exposure (Baba et al. 2007). This would lower the concentration of both glucose and ^{18}FDG in the blood and consequently that in the brain, thus resulting in a relatively lower prefrontal glucose concentration measured by ^{1}H-MRS. The $rCMR_{Glu}$, calculated as a ratio between the concentration of ^{18}FDG in the blood and the brain, would however not be influenced. Although this seems a plausible explanation for our results, more data should be gathered to confirm the lower glucose levels after nicotine administration, as well as the lack of effect on the central ^{18}FDG uptake by nicotine assumed now.

All drugs of abuse evaluated here were able to increase the prefrontal concentration of creatine, an organic acid involved in energy metabolism, although only alcohol and cocaine did so significantly. Creatine can be degraded to regenerate ATP and functions as an energy reserve for the brain (Wyss and Kaddurah-Daouk 2000; Gatfield et al. 1966). Using ^{18}FDG PET we show that drugs of abuse can reduce the $rCMR_{Glu}$, as a consequence of this decrease in metabolic activity, creatine reserves might have the opportunity to replenish (Sauter and Rudin 1993). Next to creatine, ethanol and glutamate were also influenced by the intravenous injection of alcohol as measured with ^{1}H-MRS. On the one hand, ethanol itself was observed to rise rapidly after the administration, this highlights however predominantly the benefits of dynamic ^{1}H-MRS, which are discussed below. On the other hand, a decrease in glutamate was also observed. More specifically, using high resolution dynamic ^{1}H-MRS we were able to demonstrate that this decrease was mainly caused by a transient decrease in the measure glutamate concentration immediately after the alcohol administration. As ^{1}H-MRS measures both intra- and extra-cellular concentrations, any decrease is likely due to changes in the molecular structure. For example, an ethanol induced glutamate release is taken up from the synapse by glial excitatory amino acid transporters (EAATs) to be converted by glutamine synthetase to glutamine (Woodward 1990; Roberto et al. 2004). Interestingly, alcohol abuse has been shown to decrease the level of EAATs, which are negatively correlated with glutamine synthetase activity (Miguel-Hidalgo et al. 2010). This increased activity in glutamine synthetase therefore, could decrease the glutamate concentration by increasing the relative glutamine contribution. A recent ^{1}H-MRS study did indeed observe this effect in alcoholic patients versus matched controls (Thoma et al. 2011). Our results corroborate the hypothesis that the reduction in $rCMR_{Glu}$ observed in humans after alcohol injection

could be based on the consequent glutamate release. Specifically, a major degradation of glutamate, such as suggested by our data, would decrease the $rCMR_{Glu}$ by reducing the metabolic activity of both neurons and astrocytes (Pellerin and Magistretti 1994).

Much interest exists in constant ^{18}FDG infusion protocols to show acute and transient changes in glucose metabolism. These protocols induce physiological responses that evolve during the scan and thus violate the steady-state assumption. However, Villien *et al*. showed that, although violated, the derivative of the free ^{18}FDG concentration in the tissue can be assumed to be zero (Villien et al. 2014). This partly relies on the temporal frame in which this is assumed, as during the entire scan the plasma concentration does change. Accurate quantification of $rCMR_{Glu}$ does therefore require further development of quantification through kinetic modelling, but the values reported here can be considered as high temporal resolution ^{18}F-FDG PET approximations. Additionally, further exploration of analysis methods for the obtained Patlak plots could prove fruitful, as the effect of an imposed stimulus could wean off during the scan. Therefore, more advanced methods allowing time-variant component might be able to provide more information about duration and amplitude of the change in $rCMR_{Glu}$ (Kim et al. 2014).

Magnetic resonance spectroscopy can be used to non-invasively quantify metabolites in the brain and has been applied in clinical and preclinical studies. Here we apply a modification of the classical ^{1}H-MRS sequence to obtain higher temporal resolution estimates (Prompers et al. 2006). A downside of this approach is the decreased signal-to-noise ratio, resulting in larger variability of estimated concentrations. Nevertheless, we were able to show here that individual pharmacokinetic-pharmacodynamic profiles of ethanol can be obtained with ^{1}H-MRS. This translational technique could therefore be of great use, particularly when combined with simultaneous plasma sampling, in alcohol research, as it has been in other pharmacokinetic-pharmacodynamic studies (Komoroski et al. 1993).

In this work, we reported that intravenous cocaine injections can induce a generalized decrease in $rCMR_{Glu}$. In addition, an increase in $rCMR_{Glu}$ was observed in the control group, but not in the alcohol and nicotine group. ^{1}H-MRS showed that cocaine injections increased glucose and creatine concentrations in the prefrontal cortex. Alcohol was found

to have a significant effect on the prefrontal concentration of glucose, creatine, ethanol, and glutamate. Moreover, using dynamic ^{1}H-MRS we were able to demonstrate a transient decrease in prefrontal glutamate concentration, simultaneous with the spike in ethanol level. In general, we showed that continuous ^{18}FDG infusion PET and dynamic ^{1}H-MRS are well suited to study the acute effects of pharmacological challenges, especially when combined for simultaneous measurements.

Chapter 9: Logan plots: A comparison between summary statistic approaches and analysis with GEE, second-level, or mixed models

Bart de Laat · Cindy Casteels · Koen Van Laere · Yves Rosseel

Manuscript in preparation

9.1 Abstract

Introduction: Positron emission tomography imaging can provide dynamic time-activity curves, which describe the concentration of radioactivity in a tissue over time. These dynamic data are typically mathematically modelled to obtain specific kinetic parameters, that can be surrogate markers for the variable of interest, such as binding potential (BP). These parameters however, are summary statistics that do not pass on all available information to the consecutive analysis. We report a comparison for Logan plot analysis between summary statistics, i.e. t-test and Mann-Whitney *U* test, and population inference approaches, i.e. second-level analysis, mixed models and general estimating equations (GEE).

Materials & Methods: We simulated reversible radiotracer PET data based on a two-tissue-compartment model with Gaussian variance on k3 and k4. Different methods were applied to detect increasing differences up to 10% in BP between two groups, as a result from increasing k3 difference. We assumed both groups as of equal size, but group size was varied between 5 and 50. Additionally, between-subject variance was evaluated at levels between 2.5 and 20% levels. Differences between groups were evaluated with a two-sample t-test and the non-parametric Mann-Whitney *U* test on the respective BP values calculated from the simulated data using the Logan reference method. A second-level analysis was performed on the same summary statistics, but also taking into account the variance of this estimate and allowing a random effect per subject. A population mean BP was estimated with mixed models, allowing for random intercept and slope, and a general estimating equation, which used an unstructured correlation structure, and an identity link-function for Gaussian data. Finally, the same methods were applied to experimental data obtained from a preclinical ^{18}F-FPEB study on 24 adult Wistar rats either exposed to cocaine or not, which resulted in approximately 5 – 15 % difference in BP.

Results: The t-test and Mann-Whitney *U* test provided stable and robust BP estimates in most simulations, although the latter was conservative in smaller samples below n = 10. A gain in power to detect group differences was achieved with mixed models and second-level analysis. All four methods resulted in a bias between 3 – 8 %, when between-subject variance was high. Interestingly, at 2.5% variance levels, mixed models showed an inflated bias when compared to higher levels of variance. Finally, GEE are shown to be less suited in smaller datasets and should generally be avoided unless group sizes larger

than 20 are achieved. This is based on the high false positive rate, but also the increasingly large bias with higher levels of between-subject variance. Results of the experimental ^{18}F-FPEB data analysis were in line with these results obtained for the simulated data.

Conclusion: A second-level analysis method is of interest due to its ease of implementation and low risk of model misspecification.

9.2 Introduction

Statistical analysis is used in biomedical research to indicate whether an observed effect is unlikely to have been observed due to chance. Several statistical methods exist to allow suitable analysis methods for data with different measurement scales and collection methods. A specific class of methods handles data that is collected in a longitudinal, hierarchical or clustered fashion. The key issue with these data is that some observations can be expected to be more correlated than with others (Galbraith, Daniel, and Vissel 2010). For example, multiple measurements on one subject are likely more correlated amongst each other than with those data points from different subjects. This effect, called within-subject correlation, decreases the amount of information per data-point, and should thus be corrected for. We could hypothesize that observations within a subject are distributed around a mean, but that this mean is a part of the distribution around the mean of all subjects. In this formulation, a specific term describes the variation of observation within a subject around their respective mean. Therefore, the observation *i* in subject *k* can be written as $y_{ik} = \mu + b_k + \varepsilon_{ik}$. In which μ represents the mean of all subjects, and b_k the between-subject variation. ε_{ik} represents the within subject variation or, in statistical terms, the residual errors. In this model, we assume b_k to be independent from ε_{ik}, i.e. although there is correlation within each subject, the different subjects are independent (Fitzmaurice et al. 2008).

Dynamic positron emission tomography (PET) data consists of multiple data points collected from the same subject during one scan. As described above, this inherently means that data points are more correlated within one subject, than between data points from separate subjects. Here we briefly introduce and compare different methods to deal with these data. For conceptual simplicity, all examples are focussed on linearized PET

data, e.g. using the Logan non-invasive model, but all principles also apply to non-transformed data.

9.2.1 Summary statistics

A relatively easy way of dealing with correlated data is to reduce all clustered data, here all measurements from one subject over time, into one summary statistic. This approach is applied in the majority of neuroimaging studies, because the resulting data points are now from different subjects and can thus be considered independent. Therefore, standard methods for independent observations can be used. We describe below the two most popular tests, namely the t-test and its non-parametric counterpart the Mann-Whitney *U* test. There are several versions of the t-test, adapted to different null hypotheses, such as differences from zero, differences between paired observations, or differences between independent samples. The test statistic for a comparison between two groups, which is the focus in this work, is described by:

$$t = \frac{\bar{X}_1 - \bar{X}_2}{\sqrt{\frac{s_{X_1}^2 + s_{X_2}^2}{2}}}$$

Since the t-test for independent samples can be considered a special case of the linear regression model, we can rewrite the test statistic for a specific variable, for example binding potential, as

$$BP = \beta_0 + \beta_1 * group$$

In which β_0 estimates the average binding potential, BP, for one group and, $\beta_0 + \beta_1 * group$ provides the estimate for the other group, with β_1 the difference between both. Since smaller samples are common in biomedical research, the non-parametric counterpart of the t-test, the Mann-Whitney *U* test, is also commonly used. This test also assumes independence between groups, as well as that the nature of the responses is at least ordinal.

The test-statistic *U* can be calculated as:

$$U_1 = R_1 - \frac{n_1(n_1+1)}{2}$$

In which R_1 is the sum of ranks in sample 1. This is calculated by combining the observations from both groups ordered from small to large value. The ranks of all observation from group 1 are then summed to obtain R_1. In doing so, the actual values of observations are not taken into account. This makes not only for good ordinal value testing, but also makes this test more robust against outliers than the t-test. When the observations originate from an underlying normal distribution the Mann-Whitney *U* test will be $3/\pi \approx 0.95$ times less powerful. However, with increasing departures from normality a threefold gain in power can be achieved (Fay and Proschan 2010; Blair and Higgins 1980).

9.2.2 Second-level analysis

An interesting approach combines the summary statistic approach, and its previously ignored measure of uncertainty (within-subject variance), with a second step to estimate the between-subject variance. This analysis, named second-level analysis in the neuroimaging field, is an adaptation of methods commonly used for meta-analysis studies. In such an analysis, an effect size and its uncertainty measure are extracted for multiple studies and analysed to estimate the overall effect size or difference between groups. Coming back to the binding potential example mentioned above, we could write the first step of this approach for the BP for the i-th individual, in the j-th group as:

$$BP_{ij} = w_i + e_{ij}$$

with variance:

$$Var[w_i] = \sigma_e^2$$

The group average, for N subjects, is then estimated as:

$$\widehat{w}_{group} = \frac{1}{N}\sum_{i=1}^{N} w_i$$

with variance:

$$Var\left[\widehat{w}_{group}\right] = Var\left[\sum_{i=1}^{N}\frac{1}{N}w_i\right]$$

This variance however contains two types of variance, which are here undistinguishable: on the one hand the between-subject variance, i.e. the actual difference between animals in binding potential for example, but on the other hand also the within-subject variance. The latter refers to the variance that remains between measurements on the same animal. This is often referred to as measurement error, which is not due to variation in the biological variable, but rather to other sources, such as the technical variation of the instruments used. When improperly separated this lumped variance can lead to faulty inference and this is the theoretical basis for applying second-level analysis.

In a second-level model, but also the mixed models described below, an estimate of the individual *i* of group w, $\widehat{w}_i$, can be defined as the sample average, $w_{population}$, plus the difference between the average of the population and the group to which *i* belongs, z_j. Finally, we add the difference between this average group level and the individual level, here denoted as e_i. Since we have $E[e_i] = E\left[z_j\right] = 0$, and we assume that $Cov(e_i, z_j) = 0$, it can be written that for the i-th individual from the j-th group:

$$\widehat{w}_i = w_{population} + z_j + e_i$$

The variance of the population mean can then be estimated as:

$$\begin{aligned} Var\left[\widehat{w}_{pop}\right] &= Var\left[\sum_{i=1}^{N}\frac{1}{N}w_i\right] \\ &= Var\left[\sum_{i=1}^{N}\frac{1}{N}z_i\right] + Var\left[\sum_{i=1}^{N}\frac{1}{N}e_i\right] \\ &= \frac{\sigma_b^2}{N} + \frac{\sigma_w^2}{N} \end{aligned}$$

Therefore, the variance estimate of the population contains both the within- and between-subject contribution. For example, the individual estimates and their within-subject variance obtained with the Logan non-invasive model are used to estimate the between-subject, i.e. the within-group, variance. The validity of this approach lies in the sample mean being used in the second-level, where its weighting adapted according to the between-subject variability can provide the right balance between within- and between-subject variance. The attraction of this method in neuroimaging analysis, compared to mixed models, lies in the fact that this approach is less computationally expensive and easier to formulate for the extensive datasets in these studies (Friston 2006).

9.2.3 Linear mixed models

Linear mixed models rely on a similar likelihood model as second-level analysis. In effect, the model can still be described in a hierarchical formulation, with the individual and population estimate respectively equal to:

$$y_{ij} = w_i + e_{ij}$$

$$\widehat{w}_i = w_{population} + z_j$$

A practical difference with the second-level analysis described above is the simultaneous estimation y_{ij}, e.g. an individual BP, and the difference between groups, contrary to the clear distinct steps in second-level analysis. However, both methods will result in the same analysis as a mixed model can also be written as:

$$\widehat{w}_{ij} = w_{population} + z_j + e_i$$

An interesting difference between approaches is that in mixed models we can explicitly formulate random intercepts and slopes. In our example of linearized PET data, both could have a positive influence on the fit of the model to the data, and therefore provide an advantage of the full mixed model approach. In effect, this explicit specification of types of random effects cannot be performed with second-level analysis. However, since the second-level model relies on the fixed effect regression or on its 'first-level', estimating a random effect based on the outcome, BP, could be considered to encompass both possible random effects, albeit non distinguishable.

9.2.4 General Estimating Equations

An alternative way to deal with correlated outcomes are the GEE method. An important aspect of GEE models is their capability of dealing with data from multiple distributions. However, since we are limiting our application to PET data, the potential benefits of these extensions are not discussed. Two main differences with the linear mixed model approach exist: the model specification and interpretation of the obtained coefficients. The model of the GEE can be written as:

$$\begin{bmatrix} Y_1 \\ \vdots \\ Y_n \end{bmatrix} = \beta_0 + \beta_1 \begin{bmatrix} X_{1,1} \\ \vdots \\ X_{n,j} \end{bmatrix} + \beta_2 + CORR + Error$$

In this formulation, *CORR* corresponds to the correlation matrix between observations. The correlation between observations in linear mixed models is assumed to amount from the random effects, which are therefore estimated per individual. However, in GEE models, a working correlation matrix has to be specified to describe the correlation between observations within an individual. The fact that this true covariance matrix is unknown, does not pose a problem as the model will estimate the correct covariance matrix. Therefore, even misspecification of the covariance matrix will still lead to unbiased estimates (Hubbard et al. 2010). This covariance matrix is assumed equal between all subjects, which also explains the difference in interpretation with linear mixed models. Estimation of the covariance matrix however, requires a relatively high number of subjects per group. In effect, estimates of variance obtained with GEE's can be heavily biased when the number of subjects is rather small (Prentice 1988). Although this depends on the amount of variance in the data, it has been recommended that more than 20 subjects per group are required to obtain reliable estimates (Horton et al. 1999).

9.3 Materials and Methods

In this work, we will compare summary statistics, second-level, mixed models, and GEE analysis, as they provide different approaches to analyze the longitudinal data obtained with PET. This will be done on simulated data to study in detail the strengths and weaknesses of each method, and to evaluate their performance with different sample sizes and noise levels. Finally, experimental data will be analyzed to evaluate the practical importance of the findings on the simulated data set.

9.3.1 Simulated data

Simulated data was generated with a two-tissue-compartment model (Figure 1), in which the rate constants between the different compartments were set to values typically observed for reversible PET tracers, i.e. K1 = 0.4 mL min^{-1} mL^{-1}, k2 = 0.8 min^{-1}, and k4 = 0.8 min^{-1}. For group 1, k3 was set to 0.80 min^{-1}, whereas group 2 looped over each value of the vector [0.80, 0.82, 0.84, 0.86, 0.88]. Additionally, the volume-percent blood in tissue was set to $V_B = 0.1$. As input to this model we used a measured input function our group has pulished before (de Laat et al. 2015). Biological variation was introduced as random Gaussian noise on all rate constants. Furthermore, for k3 and k4, the amount of variance was a percentage of this parameter, thus introducing variance between subjects for the outcome BP = k3/k4. Additionally, a smaller amount of absolute variation, i.e. 0.001, was added to the k3 and k4 of the cerebellum. Finally, technical noise was added to the simulated time-activity curve as random Gaussian noise with variance proportional to $C_{PET} * e^{\lambda t} / dt$ (Alpert et al. 2003).

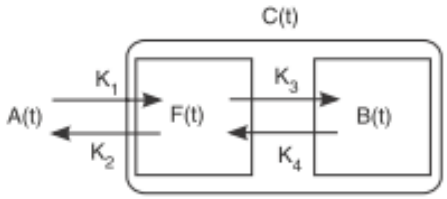


Figure 1. Schematic drawing of a two-tissue-compartment model (Watabe 2017), in which A(t) represents a function describing the arterial radioactivity concentration over time, which distributes into (K_1) and from (k_2) the free fraction of the radiotracer in the tissue. This amount of free tracer in the tissue over time is described by F(t), as is the bound fraction of the radiotracer B(t). The kinetic rate constants between these two compartments is described by k_3 and k_4. The total tissue concentration over time can be expressed as C(t).

The measured arterial input function was used to obtain data-points matching each frame of the dynamic PET scan reconstruction, i.e. 4 x 15s, 4 x 60s, 5 x 180s, and 8 x 300s. One thousand simulations were performed per k3 value. The effect of the number of subjects

per group was evaluated for n = 5, 10, 20, and 50. Only balanced designs were evaluated. Finally, the amount of biological noise, i.e. random noise on the true binding potential of an individual, was studied. This was done by adding random Gaussian noise with zero mean, and a standard deviation of 0, 2.5, 5 and 10% of the k3 value. Between both groups the K1 and k2 constant are assumed to remain stable. A summary of the chosen parameters can be found in Table 1.

Variable	**Unit**	**Value**	**Meaning**
Group size	Animals	[5, 10, 20, 50]	Size of each group
Simulations	number	1000	For each condition
Std. dev. noise	%	[0.025, 0.05 0.1, 0.2]	Expressed as % of k3*
K1	mL min^{-1} mL^{-1}	0.4	RC plasma to tissue
k2	min^{-1}	0.8	RC tissue to plasma
k3*	min^{-1}	[0.80, 0.82, 0.84, 0.86, 0.88]	RC free to bound
k4	min^{-1}	0.15	RC bound to free
Blood volume	%	0.1	Ratio blood / tissue

Table 1. Simulation parameters. * = for group 1, k3 was set to 0.80, whereas group 2 looped over each value. Additionally, k3 and k4 were set to zero for the reference region. Random Gaussian noise with zero mean was added to all rate constants and Vb. For k3 and k4 in the reference region, noise was constrained to be absolute to avoid conceptually impossible negative values. RC = rate constant.

Experimental data were obtained from 24 adult Wistar rats, which were scanned on a FOCUS 220 for 60 min upon injection of 17.4 ± 2.3 MBq ^{18}F-FPEB into the tail vein. Rats were scanned, three at a time, and attenuation correction was performed by means of a ^{57}Co point source. List mode data were reconstructed using the Maximing a posteriori information algorithm (MAP) with 12 iterations. After registration of each scan to an in-house brain template, time-activity curves were extracted for the cortex, hippocampus, striatum, nucleus accumbens, and thalamus using the PMOD 3.6 software package (PMOD, Zurich, Switzerland).

Reference models are commonly used, if a suitable region is present, because of their practical advantages. Several equivalent models are available, with only minor changes in their mathematical framework, to estimate the specific binding (k3/k4) of a reversible radiotracer using a reference region input as a measure of the nonspecific binding (K1/k2). Here we use the popular Logan reference model, because of the relatively simple operational formulas, allowing a clear specification of relevant random effects, as can be seen from its operational formula (Logan et al. 1996):

$$\frac{\int_0^T C_{ROI}(t)dt}{C_{ROI}(T)} = \frac{V_T}{V_T^{ref}} \times \frac{\int_0^T C_{ref}(t)dt + (C_{ref}(T)/\overline{k'_2}}{C_{ROI}(T)} + Int$$

In which V_T / V_T^{ref} can be considered as the distribution volume ratio, a surrogate measure of binding potential + 1. Note that the BP_{ij}, or w_i as it was defined in the introduction, is here the covariate written as V_T/V_T^{Ref}. Furthermore, the radiotracer binding region, C_{ROI}, is taken as one compartment comprising both the specific and non-specific binding. However, specific binding is based on chemical equilibria, which can slow down the influx of the tracer into the tissue. Since this delay only occurs in the specific compartment the linearization will not become linear in the first frames (Logan et al. 1996). Since the outcome of this model is the slope of the linear part, we select only the time-points within this linear section of the curve. We determined the linear part empirically and found to be after the initial 8 min (t* = 8 min), which were excluded therefore.

9.3.2 Analysis methods

9.3.2.1 Summary statistic

A linear model was used to determine BP, i.e. the slope of the linearization, for every subject using lm() from the stats package (Lehrer et al. 2010) in R(R Core Team 2016). Differences between both groups in BP were determined by the application of a t-test (t.test()) or Mann-Whitney *U* test (wilcox.test()) from the same package. For each simulation, the obtained p-value was stored and the proportion of p-values < 0.05 was taken as the proportion of significant tests.

9.3.2.2 Second-level

The BP values obtained with the linear method described above were, together with their standard errors, fed into a second-level model with the subject's respective membership as covariate. This was performed using the rma.uni() function from the metafor package (Viechtbauer 2010), which was originally designed for meta-analysis. Based on this information an estimation was obtained, inversely weighted to the variance of the estimate, of the between-subject variation observed in each group. Taking this variation into account, the model evaluated if both groups differed significantly with respect to their BP values.

9.3.2.3 Mixed model

Mixed model analysis was performed using the lmer() function from the lme4 package (Bates et al. 2015). Model selection showed that the optimal model in general could be written as:

$$\frac{\int_0^T C_{ROI}(t)dt}{C_{ROI}(T)} = Intercept + Group + BP \times \frac{\int_0^T C_{ref}(t)dt + (C_{ref}(T)/\overline{k'_2}}{C_{ROI}(T)} + BP \times Group \times \frac{\int_0^T C_{ref}(t)dt + (C_{ref}(T)/\overline{k'_2}}{C_{ROI}(T)}$$

This model allows for both a difference in intercept and slope per group. Since our outcome, BP_{ij}, is assumed equal to the slope of this regression, we have to write $BP_{ij} = BP + BP \times Group$, where group is a dummy variable being 0 for the control group. Therefore, this can be rewritten to:

$$\widehat{BP}_{ij} = (BP + group * BP)_{population} + (BP + group * BP)_{group} + (BP + group * BP)_{individual}$$

In addition, a random effect was included for both intercept and slope per individual subject. In outlying cases this model would not converge (<2%). In this case obtained estimates and p-values would be excluded from further analysis.

9.3.2.4 General Estimating Equations

For GEE fitting we made use of the geeglm() function in the geepack package (Højsgaard, Halekoh, and Yan 2006),with which a model identical the one described above for mixed model analysis was fitted. However, instead of random effects, the covariance matrix was modeled using an autoregressive correlation structure. Additionally, due to the data's distribution being close to normal an identity link function was chosen for Gaussian family data.

9.4 Results

9.4.1 Simulations

Time-activity curves were simulated using the data generating mechanism described above for each subject of both groups at every pre-specified difference level (Figure 8). Sample sizes of 5, 10, 20, and 50 subjects per group were evaluated. This was repeated 1000 times for each parameter level. Binding potentials were estimated using the above described Logan linearization, for which the first eight non-linear data points were excluded, to obtain a minimally biased slope estimate (Figure 2). Every analysis method was applied to these generated data and their results were stored.

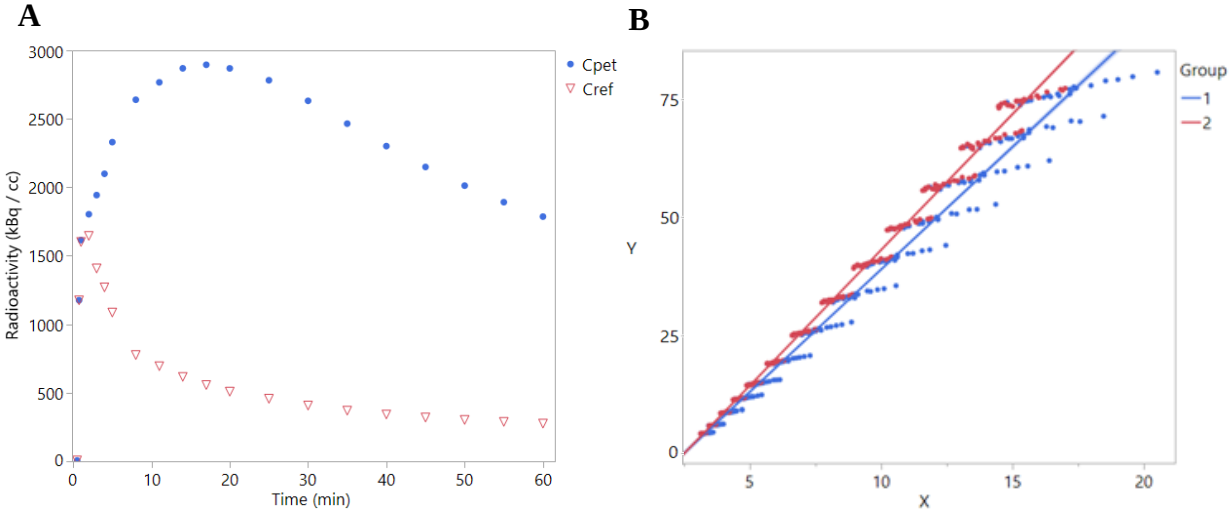


Figure 2. **A**) A typical time-activity curve simulated for a receptor-rich and receptor-free reference region. **B**) Time-activity curves after Logan linearization for one simulation.

Bias was evaluated as the difference between the obtained estimate minus the input k3/k4 (Figure 3). As can be observed, the bias introduced by GEE is considerably larger than that of other methods, and seemed to increase exponentially with increasing between-subject (BS) variance. For example, with 20% BS variance, a bias of 0.65 was found, amounting to more than 10% of the estimated BP. The second-level and mixed models performed almost identical, but did show a negative trend with increasing BS variance, contrasting the exponential increase in bias obtained with GEE.

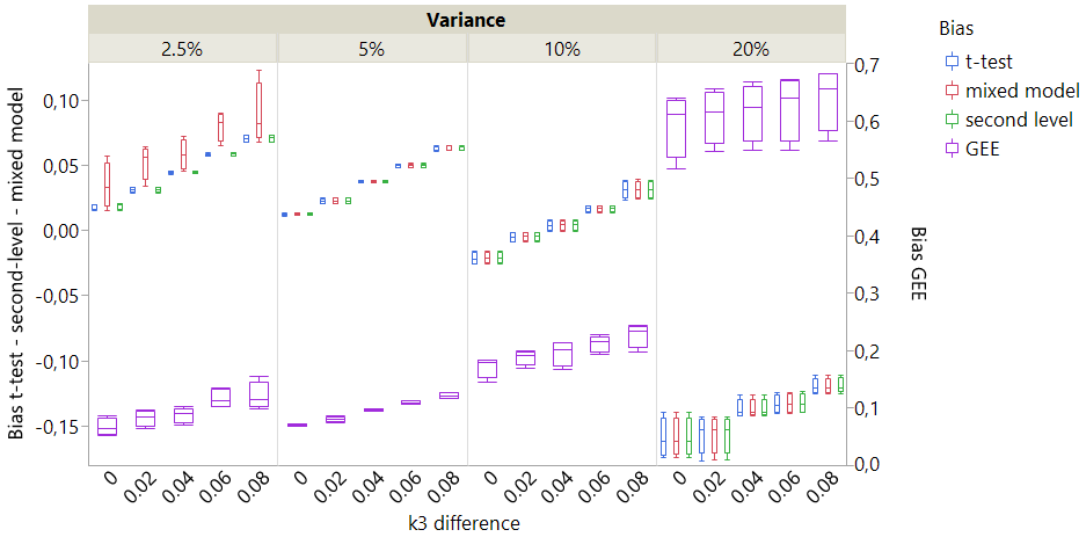


Figure 3. Bias obtained with the different models in function of between-subject variance. The magnitude of this bias should be compared to the corresponding BP values, here between 5.3 and 5.9.

Next, Type I error rate was assessed as the number of significant outcomes when no difference in k3 was present (Figure 4). On average, the t-test applied to summary statistics provided a stable 5% Type I error. Mann-Whitney is shown to perform similarly, and is only more conservative in the smallest evaluated group size of n = 5. Both second-level and mixed model analysis were too liberal particularly in smaller samples, with negligible overestimations of 2 – 3% at n=10, and virtually no differences at n = 20 or 50.

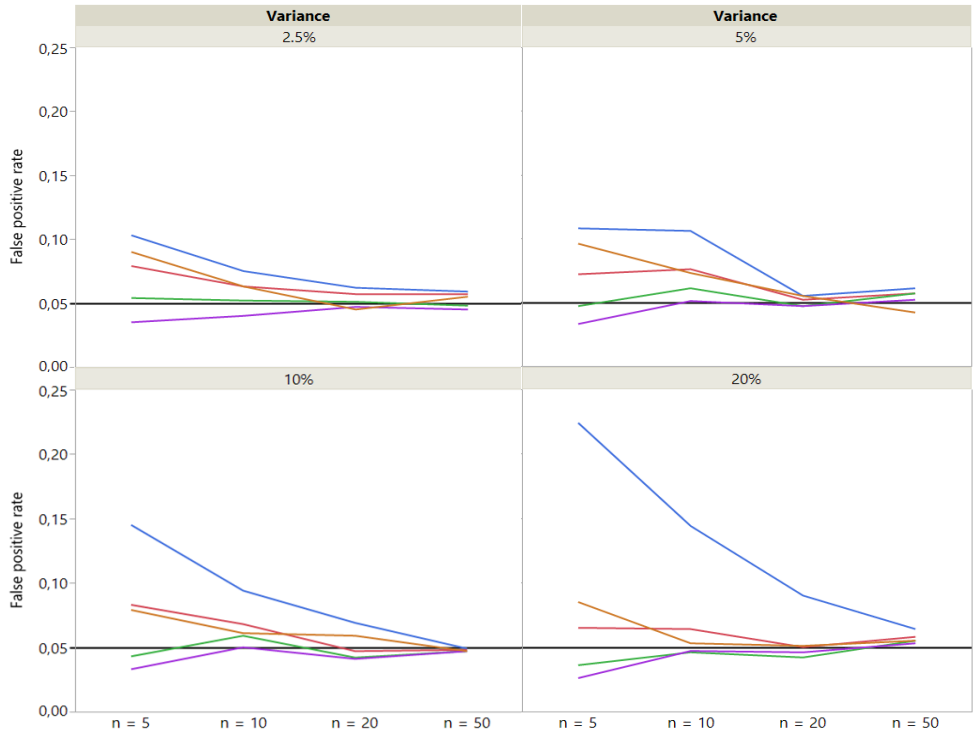


Figure 4. False positive rate for Mann-Whitney (purple), t-test (green), second-level (red), mixed model (orange), and GEE (blue) with different levels of between-subject variance.

Finally, we varied the amount of BS variance, 2.5, 5, 10 and 20% of k3 and k4, to evaluate its influence on each analysis approach. As can be concluded from Figure 5, the Mann-Whitney U test remains most conservative and least powerful in all evaluated situations, with a similar but less conservative pattern resulting from the t-test evaluation of the summary statistics. Power differences between the second-level and mixed model approach were small independent of group, effect of variance amplitude. The GEE finally was the most powerful test on every occasion, as was also reflected on the false positive rate. Interestingly, GEE showed the largest gain in power in samples with higher BS variation levels of 5 and 10%.

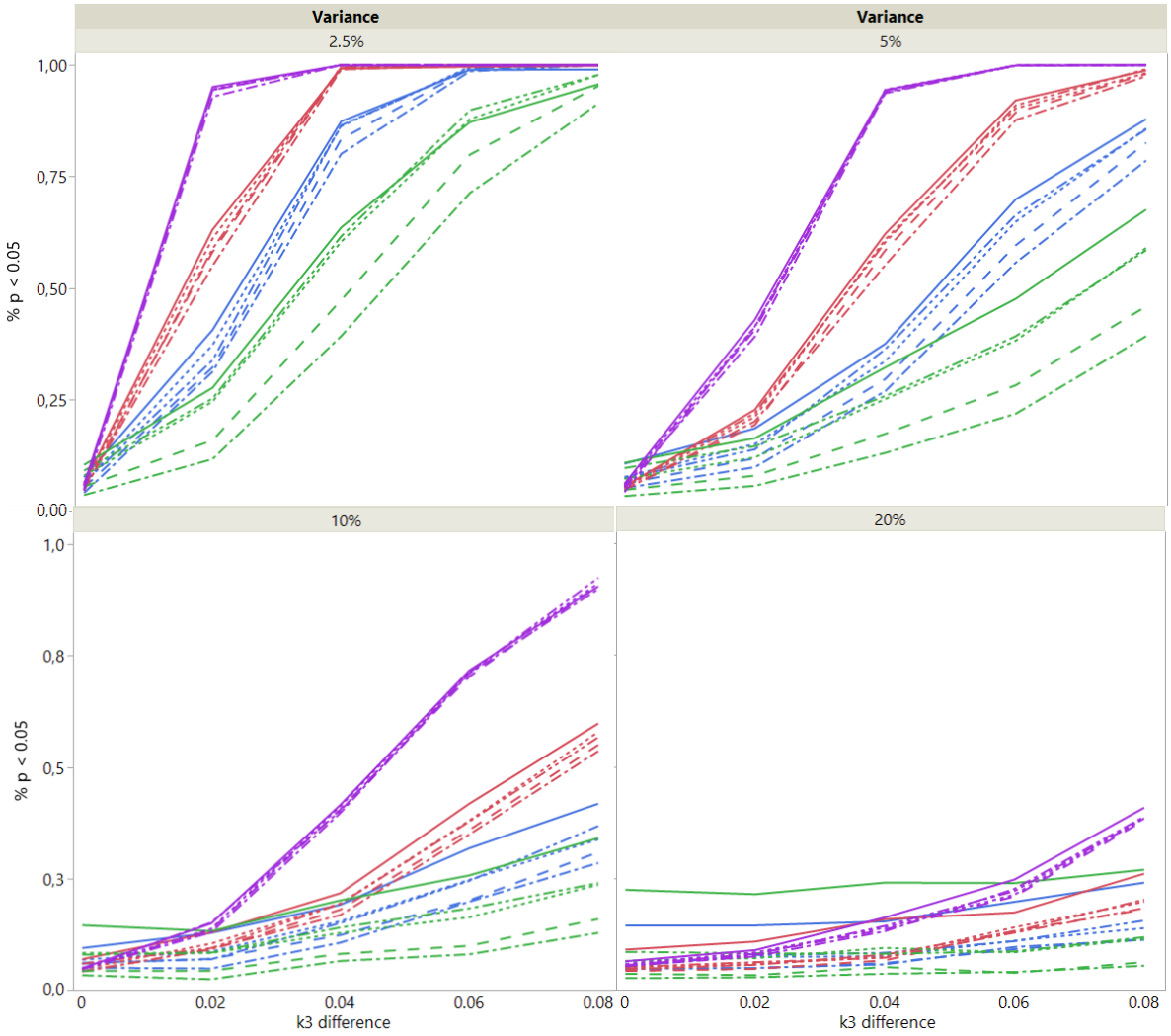


Figure 5. Percentage of p-values smaller than 0.05 plotted against an increasing difference in k3 between two simulated groups. Mann-Whitney (- • -), t-test (- - -), second-level (•••), mixed model (- •• -) and gee (---) are evaluated for group sizes of 5 (green), 10 (blue), 20 (red), and 50 (purple). Additionally, the influence of increasing between-subject variance is shown for 2.5% (top left), 5% (top right), 10% (bottom left) and 20% (bottom right).

9.4.2 Experimental data

Experimental data obtained from two groups, both consisting of 12 animals that underwent a 60 min ^{18}F-FPEB scan, were analyzed according to the method described above. In brief, the obtained time-activity curves from the cortex, hippocampus, nucleus accumbens, striatum, and thalamus were linearized according to Logan's reference method (Figure 6).

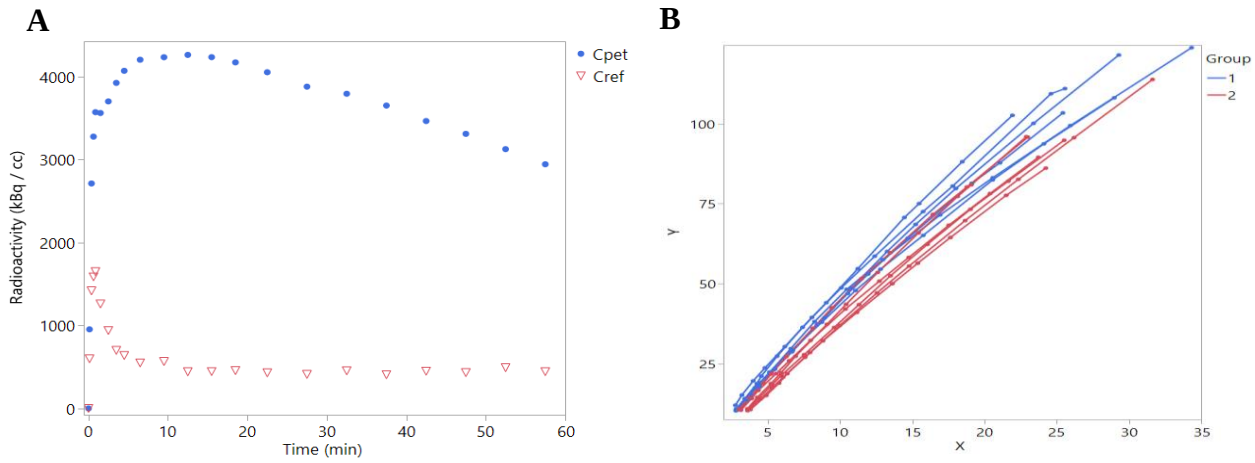


Figure 6. **A)** A time-activity curve from the experimental data for the striatum (receptor-rich) and receptor-free reference region. **B)** Striatal time-activity curves after Logan linearization for all subject colored by group membership.

Analysis of the experimental data with each method provided highly similar estimates for each region (Table 2). An interesting difference between models is the identical variance in both group estimates for the second-level and mixed model analysis, whereas this is not the case for the summary statistic or GEE approach.

Group 1	**Summary Statistic**		**Second-level**		**Mixed Model**		**GEE**	
	Mean	SE	Mean	SE	Mean	SE	Mean	SE
Cortex	4.33	0.20	4.33	0.18	4.32	0.17	3.86	4.62
Hippocampus	7.88	0.27	7.89	0.24	7.88	0.23	6.57	0.31
NAC	5.09	0.32	5.08	0.25	5.08	0.24	4.16	0.28
Striatum	8.72	0.35	8.72	0.32	8.71	0.30	6.66	0.40
Thalamus	4.45	0.15	4.45	0.13	4.44	0.13	4.40	0.19
Group 2								
Cortex	3.98	0.16	3.98	0.18	3.98	0.17	3.57	0.35
Hippocampus	6.82	0.21	6.82	0.24	6.82	0.23	5.90	0.20
NAC	4.59	0.15	4.59	0.25	4.59	0.24	3.92	0.12
Striatum	7.80	0.27	7.79	0.31	7.79	0.30	5.89	0.41
Thalamus	3.94	0.11	3.94	0.13	3.94	0.13	3.51	0.13

Table 2. Estimates and their standard error as obtained with fixed effect, second-level or random-effect analysis. NAC = nucleus accumbens.

P-values obtained with the different methods were in line with the simulations above (Figure 7). Mann-Whitney and the t-test were slightly more conservative than the second-level and mixed model approach for all regions. An interesting exception was the nucleus accumbens, for which the Mann-Whitney *U* test found a lower p-value than all other methods, a situation not procured in the simulations. The GEE model proved to be unstable and provides the lowest p-values for the thalamus, but the highest for the cortex, nucleus accumbens, and striatum.

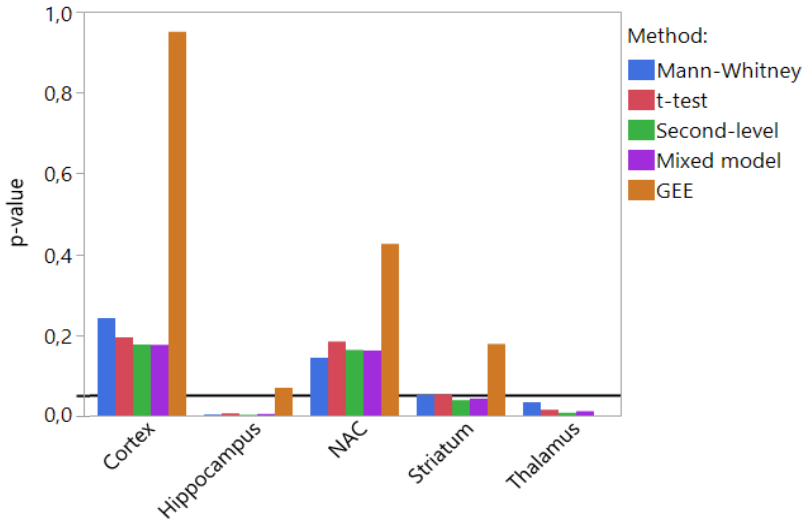


Figure 7. P-values obtained with fixed effect, second-level, and random effect analysis for the five evaluated regions. A horizontal reference line is drawn at p = 0.05.

9.5 Discussion

Longitudinal data can be summarized with a summary statistic. This is common in biomedical sciences, although more appropriate statistical models exist. We evaluate here the potential advantages these more complex models and compare them with the summary statistic approach. Differences in performance of summary statistic and second-level analysis, mixed models and GEE were evaluated in the analysis of both simulated and experimental PET data. Using simulated time-activity curves, based on a two-tissue-compartment model, we show that a gain in power can be achieved by accounting for random effects either with a second-level or mixed model analysis. This gain in power however diminishes when sample sizes become larger, e.g. up to n = 50 in our examples. Furthermore, we report that the false positive rate is higher for both second-level and

random effect analysis, although this effect also becomes negligible for larger group sizes. Summary statistic analysis on the other hand was shown to be slightly conservative in smaller samples, when evaluated with the non-parametric Mann-Whitney *U* test. Generalized Estimating Equations performed poorly in the evaluated situations, as this method introduced large biases, particularly for high levels of between-subject variance. In addition, it was shown to be problematically liberal in small sample sizes. Application of these analysis methods to experimental data showed similar results as obtained by simulation: for both second-level and random effect analysis provided slightly more power than the summary statistic analysis.

The reduction of clustered data into a summary statistic overcomes the nested nature of the original data, thus validating simple analysis methods, such as the t-test between groups. This approach is however not suitable for all settings, for example observations from both groups within one cluster cannot be simply averaged. Secondly, an unequal number of observations per cluster between groups is not taken into account when calculating a summary without confidence intervals. A higher number of observations would indeed contribute more information, and should therefore be given more weight in the analysis. Additionally, all information is lost about the individual measurements, which can be of interest (Galbraith, Daniel, and Vissel 2010). For example, when investigating the reduction of skin inflammation after topical treatment application by multiple biopsies of the same subject, it would be interesting to know whether there is a general down-regulation or rather a more heterogeneous, focal decrease. Both these concerns however, do not apply to PET data with our hypotheses: data originate from individuals who belong exclusively to one group and consist only of entire scans, which are reconstructed with a fixed number of frames independent from group membership.

Here we show that the parametric t-test performs well when comparing BP between two groups. Its false positive rate remains stably around the desired 5% for all simulated situations. A situation which was not assessed here, namely with large difference in BS variance between groups, would violate a key assumption and thus undermine the validity of the t-test. The non-parametric Mann-Whitney *U* test shows the same robustness against increases in between-subject variance, but its conservativeness makes it the least powerful method evaluated here, particularly in lower sample sizes. This is

inherent to its non-parametric nature, which cannot fall back to a pre-defined distribution. In addition, with a more skewed BP distribution, due to the increased BS variance in k3, the Mann-Whitney test's power increased to the t-test level.

Second-level analysis, which bases itself on the summary statistics and their variances, and allows a random effect per subject has been reported to perform similarly to mixed model approaches (Friston 2006). Our findings corroborate this, although second-level analysis consistently had a lower Type I error rate in the smaller samples of n = 5, than the specified mixed model. In addition, the inverted variance weighting, applied here, assured that subjects with particularly noisy linearizations were less influential on the predicted population mean (Marín-Martínez and Sánchez-Meca 2010). Finally, from a practical point of view, the most important advantage is that the second-level analysis approach consists of one additional step, which can be performed with a minimum of extra information, i.e. the variance of the summary statistic. Effectively, mixed models require a more extensive statistical knowledge to build the appropriate model, including the random effect specification. For the data evaluated here, we feel that this required knowledge, and the inherently higher risk of model misspecification, should guide researchers in the PET field towards second-level analysis of their data.

General estimating equations are considered as robust alternatives to (generalized) linear mixed models, as they can overcome misspecification of the correlation matrix, and departures from normality (Hubbard et al. 2010). However, this robustness comes at a price, as these models typically require a large number of observations to result in reliable estimates. In both the simulated and observed data-sets it can be observed that GEEs indeed provide a maximal power, particularly in the case of the skewed binding potential simulations. This power however, is also reflected in the highest false positive rate, particularly in smaller samples and higher levels of between-subject variance. Due to these reasons GEEs seem less convenient for the sample sizes typically encountered in PET studies (Mancl and DeRouen 2001).

In this work, we assessed several situations that could be encountered in neuroimaging practice. However, two additional simulation studies could contribute to the quality of this work. Firstly, the noise added to this data is based on previously published reports

(Alpert et al. 2003). We did not investigate however the noise distributions in our own data, which might have been different. Outliers are another issue that were not addressed here. In effect, outliers are commonly encountered in neuroimaging data, and could have a differential effect on the reliability of parametric and non-parametric methods. In conclusion, we show that the naïve summary statistic approach is defendable in most situations, although non-parametric comparison of groups is overly conservative. An increase in power can be achieved with both second-level analysis and mixed models. Second-level analysis could be considered the better choice, as these models are simpler to specify and do not have the minor performance issues of mixed models. Finally, GEEs are evaluated for their use in this application, but samples smaller than 20 subjects per group, common to most PET studies are not sufficient to profit from the advantages this family of models has to offer.

Chapter 10: General discussion

One of the central questions of this PhD project, was to determine whether mGluR5 was affected by different drugs, thus potentially aiding with the identification of a common pathway for all, or at least multiple, addictive substances. In addition, we aimed to evaluate whether mGluR5 availability, and other biomarkers, before drug exposure, could be associated with future drug use. In this thesis, we investigated these possible relationships for cocaine and alcohol self-administration in rats using ^{18}F-FPEB PET. At the beginning of our work, this novel tracer was not sufficiently validated for preclinical use. Therefore, our first efforts have been focused on the extensive validation as described in Chapter 2.

In the consequent experiments, both cocaine and alcohol were shown to cause a reversible decrease in mGluR5 expression during self-administration, although the magnitude and extent of this effect was larger for cocaine. Longitundinally, the effect of both drugs on mGluR5 availability normalized after approximately one week of forced withdrawal implicating a reversible effect. In cross-sectional human PET studies, alcohol and cocaine exposure have also been found to reduce mGluR5 availability when compared to healthy controls (Milella et al. 2014) (Leurquin-Sterk, JNM 2017, in press). In addition, nicotine use, as well as ketamine infusions can reduce temporary availability of mGluR5 (Akkus et al. 2013; DeLorenzo et al. 2015). These data suggest therefore, that mGluR5 is indeed involved in a common pathway influenced by most drugs of abuse.

Our findings that both alcohol and cocaine reduce mGluR5 availability, is despite the subjective experience of both drugs is significantly different. In effect, cocaine is classified as a stimulant, whereas alcohol is classified as a dose-dependent depressant (Schuckit 2006). In addition, both these drugs rely on different mechanisms to achieve their addictive potential. A common mechanistic pathway however is their interference with the dopaminergic system (Rossetti et al.). The complex relationship between the mGluRs and the glutamate and dopamine release in brain regions, such as the striatum,

has repeatedly been reported. For example, it has been shown *ex vivo* that group I mGluR agonists can elicit both glutamate and dopamine release in the striatum, potentially through transsynaptic mechanisms (David, Ansseau, and Abraini 2005). Considering this body of literature and our results, it would be interesting to elucidate the direction of causality: does a large dopamine release trigger the downregulation of mGluR5, and does this downregulation enforce a negative feedback mechanism through which dopamine release is decreased. Among the many possible experiments to explore this hypothesis, most translational value might come from a combination of two. The first part, i.e. dopamine downregulates mGluR5, could be assessed *in vivo* through infusions of dopamine in combination with PET assessment of mGluR5 availability. It should be ascertained however, that a downregulation of mGluR5 is obtained, as this might only be achieved after prolonged exposure to large dopamine releases, such as described in our self-administration paradigms. The second part of this proposed mechanism, i.e. decrease of dopamine release through downregulation of mGluR5, could be studied in animals with, ideally inducible, localized knock-down, that would be subject to a dopamine releasing challenge. Data supporting this part of the hypothesis has already been obtained through microdialysis studies, in which dopamine release after nicotine challenges could be inhibited by administration of the mGluR5 antagonist MPEP (Tronci and Balfour 2011). Positive results could explain the link between the anhedonia experienced by addicted patients on the one hand, and their lower mGluR5 availability on the other (Akkus et al. 2013; Leurquin-Sterk et al. 2016; Janiri et al. 2005; Martinotti, Cloninger, and Janiri 2008; Wise 2008). Potentially the most interesting consequence of the confirmation of this relation would be a new possible point of action: the development of new addiction therapy strategies might need to consider reversing the mechanisms through which the dopamine release in the addicted patients is inhibited. In effect, an individual motivated to abandon their habit, but unable to cope with how colorless their lives are without their addictive habit, could benefit from such a therapy.

In chapters 4 and 5, we found biological variables that, at baseline, were associated with drug use later in the experiment. The search for such predictive biomarkers is motivated by a direct translational value, as such a ‘risk biomarker’ could help with the prevention of this disorder in high-risk individuals. Secondly, identification of such biomarkers is of

great interest, as they may highlight aspects of the neurobiology of addiction that could be new targets for therapy development. In this thesis we show that the glutamate concentration in the prefrontal cortex was affected in a very similar way by both alcohol and cocaine self-administration. However, prefrontal glutamate concentrations were only associated with future cocaine-use, but not alcohol preference. The opposite was true for the mGluR5 availability in the nucleus accumbens, which was only related to alcohol preference. These discrepant results could be associated with the difference in the effects of alcohol and cocaine on the brain. This is in line with previous reports that showed that MPEP, a selective mGluR5 antagonist, prevented the conditioned rewarding effects of cocaine, but not alcohol or nicotine (McGeehan and Olive 2003). These results might in part also be explained by the different kind of reward experienced after exposure to alcohol or cocaine, as discussed below. In spite of the reports on differential influences of cocaine and alcohol, many findings have in fact shown similarities between both drugs. For example, D2/D3 receptor densities in the nucleus accumbens have been found pivotal for both alcohol and cocaine self-administration, although a predictive relationship has only been reported for cocaine (Thanos et al. 2001; Michaelides et al. 2012; Dalley et al. 2007). In parallel, the character trait of impulsiSvity has been found predictive for both alcohol and cocaine use in rats (Poulos, Le, and Parker 1995; Perry et al. 2005). Therefore, it would be of interest to further investigate the molecular basis of the observed predictive associations, and evaluate whether a difference between alcohol and cocaine is indeed plausible

Extrapolation of preclinical results from addiction research to clinical practice should be done with care. The most important reason for this is the lack of the psychosocial dimension in most self-administration paradigms and the much more elaborated prefrontal functions in humans (e.g. relating to impulse inhibition and control). As described in the general introduction, drugs are typically taken by patients because they want to feel good, better, or perform better (National Institute for Drug Abuse 2007). The latter two classes are motivated by an array of complex psychosocial emotions, which are unlikely to be matched by rodents (Belin and Deroche-Gamonet 2012). This likely explains the little motivation of rodents to self-administer drugs like alcohol, typically abused for their negative rewarding properties, whereas stimulants, experienced as directly pleasurable by virtually any species, are self-administered by animals in lethal

amounts (Pickens and Thompson 1968). An extensive discussion continues to be held between specialists from different fields on whether animals can become addicted and how this diagnosis should be made (Deroche-Gamonet, Belin, and Piazza 2004). Several options have been raised, all involving a means to measure behavioral outcomes, such as compulsion, motivation and continuance despite negative effects. These measures can indeed place animals on a relative scale, thus allowing comparison with other animals in the same experiment. However, most results indicate that animals with a higher level of "addiction-like" behavior also self-administer more. Whether the considerable extra effort of installing the required behavioral procedures for these additional measures is worthwhile can therefore be called in question.

In this work, we have used two behavioral tests: the rodent Iowa Gambling Task and the Open Field Test. Although the experiment described in the fifth chapter on alcohol self-administration, was initially designed to also include the rIGT, practical circumstances forced us to abandon this behavioral test. In effect, one of the disadvantages of the rIGT is the long training period that is required to obtain reliable results (Zeeb, Robbins, and Winstanley 2009). This period can span over three weeks before all animals in a sample show a sufficient operational understanding of the test. This is a clear plus of the open field test, where naïve rats can be placed in the open space to assess their mobility. However, the interpretation of the open field test is not straightforward. Researchers have applied this test in research on anxiety, fear, stress, and depression (Hicks and Moore 1979; Katz, Roth, and Carrol 1981; DeMar et al. 2006). The open field test can be used to assess multiple outcomes, such as latency (initial immobility), rearing, defecation, grooming, freezing, locomotor activity. Additional outcomes have been described since automated video-tracking became available, e.g. frequency, distance and duration of movements, stereotypies, and margin occupation. In effect, locomotor activity can be divided into activity demonstrated in the periphery or in the center, where the center is likely to be experienced by rodents as more frightening than the, near a wall, peripheral regions. Most studies have used centrality of the animals as a measure of anxiety, whereas total locomotor activity is interpreted as a measure of explorative behavior. However both measures have also been applied to assess anxiety (Bert et al. 2001; Prut and Belzung 2003).

Preclinical neuroimaging provides challenges additional to the neuroimaging of humans. Arguably, the most influential difference is the use of anesthesia to immobilize animals during their scan. Although common practice, all employed anesthetics have a multifaceted influence on several organ systems, including the brain and cardiovascular system (Hildebrandt, Su, and Weber 2008). Since every animal is exposed to the same dose and agent within an experiment, these influences might seem negligible. However, in the majority of studies there is a lack of information on several aspects: 1) Does the influence change within a scan? Accumulation and continually decreasing brain activity can potentially increase the effect of the anesthetic agent towards the end of a scan. 2) Is there an interaction with the drug under investigation? Particularly in experiments with control animals, not exposed to the drug, this can potentially lead to confounded results. 3) Do animals get resistance after repeated exposure? Rodents with previous exposure to anesthetic agents can be increasingly challenging to reach a sufficient anesthetic plane with concentrations that were previously used. Increasing this concentration however might achieve the same macroscopic effect, i.e. an anesthetized animal, but can simultaneously cause a more profound disturbance of the cardiovascular system. To circumvent these issues, several developments have recently been reported, also by our group, to scan awake animals (Spangler-Bickell et al. 2016). Most interesting results have been obtained in setups were rats were allowed to move freely and their collected data were motion corrected during data analysis. Although these methods can be implemented in PET imaging with relative ease, the reliance on additional, often magnetic, instruments have precluded the implementation in MR imaging so far. In addition, these techniques require a substantial amount of extra time per animal in both preparation and actual scanning, which has precluded their implementation in practice so far.

Preclinical PET and MRI scanners typically have better absolute spatial resolution than their clinical counterparts. However, the rodent brain is so much smaller that there still is a much lower relative resolution or the number of identifiable voxel in the brain. This influences not only the accuracy of cluster localization, but also the segmentation and registration of acquired images (Moses 2011). The less accurate registration is amplified by the sparseness of high-quality rodent atlases, templates, and software applications. In addition, phenotypical differences between different strains of rats exist and can further

increase the inaccuracy of the registration when ignored (Yanai 1979). Another effect, common in clinical and preclinical neuroimaging, is the effect of age on both brain structural and functional morphology. In effect, different regions of the brain have different post-partum development (Moll et al. 2000). For example, the brain will develop on a molecular level, which can be reflected in, amongst others, altered receptor expressions. In chapter 3, we show that mGluR5 availability in rats does indeed change between birth and adulthood. We did not control for this effect in the longitudinal self-administration protocols in this work, which can be considered a limitation. These experiments and their analysis were performed in parallel, therefore precluding integration of these results. However, we feel that our results did not decrease in value because of this: On the one hand, a control group was installed in both experiments, which prevented, assuming equal growth in both groups, misinterpretation of observed results. On the other hand, we have reported a consistent lower mGluR5 availability throughout the experiments, whereas the age effect we described was an increased availability. In effect, we potentially underestimated the mGluR5 reduction by not taking into account a potential increase over time.

We observed a strong correlation between mGluR5 availability, in both rats and humans, in different brain regions with both *in vivo* and *in vitro* quantification methods (Figure 1). Possible explanations for this phenomenon can be found in other fields. For example, several gene expression studies have investigated expression correlation patterns and their relation with functional connectivity data (Richiardi et al. 2015). Although the exact mechanisms of this global expression regulation are unknown, it has been hypothesized to be associated with the embryological origin of regions (Kirsch and Chechik 2016). This provides an intriguing perspective on the importance of locally induced effects, by for example receptor binding, as well on the potential ways of communication of harmonic neuron populations. Another consequence of this observed correlation between regions, is that classic multiple testing methods, such as the Bonferroni method, will be too stringent due to their assumption of independence (McDonald 2014). In addition, this functional network-like property of receptor expression could motivate the study of the existence of these networks for different receptors, and their response to different pathophysiological situations (Feigin et al. 2001).

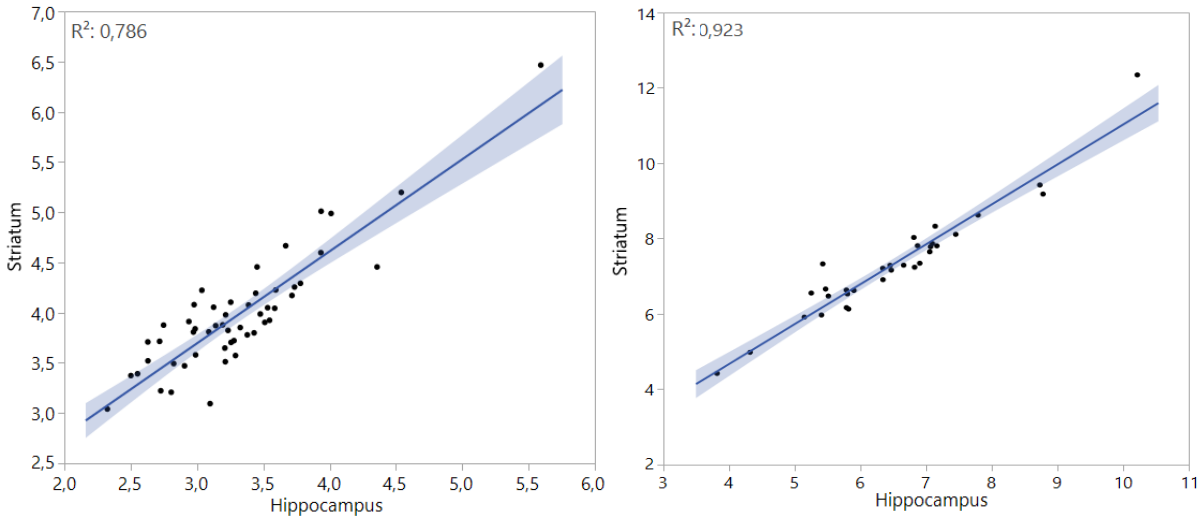


Figure 1. Correlation with the measured ^{18}FPEB uptake in the hippocampus and striatum, as measured with **A**) in vitro autoradiography and **B**) PET imaging using SRTM.

Almost every stimulus, which changes the homeostasis of the organism, will be countered by a response to restore the system to its original state. This response can contribute knowledge, which is inaccessible when the system remains in rest. For example, it could be difficult to assess the cardiovascular stamina of two, similarly build, individuals at the start of a track. However, after running a mile, a large difference may become apparent. This principle has been applied in diagnostic tests in both medicine and other fields, such as economics (Frye et al. 2003; Koyner et al. 2015; Alvarez et al. 1996; Vazquez, Tabak, and Souto 2012). This rationale also applies to many systems in the brain: additional information can be gained by putting a system under duress. In this work, we aimed to exploit this mechanism by intravenously injecting drugs, while animals were being simultaneously scanned with PET and MRS. The results of this experiment were of a preliminary nature, and should be repeated before too strong conclusions are drawn. However, the obtained data does show interesting aspects that have not been described previously. The innovative application of techniques, however does also require an extensive substantiation of the required quantification methods for both PET and MRS (Villien et al. 2014). On the one hand, MRS is a technique that is sensitive to many factors, such as motion, temperature and magnetic shift (Blüml 2013). Although many metabolite concentrations remained stable during the scan, hinting towards stable quantification, further phantom studies to validate the obtained results are advised. Better theoretical and in vitro frameworks, to assess the influence of the

assumptions that were violated, should also support quantification of the PET signal. It is our hope that our results will aid in drawing attention to these interesting methods and consequently inspire future research to elucidate these important details.

The study of biological systems often aims to describe very complex interactions, which happen in different time spans, on different levels, and in different locations at the same time. To understand such a complex system studying one protein, one region, or one time-point severely limits the contribution of such work to our understanding of the entire system (Figure 2). In this work, we have always aimed to combine different techniques, each investigating specific aspects, at multiple time-points.

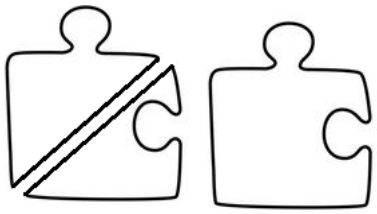


Figure 2. Investigating a single biological unit can be compared with studying half a puzzle piece: it will provide information, but cannot aid in solving the puzzle.

In addition to studying multiple targets or combining multiple techniques, an elegant way of increasing the amount of information of the obtained data is by using multiple analysis methods. In neuroimaging, we believe that machine learning could be an interesting and logical extension of the current analysis pipelines. The multivariate nature of these new methods in particular, can provide complementary information to the classic univariate ones, such as SPM or region-of-interest based analysis (McGettigan et al. 2011). For all methods that require no *a priori* identification of regions of interest, like SPM or independent component analyses, a risk lies in this free reign. In effect, subtle artifacts, not detected by the researcher, can steer a machine learning algorithm to obtain good, but false results. A concrete example of this is the U.S. Army aiming to identify tanks in aerial photos of forested areas. Results were promising on the obtained, both test and training, data set. However, generalizability was extremely poor when the algorithm was exposed to real world data. It turned out that in the original data set, used for both training and testing the algorithm, aerial photographs were taken with tanks on a sunny day, whereas the day without tanks was cloudy. The algorithm had effectively taught itself to

recognizes shadows in a forest (Dreyfus and Dreyfus 1992). In our view, an important protection against this phenomenon in neuroimaging is the ability to map the relative importance of each voxel back to the original three-dimensional space. This poses however some challenges, particularly for four dimensional data, such as resting-state fMRI.

fMRI data is typically analyzed in two steps, a first level to obtain individual beta images, and a second level to allow for population inference (Mumford and Nichols 2006). This is a discrepancy with our typical analysis pipeline of PET experiments. In effect, after a first-level analysis, groups are typically compared using classical group comparison tests. Although this can detect a difference between both samples, population inference cannot be made (Beckmann, Jenkinson, and Smith 2003). A specific example, of this subtle difference is the positive-negative word fMRI paradigm. The response of an individual is assessed when exposed to a positive word, such as "puppies", or a negative word, such as "murder". In general however, we would like to conclude from this experiment which brain regions are activated by positive and negative words, i.e. inference on the entire "population" of words, and not only by the words puppies and murder. Therefore, the final chapter of this work aimed to investigate this issue. We were able to show that these correct methods, which are readily available and easily implemented, can also lead to a gain in efficiency. This study however, only investigated very specific situations and quantification methods, which should be expanded to explore the usefulness of the recommendations, made in this chapter, in other settings.

The brain is unquestionably the most complex organ in the human body. Our knowledge about every aspect of it has exponentially increased in the last decades, but our overall understanding has not. It might even be argued that the growing amount of evidence has complicated the field to a point that is beyond understanding. A meagre upside is that we do not require full understanding to develop new therapies for those suffering from specific brain diseases. Therefore, we hope that the results described here will contribute to the development and optimization of new therapeutic strategies for addiction, as well as to our understanding of this important disease. Finally, we have attempted to unite both sub-fields in neuroimaging, as well as different worlds such as imaging, statistics and machine learning. We feel that this has strengthened the quality of this work, and hope that it may inspire other researchers to do the same.

Bibliography

Aarts, E., M. Verhage, J. V. Veenvliet, C. V. Dolan, and S. van der Sluis. 2014. 'A solution to dependency: using multilevel analysis to accommodate nested data', *Nat Neurosci*, 17: 491-6.

Abou Farha, K., R. Bruggeman, and C. Balje-Volkers. 2014. 'Metabotropic glutamate receptor 5 negative modulation in phase I clinical trial: potential impact of circadian rhythm on the neuropsychiatric adverse reactions-do hallucinations matter?', *ISRN Psychiatry*, 2014: 652750.

Acker, C. J. 1993. 'Stigma or legitimation? A historical examination of the social potentials of addiction disease models', *J Psychoactive Drugs*, 25: 193-205.

Adcock, R. A., A. Thangavel, S. Whitfield-Gabrieli, B. Knutson, and J. D. Gabrieli. 2006. 'Reward-motivated learning: mesolimbic activation precedes memory formation', *Neuron*, 50: 507-17.

Adinoff, B. 2004. 'Neurobiologic processes in drug reward and addiction', *Harv Rev Psychiatry*, 12: 305-20.

Akaike, H. 1974. 'A new look at the statistical model identification', *IEEE Transactions on Automatic Control*, 19: 716-23.

Akkus, F., S. M. Ametamey, V. Treyer, C. Burger, A. Johayem, D. Umbricht, B. Gomez Mancilla, J. Sovago, A. Buck, and G. Hasler. 2013. 'Marked global reduction in mGluR5 receptor binding in smokers and ex-smokers determined by [11C]ABP688 positron emission tomography', *Proc Natl Acad Sci U S A*, 110: 737-42.

Akkus, F., S. Terbeck, S. M. Ametamey, M. Rufer, V. Treyer, C. Burger, A. Johayem, B. G. Mancilla, J. Sovago, A. Buck, and G. Hasler. 2014. 'Metabotropic glutamate receptor 5 binding in patients with obsessive-compulsive disorder', *Int J Neuropsychopharmacol*, 17: 1915-22.

Alpert, Nathaniel M., Rajendra D. Badgaiyan, Elijahu Livni, and Alan J. Fischman. 2003. 'A novel method for noninvasive detection of neuromodulatory changes in specific neurotransmitter systems', *Neuroimage*, 19: 1049-60.

Alvarez, Juan G., Demetrios Minaretzis, C. Brent Barrett, Joseph F. Mortola, and Irwin E. Thompson. 1996. 'The sperm stress test: a novel test that predicts pregnancy in assisted reproductive technologies**Presented at the 50th Annual Meeting of The American Fertility Society, San Antonio, Texas, November 5 to 10, 1994', *Fertility and Sterility*, 65: 400-05.

American Psychiatric Association. 2013. *Diagnostic and Statistical Manual of Mental Disorders* (Washington, D.C.).

Ametamey, S., L. J. Kessler, M. Honer, M.T. Wyss, A. Buck, S. Hintermann, Y. Auberson, F. Gasparini, and P. A. Schubiger. 2006. 'Radiosynthesis and preclinical evaluation of 11C-ABP688 as a probe for imaging the metabotropic glutamate receptor subtype 5', *J Nucl Med*, 47: 7.

Ametamey, S. M., V. Treyer, J. Streffer, M. T. Wyss, M. Schmidt, and M. Blagoev. 2007. 'Human PET studies of the Metabotropic Glutamate Receptor Subtype 5 with 11C-ABP688', *J Nucl Med*, 48: 247-52.

Amunts, K., and K. Zilles. 2015. 'Architectonic Mapping of the Human Brain beyond Brodmann', *Neuron*, 88: 1086-107.

Anderson, Jeffery J., Margaret J. Bradbury, Darlene R. Giracello, Deborah F. Chapman, Greg Holtz, Jeffrey Roppe, Chris King, Nicholas D. P. Cosford, and Mark A. Varney. 2003. 'In vivo receptor occupancy of mGlu5 receptor antagonists using the novel radioligand [3H]3-methoxy-5-(pyridin-2-ylethynyl)pyridine)', *European Journal of Pharmacology*, 473: 35-40.

Anderson, K. G., and J. W. Diller. 2010. 'Effects of acute and repeated nicotine administration on delay discounting in Lewis and Fischer 344 rats', *Behav Pharmacol*, 21: 754-64.

Anker, J. J., M. G. Kushner, P. Thuras, J. Menk, and A. S. Unruh. 2016. 'Drinking to cope with negative emotions moderates alcohol use disorder treatment response in patients with co-occurring anxiety disorder', *Drug Alcohol Depend*, 159: 93-100.

Antonini, A., and K.L. Leenders. 1993. 'Dopamine D2 receptors in normal human brain: Effect of age measured by positron emission tomography (PET) and ^{11}C-Raclopride', *Annals New York Academy of Sciences*, 695: 5.

Anwyl, R. 2009. 'Metabotropic glutamate receptor-dependent long-term potentiation', *Neuropharmacology*, 56: 735-40.

Arias-Carrion, O., and E. Poppel. 2007. 'Dopamine, learning, and reward-seeking behavior', *Acta Neurobiol Exp*, 67: 8.

Arias-Carrion, O., M. Stamelou, E. Murillo-Rodriguez, M. Menendez-Gonzalez, and E. Poppel. 2010. 'Dopaminergic reward system: a short integrative review', *Int Arch Med*, 3: 24.

Arvey, A., E. Larsson, C. Sander, C. S. Leslie, and D. S. Marks. 2010. 'Target mRNA abundance dilutes microRNA and siRNA activity', *Mol Syst Biol*, 6: 7.

Aunger, Robert, and Valerie Curtis. 2013. 'The Anatomy of Motivation: An Evolutionary-Ecological Approach', *Biological Theory*, 8: 49-63.

Baba, S., M. Tatsumi, T. Ishimori, D. L. Lilien, J. M. Engles, and R. L. Wahl. 2007. 'Effect of nicotine and ephedrine on the accumulation of 18F-FDG in brown adipose tissue', *J Nucl Med*, 48: 981-6.

Babb, S., A. Malarcher, G. Schauer, K. Asman, and A. Jamal. 2017. "Quitting Smoking Among Adults — United States 2000 - 2015." In, edited by Center for Disease Control, 1457-64.

Backes, H., M. Walberer, H. Endepols, B. Neumaier, R. Graf, K. Wienhard, and G. Mies. 2011. 'Whiskers area as extracerebral reference tissue for quantifcation of rat brain metabolism using 18F-FDG PET: Application to focal cerebral ischemia', *J Nucl Med*, 52: 8.

Backstrom, P., D. Bachteler, S. Koch, P. Hyytia, and R. Spanagel. 2004. 'mGluR5 antagonist MPEP reduces ethanol-seeking and relapse behavior', *Neuropsychopharmacology*, 29: 921-8.

Badanich, K. A., P. J. Mulholland, J. T. Beckley, H. Trantham-Davidson, and J. J. Woodward. 2013. 'Ethanol reduces neuronal excitability of lateral orbitofrontal cortex neurons via a glycine receptor dependent mechanism', *Neuropsychopharmacology*, 38: 1176-88.

Baker, D. A., Z. X. Xi, H. Shen, C. J. Swanson, and P. W. Kalivas. 2002. 'The origin and neuronal function of in vivo nonsynaptic glutamate', *J Neurosci*, 22: 9134-41.

Ballard, T. M., M. L. Woolley, E. Prinssen, J. Huwyler, R. Porter, and W. Spooren. 2005. 'The effect of the mGlu5 receptor antagonist MPEP in rodent tests of anxiety and cognition: a comparison', *Psychopharmacology (Berl)*, 179: 218-29.

Barron, A. B., E. Sovik, and J. L. Cornish. 2010. 'The roles of dopamine and related compounds in reward-seeking behavior across animal phyla', *Front Behav Neurosci*, 4: 163.

Barry, C. L., E. E. McGinty, B. A. Pescosolido, and H. H. Goldman. 2014. 'Stigma, discrimination, treatment effectiveness, and policy: public views about drug addiction and mental illness', *Psychiatr Serv*, 65: 1269-72.

Bartlett, D. W., and M. E. Davis. 2006. 'Insights into the kinetics of siRNA-mediated gene silencing from live-cell and live-animal bioluminescent imaging', *Nucleic Acids Res*, 34: 322-33.

Bates, D., M. Maechler, B. Bolker, and S. Walker. 2015. 'Fitting Linear Mixed-Effects Models Using lme4', *Journal of Statistical Software*, 67: 47.

Bauer, J., A. Pedersen, N. Scherbaum, J. Bening, J. Patschke, H. Kugel, W. Heindel, V. Arolt, and P. Ohrmann. 2013. 'Craving in alcohol-dependent patients after detoxification is related to glutamatergic dysfunction in the nucleus accumbens and the anterior cingulate cortex', *Neuropsychopharmacology*, 38: 1401-8.

Beauvais, F. 1998. 'American indians and alcohol', *Alcohol Health & Research World*, 22: 7.

Bechara, A. 2005. 'Decision making, impulse control and loss of willpower to resist drugs: a neurocognitive perspective', *Nat Neurosci*, 8: 1458-63.

Beckley, J. T., S. Laguesse, K. Phamluong, N. Morisot, S. A. Wegner, and D. Ron. 2016. 'The First Alcohol Drink Triggers mTORC1-Dependent Synaptic Plasticity in Nucleus Accumbens Dopamine D1 Receptor Neurons', *J Neurosci*, 36: 701-13.

Beckmann, Christian F., Mark Jenkinson, and Stephen M. Smith. 2003. 'General multilevel linear modeling for group analysis in FMRI', *Neuroimage*, 20: 1052-63.

Begley, C. Glenn, and John P.A. Ioannidis. 2015. 'Reproducibility in Science', *Improving the Standard for Basic and Preclinical Research*, 116: 116-26.

Belin, D., and V. Deroche-Gamonet. 2012. 'Responses to novelty and vulnerability to cocaine addiction: contribution of a multi-symptomatic animal model', *Cold Spring Harb Perspect Med*, 2.

Benowitz, N. 2010a. 'Nicotine Addiction', *N Engl J Med*, 362: 2295-303.

Benowitz, N. L. 2010b. 'Nicotine addiction', *N Engl J Med*, 362: 2295-303.

Berridge, K. C., T. E. Robinson, and J. W. Aldridge. 2009. 'Dissecting components of reward: 'liking', 'wanting', and learning', *Curr Opin Pharmacol*, 9: 65-73.

Berry, M. R., and M. D. Likar. 2007. 'Statistical assessment of dissolution and drug release profile similarity using a model-dependent approach', *J Pharm Biomed Anal*, 45: 194-200.

Bert, B., H. Fink, R. Sohr, and A. Rex. 2001. 'Different effects of diazepam in Fischer rats and two stocks of Wistar rats in tests of anxiety', *Pharmacology Biochemistry and Behavior*, 70: 9.

Berthele, A., S.J. Boxall, A. Urban, J.M.H. Anneser, W. Zieglgansberger, L. Urban, and T.R. Tolle. 1999. 'Distribution and developmental changes in metabotropic glutamate receptor messenger RNA expression in the rat lumbar spinal cord', *Developmental Brain Research*, 112: 14.

Bird, M. K., C. A. Reid, F. Chen, H. O. Tan, S. Petrou, and A. J. Lawrence. 2010. 'Cocaine-mediated synaptic potentiation is absent in VTA neurons from mGlu5-deficient mice', *Int J Neuropsychopharmacol*, 13: 133-41.

Bischoff-Ferrari, H.A., M. Borchers, F. Gudat, U. Durmuller, H.B. Stahelin, and W. Dick. 2004. 'Vitamin D receptor expression in human muscle tissue decreases with age', *Journal of bone and mineral research*, 19: 4.

Biswal, B., F. Z. Yetkin, V. M. Haughton, and J. S. Hyde. 1995. 'Functional connectivity in the motor cortex of resting human brain using echo-planar MRI', *Magn Reson Med Oct*, 34: 537-41.

Blair, R.C., and J.J. Higgins. 1980. 'A comparison of the power of Wilcoxon's rank-sum statistic to that of the students t statistic under various non-normal distributions', *Journal of Educational Statistics*, 5: 26.

Bland, I. M., A. Guthrie-Jones, R. D. Taylor, and J. Hill. 2009. 'Dog obesity: owner attitudes and behaviour', *Prev Vet Med*, 92: 333-40.

Bland, J. M., and D. G. Altman. 1986. 'Statistical methods for assessing agreement between two methods of clinical measurement', *Lancet*, 1: 307-10.

Blum, K., A. L. Chen, J. Giordano, J. Borsten, T. J. Chen, M. Hauser, T. Simpatico, J. Femino, E. R. Braverman, and D. Barh. 2012. 'The addictive brain: all roads lead to dopamine', *J Psychoactive Drugs*, 44: 134-43.

Blüml, Stefan. 2013. 'Magnetic Resonance Spectroscopy: Basics.' in Stefan Blüml and Ashok Panigrahy (eds.), *MR Spectroscopy of Pediatric Brain Disorders* (Springer New York: New York, NY).

Brazas, R. M., J. E. Hagstrom, R. N. A. Interfiring, D. R. Engelke, and J. J. Rossi. 2005. *Delivery of Small to Mammalian Cells in Culture by Using Cationic Lipid/Polymer Based Transfection Reagens* (Academic Press: USA).

Brechtel, K., D.B. Dahl, J. Machann, O.P. Bachmann, I. Wenzel, T. Maier, C.D. Claussen, H.U. Haring, S. Jacob, and F. Schick. 2001. 'Fast elevation of the intramyocellular lipid content in the presence of circulating free fatty acids and hyperinsulinemia A dynamic 1H-MRS study', *Magnetic Resonance in Medicine*, 45: 4.

Brier, M. R., G. S. Day, A. Z. Snyder, A. B. Tanenbaum, and B. M. Ances. 2016. 'N-methyl-D-aspartate receptor encephalitis mediates loss of intrinsic activity measured by functional MRI', *J Neurol*, 263: 1083-91.

Brown, R. M., Y. M. Kupchik, and P. W. Kalivas. 2013. 'The story of glutamate in drug addiction and of N-acetylcysteine as a potential pharmacotherapy', *JAMA Psychiatry*, 70: 895-7.

Brown, R. M., M. R. Stagnitti, J. R. Duncan, and A. J. Lawrence. 2012. 'The mGlu5 receptor antagonist MTEP attenuates opiate self-administration and cue-induced opiate-seeking behaviour in mice', *Drug Alcohol Depend*, 123: 264-8.

Buchman, D. Z., W. Skinner, and J. Illes. 2010. 'Negotiating the Relationship Between Addiction, Ethics, and Brain Science', *AJOB Neurosci*, 1: 36-45.

Bueno, C.H., H. Zangrossi, and M.B. Viana. 2005. 'The inactivation of the basolateral nucleus of the rat amygdala has an anxiolytic effect in the elevated T-maze and light dark transition tests', *Brazilian Journal of Medical and Biological Research*, 38: 4.

Buller, A.L., H.C. Larson, R.A. Morriset, and D.T. Monaghan. 1996. 'Glycine modulates ethanol inhibition of heteromeric NMDA receptors expressed in Xenopus Oocytes', *Molecular pharmacology*, 48: 6.

Caine, S.B., T. Humby, T. W. Robbins, and B. J. Everitt. 2001. 'Behavioral effects of psychomotor stimulants in rats with dorsal or ventral subiculum lesions: Locomotion, cocaine self-administration and prepulse inhibition of startle.', *Behavioral Neuroscience*, 15: 14.

Campbell, U. C., K. Lalwani, L. Hernandez, G. G. Kinney, P. J. Conn, and L. J. Bristow. 2004. 'The mGluR5 antagonist 2-methyl-6-(phenylethynyl)-pyridine (MPEP) potentiates PCP-induced cognitive deficits in rats', *Psychopharmacology (Berl)*, 175: 310-8.

Cantin, L., M. Lenoir, E. Augier, N. Vanhille, S. Dubreucq, F. Serre, C. Vouillac, and S. H. Ahmed. 2010. 'Cocaine is low on the value ladder of rats: possible evidence for resilience to addiction', *PLoS One*, 5: e11592.

Cao, Y. J., C. S. Surowy, and P. S. Puttfarcken. 2005. 'Different nicotinic acetylcholine receptor subtypes mediating striatal and prefrontal cortical [3H]dopamine release', *Neuropharmacology*, 48: 72-9.

Carlson, R. W., N. N. Kumar, E. Wong-Mckinstry, S. Ayyagari, N. Puri, F. K. Jackson, and S. Shashikumar. 2012. 'Alcohol withdrawal syndrome', *Crit Care Clin*, 28: 549-85.

Casabona, G., T. Knopfel, R. Kuhn, F. Gasparini, P. Baumann, M.A. Sortino, A. Copani, and F. Nicoletti. 1997. 'Expression and coupling to polyphosphoinositide hydrolysis of Group I metabotropic glutamate receptors in early postnatal and adult rat brain', *European Journal of Neuroscience*, 9: 5.

Casteels, C., P. Vermaelen, J. Nuyts, A. Van Der Linden, V. Baekelandt, L. Mortelmans, G. Bormans, and K. Van Laere. 2006a. 'Construction and evaluation of multitracer small-animal PET probabilistic atlases for voxel-based functional mapping of the rat brain', *J Nucl Med*, 47: 1858-66.

———. 2006b. 'Construction and evaluation of multitracer small-animal PET probabilistic atlases for voxel-based functional mapping of the rat brain', *Journal of Nuclear Medicine*, 47: 8.

Casteels, C., K. Vunckx, S. A. Aelvoet, V. Baekelandt, G. Bormans, K. Van Laere, and M. Koole. 2013. 'Construction and evaluation of quantitative small-animal PET probabilistic atlases for [18F]FDG and [18F]FECT functional mapping of the mouse brain', *PLoS One*, 8: e65286.

Chau, P., B. Soderpalm, and M. Ericson. 2011. 'The mGluR5 antagonist MPEP elevates accumbal dopamine and glycine levels; interaction with strychnine-sensitive glycine receptors', *Addict Biol*, 16: 591-9.

Chen, B., and K. Roche. 2007. 'Regulation of NMDA receptors by phosphorylation', *Neuropharmacology*, 53: 6.

Chen, X., M. L. Michaelis, and E. K. Michaelis. 1997. 'Effects of chronic ethnol treatment on the expression of Ca transport carriers and NMDA Glutamate receptor proteins in brain synaptic membranes', *J Neurochem*, 69: 10.

Cheng, J. C., K. Shoghi, and R. Laforest. 2012. 'Quantitative accuracy of MAP reconstruction for dynamic PET imaging in small animals', *Med Phys*, 39: 1029-41.

Chesworth, R., R. M. Brown, J. H. Kim, and A. J. Lawrence. 2013. 'The metabotropic glutamate 5 receptor modulates extinction and reinstatement of methamphetamine-seeking in mice', *PLoS One*, 8: e68371.

Chiamulera, C., M.P. Epping-Jordan, A. Zocchi, C. Marcon, C. Cottiny, S. Tacconi, M. Corsi, F. Orzi, and F. Conquet. 2001. 'Reinforcing and locomotor stimulant effects of cocaine are absent in mGluR5 null mutant mice', *Nature Neuroscience*, 4: 2.

Chou, S. P., R. B. Goldstein, S. M. Smith, B. Huang, W. J. Ruan, H. Zhang, J. Jung, T. D. Saha, R. P. Pickering, and B. F. Grant. 2016. 'The Epidemiology of DSM-5 Nicotine Use Disorder: Results From the National Epidemiologic Survey on Alcohol and Related Conditions-III', *J Clin Psychiatry*, 77: 1404-12.

Cole, D. M., C. F. Beckmann, C. J. Long, P. M. Matthews, M. J. Durcan, and J. D. Beaver. 2010. 'Nicotine replacement in abstinent smokers improves cognitive withdrawal symptoms with modulation of resting brain network dynamics', *Neuroimage*, 52: 590-9.

Conn, P. J., and C. K. Jones. 2009. 'Promise of mGluR2/3 activators in psychiatry', *Neuropsychopharmacology*, 34: 248-9.
Conti, M. 2009. 'State of the art and challenges of time-of-flight PET', *Phys Med*, 25: 1-11.
Coolidge, F. L., and T. Wynn. 2009. *The rise of Homo Sapiens: The evolution of modern thinking* (Wiley-Blackwell: Singapore).
Coolidge, F.L., and T. Wynn. 2001. 'Executive functions of the frontal lobes and the evolutionary ascendancy of *Homo Sapiens*', *Cambridge Archaelogical Journal*, 11: 5.
Corrigall, W. A., K. M. Coen, and K. L. Adamson. 1994. 'Self-administered nicotine activates the mesolimbic dopamine system through the ventral tegmental area', *Brain Res*, 653: 278 - 84.
Corrigall, W. A., K. B. Franklin, K. M. Coen, and P. B. Clarke. 1992. 'The mesolimbic dopaminergic system is implicated in the reinforcing effects of nicotine', *Psychopharmacology*, 107: 285 - 89.
Cosford, N. D., L. Tehrani, J. Roppe, E. Schweiger, N. D. Smith, J. Anderson, L. Bristow, J. Brodkin, X. Jiang, I. McDonald, S. Rao, M. Washburn, and M. A. Varney. 2003. '3-[(2-Methyl-1,3-thiazol-4-yl)ethynyl]-pyridine: a potent and highly selective metabotropic glutamate subtype 5 receptor antagonist with anxiolytic activity', *J Med Chem*, 46: 204-6.
Cosgrove, K. P. 2016. 'A Need for Longitudinal Studies in the Addiction Field', *Biol Psychiatry*, 80: 174-5.
Coutinho, V., and T. Knopfel. 2002. 'Book Review: Metabotropic Glutamate Receptors: Electrical and Chemical Signaling Properties', *The Neuroscientist*, 8: 551-61.
Cozzoli, D. K., J. Courson, A. L. Caruana, B. W. Miller, D. I. Greentree, A. B. Thompson, M. G. Wroten, P. W. Zhang, B. Xiao, J. H. Hu, M. Klugmann, P. Metten, P. F. Worley, J. C. Crabbe, and K. K. Szumlinski. 2012. 'Nucleus accumbens mGluR5-associated signaling regulates binge alcohol drinking under drinking-in-the-dark procedures', *Alcohol Clin Exp Res*, 36: 1623-33.
Cozzoli, D. K., J. Courson, C. Rostock, R. R. Campbell, M. G. Wroten, H. McGregor, A. L. Caruana, B. W. Miller, J. H. Hu, P. Wu Zhang, B. Xiao, P. F. Worley, J. C. Crabbe, D. A. Finn, and K. K. Szumlinski. 2016. 'Protein Kinase C Epsilon Activity in the Nucleus Accumbens and Central Nucleus of the Amygdala Mediates Binge Alcohol Consumption', *Biol Psychiatry*, 79: 443-51.
Cruz, N. F., A. Lasater, H. R. Zielke, and G. A. Dienel. 2005. 'Activation of astrocytes in brain of conscious rats during acoustic stimulation: acetate utilization in working brain', *J Neurochem*, 92: 934-47.
Cunningham, J. P. 2004. 'Learning, odour preference and flower foraging in moths', *Journal of Experimental Biology*, 207: 87-94.
Dahchour, A., P. De Witte, N. Bolo, J. Nédélec, M. Muzet, P. Durbin, and J. Macher. 1998. 'Central effects of acamprosate: Part1. Acamprosate blocks the glutamate increase in the nucleus accumbens microdialysate in ethanol withdrawn rats', *Pyschiatry Research*, 82: 7.
Dailly, E., F. Chenu, C. E. Renard, and M. Bourin. 2004. 'Dopamine, depression and antidepressants', *Fundam Clin Pharmacol*, 18: 601-7.
Dajas-Bailador, F., and S. Wonnacott. 2004. 'Nicotinic acetylcholine receptors and the regulation of neuronal signalling', *Trends Pharmacol Sci*, 25: 317-24.
Dalley, Jeffrey W., Tim D. Fryer, Laurent Brichard, Emma S. J. Robinson, David E. H. Theobald, Kristjan Lääne, Yolanda Peña, Emily R. Murphy, Yasmene Shah, Katrin Probst, Irina Abakumova, Franklin I. Aigbirhio, Hugh K. Richards, Young

Hong, Jean-Claude Baron, Barry J. Everitt, and Trevor W. Robbins. 2007. 'Nucleus Accumbens D2/3 Receptors Predict Trait Impulsivity and Cocaine Reinforcement', *Science*, 315: 1267.

Dani, J. A., and M. De Biasi. 2001. 'Cellular mechanisms of nicotine addiction', *Pharmacol Biochem Behav*, 70: 439-46.

David, H. N., M. Ansseau, and J. H. Abraini. 2005. 'Dopamine-glutamate reciprocal modulation of release and motor responses in the rat caudate-putamen and nucleus accumbens of "intact" animals', *Brain Res Brain Res Rev*, 50: 336-60.

de Bejczy, A., K. R. Nations, A. Szegedi, J. Schoemaker, F. Ruwe, and B. Soderpalm. 2014. 'Efficacy and safety of the glycine transporter-1 inhibitor org 25935 for the prevention of relapse in alcohol-dependent patients: a randomized, double-blind, placebo-controlled trial', *Alcohol Clin Exp Res*, 38: 2427-35.

de Laat, B., G. Leurquin-Sterk, S. Celen, G. Bormans, M. Koole, K. Van Laere, and C. Casteels. 2015. 'Preclinical Evaluation and Quantification of 18F-FPEB as a Radioligand for PET Imaging of the Metabotropic Glutamate Receptor 5', *J Nucl Med*, 56: 1954-9.

De Vico Fallani, F., J. Richiardi, M. Chavez, and S. Achard. 2014. 'Graph analysis of functional brain networks: practical issues in translational neuroscience', *Philos Trans R Soc Lond B Biol Sci*, 369.

DeLorenzo, C., N. DellaGioia, M. Bloch, G. Sanacora, N. Nabulsi, C. Abdallah, J. Yang, R. Wen, J. J. Mann, J. H. Krystal, R. V. Parsey, R. E. Carson, and I. Esterlis. 2015. 'In vivo ketamine-induced changes in [11C]ABP688 binding to metabotropic glutamate receptor subtype 5', *Biol Psychiatry*, 77: 266-75.

DeLorenzo, C., J. S. Kumar, J. J. Mann, and R. V. Parsey. 2011. 'In vivo variation in metabotropic glutamate receptor subtype 5 binding using positron emission tomography and [11C]ABP688', *J Cereb Blood Flow Metab*, 31: 2169-80.

DeMar, J. C., Jr., K. Ma, J. M. Bell, M. Igarashi, D. Greenstein, and S. I. Rapoport. 2006. 'One generation of n-3 polyunsaturated fatty acid deprivation increases depression and aggression test scores in rats', *J Lipid Res*, 47: 172-80.

den Hartog, C. R., J. T. Beckley, T. C. Smothers, D. H. Lench, Z. L. Holseberg, H. Fedarovich, M. J. Gilstrap, G. E. Homanics, and J. J. Woodward. 2013. 'Alterations in ethanol-induced behaviors and consumption in knock-in mice expressing ethanol-resistant NMDA receptors', *PLoS One*, 8: e80541.

Deroche-Gamonet, V., D. Belin, and P. V. Piazza. 2004. 'Evidence for addiction-like behavior in the rat', *Science*, 305: 1014-7.

Dichter, G.S., C.A. Damiano, and J.A. Allen. 2012. 'Reward circuitry dysfunction in psychiatric and neurodevelopmental disorders and genetic syndromes: animal models and clinical findings', *Journal of Neurodevelopmental Disorders*, 4: 43.

DiLeone, R. J., J. R. Taylor, and M. R. Picciotto. 2012. 'The drive to eat: comparisons and distinctions between mechanisms of food reward and drug addiction', *Nat Neurosci*, 15: 1330-5.

Ding, R., Y. Li, A. Du, H. Yu, B. He, R. Shen, J. Zhou, L. Li, W. Cui, G. Zhang, Y. Lu, and X. Wu. 2016. 'Changes in hippocampal AMPA receptors and cognitive impairments in chronic ketamine addiction models: another understanding of ketamine CNS toxicity', *Sci Rep*, 6: 38771.

Doll, R., R. Peto, J. Boreham, and I. Sutherland. 2004. 'Mortality in relation to smoking: 50 years' observations on male British doctors', *BMJ*, 328: 9.

Domino, E. F., S. Minoshima, S. K. Guthrie, L. Ohl, L. Ni, R. A. Koeppe, D. J. Cross, and J. K. Zubieta. 2000. 'Effects of nicotine on regional cerebral glucose metabolism in awake resting tobacco smokers', *Neuroscience*, 101: 277-82.

Dorri, F., D. R. Hampson, A. Baskys, and J. M. Wojtowicz. 1997. 'Down-regulation of mGluR5 by antisense deoxynucleotides alters pharmacological responses to applications of ACPD in the rat hippocampus', *Exp Neurol*, 147: 48-54.

Dreyfus, H.L., and S.E. Dreyfus. 1992. 'What artificial experts can and cannot do', *AI & Society*, 6: 8.

DuBois, J. M., O. G. Rousset, J. Rowley, M. Porras-Betancourt, A. J. Reader, A. Labbe, G. Massarweh, J. P. Soucy, P. Rosa-Neto, and E. Kobayashi. 2016. 'Characterization of age/sex and the regional distribution of mGluR5 availability in the healthy human brain measured by high-resolution [(11)C]ABP688 PET', *Eur J Nucl Med Mol Imaging*, 43: 152-62.

Effertz, T., and K. Mann. 2013. 'The burden and cost of disorders of the brain in Europe with the inclusion of harmful alcohol use and nicotine addiction', *Eur Neuropsychopharmacol*, 23: 742-8.

Elmenhorst, D., A. Aliaga, A. Bauer, and P. Rosa-Neto. 2012. 'Test-retest stability of cerebral mGluR(5) quantification using [(1)(1)C]ABP688 and positron emission tomography in rats', *Synapse*, 66: 552-60.

Elmenhorst, D., K. Mertens, T. Kroll, A. Oskamp, J. Ermert, E. M. Elmenhorst, F. Wedekind, S. Beer, H. H. Coenen, and A. Bauer. 2016. 'Circadian variation of metabotropic glutamate receptor 5 availability in the rat brain', *J Sleep Res*, 25: 754-61.

Elmenhorst, D., L. Minuzzi, A. Aliaga, J. Rowley, G. Massarweh, M. Diksic, A. Bauer, and P. Rosa-Neto. 2010. 'In vivo and in vitro validation of reference tissue models for the mGluR(5) ligand [(11)C]ABP688', *J Cereb Blood Flow Metab*, 30: 1538-49.

Elsworth, J.D., and R.H. Roth. 1997. 'Dopamine synthesis, uptake, metabolism, and receptors: Relevance to gene therapy of Parkinson's disease', *Experimental Neurology*, 144: 5.

Everitt, B. J., J.A. Parkinson, M. C. Olmstead, M. Arroyo, P. Robledo, and T. W. Robbins. 1999. 'Associative processes in addiction and reward. The role of amygdala-ventral striatal subsystems.', *Annals New York Academy of Sciences*, 877: 27.

Everitt, B. J., and T. W. Robbins. 2005. 'Neural systems of reinforcement for drug addiction: from actions to habits to compulsion', *Nat Neurosci*, 8: 1481-9.

Fatemi, S. H., T. D. Folsom, R. E. Kneeland, M. K. Yousefi, S. B. Liesch, and P. D. Thuras. 2013. 'Impairment of fragile X mental retardation protein-metabotropic glutamate receptor 5 signaling and its downstream cognates ras-related C3 botulinum toxin substrate 1, amyloid beta A4 precursor protein, striatal-enriched protein tyrosine phosphatase, and homer 1, in autism: a postmortem study in cerebellar vermis and superior frontal cortex', *Mol Autism*, 4: 21.

Fay, M. P., and M. A. Proschan. 2010. 'Wilcoxon-Mann-Whitney or t-test? On assumptions for hypothesis tests and multiple interpretations of decision rules', *Stat Surv*, 4: 1-39.

Feigin, Andrew, Klaus L. Leenders, James R. Moeller, John Missimer, Gabriella Kuenig, Phoebe Spetsieris, Angelo Antonini, and David Eidelberg. 2001. 'Metabolic Network Abnormalities in Early Huntington's Disease: An [18F]FDG PET Study', *Journal of Nuclear Medicine*, 42: 1591-95.

Fitzmaurice, Garrett, Marie Davidian, Geert Verbeke, and Geert Molenberghs. 2008. *Longitudinal data analysis* (CRC Press).

Flores, J. E., L. M. McFarland, A. Vanderbilt, A. K. Ogasawara, and S. P. Williams. 2008. 'The effects of anesthetic agent and carrier gas on blood glucose and tissue

uptake in mice undergoing dynamic FDG-PET imaging: sevoflurane and isoflurane compared in air and in oxygen', *Mol Imaging Biol*, 10: 192-200.

Fonseca, U. N., S. G. Nielsen, J. Hau, and A. K. Hansen. 2010. 'Permanent catheterization of the carotid artery induces kidney infection and inflammation in the rat', *Lab Anim*, 44: 46-53.

Foster, K.R., R. Koprowski, and J.D. Skufca. 2014. 'Machine learning, medical diagnosis, and biomedical engineering research - commentary', *Biomedical Engineering*, 13: 9.

Fourgeaud, L., A. S. Bessis, F. Rossignol, J. P. Pin, J. C. Olivo-Marin, and A. Hemar. 2003. 'The metabotropic glutamate receptor mGluR5 is endocytosed by a clathrin-independent pathway', *J Biol Chem*, 278: 12222-30.

Friston, K. J. 2006. 'Statistical Parametric Mapping.' in W.D. Penny, K. J. Friston and S.J.K. Ashburner (eds.), *Statistical Parametric Mapping: The analysis of functional brain images* (Academic Press: Cambridge, U.S.A.).

Frye, M. A., J. M. Bright, D. A. Dargatz, M. J. Fettman, D. D. Frisbie, D. C. Baker, and J. L. Traub-Dargatz. 2003. 'A Comparison of Dobutamine Infusion to Exercise as a Cardiac Stress Test in Healthy Horses', *Journal of Veterinary Internal Medicine*, 17: 58-64.

Galbraith, S., J. A. Daniel, and B. Vissel. 2010. 'A study of clustered data and approaches to its analysis', *J Neurosci*, 30: 10601-8.

Gao, Y., P. Li, L. Ma, K. Du, X. Wang, M. Tang, H. He, X. Yu, W. Zang, and H. Hu. 2012. 'Effects of Acute Administration of Ethanol on Experimental Arrhythmia', *The Chinese Journal of Physiology*, 55: 6.

Gardner, E. L. 2000. 'What have we learned about addiction from animal models of drug self-administration', *The American Journal on Addictions*, 9: 28.

Garrison, K. A., and M. N. Potenza. 2014. 'Neuroimaging and biomarkers in addiction treatment', *Curr Psychiatry Rep*, 16: 513.

Gass, J. T., and M. F. Olive. 2008. 'Glutamatergic substrates of drug addiction and alcoholism', *Biochem Pharmacol*, 75: 47.

Gatfield, P. David, Oliver H. Lowry, Demoy W. Schulz, and Janet V. Passonneau. 1966. 'REGIONAL ENERGY RESERVES IN MOUSE BRAIN AND CHANGES WITH ISCHAEMIA AND ANAESTHESIA*', *Journal of Neurochemistry*, 13: 185-95.

Gilpin, N. W., M. A. Herman, and M. Roberto. 2015. 'The central amygdala as an integrative hub for anxiety and alcohol use disorders', *Biol Psychiatry*, 77: 859-69.

Ginovart, N., W. Hassoun, M. Le Cavorsin, L. Veyre, D. Le Bars, and V. Leviel. 2002. 'Effects of amphetamine and evoked dopamine release on [11C]raclopride binding in anesthetized cats', *Neuropsychopharmacology*, 27: 72-84.

Glover, G. H. 2011. 'Overview of functional magnetic resonance imaging', *Neurosurg Clin N Am*, 22: 133-9, vii.

Goldman, D., G. Oroszi, and F. Ducci. 2005. 'The genetics of addictions: uncovering the genes', *Nat Rev Genet*, 6: 521-32.

Golembiowska, K. 2003. 'Neuroprotective action of MPEP, a selective mGluR5 antagonist, in methamphetamine-induced dopaminergic neurotoxicity is associated with a decrease in dopamine outflow and inhibition of hyperthermia in rats', *Neuropharmacology*, 45: 484-92.

Gosnell, B.A., and D.D. Krahn. 1992. 'The relationship between saccharin and alcohol intake in rats', *Alcohol*, 9: 3.

Gossop, M., D. Stewart, S. Treacy, and J. Marsden. 2002. 'A prospective study of mortality among drug misusers during a 4-year period after seeking treatment', *Addiction*, 97: 8.

Gould, S. E., M. R. Junttila, and F. J. de Sauvage. 2015. 'Translational value of mouse models in oncology drug development', *Nat Med*, 21: 431-9.

Graham, J.S., H.G. Wall, J.B. Nold, I.J. Hayward, and T.W. Slone. 1990. 'Cardiac perfusion versus immersion fixation for the production of brain sections', *U.S. Army Medical Research Institute of Chemical Defense*.

Grant, B. F., R. B. Goldstein, T. D. Saha, S. P. Chou, J. Jung, H. Zhang, R. P. Pickering, W. J. Ruan, S. M. Smith, B. Huang, and D. S. Hasin. 2015. 'Epidemiology of DSM-5 Alcohol Use Disorder: Results From the National Epidemiologic Survey on Alcohol and Related Conditions III', *JAMA Psychiatry*, 72: 757-66.

Grant, J. E., and S. R. Chamberlain. 2014. 'Impulsive action and impulsive choice across substance and behavioral addictions: cause or consequence?', *Addict Behav*, 39: 1632-9.

Graveron-Demilly, D. 2014. 'Quantification in magnetic resonance spectroscopy based on semi-parametric approaches', *MAGMA*, 27: 113-30.

Groenewegen, H.J. 2003. 'The basal ganglia and motor control', *Neural plasticity*, 10: 14.

Groenewegen, H.J., C.I. Wright, A.V.J. Beijer, and P. Voorn. 2006. 'Convergence and segregation of central striatal inputs and outputs', *Annals New York Academy of Sciences*, 877: 15.

Gunn, R. N., S. R. Gunn, F. E. Turkheimer, J.A.D. Aston, and V. J. Cunningham. 2002. 'Positron Emission Tomography compartment models: A basis pursuit strategy for kinetic modelling', *J Cereb Blood Flow Metab*, 22: 14.

Hadar, R., V. Vengeliene, E. Barroeta Hlusicke, S. Canals, H. R. Noori, F. Wieske, J. Rummel, D. Harnack, A. Heinz, R. Spanagel, and C. Winter. 2016. 'Paradoxical augmented relapse in alcohol-dependent rats during deep-brain stimulation in the nucleus accumbens', *Transl Psychiatry*, 6: e840.

Hahn, A., G. Gryglewski, L. Nics, M. Hienert, L. Rischka, C. Vraka, H. Sigurdardottir, T. Vanicek, G. M. James, R. Seiger, A. Kautzky, L. Silberbauer, W. Wadsak, M. Mitterhauser, M. Hacker, S. Kasper, and R. Lanzenberger. 2016. 'Quantification of Task-Specific Glucose Metabolism with Constant Infusion of 18F-FDG', *J Nucl Med*, 57: 1933-40.

Hall, Wayne, Adrian Carter, and Cynthia Forlini. 2015. 'The brain disease model of addiction: is it supported by the evidence and has it delivered on its promises?', *The Lancet Psychiatry*, 2: 105-10.

Hall, Z. J., S. D. Healy, and S. L. Meddle. 2015. 'A role for nonapeptides and dopamine in nest-building behaviour', *J Neuroendocrinol*, 27: 158-65.

Hamill, T. G., S. Krause, C. Ryan, C. Bonnefous, S. Govek, T. J. Seiders, N. D. Cosford, J. Roppe, T. Kamenecka, S. Patel, R. E. Gibson, S. Sanabria, K. Riffel, W. Eng, C. King, X. Yang, M. D. Green, S. S. O'Malley, R. Hargreaves, and H. D. Burns. 2005. 'Synthesis, characterization, and first successful monkey imaging studies of metabotropic glutamate receptor subtype 5 (mGluR5) PET radiotracers', *Synapse*, 56: 205-16.

Hamill, T., T. J. Seiders, S. Krause, C. Ryan, S. Sanabria, R. E. Gibson, S. Patel, N. D. Cosford, J. Roppe, J. Yang, C. King, R. Hargreaves, and H. D. Burns. 2003. 'The synthesis and characterization of mGluR5 receptor PET ligands', *J Labelled Compd Rad*, 46: 1.

Hao, Y., R. Martin-Fardon, and F. Weiss. 2010. 'Behavioral and functional evidence of metabotropic glutamate receptor 2/3 and metabotropic glutamate receptor 5

dysregulation in cocaine-escalated rats: factor in the transition to dependence', *Biol Psychiatry*, 68: 240-8.

Hefti, K., S. C. Holst, J. Sovago, V. Bachmann, A. Buck, S. M. Ametamey, M. Scheidegger, T. Berthold, B. Gomez-Mancilla, E. Seifritz, and H. P. Landolt. 2013. 'Increased metabotropic glutamate receptor subtype 5 availability in human brain after one night without sleep', *Biol Psychiatry*, 73: 161-8.

Heimer, L. 2003. 'A new anatomical framework for neuropsychiatric disorders and drug abuse', *Am J Psychiatry*, 160: 14.

Heishman, S. J., and E. G. Singleton. 2010. 'Meta-analysis of the acute effects of nicotine and smoking on human performance', *Psychopharmacology*, 210: 453-69.

Hellwig, S., S. Brioschi, S. Dieni, L. Frings, A. Masuch, T. Blank, and K. Biber. 2016. 'Altered microglia morphology and higher resilience to stress-induced depression-like behavior in CX3CR1-deficient mice', *Brain Behav Immun*, 55: 126-37.

Helzer, J.E., W. Van den Brink, and S.E. Guth. 2006. 'Should there be both categorical and dimensional criteria for the substance use disorders in DSM-V', *Addiction*, 101: 5.

Hermann, D., W. Weber-Fahr, A. Sartorius, M. Hoerst, U. Frischknecht, N. Tunc-Skarka, S. Perreau-Lenz, A. C. Hansson, B. Krumm, F. Kiefer, R. Spanagel, K. Mann, G. Ende, and W. H. Sommer. 2012. 'Translational magnetic resonance spectroscopy reveals excessive central glutamate levels during alcohol withdrawal in humans and rats', *Biol Psychiatry*, 71: 1015-21.

Hermans, E., and R.A.J. Challiss. 2001. 'Structural, signalling and regulatory properties of the group I metabotropic glutamate receptors: Prototypic family C G-protein-coupled receptors', *Biochem J*, 359: 19.

Hicks, R.A., and J.D. Moore. 1979. 'REM sleep deprivation diminishes fear in rats', *Physiology & Behavior*, 22: 3.

Higuera-Matas, A., M. L. Soto-Montenegro, G. L. Montoya, V. Garcia-Vazquez, J. Pascau, M. Miguens, N. Del Olmo, J. J. Vaquero, C. Garcia-Lecumberri, M. Desco, and E. Ambrosio. 2011. 'Chronic cannabinoid administration to periadolescent rats modulates the metabolic response to acute cocaine in the adult brain', *Mol Imaging Biol*, 13: 411-15.

Hildebrandt, Isabel J., Helen Su, and Wolfgang A. Weber. 2008. 'Anesthesia and Other Considerations for in Vivo Imaging of Small Animals', *ILAR Journal*, 49: 17-26.

Hiroi, N., and S. Agatsuma. 2005. 'Genetic susceptibility to substance dependence', *Mol Psychiatry*, 10: 336-44.

Hodge, C. W., M. F. Miles, A. C. Sharko, R. A. Stevenson, J. R. Hillmann, V. Lepoutre, J. Besheer, and J. P. Schroeder. 2006. 'The mGluR5 antagonist MPEP selectively inhibits the onset and maintenance of ethanol self-administration in C57BL/6J mice', *Psychopharmacology (Berl)*, 183: 429-38.

Højsgaard, S., U. Halekoh, and J. Yan. 2006. 'The R package geepack for Generalized Estimating Equations', *Journal of Statistical Software*, 15: 47.

Holden, C. 2010. 'Psychiatry. Behavioral addictions debut in proposed DSM-V', *Science*, 327: 935.

Hollander, J. A., Q. Lu, M.D. Cameron, T. Kamenecka, and P. J. Kenny. 2008. 'Insular hypocretin transmission regulates nicotine reward', *Proc Natl Acad Sci*, 105: 5.

Honer, M., A. Stoffel, L. J. Kessler, P. A. Schubiger, and S. M. Ametamey. 2007. 'Radiolabeling and in vitro and in vivo evaluation of [18F]-FE-DABP688 as a PET radioligand for the metabotropic glutamate receptor subtype 5', *Nucl Med Biol*, 34: 973-80.

Hons, J., R. Zirko, M. Ulrychova, E. Cermakova, P. Doubek, and J. Libiger. 2010. 'Glycine serum level in schizophrenia: relation to negative symptoms', *Psychiatry Res*, 176: 103-8.

Horton, N.J., J.D. Bebchuck, C.L. Jones, S.R. Lipsitz, P.J. Catalano, G.P. Zahner, and G.M. Fitzmaurice. 1999. 'Goodness-of-fit for GEE: An example with mental health service utilization', *Statistics in Medicine*, 18: 9.

Hu, X., P. Follesa, and M.K. Ticku. 1996. 'Chronic ethanol treatment produces a selective upregulation of the NMDA receptor subunit gene expression in mammalian cultured cortical neurons', *Molecular Brain Research*, 36: 7.

Huang, L., P. Sherchan, Y. Wang, C. Reis, R. L. Applegate, 2nd, J. Tang, and J. H. Zhang. 2015. 'Phosphoinositide 3-Kinase Gamma Contributes to Neuroinflammation in a Rat Model of Surgical Brain Injury', *J Neurosci*, 35: 10390-401.

Hubbard, A. E., J. Ahern, N. L. Fleischer, M. Van der Laan, S. A. Lippman, N. Jewell, T. Bruckner, and W. A. Satariano. 2010. 'To GEE or not to GEE: comparing population average and mixed models for estimating the associations between neighborhood risk factors and health', *Epidemiology*, 21: 467-74.

Hughes, J. R., and D. Hatsukami. 1986. 'Signs and symptoms of tobacco withdrawal', *Arch Gen Psychiatry Mar*, 43: 289-94.

Hulka, L. M., V. Treyer, M. Scheidegger, K. H. Preller, M. Vonmoos, M. R. Baumgartner, A. Johayem, S. M. Ametamey, A. Buck, E. Seifritz, and B. B. Quednow. 2014. 'Smoking but not cocaine use is associated with lower cerebral metabotropic glutamate receptor 5 density in humans', *Mol Psychiatry*, 19: 625-32.

Ichise, M., J. S. Liow, J. Q. Lu, A. Takano, K. Model, H. Toyama, T. Suhara, K. Suzuki, R. B. Innis, and R. E. Carson. 2003. 'Linearized reference tissue parametric imaging methods: application to [11C]DASB positron emission tomography studies of the serotonin transporter in human brain', *J Cereb Blood Flow Metab*, 23: 1096-112.

Innis, R. B., V. J. Cunningham, J. Delforge, M. Fujita, A. Gjedde, R. N. Gunn, J. Holden, S. Houle, S. C. Huang, M. Ichise, H. Iida, H. Ito, Y. Kimura, R. A. Koeppe, G. M. Knudsen, J. Knuuti, A. A. Lammertsma, M. Laruelle, J. Logan, R. P. Maguire, M. A. Mintun, E. D. Morris, R. Parsey, J. C. Price, M. Slifstein, V. Sossi, T. Suhara, J. R. Votaw, D. F. Wong, and R. E. Carson. 2007. 'Consensus nomenclature for in vivo imaging of reversibly binding radioligands', *J Cereb Blood Flow Metab*, 27: 1533-9.

Ishida, M., H. Akagi, K. Shimamoto, Y. Ohfune, and H. Shinozaki. 1990. 'A potent metabotropic glutamate receptor agonist: Electrophysiological actions of a conformationally restricted glutamate analogue in the rat spinal cord and Xenopus oocytes.', *Brain Res*, 537: 3.

Janes, A. C., L. D. Nickerson, B. Frederick Bde, and M. J. Kaufman. 2012. 'Prefrontal and limbic resting state brain network functional connectivity differs between nicotine-dependent smokers and non-smoking controls', *Drug Alcohol Depend*, 125: 252-9.

Janiri, L., G. Martinotti, T. Dario, D. Reina, F. Paparello, G. Pozzi, G. Addolorato, M. Di Giannantonio, and S. De Risio. 2005. 'Anhedonia and substance-related symptoms in detoxified substance-dependent subjects: a correlation study', *Neuropsychobiology*, 52: 37-44.

Jenkinson, M., P. Bannister, M. Brady, and S. Smith. 2002. 'Improved optimization for the robust and accurate linear registration and motion correction of brain images', *Neuroimage*, 17: 825-41.

Jenkinson, M., and S. Smith. 2001. 'A global optimisation method for robust affine registration of brain images', *Med Image Anal*, 5: 143-56.
Johnson, M.W., and W.K. Bickel. 2002. 'Within-subject comparison of real and hypothetical money rewards in delay discounting', *J Exp Anal Behav*, 77: 17.
Jones, J. D., S. Mogali, and S. D. Comer. 2012. 'Polydrug abuse: a review of opioid and benzodiazepine combination use', *Drug Alcohol Depend*, 125: 8-18.
Kaiser, T., and G. Feng. 2015. 'Modeling psychiatric disorders for developing effective treatments', *Nat Med*, 21: 979-88.
Kalivas, P. W. 2009. 'The glutamate homeostasis hypothesis of addiction', *Nat Rev Neurosci*, 10: 561-72.
Kalivas, P. W., and N. D. Volkow. 2005. 'The neural basis of addiction: A pathology of motivation and choice', *Am J Psychiatry*, 162: 10.
Kalivas, P. W., N. Volkow, and J. Seamans. 2005. 'Unmanageable motivation in addiction: a pathology in prefrontal-accumbens glutamate transmission', *Neuron*, 45: 647-50.
Katz, R.J., K.A. Roth, and B.J. Carrol. 1981. 'Acute and chronic stress effects on open field activity in the rat Implications for a model of depression', *Neuroscience & Biobehavioral Reviews*, 5: 4.
Kearfott, K.J., and J. R. Votaw. 1995. 'The basics of Positron Emission Tomography (PET) imaging.' in A.M. Emran (ed.), *Chemists' Views of Imaging Centers* (Springer US: New York, U.S.A.).
Kelley, A. E., and K. C. Berridge. 2002. 'The neuroscience of natural rewards Relevance to addictive drugs', *The journal of neuroscience*, 22: 5.
Kenny, P. J., and A. Markou. 2006. 'Nicotine self-administration acutely activates brain reward systems and induces a long-lasting increase in reward sensitivity', *Neuropsychopharmacology*, 31: 1203-11.
Kessler, R. M., J. Seibyl, R. L. Cowan, D. Zald, J. S. Young, M. S. Ansari, and M. G. Stabin. 2014. 'Radiation Dosimetry of (18)F-FPEB in Humans', *J Nucl Med*, 55: 1119-21.
Kew, J. N. C., and J. Kemp. 2005. 'Ionotropic and metabotropic glutamate receptor structure and pharmacology', *Psychopharmacology*, 179: 4-29.
Kim, D. H., and J. J. Rossi. 2008. 'RNAi mechanisms and applications', *Biotechniques*, 44: 613-6.
Kim, I. D., J. H. Shin, S. W. Kim, S. Choi, J. Ahn, P. L. Han, J. S. Park, and J. K. Lee. 2012. 'Intranasal delivery of HMGB1 siRNA confers target gene knockdown and robust neuroprotection in the postischemic brain', *Mol Ther*, 20: 829-39.
Kim, S. J., J. M. Sullivan, S. Wang, K. P. Cosgrove, and E. D. Morris. 2014. 'Voxelwise lp-ntPET for detecting localized, transient dopamine release of unknown timing: sensitivity analysis and application to cigarette smoking in the PET scanner', *Hum Brain Mapp*, 35: 4876-91.
Kirsch, L., and G. Chechik. 2016. 'On Expression Patterns and Developmental Origin of Human Brain Regions', *PLoS Comput Biol*, 12: e1005064.
Kloppel, S., A. Abdulkadir, C. R. Jack, Jr., N. Koutsouleris, J. Mourao-Miranda, and P. Vemuri. 2012. 'Diagnostic neuroimaging across diseases', *Neuroimage*, 61: 457-63.
Komoroski, R.A., J.E.O Newton, J.R. Sprigg, D. Cardwell, P. Mohanakrishnan, and C.N. Karson. 1993. 'In vivo 7Li nuclear magnetic resonance study of lithium pharmacokinetics and chemical shift imaging in psychiatric patients', *Psychiatry Res*, 50: 9.

Koob, G. F. 2013. 'Addiction is a Reward Deficit and Stress Surfeit Disorder', *Front Psychiatry*, 4: 72.

———. 2014. 'Neurocircuitry of alcohol addiction: synthesis from animal models.' in E.V. Sullivan and A. Pfefferbaum (eds.), *Alcohol and the Nervous System* (Elsevier: Oxford).

Koob, G. F., and B. J. Mason. 2016. 'Existing and Future Drugs for the Treatment of the Dark Side of Addiction', *Annu Rev Pharmacol Toxicol*, 56: 299-322.

Koob, G. F., and N. D. Volkow. 2016. 'Neurobiology of addiction: a neurocircuitry analysis', *Lancet Psychiatry*, 3: 13.

Koyner, J. L., D. L. Davison, E. Brasha-Mitchell, D. M. Chalikonda, J. M. Arthur, A. D. Shaw, J. A. Tumlin, S. A. Trevino, M. R. Bennett, P. L. Kimmel, M. G. Seneff, and L. S. Chawla. 2015. 'Furosemide Stress Test and Biomarkers for the Prediction of AKI Severity', *J Am Soc Nephrol*, 26: 2023-31.

Kreek, M. J., D. Nielsen, E. R. Butelman, and K. S. LaForge. 2005. 'Genetic influences on impulsivity, risk taking, stress responsivity and vulnerability to drug abuse and addiction', *Nat Neurosci*, 8: 1450-7.

Kuhn, S., F. Schubert, R. Mekle, E. Wenger, B. Ittermann, U. Lindenberger, and J. Gallinat. 2016. 'Neurotransmitter changes during interference task in anterior cingulate cortex: evidence from fMRI-guided functional MRS at 3 T', *Brain Struct Funct*, 221: 2541-51.

Kumar, K., S. Sharma, P. Kumar, and R. Deshmukh. 2013. 'Therapeutic potential of GABA(B) receptor ligands in drug addiction, anxiety, depression and other CNS disorders', *Pharmacol Biochem Behav*, 110: 174-84.

Kunstler, G., D. Falster, D. A. Coomes, F. Hui, R. M. Kooyman, D. C. Laughlin, L. Poorter, M. Vanderwel, G. Vieilledent, S. J. Wright, M. Aiba, C. Baraloto, J. Caspersen, J. H. Cornelissen, S. Gourlet-Fleury, M. Hanewinkel, B. Herault, J. Kattge, H. Kurokawa, Y. Onoda, J. Penuelas, H. Poorter, M. Uriarte, S. Richardson, P. Ruiz-Benito, I. F. Sun, G. Stahl, N. G. Swenson, J. Thompson, B. Westerlund, C. Wirth, M. A. Zavala, H. Zeng, J. K. Zimmerman, N. E. Zimmermann, and M. Westoby. 2016. 'Plant functional traits have globally consistent effects on competition', *Nature*, 529: 204-7.

Kushner, M. G., K. Abrams, and C. Borchardt. 2000. 'The relationship between anxiety disorders and alcohol use disorders: a review of major perspectives and findings', *Clinical Psychology Review*, 20: 22.

Lai, H. M., M. Cleary, T. Sitharthan, and G. E. Hunt. 2015. 'Prevalence of comorbid substance use, anxiety and mood disorders in epidemiological surveys, 1990-2014: A systematic review and meta-analysis', *Drug Alcohol Depend*, 154: 1-13.

Lammertsma, A. A., and S. P. Hume. 1996. 'Simplified reference tissue model for PET receptor studies', *Neuroimage*, 4: 153-8.

Larson, M. H., L. Gilbert, X. Wang, W. Lim, J. S. Weissman, and L. S. Qi. 2013. 'CRISPR interference (CRISPRi) for sequence-specific control of gene expression', *Nat Protoc*, 8: 2180-96.

Larsson, E., C. Sander, and D. Marks. 2010. 'mRNA turnover rate limits siRNA and microRNA efficacy', *Mol Syst Biol*, 6: 7.

Le Foll, B., S. I. Chefer, A. S. Kimes, D. Shumway, E. A. Stein, A. G. Mukhin, and S. R. Goldberg. 2009. 'Baseline expression of alpha4beta2* nicotinic acetylcholine receptors predicts motivation to self-administer nicotine', *Biol Psychiatry*, 65: 714-6.

Lebedeva, I., and C. A. Stein. 2001. 'Antisense oligonucleotides: promise and reality', *Annu Rev Pharmacol Toxicol*, 41: 403-19.

Lehrer, D. S., B. T. Christian, C. Kirbas, M. Chiang, S. Sidhu, H. Short, B. Wang, B. Shi, K. W. Chu, B. Merrill, and M. S. Buchsbaum. 2010. '18F-fallypride binding potential in patients with schizophrenia compared to healthy controls', *Schizophr Res*, 122: 43-52.

Lemm, S., B. Blankertz, T. Dickhaus, and K. R. Muller. 2011. 'Introduction to machine learning for brain imaging', *Neuroimage*, 56: 387-99.

Leroy, C., V. Bragulat, I. Berlin, M. C. Gregoire, M. Bottlaender, D. Roumenov, F. Dolle, S. Bourgeois, J. Penttila, E. Artiges, J. L. Martinot, and C. Trichard. 2009. 'Cerebral monoamine oxidase A inhibition in tobacco smokers confirmed with PET and [11C]befloxatone', *J Clin Psychopharmacol*, 29: 86-8.

Letiembre, M., W. Hao, Y. Liu, S. Walter, I. Mihaljevic, S. Rivest, T. Hartmann, and K. Fassbender. 2007. 'Innate immune receptor expression in normal brain aging', *Neuroscience*, 146: 248-54.

Leurquin-Sterk, G., C. Crunelle, J. Ceccarini, B. De Laat, H. Peuskens, G. Bormans, and K. Van Laere. 2016. 'Alcohol addiction is associated with decreased limbic mGluR5 availability: a 18F-FPEB PET study in human.', *Journal of Nuclear Medicine*, 57: 1.

Leurquin-Sterk, G., A. Postnov, S. Celen, A. Weerasekera, B. De Laat, L. De Backer, G. Bormans, and K. Van Laere. 2015. 'Age-dependency of mGluR5 and its relationship to novelty seeking and MRS-derived glutamate concentrations: a ^{18}F-FPEB PET study in healthy volunteers', *Journal of Nuclear Medicine*, 56: 1.

Lewis, A., J. H. Miller, and R. A. Lea. 2007. 'Monoamine oxidase and tobacco dependence', *Neurotoxicology*, 28: 182-95.

Li, D., H. Shan, P. Conti, and Z. Li. 2012. 'PET imaging of metabotropic glutamate receptor subtype 5 (mGluR5)', *American journal of nuclear medicine and molecular imaging*, 2: 3.

Livieratos, Lefteris. 2012. 'Basic Principles of SPECT and PET Imaging': 345-59.

Lochhead, J. J., and R. G. Thorne. 2012. 'Intranasal delivery of biologics to the central nervous system', *Adv Drug Deliv Rev*, 64: 614-28.

Logan, Jean, Joanna S. Fowler, Nora D. Volkow, Gene-Jack Wang, Yu-Shin Ding, and David L. Alexoff. 1996. 'Distribution Volume Ratios without Blood Sampling from Graphical Analysis of PET Data', *Journal of Cerebral Blood Flow & Metabolism*, 16: 834-40.

Logrip, M. L., L. F. Vendruscolo, J. E. Schlosburg, G. F. Koob, and E. P. Zorrilla. 2014. 'Phosphodiesterase 10A regulates alcohol and saccharin self-administration in rats', *Neuropsychopharmacology*, 39: 1722-31.

Lohith, T.G., E. K. Osterweil, M. Fujita, K.J. Jenko, M. F. Bear, and R. B. Innis. 2013. 'Is metabotropic glutamate receptor 5 upergulated in prefrontal cortex in fragile X syndrome', *Molecular Autism*, 4: 8.

Lohmann, G., D. S. Margulies, A. Horstmann, B. Pleger, J. Lepsien, D. Goldhahn, H. Schloegl, M. Stumvoll, A. Villringer, and R. Turner. 2010. 'Eigenvector centrality mapping for analyzing connectivity patterns in fMRI data of the human brain', *PLoS One*, 5: e10232.

London, E. D., N.G. Cascella, D. F. Wong, R.L. Phillips, R.F. Dannals, J.M. links, R. Herning, R. Grayson, J.H. Jaffe, and H.N. Wagner. 1990. 'Cocaine-induced reduction of glucose utilization in human brain: A study using positron emission tomography and [Fluorine 18]-Fluorodeoxyglucose.', *Arch Gen Psychiatry*, 47: 7.

London, E. D., R. J. Connolly, M. Szikszay, J. K. Wamsley, and M. Dam. 1988. 'Effects of nicotine on local cerebral glucose utilization in the rat', *The journal of neuroscience*, 8: 3920.

López-Bendito, G., R. Shigemoto, A. Fairén, and R. lujan. 2002. 'Differential distribution of Group I mGluRs during rat cortical development', *Cerebral cortex*, 12: 13.

Lovinger, David M. 1999. '5-HT3 receptors and the neural actions of alcohols: an increasingly exciting topic', *Neurochemistry International*, 35: 125-30.

Lucantonio, F., S. Kambhampati, R. Z. Haney, D. Atalayer, N. E. Rowland, Y. Shaham, and G. Schoenbaum. 2015. 'Effects of prior cocaine versus morphine or heroin self-administration on extinction learning driven by overexpectation versus omission of reward', *Biol Psychiatry*, 77: 912-20.

Lucatelli, C., M. Honer, J. F. Salazar, T. L. Ross, P. A. Schubiger, and S. M. Ametamey. 2009. 'Synthesis, radiolabeling, in vitro and in vivo evaluation of [18F]-FPECMO as a positron emission tomography radioligand for imaging the metabotropic glutamate receptor subtype 5', *Nucl Med Biol*, 36: 613-22.

Maddock, R. J., M. H. Buonocore, L.E. Copeland, and A.L. Richards. 2009. 'Elevated brain lactate responses to neural activation in panic disorder: A dynamic 1H-MRS study', *Molecular Psychiatry*, 14: 8.

Maddock, R. J., G. A. Casazza, M. H. Buonocore, and C. Tanase. 2011. 'Vigorous exercise increases brain lactate and Glx (glutamate+glutamine): a dynamic 1H-MRS study', *Neuroimage*, 57: 1324-30.

Maisel, N. C., J. C. Blodgett, P. L. Wilbourne, K. Humphreys, and J. W. Finney. 2013. 'Meta-analysis of naltrexone and acamprosate for treating alcohol use disorders: when are these medications most helpful?', *Addiction*, 108: 275-93.

Mancl, Lloyd A., and Timothy A. DeRouen. 2001. 'A Covariance Estimator for GEE with Improved Small-Sample Properties', *Biometrics*, 57: 126-34.

Mansvelder, H. D., and D. S. McGehee. 2002. 'Cellular and synaptic mechanisms of nicotine addiction', *J Neurobiol*, 53: 606 - 17.

Mao, L., and J. Q. Wang. 2003. 'Phosphorylation of cAMP response element-binding protein in cultured striatal neurons by metabotropic glutamate receptor subtype 5', *J Neurochem*, 84: 233-43.

Marchant, N. J., E. J. Campbell, L. R. Whitaker, B. K. Harvey, K. Kaganovsky, S. Adhikary, B. T. Hope, R. C. Heins, T. E. Prisinzano, E. Vardy, A. Bonci, J. M. Bossert, and Y. Shaham. 2016. 'Role of Ventral Subiculum in Context-Induced Relapse to Alcohol Seeking after Punishment-Imposed Abstinence', *J Neurosci*, 36: 3281-94.

Marín-Martínez, Fulgencio, and Julio Sánchez-Meca. 2010. 'Weighting by Inverse Variance or by Sample Size in Random-Effects Meta-Analysis', *Educational and Psychological Measurement*, 70: 56-73.

Martinez, D., M. Slifstein, N. Nabulsi, A. Grassetti, N. B. Urban, A. Perez, F. Liu, S. F. Lin, J. Ropchan, X. Mao, L. S. Kegeles, D. C. Shungu, R. E. Carson, and Y. Huang. 2014. 'Imaging glutamate homeostasis in cocaine addiction with the metabotropic glutamate receptor 5 positron emission tomography radiotracer [(11)C]ABP688 and magnetic resonance spectroscopy', *Biol Psychiatry*, 75: 165-71.

Martinotti, G., C. R. Cloninger, and L. Janiri. 2008. 'Temperament and character inventory dimensions and anhedonia in detoxified substance-dependent subjects', *Am J Drug Alcohol Abuse*, 34: 177-83.

Marton, T. M., M. G. Hussain Shuler, and P. F. Worley. 2015. 'Homer 1a and mGluR5 phosphorylation in reward-sensitive metaplasticity: A hypothesis of neuronal selection and bidirectional synaptic plasticity', *Brain Res*, 1628: 17-28.

Matosin, N., and S. J. Siegel. 2016. 'Metabotropic Glutamate Receptor 5 as a Point of Convergence for Models of Obsessive-Compulsive Disorder and Autism Spectrum Disorder', *Biol Psychiatry*, 80: 504-6.

Mayr, M., and R. M. Schmid. 2010. 'Depression in pancreatic cancer: sense of impending doom', *Digestion*, 82: 1-3.

McDonald, J.H. 2014. *Handbook of biological statistics* (Sparky Hous Publishing: Baltimore, USA).

McGeehan, A. J., and M. F. Olive. 2003. 'The mGluR5 antagonist MPEP reduces the conditioned rewarding effects of cocaine but not other drugs of abuse', *Synapse*, 47: 240-2.

McGettigan, Carolyn, Samuel Evans, Stuart Rosen, Zarinah K. Agnew, Poonam Shah, and Sophie K. Scott. 2011. 'An Application of Univariate and Multivariate Approaches in fMRI to Quantifying the Hemispheric Lateralization of Acoustic and Linguistic Processes', *Journal of Cognitive Neuroscience*, 24: 636-52.

McManus, M. T., and P. A. Sharp. 2002. 'Gene silencing in mammals by small interfering RNAs', *Nat Rev Genet*, 3: 737-47.

Meredith, G. E., B. A. Baldo, M. E. Andrezjewski, and A. E. Kelley. 2008. 'The structural basis for mapping behavior onto the ventral striatum and its subdivisions', *Brain Struct Funct*, 213: 17-27.

Merriam-Webster.com. 2011. 'Addiction', Accessed May 8.

Meshul, C.K., K. Noguchi, N. Emre, and G. Ellison. 1998. 'Cocaine induced changes in glutamate and GABA immunolabeling within rat habenula and nucleus accumbens', *Synapse*, 30: 9.

Michaelides, M., P. K. Thanos, R. Kim, J. Cho, M. Ananth, G. J. Wang, and N. D. Volkow. 2012. 'PET imaging predicts future body weight and cocaine preference', *Neuroimage*, 59: 1508-13.

MicroMath. 1995. 'Scientist User Manual 2.0', *Chapter 10 - Statistical output*.

Middleton, L. S., W. A. Cass, and L. P. Dwoskin. 2004. 'Nicotinic receptor modulation of dopamine transporter function in rat striatum and medial prefrontal cortex', *J Pharmacol Exp Ther*, 308: 367-77.

Miguel-Hidalgo, J. J., R. Waltzer, A. A. Whittom, M. C. Austin, G. Rajkowska, and C. A. Stockmeier. 2010. 'Glial and glutamatergic markers in depression, alcoholism, and their comorbidity', *J Affect Disord*, 127: 230-40.

Mihic, S. John. 1999. 'Acute effects of ethanol on GABAA and glycine receptor function', *Neurochemistry International*, 35: 115-23.

Milella, M. S., L. Marengo, K. Larcher, A. Fotros, A. Dagher, P. Rosa-Neto, C. Benkelfat, and M. Leyton. 2014. 'Limbic system mGluR5 availability in cocaine dependent subjects: a high-resolution PET [(11)C]ABP688 study', *Neuroimage*, 98: 195-202.

Mitchnick, K. A., S. Creighton, M. O'Hara, B. E. Kalisch, and B. D. Winters. 2015. 'Differential contributions of de novo and maintenance DNA methyltransferases to object memory processing in the rat hippocampus and perirhinal cortex--a double dissociation', *Eur J Neurosci*, 41: 773-86.

Moll, Gunther H., Claas Mehnert, Maike Wicker, Nathalie Bock, Aribert Rothenberger, Eckart Rüther, and Gerald Huether. 2000. 'Age-associated changes in the densities of presynaptic monoamine transporters in different regions of the rat

brain from early juvenile life to late adulthood', *Developmental Brain Research*, 119: 251-57.

Moller, A.P. 1995. 'Bumblebee preference for symmetrical flowers', *Proc Natl Acad Sci U S A*, 92: 4.

Montgomery, A. J., A. R. Lingford-Hughes, A. Egerton, D. J. Nutt, and P. M. Grasby. 2007. 'The effect of nicotine on striatal dopamine release in man: A [11C]raclopride PET study', *Synapse*, 61: 637-45.

Moonat, S., A. J. Sakharkar, H. Zhang, L. Tang, and S. C. Pandey. 2013. 'Aberrant histone deacetylase2-mediated histone modifications and synaptic plasticity in the amygdala predisposes to anxiety and alcoholism', *Biol Psychiatry*, 73: 763-73.

Moore, Charles James. 2008. 'Synthetic polymers in the marine environment: A rapidly increasing, long-term threat', *Environmental Research*, 108: 131-39.

Morris, E. D., C.J. Endres, K.C. Schmidt, B.T. Christian, R.F. Muzic, and R.E. Fisher. 2004. 'Kinetic modelling in positron emission tomography.' in M. Wernick and J. Aarsvold (eds.), *Emission Tomography* (Elsevier: Amsterdam, Netherlands).

Moses, W. W. 2011. 'Fundamental Limits of Spatial Resolution in PET', *Nucl Instrum Methods Phys Res A*, 648 Supplement 1: S236-40.

Mourao-Miranda, J., A. A. Reinders, V. Rocha-Rego, J. Lappin, J. Rondina, C. Morgan, K. D. Morgan, P. Fearon, P. B. Jones, G. A. Doody, R. M. Murray, S. Kapur, and P. Dazzan. 2012. 'Individualized prediction of illness course at the first psychotic episode: a support vector machine MRI study', *Psychol Med*, 42: 1037-47.

Mourik, J. E., M. Lubberink, A. Schuitemaker, N. Tolboom, B. N. van Berckel, A. A. Lammertsma, and R. Boellaard. 2009. 'Image-derived input functions for PET brain studies', *Eur J Nucl Med Mol Imaging*, 36: 463-71.

Moussawi, K., and P. W. Kalivas. 2010. 'Group II metabotropic glutamate receptors (mGlu2/3) in drug addiction', *Eur J Pharmacol*, 639: 115-22.

Mukhin, A. G., A. S. Kimes, S. I. Chefer, J. A. Matochik, C. S. Contoreggi, A. G. Horti, D. B. Vaupel, O. Pavlova, and E. A. Stein. 2008. 'Greater nicotinic acetylcholine receptor density in smokers than in nonsmokers: a PET study with 2-18F-FA-85380', *J Nucl Med*, 49: 1628-35.

Muller, C. P., and J. R. Homberg. 2015. 'The role of serotonin in drug use and addiction', *Behav Brain Res*, 277: 146-92.

Muller Herde, A., C. Keller, S. Milicevic Sephton, L. Mu, R. Schibli, S. M. Ametamey, and S. D. Kramer. 2015. 'Quantitative positron emission tomography of mGluR5 in rat brain with [(18) F]PSS232 at minimal invasiveness and reduced model complexity', *J Neurochem*, 133: 330-42.

Muller, U. J., J. Voges, J. Steiner, I. Galazky, H. J. Heinze, M. Moller, J. Pisapia, C. Halpern, A. Caplan, B. Bogerts, and J. Kuhn. 2013. 'Deep brain stimulation of the nucleus accumbens for the treatment of addiction', *Ann N Y Acad Sci*, 1282: 119-28.

Mumford, J. A., and T. Nichols. 2006. 'Modeling and inference of multisubject fMRI data', *IEEE Engineering in Medicine and Biology Magazine*, 25: 42-51.

Nair, G., and T. Q. Duong. 2004. 'Echo-planar BOLD fMRI of mice on a narrow-bore 9.4 T magnet', *Magn Reson Med*, 52: 430-4.

Nakajima, H., T. Kubo, Y. Semi, M. Itakura, M. Kuwamura, T. Izawa, Y. T. Azuma, and T. Takeuchi. 2012. 'A rapid, targeted, neuron-selective, in vivo knockdown following a single intracerebroventricular injection of a novel chemically modified siRNA in the adult rat brain', *J Biotechnol*, 157: 326-33.

Nam, H. W., V. M. Karpyak, D. J. Hinton, J. R. Geske, A. M. Ho, M. L. Prieto, J. M. Biernacka, M. A. Frye, R. M. Weinshilboum, and D. S. Choi. 2015. 'Elevated baseline serum glutamate as a pharmacometabolomic biomarker for acamprosate treatment outcome in alcohol-dependent subjects', *Transl Psychiatry*, 5: e621.

Nandi, Ayon, Heather Valentine, Mary McCaul, and Dean Wong. 2016. 'Glutamatergic Abnormalities in a Rodent Model of Alcohol Abuse', *Journal of Nuclear Medicine*, 57: 1866a.

Narahashi, Toshio, Gary L. Aistrup, William Marszalec, and Keiichi Nagata. 1999. 'Neuronal nicotinic acetylcholine receptors: a new target site of ethanol', *Neurochemistry International*, 35: 131-41.

National Institute for Drug Abuse. 2007. "Drugs, brains, and behavior: The science of addiction." In, edited by N. Volkow.

———. 2017. 'Commonly abused drug charts'.

Ng, M., M. K. Freeman, T. D. Fleming, M. Robinson, L. Dwyer-Lindgren, B. Thomson, A. Wollum, E. Sanman, S. Wulf, A. D. Lopez, C. J. Murray, and E. Gakidou. 2014. 'Smoking prevalence and cigarette consumption in 187 countries, 1980-2012', *JAMA*, 311: 183-92.

Nickols, H. H., J. P. Yuh, K. J. Gregory, R. D. Morrison, B. S. Bates, S. R. Stauffer, K. A. Emmitte, M. Bubser, W. Peng, M. T. Nedelcovych, A. Thompson, X. Lv, Z. Xiang, J. S. Daniels, C. M. Niswender, C. W. Lindsley, C. K. Jones, and P. J. Conn. 2016. 'VU0477573: Partial Negative Allosteric Modulator of the Subtype 5 Metabotropic Glutamate Receptor with In Vivo Efficacy', *J Pharmacol Exp Ther*, 356: 123-36.

Nona, C. N., R. Li, and J. N. Nobrega. 2014. 'Altered NMDA receptor subunit gene expression in brains of mice showing high vs. low sensitization to ethanol', *Behav Brain Res*, 260: 58-66.

O'Brien, C. P. 1997. 'A range of research-based pharmacotherapies for addiction', *Science*, 278: 5.

O'Neill, J., M. C. Tobias, M. Hudkins, and E. D. London. 2015. 'Glutamatergic neurometabolites during early abstinence from chronic methamphetamine abuse', *Int J Neuropsychopharmacol*, 18.

Ohnuma, T., S. J. Augood, H. Arai, P. J. McKenna, and P. C. Emson. 1998. 'Expression of the human excitatory amino acid transporter 2 and metabotropic glutamate receptors 3 and 5 in the prefrontal cortex from normal individuals and patients with schizophrenia', *Brain Res Mol Brain Res*, 56: 207-17.

Oldendorf, W., and W. Jr. Oldendorf. 1988. *Basics of Magnetic Resonance Imaging* (Springer US: Boston).

Olive, M. F., A. J. McGeehan, J. R. Kinder, T. McMahon, C. W. Hodge, P. H. Janak, and R. O. Messing. 2005. 'The mGluR5 antagonist 6-methyl-2-(phenylethynyl)pyridine decreases ethanol consumption via a protein kinase C epsilon-dependent mechanism', *Mol Pharmacol*, 67: 349-55.

Olsen, C. M., D. S. Childs, G. D. Stanwood, and D. G. Winder. 2010. 'Operant sensation seeking requires metabotropic glutamate receptor 5 (mGluR5)', *PLoS One*, 5: e15085.

Ongur, D., and J.L. Price. 2000. 'The organization of networks within the orbital and medial prefrontal cortex of rats, monkeys and humans', *Cerebral cortex*, 10: 13.

Osokine, I., R. Hsu, G.B. Loeb, and M.T. McManus. 2008. 'Unintentional miRNA ablation is a risk factor in gene knockout studies A short report', *PLOS Genetics*, 4: 3.

Page, G., M. Peeters, M. Najimi, J. M. Maloteaux, and E. Hermans. 2001. 'Modulation of the neuronal dopamine transporter activity by the mGluR5 in rat striatal synaptosomes through phosphorylation mediated processes', *J Neurochem*, 76: 8.

Paille, F. M., J.D. Guelfi, A.C. Perkins, R. J. Royer, L. Steru, and P. Parot. 1995. 'Double-blind randomized multicentre trial of acamprosate in maintaining abstinence from alcohol', *Alcohol and Alcoholism*, 30: 8.

Parkitna, J. R., M. Sikora, S. Golda, K. Golembiowska, B. Bystrowska, D. Engblom, A. Bilbao, and R. Przewlocki. 2013. 'Novelty-seeking behaviors and the escalation of alcohol drinking after abstinence in mice are controlled by metabotropic glutamate receptor 5 on neurons expressing dopamine d1 receptors', *Biol Psychiatry*, 73: 263-70.

Parsegian, A., and R. E. See. 2014. 'Dysregulation of dopamine and glutamate release in the prefrontal cortex and nucleus accumbens following methamphetamine self-administration and during reinstatement in rats', *Neuropsychopharmacology*, 39: 811-22.

Parsons, L. H., and Y. L. Hurd. 2015. 'Endocannabinoid signalling in reward and addiction', *Nat Rev Neurosci*, 16: 579-94.

Patel, S., T. G. Hamill, B. Connolly, E. Jagoda, W. Li, and R. E. Gibson. 2007. 'Species differences in mGluR5 binding sites in mammalian central nervous system determined using in vitro binding with [18F]F-PEB', *Nucl Med Biol*, 34: 1009-17.

Paterson, N. E., S. Semenova, F. Gasparini, and A. Markou. 2003. 'The mGluR5 antagonist MPEP decreased nicotine self-administration in rats and mice', *Psychopharmacology (Berl)*, 167: 257-64.

Paulus, M.P. 2007. 'Decision-making dysfunctions in psychiatry - Altered homeostatic processing?', *Science*, 318: 5.

Paxinos, G., C. Watson, M. Pennisi, and A. Topple. 1985. 'Bregma, lambda and the interaural midpoint in stereotaxic surgery with rats of different sex, strain and weight', *J Neurosci Methods*, 13: 139-43.

Paxinos, G., R.R.W. Watson, and P.C. Emson. 1980. 'AChE-stained horizontal sections of the rat brain in stereotaxic coordinates', *Journal of Neuroscience Methods*, 3: 20.

Pellegrini-Giampietro, D.E., M.V.L. Bennet, and R.S. Zukin. 1991. 'Differential expression of three glutamate receptor genes in developing rat brain: An *in situ* hybridization study', *Proc Natl Acad Sci U S A*, 88: 4.

Pellerin, L., and P. J. Magistretti. 1994. 'Glutamate uptake into astrocytes stimulates aerobic glycolysis: a mechanism coupling neuronal activity to glucose utilization', *Proceedings of the National Academy of Sciences*, 91: 10625-29.

Pelloux, Y., J. Costentin, and D. Duterte-Boucher. 2015. 'Differential involvement of anxiety and novelty preference levels on oral ethanol consumption in rats', *Psychopharmacology*, 232: 10.

Peoples, R.W., G. White, D. M. lovinger, and F.F. Weight. 1997. 'Ethanol inhibition of N-methyl-D-aspartate-activated current in mouse hippocampal neurones Whole-cell patch-clamp analysis', *British Journal of Pharmacology*, 122: 7.

Perry, J. L., E. B. Larson, J. P. German, G. J. Madden, and M. E. Carroll. 2005. 'Impulsivity (delay discounting) as a predictor of acquisition of IV cocaine self-administration in female rats', *Psychopharmacology (Berl)*, 178: 193-201.

Peto, R., A.D. Lopez, J. Boreham, M. Thun, C. Heath, and R. Doll. 1996. 'Mortality from smoking worldwide', *British Medical Bulletin*, 52: 9.

Pfeuffer, J., I. Tkác, S.W. Provencher, and R. Gruetter. 1999. 'Toward an in Vivo neurochemical profile: Quantification of 18 metabolites in Short-Echo-Time ^{1}H-NMR spectra of the rat brain', *Journal of Magnetic Resonance*, 141: 16.

Phillips, A. G., G. Vacca, and S. Ahn. 2008. 'A top-down perspective on dopamine, motivation and memory', *Pharmacol Biochem Behav*, 90: 236-49.

Picetti, R., A. Ho, E.R. Butelman, and M.J. Kreek. 2010. 'Dose preference and dose escalation in extended-access cocaine self-administration in Fischer and Lewis rats', *Psychopharmacology*, 211: 10.

Pickens, Roy, and Travis Thompson. 1968. 'COCAINE-REINFORCED BEHAVIOR IN RATS: EFFECTS OF REINFORCEMENT MAGNITUDE AND FIXED-RATIO SIZE', *Journal of pharmacology and experimental therapeutics*, 161: 122-29.

Piers, T. M., D. H. Kim, B. C. Kim, P. Regan, D. J. Whitcomb, and K. Cho. 2012. 'Translational Concepts of mGluR5 in Synaptic Diseases of the Brain', *Front Pharmacol*, 3: 199.

Portugal, L. C., M. J. Rosa, A. Rao, G. Bebko, M. A. Bertocci, A. K. Hinze, L. Bonar, J. R. Almeida, S. B. Perlman, A. Versace, C. Schirda, M. Travis, M. K. Gill, C. Demeter, V. A. Diwadkar, G. Ciuffetelli, E. Rodriguez, E. E. Forbes, J. L. Sunshine, S. K. Holland, R. A. Kowatch, B. Birmaher, D. Axelson, S. M. Horwitz, E. L. Arnold, M. A. Fristad, E. A. Youngstrom, R. L. Findling, M. Pereira, L. Oliveira, M. L. Phillips, and J. Mourao-Miranda. 2016. 'Can Emotional and Behavioral Dysregulation in Youth Be Decoded from Functional Neuroimaging?', *PLoS One*, 11: e0117603.

Poulos, Constantine X., A. D. Le, and J. L. Parker. 1995. 'Impulsivity predicts individual susceptibility to high levels of alcohol self-administration', *Behavioural Pharmacology*, 6.

Prentice, R. 1988. 'Correlated binary regression with covariates specific to each binary observation', *Biometrics*, 44: 15.

Program, National Toxicology. 2015. "Report on Carcinogens." In, edited by US Department of Health and Human Program.

Prompers, J. J., J. A. Jeneson, M. R. Drost, C. C. Oomens, G. J. Strijkers, and K. Nicolay. 2006. 'Dynamic MRS and MRI of skeletal muscle function and biomechanics', *NMR Biomed*, 19: 927-53.

Prut, Laetitia, and Catherine Belzung. 2003. 'The open field as a paradigm to measure the effects of drugs on anxiety-like behaviors: a review', *European Journal of Pharmacology*, 463: 3-33.

Quadros, P. S., and C. K. Wagner. 2008. 'Regulation of progesterone receptor expression by estradiol is dependent on age, sex and region in the rat brain', *Endocrinology*, 149: 3054-61.

R Core Team. 2016. "R: A language and environment for statistical computing." In. Vienne, Austria: R Foundation for Statistical Computing.

Ratiney, H., Y. Coenradie, S. Cavassila, D. van Ormondt, and D. Graveron-Demilly. 2004. 'Time-domain quantitation of 1H short echo-time signals: background accommodation', *MAGMA*, 16: 284-96.

Richiardi, J., A. Altmann, A. C. Milazzo, C. Chang, M. M. Chakravarty, T. Banaschewski, G. J. Barker, A. L. W. Bokde, U. Bromberg, C. Büchel, P. Conrod, M. Fauth-Bühler, H. Flor, V. Frouin, J. Gallinat, H. Garavan, P. Gowland, A. Heinz, H. Lemaître, K. F. Mann, J. L. Martinot, F. Nees, T. Paus, Z. Pausova, M. Rietschel, T. W. Robbins, M. N. Smolka, R. Spanagel, A. Ströhle, G. Schumann, M. Hawrylycz, J. B. Poline, and M. D. Greicius. 2015. 'Correlated gene

expression supports synchronous activity in brain networks', *Science*, 348: 1241-4.

Ritz, M. C., E. J. Cone, and M. J. Kuhar. 1990. 'Cocaine inhibition of ligand binding at dopamine, norepinephrine and serotonin transporters: A structure-activity study', *Life Sciences*, 46: 635-45.

Roberto, M., P. Schweitzer, S. G. Madamba, D. G. Stouffer, L. H. Parsons, and G. R. Siggins. 2004. 'Acute and chronic ethanol alter glutamatergic transmission in rat central amygdala: an in vitro and in vivo analysis', *J Neurosci*, 24: 1594-603.

Rogers, J., S.G. Wiener, and F.E. Bloom. 1979. 'Long-term ethanol administration methods for rats Advantages of inhalation over intubation or liquid diets', *Behavioral and Neural Biology*, 27: 20.

Romano, C., M.A. Sesma, C.T. McDonald, K. O'Malley, A.N. Van den Pol, and J.W. Olney. 1995. 'Distribution of metabotropic glutamate receptor mGluR5 immunoreactivity in rat brain', *J Comp Neurol*, 355: 14.

Romano, C., A.N. Van den Pol, and K. O'Malley. 1996. 'Enhanced early development expression of the mGluR5 in rat brain Protein, mRNA, splice variants, and regional distribution', *The journal of comparative neurology*, 367: 9.

Rose, J. E., F. M. Behm, A. N. Salley, J. E. Bates, R. E. Coleman, T. C. Hawk, and T. G. Turkington. 2007. 'Regional brain activity correlates of nicotine dependence', *Neuropsychopharmacology*, 32: 2441-52.

Rossetti, Z.L., Y. Hmaidan, and G.L. Gessa. 1992. 'Marked inhibition of mesolimbic dopamine release A common feature of ethanol, morphine, cocaine and aphetamine abstinence in rats', *European Journal of Pharmacology*, 221: 8.

Rossetti, Zvani L., Franco Melis, Susanna Carboni, and Gian L. Gessa. 'Dramatic Depletion of Mesolimbic Extracellular Dopamine after Withdrawal from Morphine, Alcohol or Cocaine: A Common Neurochemical Substrate for Drug Dependence'.

Rossi, A., Z. Kontarakis, C. Gerri, H. Nolte, S. Holper, M. Kruger, and D. Y. Stainier. 2015. 'Genetic compensation induced by deleterious mutations but not gene knockdowns', *Nature*, 524: 230-3.

Roth, B. L. 2006. 'CNS dopamine autoreceptors Distribution, pharmacology, and function', *Annals New York Academy of Sciences*, 430: 27.

Rowntree, L.G. 1926. 'The effects on mammals of the administration of excessive quantities of water', *Journal of pharmacology and experimental therapeutics*, 29: 25.

Sanfey, A. G., G. Loewenstein, S. M. McClure, and J. D. Cohen. 2006. 'Neuroeconomics: cross-currents in research on decision-making', *Trends Cogn Sci*, 10: 108-16.

Sauter, A., and M. Rudin. 1993. 'Determination of creatine kinase kinetic parameters in rat brain by NMR magnetization transfer', *Journal of Biological Chemistry*, 268: 5.

Schilstrom, B., H.M. Svensson, T.H. Svensson, and G.G. Nomikos. 1998. 'Nicotine and food induced dopamine release in the nucleus accumbens of the rat Putative role of alpha-7 nicotinic receptors in the ventral tegmental area', *Neuroscience*, 85: 4.

Schmidt, E. D., P. Voorn, R. Binnekade, A. N. Schoffelmeer, and T. J. De Vries. 2005. 'Differential involvement of the prelimbic cortex and striatum in conditioned heroin and sucrose seeking following long-term extinction', *Eur J Neurosci*, 22: 2347-56.

Schmidt, H. D., and R. C. Pierce. 2010. 'Cocaine-induced neuroadaptations in glutamate transmission: potential therapeutic targets for craving and addiction', *Ann N Y Acad Sci*, 1187: 35-75.

Schober, G., M. Arnold, S. Birtles, L. K. Buckett, G. Pacheco-Lopez, A. V. Turnbull, W. Langhans, and A. Mansouri. 2013. 'Diacylglycerol acyltransferase-1 inhibition enhances intestinal fatty acid oxidation and reduces energy intake in rats', *J Lipid Res*, 54: 1369-84.

Scholvinck, M. L., A. Maier, F. Q. Ye, J. H. Duyn, and D. A. Leopold. 2010. 'Neural basis of global resting-state fMRI activity', *Proc Natl Acad Sci U S A*, 107: 10238-43.

Schrouff, J., J. Cremers, G. Garraux, L. Baldassarre, J. Mourao-Miranda, and C. Phillips. 2013. "Localizing and Comparing Weight Maps Generated from Linear Kernel Machine Learning Models." In *2013 International Workshop on Pattern Recognition in Neuroimaging*, 124-27.

Schrouff, J., M. J. Rosa, J. M. Rondina, A. F. Marquand, C. Chu, J. Ashburner, C. Phillips, J. Richiardi, and J. Mourao-Miranda. 2013. 'PRoNTo: pattern recognition for neuroimaging toolbox', *Neuroinformatics*, 11: 319-37.

Schuckit, M.A. 2006. *Drug and Alcohol abuse A clinical guide to diagnosis and treatment* (Springer: U.S.A).

Schulte, E. M., M. A. Joyner, M. N. Potenza, C. M. Grilo, and A. N. Gearhardt. 2015. 'Current considerations regarding food addiction', *Curr Psychiatry Rep*, 17: 563.

Schumann, G., M. Johann, J. Frank, U. Preuss, N. Dahmen, M. Laucht, M. Rietschel, D. Rujescu, A. Lourdusamy, T. K. Clarke, K. Krause, A. Dyer, M. Depner, S. Wellek, J. Treutlein, A. Szegedi, I. Giegling, S. Cichon, D. Blomeyer, A. Heinz, S. Heath, M. Lathrop, N. Wodarz, M. Soyka, R. Spanagel, and K. Mann. 2008. 'Systematic analysis of glutamatergic neurotransmission genes in alcohol dependence and adolescent risky drinking behavior', *Arch Gen Psychiatry*, 65: 826-38.

Schwendt, M., and M. F. Olive. 2016. 'Protein kinase Cvarepsilon activity regulates mGluR5 surface expression in the rat nucleus accumbens', *J Neurosci Res*.

Sengmany, K., and K. J. Gregory. 2015. 'Metabotropic glutamate receptor subtype molecular pharmacology, allosteric modulation and stimulus bias', *Br J Pharmacol*, 173: 16.

Sephton, S. M., P. Dennler, D. S. Leutwiler, L. Mu, R. Schibli, S. D. Kramer, and S. M. Ametamey. 2012. 'Development of [(18)F]-PSS223 as a PET tracer for imaging of metabotropic glutamate receptor subtype 5 (mGluR5)', *Chimia (Aarau)*, 66: 201-4.

Shigemoto, R., S. Nomura, H. Ohishi, H. Sugihara, S. Nakanishi, and N. Mizuno. 1993. 'Immunohistochemical localization of a metabotropic glutamate receptor, mGluR5, in the rat brain', *Neurosci Lett*, 163: 53-7.

Shim, M. S., and Y. J. Kwon. 2010. 'Efficient and targeted delivery of siRNA in vivo', *FEBS J*, 277: 4814-27.

Shum, K., and J. J. Rossi. 2016. "siRNA delivery methods." In. New York: Springer.

Simeon, F. G., A. K. Brown, S. S. Zoghbi, V. M. Patterson, R. B. Innis, and V. W. Pike. 2007. 'Synthesis and simple 18F-labeling of 3-fluoro-5-(2-(2-(fluoromethyl)thiazol-4-yl)ethynyl)benzonitrile as a high affinity radioligand for imaging monkey brain metabotropic glutamate subtype-5 receptors with positron emission tomography', *J Med Chem*, 50: 3256-66.

Simms, J. A., P. Steensland, B. Medina, K. E. Abernathy, L. J. Chandler, R. Wise, and S. E. Bartlett. 2008. 'Intermittent access to 20% ethanol induces high ethanol consumption in Long-Evans and Wistar rats', *Alcohol Clin Exp Res*, 32: 1816-23.

Simonyi, A., R. T. Ngomba, M. Storto, M. V. Catania, L. A. Miller, B. Youngs, V. DiGiorgi-Gerevini, F. Nicoletti, and G. Y. Sun. 2005. 'Expression of groups I and

II metabotropic glutamate receptors in the rat brain during aging', *Brain Res*, 1043: 95-106.
Singh, M. K. 2012. 'Volumetric reductions in the subgenual anterior cingulate cortex in adolescents with bipolar I disorder', 14: 585-96.
Singh, M. K., K. D. Chang, R. G. Kelley, X. Cui, L. Sherdell, M. E. Howe, I. H. Gotlib, and A. L. Reiss. 2013. 'Reward Processing in Adolescents with Bipolar I Disorder', *J Am Acad Child Adolesc Psychiatry*, 52: 68-83.
Smith, Y., and R. Villalba. 2008. 'Striatal and extrastriatal dopamine in the basal ganglia: an overview of its anatomical organization in normal and Parkinsonian brains', *Mov Disord*, 23 Suppl 3: S534-47.
Soyka, M., and J. Mutschler. 2016. 'Treatment-refractory substance use disorder: Focus on alcohol, opioids, and cocaine', *Prog Neuropsychopharmacol Biol Psychiatry*, 70: 148-61.
Spanagel, R. 2003. 'Alcohol addiction research from animal models to clinics', *Best Pract Res Cl Ga*, 17: 11.
Spangler-Bickell, M. G., B. de Laat, R. Fulton, G. Bormans, and J. Nuyts. 2016. 'The effect of isoflurane on 18F-FDG uptake in the rat brain: a fully conscious dynamic PET study using motion compensation', *EJNMMI Res*, 6: 86.
Stapleton, J. M., S. F. Gilson, D. F. Wong, V. L. Villemagne, R. F. Dannals, R. F. Grayson, J. E. Henningfield, and E. D. London. 2003. 'Intravenous nicotine reduces cerebral glucose metabolism: a preliminary study', *Neuropsychopharmacology*, 28: 765-72.
Stefan, D., F. Di Cesare, A. Andrasescu, E. Popa, A. Lazariev, E. Vescovo, O. Strbak, S. Williams, Z. Starcuk, M. Cabanas, D. van Ormondt, and D. Graveron-Demilly. 2009. 'Quantitation of magnetic resonance spectroscopy signals: the jMRUI software package', *Measurement Science and Technology*, 20: 104035.
Stein, E. A., J. Pankiewicz, H. H. Harsch, J. K. Cho, S. A. Fuller, R. G. Hoffmann, M. Hawkins, S. M. Rao, P. A. Bandettini, and A. S. Bloom. 1998. 'Nicotine-induced limbic cortical activation in the human brain: a functional MRI study', *Am J Psychiatry*, 155: 1009-15.
Stice, E., D. P. Figlewicz, B. A. Gosnell, A. S. Levine, and W. E. Pratt. 2013. 'The contribution of brain reward circuits to the obesity epidemic', *Neurosci Biobehav Rev*, 37: 2047-58.
Sullivan, J. M., K. Lim, D. Labaree, S. F. Lin, T. J. McCarthy, J. P. Seibyl, G. Tamagnan, Y. Huang, R. E. Carson, Y. S. Ding, and E. D. Morris. 2013. 'Kinetic analysis of the metabotropic glutamate subtype 5 tracer [(18)F]FPEB in bolus and bolus-plus-constant-infusion studies in humans', *J Cereb Blood Flow Metab*, 33: 532-41.
Tabakoff, B., and P. L. Hoffman. 2013. 'The neurobiology of alcohol consumption and alcoholism: an integrative history', *Pharmacol Biochem Behav*, 113: 20-37.
Tai, Y. C., A. Ruangma, D. Rowland, S. Siegel, D. F. Newport, P. L. Chow, and R. Laforest. 2005. 'Performance evaluation of the microPET focus: a third-generation microPET scanner dedicated to animal imaging', *J Nucl Med*, 46: 455-63.
Thanos, Panayotis K., Nora D. Volkow, Paul Freimuth, Hiroyuki Umegaki, Hiroyuki Ikari, George Roth, Donald K. Ingram, and Robert Hitzemann. 2001. 'Overexpression of dopamine D2 receptors reduces alcohol self-administration', *Journal of Neurochemistry*, 78: 1094-103.

Thierry, AM., Y. Gioanni, E. Dégénétais, and J. Glowinski. 2000. 'Hippocamp-prefrontal cortex pathway: Anatomical and electrophysiological characteristics', *Hippocampus*, 10: 8.

Thoma, R., P. Mullins, D. Ruhl, M. Monnig, R. A. Yeo, A. Caprihan, M. Bogenschutz, P. Lysne, S. Tonigan, R. Kalyanam, and C. Gasparovic. 2011. 'Perturbation of the glutamate-glutamine system in alcohol dependence and remission', *Neuropsychopharmacology*, 36: 1359-65.

Thulborn, Keith R., John C. Waterton, Paul M. Matthews, and George K. Radda. 1982. 'Oxygenation dependence of the transverse relaxation time of water protons in whole blood at high field', *Biochimica et Biophysica Acta (BBA) - General Subjects*, 714: 265-70.

Tijsterman, M., R. F. Ketting, and R. H. Plasterk. 2002. 'The genetics of RNA silencing', *Annu Rev Genet*, 36: 489-519.

Tison, F., C. Keywood, M. Wakefield, F. Durif, J. C. Corvol, K. Eggert, M. Lew, S. Isaacson, E. Bezard, S. M. Poli, C. G. Goetz, C. Trenkwalder, and O. Rascol. 2016. 'A Phase 2A Trial of the Novel mGluR5-Negative Allosteric Modulator Dipraglurant for Levodopa-Induced Dyskinesia in Parkinson's Disease', *Mov Disord*, 31: 1373-80.

Tomek, S. E., A. L. Lacrosse, N. E. Nemirovsky, and M. F. Olive. 2013. 'NMDA Receptor Modulators in the Treatment of Drug Addiction', *Pharmaceuticals (Basel)*, 6: 251-68.

Trantham-Davidson, H., and L. J. Chandler. 2015. 'Alcohol-induced alterations in dopamine modulation of prefrontal activity', *Alcohol*, 49: 773-9.

Tremblay, L., Y. Worbe, S. Thobois, V. Sgambato-Faure, and J. Feger. 2015. 'Selective dysfunction of basal ganglia subterritories: From movement to behavioral disorders', *Mov Disord*, 30: 1155-70.

Trigo, J. M., E. Martin-Garcia, F. Berrendero, P. Robledo, and R. Maldonado. 2010. 'The endogenous opioid system: a common substrate in drug addiction', *Drug Alcohol Depend*, 108: 183-94.

Tronci, V., and D. J. Balfour. 2011. 'The effects of the mGluR5 receptor antagonist 6-methyl-2-(phenylethynyl)-pyridine (MPEP) on the stimulation of dopamine release evoked by nicotine in the rat brain', *Behav Brain Res*, 219: 354-7.

Tsai, G., D.R. Gastfriend, and J. T. Coyle. 1995. 'The glutamatergic basis of human alcoholism', *Am J Psychiatry*, 152: 8.

Turecek, R., and L.O. Trussel. 2001. 'Presynaptic glycine receptors enhance transmitter release at a mammalian central synapse', *Nature*, 411: 4.

Tyrell, I. 1997. 'The US prohibition experiment Myths, history and implications', *Addiction*, 92: 4.

Tzschentke, T. M., and W. J. Schmidt. 2003. 'Glutamatergic mechanisms in addiction', *Mol Psychiatry*, 8: 373-82.

Ullensvang, K., K.P. Lehre, J. Storm-Mathisen, and N.C. Danbolt. 1997. 'Differential developmental expression of the two rat brain glutamate transporter proteins GLAST and GLT', *European Journal of Neuroscience*, 9: 9.

Umhau, J.C., R. Momenan, M.L. Schwandt, E. Singley, M. Lifshitz, L. Doty, L.J. Adams, V. Vengeliene, R. Spanagel, Y. Zhang, J. Shen, D.T. George, D. Hommer, and M. Heilig. 2010. 'Effect of Acamprosate on magnetic resonance spectroscopy measures of central glutamate in detoxified alcoholics: A randomized controlled experimental medicine study', *Arch Gen Psychiatry*, 67: 8.

UN office on drugs and crime. 2015. 'World drug report'.

Valles, A., G. J. Martens, P. De Weerd, G. Poelmans, and A. Aschrafi. 2014. 'MicroRNA-137 regulates a glucocorticoid receptor-dependent signalling network: implications for the etiology of schizophrenia', *J Psychiatry Neurosci*, 39: 312-20.

van den Bos, R., and D. de Ridder. 2006. 'Evolved to satisfy our immediate needs: self-control and the rewarding properties of food', *Appetite*, 47: 24-9.

van den Heuvel, M. P., and H. E. Hulshoff Pol. 2010. 'Exploring the brain network: a review on resting-state fMRI functional connectivity', *Eur Neuropsychopharmacol*, 20: 519-34.

Vazquez, Francisco, Benjamin M. Tabak, and Marcos Souto. 2012. 'A macro stress test model of credit risk for the Brazilian banking sector', *Journal of Financial Stability*, 8: 69-83.

Veeneman, M. M., H. Boleij, M. H. Broekhoven, E. M. Snoeren, M. Guitart Masip, J. Cousijn, W. Spooren, and L. J. Vanderschuren. 2011. 'Dissociable roles of mGlu5 and dopamine receptors in the rewarding and sensitizing properties of morphine and cocaine', *Psychopharmacology (Berl)*, 214: 863-76.

Vengeliene, V., A. Bilbao, A. Molander, and R. Spanagel. 2008. 'Neuropharmacology of alcohol addiction', *Br J Pharmacol*, 154: 299-315.

Verdejo-Garcia, A., A. Benbrook, F. Funderburk, P. David, J. L. Cadet, and K. I. Bolla. 2007. 'The differential relationship between cocaine use and marijuana use on decision-making performance over repeat testing with the Iowa Gambling Task', *Drug Alcohol Depend*, 90: 2-11.

Vermeiren, C., M. Najimi, N. Vanhoutte, S. Tilleux, I. de Hemptinne, J. M. Maloteaux, and E. Hermans. 2005. 'Acute up-regulation of glutamate uptake mediated by mGluR5a in reactive astrocytes', *J Neurochem*, 94: 405-16.

Viechtbauer, W. . 2010. 'Conducting meta-analyses in R with the metafor package', *Journal of Statistical Software*, 36: 47.

Villien, M., H. Y. Wey, J. B. Mandeville, C. Catana, J. R. Polimeni, C. Y. Sander, N. R. Zurcher, D. B. Chonde, J. S. Fowler, B. R. Rosen, and J. M. Hooker. 2014. 'Dynamic functional imaging of brain glucose utilization using fPET-FDG', *Neuroimage*, 100: 192-9.

Volkow, N. D., G. J. Wang, D. Franceschi, J. S. Fowler, P. P. Thanos, L. Maynard, S. J. Gatley, C. Wong, R. L. Veech, G. Kunos, and T. Kai Li. 2006. 'Low doses of alcohol substantially decrease glucose metabolism in the human brain', *Neuroimage*, 29: 295-301.

Volkow, N., and T. Li. 2004. 'Drug addiction: The neurobiology of behaviour gone awry', *Nature Reviews*, 5: 8.

Voytas, D., and N. Ke. 2001. *Detection and Quantitation of Radiolabeled Proteins and DNA in Gels and Blots*.

Wagner, J.G. 1993. *Pharmacokinetics for the pharmaceutical scientist* (CRC Press: Lancaster, U.S.A.).

Wang, G., N. Volkow, L. Chang, E. Miller, M. Sedler, R. Hitzemann, W. L. Zhu, J. logan, Y. Ma, and J. S. Fowler. 2004. 'Partial recovery of brain metabolism in methamphetamine abusers after protracted abstinence', *Am J Psychiatry*, 161: 6.

Wang, X., K. Moussawi, L. Knackstedt, H. Shen, and P. W. Kalivas. 2013. 'Role of mGluR5 neurotransmission in reinstated cocaine-seeking', *Addict Biol*, 18: 40-9.

Wanger-Baumann, C. A., L. Mu, M. Honer, S. Belli, M. F. Alf, P. A. Schubiger, S. D. Kramer, and S. M. Ametamey. 2011. 'In vitro and in vivo evaluation of [18F]-FDEGPECO as a PET tracer for imaging the metabotropic glutamate receptor subtype 5 (mGluR5)', *Neuroimage*, 56: 984-91.

Waniewski, Robert A., and David L. Martin. 1998. 'Preferential Utilization of Acetate by Astrocytes Is Attributable to Transport', *The journal of neuroscience*, 18: 5225.
Watabe, Hiroshi. 2017. 'Compartmental Modeling in PET Kinetics': 323-52.
Watabe, T., M. Amend, A. Thielcke, J. Hatazawa, B. Pichler, and H. Wehrl. 2016. 'Constant infusion of 18F-FDG can detect changes in cerebral metabolic rate of glucose during multiple stimulations in a single scan: A quantitative PET study in rats.', *J Nucl Med*, 57: 1.
Weinstein, N. D., S. E. Marcus, and R. P. Moser. 2005. 'Smokers' unrealistic optimism about their risk', *Tob Control*, 14: 55-9.
Wexler, D.B. 1981. *Mental health law: Major issues* (Plenum Publishing: New York, USA).
Whitehead, K., R. Langer, and D. G. Anderson. 2009. 'Knocking down barriers: advances in siRNA delivery', *Nat Rev Drug Discov*, 8: 129-38.
Williams-Hemby, Lisa, and Linda J. Porrino. 1994. 'Low and Moderate Doses of Ethanol Produce Distinct Patterns of Cerebral Metabolic Changes in Rats', *Alcoholism: Clinical and Experimental Research*, 18: 982-88.
Wilson, M.E., K.L. Rosewell, M.L. Kashon, P.J. Shughrue, I. Merchenthaler, and P.M. Wise. 2002. 'Age differentially influences estrogen receptor-alpha (ERalpha) and estrogen receptor-beta (ERbeta) gene expression in specific regions of the rat brain', *Mechanisms of Ageing and Development*, 123: 8.
Wink, A. M., J. C. de Munck, Y. D. van der Werf, O. A. van den Heuvel, and F. Barkhof. 2012. 'Fast eigenvector centrality mapping of voxel-wise connectivity in functional magnetic resonance imaging: implementation, validation, and interpretation', *Brain Connect*, 2: 265-74.
Winstanley, C. A., Q. LaPlant, D. E. Theobald, T. A. Green, R. K. Bachtell, L. I. Perrotti, R. J. DiLeone, S. J. Russo, W. J. Garth, D. W. Self, and E. J. Nestler. 2007. 'DeltaFosB induction in orbitofrontal cortex mediates tolerance to cocaine-induced cognitive dysfunction', *J Neurosci*, 27: 10497-507.
Wise, R. A. 2005. 'Forebrain substrates of reward and motivation', *J Comp Neurol*, 493: 115-21.
———. 2008. 'Dopamine and reward: the anhedonia hypothesis 30 years on', *Neurotox Res*, 14: 169-83.
Wong, D. F., H.N. Wagner, R. F. Dannals, J.M. Links, J.J. Frost, H.T. Ravert, A.A. Wilson, A.E. Rosenbaum, A. Gjedde, K.H. Douglass, J.D. Petronis, M.F. Folstein, J.K.T. Toung, H. D. Burns, and M.J. Kuhar. 1984. 'Effects of age on dopamine and serotinin receptors measured by positron tomography in the living human brain', *Science*, 226: 1.
Wong, D. F., R. Waterhouse, H. Kuwabara, J. Kim, J. R. Brasic, W. Chamroonrat, M. Stabins, D. P. Holt, R. F. Dannals, T. G. Hamill, and P. D. Mozley. 2013. '18F-FPEB, a PET radiopharmaceutical for quantifying metabotropic glutamate 5 receptors: a first-in-human study of radiochemical safety, biokinetics, and radiation dosimetry', *J Nucl Med*, 54: 388-96.
Woodward, J. J. 1990. 'Ethanol inhibition of *N*-Methyl-D-Aspartate-stimulated endogenous dopamine release from rat striatal slices: reversal by glycine', *J Neurochem*, 54: 3.
Woolrich, M. W., S. Jbabdi, B. Patenaude, M. Chappell, S. Makni, T. Behrens, C. Beckmann, M. Jenkinson, and S. M. Smith. 2009. 'Bayesian analysis of neuroimaging data in FSL', *Neuroimage*, 45: S173-86.
World Health Organization. 2014. "Global status report on alcohol and health 2014." In.
———. 2015. 'WHO report on the global tobacco epidemic'.

Wyckhuys, T., J. Verhaeghe, L. Wyffels, X. Langlois, M. Schmidt, S. Stroobants, and S. Staelens. 2013. 'N-acetylcysteine- and MK-801-induced changes in glutamate levels do not affect in vivo binding of metabotropic glutamate 5 receptor radioligand 11C-ABP688 in rat brain', *J Nucl Med*, 54: 1954-61.

Wyss, M., and R. Kaddurah-Daouk. 2000. 'Creatine and creatinine metabolism', *Physiological Reviews*, 80: 74.

Xiao, C., and J. Ye. 2008. 'Ethanol dually modulates GABAergic synaptic transmission onto dopaminergic neurons in ventral tegmental area: role of mu-opioid receptors', *Neuroscience*, 153: 18.

Yanai, Joseph. 1979. *Strain and sex differences in the rat brain*.

Yang, S., B. J. Salmeron, T. J. Ross, Z. X. Xi, E. A. Stein, and Y. Yang. 2009. 'Lower glutamate levels in rostral anterior cingulate of chronic cocaine users - A (1)H-MRS study using TE-averaged PRESS at 3 T with an optimized quantification strategy', *Psychiatry Res*, 174: 171-6.

Zafra, M. P., C. Mazzeo, C. Gámez, A. Roderiguez, A. de Zulueta, and V. Sanz. 1996. 'Gene silencing of SOCS3 by siRNA intranasal delivery inhibits asthma phenotype in mice', *PLoS One*, 9: 11.

Zeeb, F. D., T. W. Robbins, and C. A. Winstanley. 2009. 'Serotonergic and dopaminergic modulation of gambling behavior as assessed using a novel rat gambling task', *Neuropsychopharmacology*, 34: 2329-43.

Zeiler, F. A. 2015. 'Activated NMDA receptor imaging: a step forward in epilepsy', *J Neurol Neurosurg Psychiatry*, 86: 1053.

Zhou, S. J., L. F. Xue, X. Y. Wang, W. G. Jiang, Y. X. Xue, J. F. Liu, Y. Y. He, Y. X. Luo, and L. Lu. 2012. 'NMDA receptor glycine modulatory site in the ventral tegmental area regulates the acquisition, retrieval, and reconsolidation of cocaine reward memory', *Psychopharmacology (Berl)*, 221: 79-89.

Zilles, K., M. Bacha-Trams, N. Palomero-Gallagher, K. Amunts, and A. D. Friederici. 2015. 'Common molecular basis of the sentence comprehension network revealed by neurotransmitter receptor fingerprints', *Cortex*, 63: 79-89.

Zilles, K., N. Palomero-Gallagher, C. Grefkes, F. Scheperjans, C. Boy, K. Amunts, and A. Schleicher. 2002. 'Architectonics of the human cerebral cortex and transmitter receptor fingerprints: reconciling functional neuroanatomy and neurochemistry', *European Neuropsychopharmacology*, 12: 12.

Zocchi, Alessandro, Giuseppe Conti, and Francesco Orzi. 2001. 'Differential effects of cocaine on local cerebral glucose utilization in the mouse and in the rat', *Neuroscience Letters*, 306: 177-80.

Zubieta, Jon-Kar, Umberto Lombardi, Satoshi Minoshima, Sally Guthrie, LiSong Ni, Linda E. Ohl, Robert A. Koeppe, and Edward F. Domino. 2001. 'Regional cerebral blood flow effects of nicotine in overnight abstinent smokers', *Biological Psychiatry*, 49: 906-13.

Personal contribution

The Doctoral School regulation requires the specification of the contribution of the candidate to the experiments reported in this thesis.

All experiments have been designed, executed, analyzed, and reported by myself, in concertation with my supervisors and collaborators. No shared studies have been included in this thesis.

Conflict of interest

The candidate declares that there is no conflict of interest regarding the publication of this thesis.

Scientific Acknowledgments

We would like to thank Tinne Buelens and Ann Van Santvoort for their excellent technical assistance and the radiopharmacy team UZ Leuven for the tracer productions. In addition, we would like to thank Ivan Sannen and Pieter Haspeslagh for their technical assistance with the HPLC, gamma-counter, and mass spectrometer. Julie Cornelis is thanked for her exceptional help, in particular with the arterial sampling and autoradiography experiments.

Curriculum Vitae

BART DE LAAT
Rue de la Hocaille 14
1390, Archennes, Belgium
+32 (0)472 61 70 53
bart.delaat@kuleuven.com | bartdelaat@gmail.com

Personal information Nationality: Dutch
Date of Birth: 12 October 1986, Heerenveen

Education

2013 - 2017 **PhD in Biomedical Sciences**
University of Leuven, Leuven, Belgium
Thesis title: PET-MR in animal models of addiction: Focus on the glutamatergic system

2012 **Veterinary Neurology research internship**
Ghent University, Ghent, Belgium

2011 – 2012 **Veterinarian for Companionship Animals**
University of Liège, Liège, Belgium
Thesis title: Non-invasive intracranial pressure measurement in dogs

2013 - 2017 **Master of Statistical Data Analysis**
Ghent University, Belgium
Thesis title: Analysis of Positron Emission Tomography data: A comparison between approaches for linearized time-activity curves

2008 – 2011 **Master of Veterinary Science**
Ghent University, Belgium
Thesis title: Urinary biomarkers in dogs bitten by snakes

2005 – 2008 **Bachelor of Veterinary Science**
University of Antwerp, Belgium
Thesis title: The neurobiological fundaments of thanatosis

Extracurricular activities

2017 **Strategic management in the pharmaceutical industry**
University of Leuven, Leuven, Belgium [Course]

2014 **YouReCa science communication challenge**

2013 - 2015 **Vice-president Belgian Molecular Imaging Community**

2010 **Attestation of knowledge of English C1**
University Language Centre, Ghent

2009 – 2011 **Member of Ethical Committee**
Faculty of Veterinary sciences, Ghent University

Languages Dutch: native; English: fluent; French and German: conversational.

Hobbies Sailing, boxing

Publication list

International Journal Articles

de Laat B., Leurquin-Sterk G., Celen S., Bormans G., Koole M., Van Laere K., Casteels C. (2015) Preclinical evaluation and quantification of ^{18}F-FPEB as a radioligand for PET imaging of the metabotropic glutamate receptor 5. J Nuc Med, pp. 1954 – 1959.

Leurquin-Sterk G., Crunelle CL., Ceccarini J., **de Laat B.**, Verbeek J., Deman S., Neels H., Bormans G., Peuskens H., Van Laere K. (2017) Decreased limbic metabotropic glutamate receptor 5 availability in alcohol dependence. J Nucl Med, accepted.

Leurquin-Sterk G., Ceccarini J., Crunelle CL., Weerasekera A., **de Laat B.**, Himmelreich U., Bormans G., Van Laere K. (2017) Cerebral dopaminergic and glutamatergic transmission relate to different subjective responses of acute alcohol intake: an in vivo multimodal imaging study. Addict Biol, epub ahead of print.

Ory D., Postnov A., Koole M., Celen S., **de Laat B.**, Verbruggen A., Van Laere K., Bormans G., Casteels C. (2016) Quantification of TSPO overexpression in a rat model of local neuroinflammation induced by intracerebral injection of LPS by the use of [(18)F]DPA-714 PET. Eur J Nucl Med Mol Imaging, pp 163-72.

Leurquin-Sterk G., Postnov A., **de Laat B.**, Casteels C., Celen S., Crunelle CL., Bormans G., Koole M., Van Laere K. (2016) Kinetic modelling and long-term test-retest reproducibility of the mGluR5 PET tracer (18)F-FPEB in human brain. Synapse, pp 153-62.

Spangler-Bickell M., Zhou L., Kyme A., **de Laat B.**, Fulton R., Nuyts J. (2016) Optimising rigid motion compensation for small animal brain PET imaging. Phys Med Biol, 61, 19, pp. 7074 – 7091.

Leurquin-Sterk G., Van den Stock J., Crunelle CL., **de Laat B.**, Weerasekera A., Himmelreich U., Bormans G., Van Laere K. (2016) Positive Association Between

Limbic Metabotropic Glutamate Receptor 5 Availability and Novelty-Seeking Temperament in Humans: a 18F-FPEB PET study. J Nucl Med, 57, 11, pp. 1746 – 1752.

Spangler-Bickell M., **de Laat B.**, Fulton R., Bormans G., Nuyts J. (2016) The effect of isoflurane on ^{18}F-FDG uptake in the rat brain: a fully conscious dynamic PET study using motion compensation. EJNMMI Res, 6(1), pp. 86.

Hrovat A., Schoeman JP., **de Laat B.**, Meyer E., Smets P., Goddard A., Nagel S., Daminet S. (2013) Evaluation of snake envenomation-induced renal dysfunction in dogs using early urinary biomarkers of nephrotoxicity. Vet. J. 198(1), pp. 239 – 244.

Book chapters

de Brouwer C.P.M., van Gool C.J.A.W., Kant I.J., **de Laat B.**, Denies S. (2012) Chapter 2: Systematisch literatuur zoeken; van klinische vraag naar evidence. In: Training critical appraisal of a topic. Editors: de Brouwer C.P., Mommers M., van Gool C.J., Kant I.J., Ferreira I. Maastricht, pp. 145 – 195.

Oral presentations

de Laat B., Weerasekera A., Schroyen G., Casteels C., Van Laere K., Himmelreich U., Gsell W. (2018) Acute changes in rat brain metabolism after intravenous drug administration: A simultaneous dynamic 1H-MRS and continuous infusion 18FDG study. TOPIM, Les Houches, France.

de Laat B., Weerasekera A., Leurquin-Sterk G., Bormans G., Himmelreich U., Casteels C., Van Laere K. (2017) Biomarkers for alcohol addiction: Findings from a longitudinal ^{18}F-FPEB PET and ^{1}H-MRS study in rats. EMIM, Cologne, Germany.

Leurquin-Sterk G., Crunelle CL., Ceccarini J., **de Laat B.**, Verbeek J., Deman S., Neels H., Bormans G., Peuskens H., Van Laere K. (2017) Recovery of decreased metabotropic

glutamate receptor 5 availability in abstinent alcohol-dependent subjects. SNNMI, Denver, USA.

Leurquin-Sterk G., Ceccarini J., Crunelle CL., Weerasekera A., **de Laat B.**, Himmelreich U., Bormans G., Van Laere K. (2017) Cerebral dopaminergic and glutamatergic transmission relate to different subjective responses of acute alcohol intake: an in vivo multimodal imaging study. EANM, Barcelona, Spain.

de Laat B., Weerasekera A., Crabbé M, Leurquin-Sterk G., Govaerts K., Celen S., Bormans G., Koole M., Himmelreich U., Casteels C., Van Laere K. (2016) Longitudinal multimodal self-administration study provides evidence for role of mGluR5 and glutamate in predisposition to drug addiction in rats. J Nucl Med, 57, S2, p. 294. SNMMI, San Diego, USA.

Leurquin-Sterk G., Ceccarini J., Van den Stock J., Postnov A., Crunelle CL., **de Laat B.**, Weerasekera A., Himmelreich U., Peuskens H., Bormans G., Van Laere K. (2016) PET imaging of the metabotropic glutamate receptor 5 in healthy and alcohol dependent subjects. ISBRA-ESBRA, Berlin, Germany

Leurquin-Sterk G., Postnov A., Celen S., Weerasekera A., **de Laat B.**, De Backer L., Bormans G., Van Laere K. (2015) Age-dependency of mGluR5 and its relationship to novelty seeking and MRS-derived glutamate concentrations: a ^{18}F-FPEB PET study in healthy volunteers. J Nucl Med, 56, S3, p. 305. SNMMI, Baltimore, USA.

de Laat B., Weerasekera A., Crabbé M, Leurquin-Sterk G., Govaerts K., Celen S., Bormans G., Koole M., Himmelreich U., Casteels C., Van Laere K. (2016) Longitudinal multimodal self-administration study provides evidence for role of mGluR5 and glutamate in predisposition to drug addiction in rats. EMIM 2016, Utrecht, The Netherlands.

de Laat B., Koole M., Celen S., Leurquin-Sterk G., Bormans G., Van Laere K., Casteels C. (2015) Evaluation and quantification of ^{18}F-FPEB as radioligand for PET imaging of the metabotropic glutamate receptor 5 in rat brain. EMIM 2015, Tubingen, Germany.

Leurquin-Sterk G., Crunelle C., Ceccarini J., **de Laat B.**, Peuskens H., Bormans G., Van Laere K. (2016) Alcohol addiction is associated with decreased limbic mGluR5 availability: a 18F-FPEB PET study in human. J Nucl Med, 57, S2, p. 15. SNMMI, San Diego, USA.

Leurquin-Sterk G., Postnov A., **de Laat B.**, Casteels C., Celen S., Crunelle CL., Bormans G., Koole M., Van Laere K. (2015) Kinetic modelling and long-term test-retest of ^{18}F-FPEB mGluR5 PET in healthy volunteers. SNMMI 2015, San Diego, USA.

de Laat B., Schoeman J.P., Hrovat A., Meyer E., Smets P., Goddard A., Nagel S., Daminet S. (2013). Evaluation of snake envenomation-induced renal dysfunction in dogs using early urinary biomarkers of nephrotoxicity. WVA, Prague, Czech republic.

de Laat B., Gommeren K., Denies S., Merveille A-C., Gomart S., Fergus A., Peeters D. (2012). Influence of sedatives, anticonvulsants and a negative chronotrope on transcranial doppler ultrasonography. 22nd ECVIM-CA Congress, Maastricht, The Netherlands.

Gommeren K., **de Laat B.**, Denies S., Merveille A-C., Gomart S., Fergus A., Peeters D. (2012). Repeatability and reproducibility of transcranial doppler ultrasonography in healthy beagle dogs. 22nd ECVIM-CA Congress, Maastricht, The Netherlands.

Posters

de Laat B., Gsell W., Casteels C., Van Laere K. (2017) Dual ^{18}FDG injection protocol shows changes glucose metabolism in the nucleus accumbens after cocaine challenge in rats. EMIM, Cologne, Germany.

de Laat B., Casteels C., Van Laere K. (2017) Effects of brain development and gender on metabotropic glutamate receptor type 5 availability in rats: A cross-sectional ^{18}F-FPEB PET study. EMIM, Cologne, Germany.

de Laat B., Weerasekera A., Crabbé M., Leurquin-Sterk G., Govaerts K., Celen S., Bormans G., Koole M., Himmelreich U., Casteels C., Van Laere K. (2016) Longitudinal multilevel rat study of cocaine addiction shows associations with decision-making, glutamate and the metabotropic glutamate receptor 5, EURON, Lille, France .

de Laat B., Gsell W., Govaerts K., Himmelreich U., Casteels C., Van Laere K. (2016) Resting state connectivity shows differential effects for subsets of the mesocorticolimbic circuit during drug addiction in rats. Frontiers in Aging Neuroscience. Conference Abstract: 6th Belgian Brain Congress.

de Laat B., Gsell W., Govaerts K., Himmelreich U., Casteels C., Van Laere K. (2016) Longitudinal self-administration study provides evidence for changes in resting state connectivity. FENS, Kopenhagen, Denmark.

de Laat B., Koole M., Celen S., Leurquin-Sterk G., Bormans G., Van Laere K., Casteels C. (2015) Evaluation and quantification of ^{18}F-FPEB as radioligand for PET imaging of the metabotropic glutamate receptor 5 in rat brain. BRAIN, Vancouver, Canada.

Bickell M., **de Laat B.**, Fulton R., Bormans G., Nuyts J. The Effect of Anaesthesia on 18F-FDG Uptake in the Rat Brain: a Fully Conscious Dynamic Study Using Motion Correction. 2015 IEEE MIC, San Diego, California.

Holvoet B., Quattrocelli M., Gijsbers R., **de Laat B.**, Casteels C., Wolfs E., Van Laere K., Verfaillie C., Sampaolesi M., Deroose C. (2014). Noninvasive imaging of muscle progenitors in muscular dystrophy murine models via BLI, CLI and PET. BeSSCR, Ghent, Belgium.